SAND--88-7002

DE88 009795

SAND88-7002

NUMERICAL SIMULATION OF GROUND-WATER FLOW IN THE CULEBRA DOLOMITE AT THE WASTE ISOLATION PILOT PLANT (WIPP) SITE: SECOND INTERIM REPORT

Prepared for

Sandia National Laboratories
Albuquerque, New Mexico 87185

By

A.M. LaVenue, A. Haug, V.A. Kelley

INTERA Technologies, Inc.
6850 Austin Center Blvd., Suite 300
Austin, Texas 78731

March 10, 1988

097B-00G-018F
H09700R554

DISCLAIMER

EXECUTIVE SUMMARY

This hydrogeologic modeling study has been performed as part of the regional hydrologic characterization of the Waste Isolation Pilot Plant (WIPP) Site in southeastern New Mexico. The study resulted in an estimation of the transmissivity distribution, hydraulic potentials, flow field, and fluid densities in the Culebra Dolomite Member of the Permian Rustler Formation at the WIPP site.

The three-dimensional finite-difference code SWIFT-II was employed for the numerical modeling, using variable-fluid-density and a single-porosity formulation. The variable-fluid-density approach does not, at this stage, include changes in brine density within the model due to the present flow field or due to local reactions, such as halite dissolution. The spatial scale of the model, 24 km by 25 km, was chosen to allow simulation of a 62-day pumping test conducted in the fall of 1985 at the H-3 hydropad south of the center of the WIPP site, and a 36-day pumping test conducted in early 1987 at well WIPP-13 northwest of the center of the WIPP site. The modeled area includes and extends beyond the WIPP controlled zone (Zone 3).

The work performed consisted of modeling the hydrogeology of the Culebra using two approaches: (1) steady-state modeling to develop the best estimate of the undisturbed head distribution, i.e., of the situation before sinking of the WIPP shafts, which began in 1981; and (2) superimposed transient modeling of local hydrologic responses to excavation of the three WIPP shafts at the center of the WIPP site, as well as to various well tests. Boundary conditions (prescribed constant fluid pressures and densities) were estimated using hydraulic-head and fluid-density data obtained from about 40 wells at and near the WIPP site. The transient modeling used the calculated steady-state freshwater heads as initial conditions.

The initial spatial transmissivity distribution in the Culebra dolomite was obtained using two different kriging techniques, the USGS universal kriging code, K603, and the MIT generalized kriging code, AKRIP. The resulting transmissivity distributions are very similar with low transmissivities ($< 1 \times 10^{-7}$ m^2/s) in the eastern model area, intermediate transmissivities (1×10^{-6} to 1×10^{-4} m^2/s) in the central part of the model area, and high transmissivities ($> 1 \times 10^{-3}$ m^2/s) in the western part of the model area representing Nash Draw. The transmissivity distribution estimated by AKRIP was selected for the initial steady-state simulation. The resulting initial steady-state model was calibrated such that the differences between the calculated and observed freshwater heads are below the uncertainties associated with observed heads. Calibration parameters were the prescribed boundary conditions and transmissivities. AKRIP was used in the estimation of the transmissivity distributions during calibration.

The steady-state calibrated transmissivity distribution contains a relatively high-transmissivity zone between wells H-17 and P-17. Modeled transmissivities within this zone are approximately 5×10^{-5} m^2/s. The location of the zone is approximately the same as that proposed in a previous interim modeling report, but the transmissivity is four times lower in magnitude. Sensitivity analyses performed in this study demonstrate that the introduction of a higher transmissivity feature between H-17 and P-17 is required to reduce the differences between the calculated and observed heads in the vicinity of DOE-1 and H-11 below the uncertainties of the observed heads. The final transmissivity distribution is also characterized by a relatively large area of low transmissivities (less than approximately 10^{-6} m^2/s) near the center of the site. This area includes wells H-1, H-2, WIPP-12, WIPP-18, WIPP-19, WIPP-21, WIPP-22, P-18, and H-5, in addition to the WIPP shafts.

After final calibration of the steady-state model, the following drilling and testing activities at the WIPP shafts and well locations were

incorporated into the model and superimposed onto the steady-state head distribution: (1) a simplified but complete shaft history since 1981; (2) three pumping tests and a series of slug tests conducted at the H-2 hydropad in 1982 and 1981; (3) the H-3 convergent-flow tracer test conducted in 1984; (4) the H-3 step-drawdown test conducted in 1985; (5) the H-3 multipad pumping test in 1985 and 1986; (6) the convergent-flow tracer test at the H-4 hydropad conducted between 1982 and 1984; and (7) the WIPP-13 multipad pumping test conducted in 1987. The transient simulation of the above hydraulic stresses in the Culebra dolomite extended from January 1, 1981 to December 31, 1987.

The initial transient simulation using the steady-state calibrated model adequately reproduced the observed drawdowns at P-14, DOE-2, and H-6 during the WIPP-13 multipad pumping test. The calculated drawdowns at H-11 and DOE-1 during the simulation of the H-3 multipad pumping test are also very similar to the observed drawdowns. The steady-state calibrated transmissivities do not adequately reproduce the observed transient responses generated from the shaft events or the observed drawdowns at the pumping wells used in the simulation, H-2, H-3, H-4, and WIPP-13. Generally, the calculated drawdowns at these wells are a factor of two greater than the observed drawdowns. Similarly, the calculated drawdowns due to the shaft events are a factor of two greater than the observed drawdown at H-1, H-2, and H-3.

Sensitivity analyses performed to determine the effects of the model transmissivities and storativity upon the calculated transient heads indicate that adjustments to the steady-state calibrated transmissivities are necessary to reduce the differences between the calculated and observed transient data. These analyses indicate: (1) lower transmissitivities are required between the shafts and H-1, H-2, H-3, and the WIPP wells in the vicinity of the shafts; (2) higher transmissivities are necessary in the vicinity of H-2, H-3, H-4, and WIPP-13; and (3) a higher transmissivity, low-storativity zone between WIPP-13 and the WIPP wells north of the shafts is necessary to reproduce the observed transient responses during the WIPP-13 multipad pumping test.

The modeling study discussed in this second interim report is based on the transmissivity data available as of November 1987, as well as the hydraulic-head data available as of August 1987. This modeling study represents recent progress towards a comprehensive modeling study characterizing the regional hydrogeology of the Culebra dolomite of the Rustler Formation at the WIPP site. The next step will incorporate the results of the transient effects due to the pumping during a tracer test at the H-11 hydropad and the transient effects due to the construction of the fourth shaft at the WIPP site. Improvement of the agreement between the observed and the calculated transient freshwater heads by additional calibration efforts is also planned. In addition, adjoint-sensitivity techniques will provide quantitative estimates of sensitivities of model results to the spatial distribution of the model parameters and the boundary conditions. The final report is planned to be issued in early 1989.

TABLE OF CONTENTS

TABLE OF CONTENTS

(cont.)

TABLE OF CONTENTS
(cont.)

PAGE

TABLE OF CONTENTS
(cont.)

PAGE

LIST OF FIGURES

LIST OF FIGURES
(cont.)

LIST OF FIGURES
(cont.)

LIST OF FIGURES
(cont.)

LIST OF FIGURES
(cont.)

LIST OF FIGURES
(cont.)

LIST OF FIGURES
(cont.)

LIST OF FIGURES
(cont.)

LIST OF TABLES

LIST OF TABLES
(cont.)

1.0 INTRODUCTION

Site-characterization efforts are being conducted at the Waste Isolation Pilot Plant (WIPP) site in southeastern New Mexico (Figure 1.1) as part of the evaluation of the suitability of the bedded salt in the Salado Formation for isolation of defense transuranic waste. Studies are performed in accordance with the Consultation and Cooperation Agreement between the U.S. Department of Energy and the State of New Mexico. Efforts have included regional and local geologic, geochemical, and hydrogeologic characterization. Sandia National Laboratories is coordinating the hydrogeologic studies on behalf of the Department of Energy. This report represents a summary of work conducted to date on developing a ground-water model for the Culebra Dolomite Member of the Rustler Formation on a regional scale around the WIPP site. This work was performed by INTERA Technologies under contract to Sandia National Laboratories.

The Culebra dolomite is the most transmissive, laterally-continuous, hydrogeologic unit above the Salado Formation. It is considered to be the principal pathway for radionuclide transport in the subsurface should an accidental breach of the repository occur. This study focuses on the simulation of ground-water flow within the Culebra.

A finite-difference model based on the hydrogeologic data base as of approximately November 1987 is used to calculate the undisturbed and transient equivalent freshwater head distributions at the site. The undisturbed heads represent the hydrologic conditions prior to the construction of the shafts at the WIPP site in 1981. The transient heads were generated from several hydrologic tests including two regional pumping tests. The effects of the WIPP shafts upon the hydrologic environment are also presented. This study is an update of the model presented by Haug et al. (1987) and includes an extended model area and an expanded data base.

The conclusions derived from this study and their significance to the WIPP project are presented in Section 6.0. The results are intended to provide additional information for the characterization of the WIPP site, and to support the evaluation of the suitability of the site for disposal of defense transuranic waste.

1.1 Objectives

The objectives of this report are to:

(1) document the hydrogeologic data base for the Culebra at the WIPP site (including Culebra elevations, transmissivities, storativities, formation-fluid densities, undisturbed equivalent freshwater heads, and hydrologic stresses during the period 1981-1987);

(2) continue the development of a conceptualization and modeling strategy for describing ground-water flow in the Culebra; and

(3) present the calibration approach and results for simulating ground-water flow in the Culebra under undisturbed hydraulic conditions and under transient conditions (1981 to 1987) resulting from shaft activities and well tests (in particular, two long-term pumping tests at H-3 and WIPP-13).

The spatial scale for the numerical model utilized in this study was chosen to allow a quantitative evaluation of the H-3 and WIPP-13 multipad pumping tests and to allow an assessment of ground-water flow in the Culebra at the WIPP site in a region of interest for future performance-assessment calculations and evaluations. As such, it encompasses the WIPP site and its immediate surroundings. The WIPP-site boundary (also referred to as the Zone-3 boundary) is defined approximately by a four-mile square as illustrated in Figure 1.1 and represents the boundary to the accessible environment in the context of

performance-assessment studies. The model is relatively detailed since it includes the area containing the majority of the available monitoring and testing wells in this region.

1.2 Other Modeling Studies of Ground-Water Flow in the Culebra Dolomite

Several modeling studies of ground-water flow at the WIPP site have been conducted since 1978, with particular emphasis on the Permian Rustler Formation. These studies are presented in:

- Final Environmental Impact Statement (FEIS), U.S. DOE (1980) and WIPP Safety Analysis Report, U.S. DOE (1981);
- Cole and Bond (1980);
- D'Appolonia Consulting Engineers, Inc. (1980);
- Barr et al. (1983);
- Haug et al. (1987);
- Niou and Pietz (1987);
- Davies (1988).

The approximate areal extent encompassed by these models is illustrated in Figure 1.2.

The hydrogeologic data base at the WIPP site has been significantly expanded in the period 1985-1987. Modeling studies before 1985 utilized a smaller data base for characterizing the Culebra. These earlier studies, the interim modeling report by Haug et al. (1987) which utilized the data base up to mid-1986, and the recent modeling studies by Niou and Pietz (1987) and Davies (1988) are discussed briefly below.

1.2.1 Modeling Studies Before 1985

The modeling studies presented in the Final Environmental Impact

Statement and the WIPP Safety Analysis Report (SAR) were conducted by INTERA during the period 1977-1980. The objectives of these studies were to:

(1) check the consistency between various sets of hydrogeologic data;

(2) calculate the extent of vertical hydraulic communication between various hydrologic units;

(3) delineate heterogeneities (i.e., spatial variation of permeability) existing within each geologic formation;

(4) determine potentials and/or hydraulic conductivities in areas where data are lacking; and

(5) determine boundary conditions for local scenario and nuclide-transport modeling.

The hydrologic data base of the above-mentioned studies was obtained principally from Mercer and Orr (1977), which summarized data existing through February 1977, and from a draft USGS report to Sandia National Laboratories containing the results of well tests and permeability estimates at the WIPP site. The hydrogeologic units included in the modeling studies were the Rustler Formation (modeled as a single hydrologic unit), the shallow-dissolution zone along the Rustler-Salado interface in Nash Draw (see Figure 1.2), the Delaware Mountain Group, the Capitan Reef, the Salado Formation, and the Castile Formation.

Cole and Bond (1980) conducted a benchmark check of the modeling studies done by INTERA for the FEIS. The Cole and Bond study, performed on behalf of the Office of Nuclear Waste Isolation (ONWI),

utilized the same data and conceptual model for its assessments. The numerical model they used, denoted VTT, is a two-dimensional multilayer model which solves the Boussinesque equations for groundwater flow and allows hydraulic communication between layers with an interaquifer transfer coefficient. The results of their modeling studies showed a very close correspondence to results obtained using the INTERA model.

D'Appolonia Consulting Engineers, Inc. (1980) conducted modeling studies of the WIPP site with the objectives of:

(1) verifying the basic calculational procedures implemented by INTERA in the SAR for the analyses of breach and transport events;

(2) evaluating the sensitivity of the results to basic hydrogeologic and geochemical parameters and source-term inputs; and

(3) reviewing the data base used to define the input parameters.

In their studies, the Rustler Formation and the Bell Canyon aquifer were modeled individually with separate model grids and simulations. Overall, their results and conclusions were consistent with the previously conducted studies.

The model developed by Barr et al. (1983) had the principal objectives of:

(1) simulating the freshwater potential surfaces for the Magenta and Culebra dolomites; and

(2) estimating rates and extents of migration of ideally nonsorbing contaminants injected continuously into the Culebra and Magenta dolomites without disturbing the calculated head distribution.

The model area was selected to include the majority of hydrologic wells and most of Nash Draw. The Culebra and Magenta dolomites were modeled separately using an anisotropic two-dimensional model, ISOQUAD. The hydrogeologic data base consisted primarily of Mercer (1983) and Gonzalez (1983 a,b). Travel times along selected streamlines were presented. Results of this effort indicated slower ground-water movement than presented in previous reports.

1.2.2 Interim Report by Haug et al. (1987)

In 1986, INTERA began new modeling studies of the Culebra dolomite (Haug et al., 1987). The objectives included:

(1) evaluating the H-3 multipad pumping test conducted in late 1985 and early 1986; and

(2) simulating ground-water flow in the Culebra dolomite at the WIPP site. This was meant to be a first step toward a regional model capable of simulating ground-water flow and transport at the WIPP site and its surroundings.

INTERA's efforts resulted in a single-layer model of the Culebra dolomite with an area of 12.24 x 11.7 km. SWIFT II, a three-dimensional finite-difference code with variable fluid density and double-porosity formulation, was used in the study. The model was calibrated to the best estimate of the undisturbed freshwater heads (Figure 1.3) and the best estimate of the present-day formation-water densities (Figure 1.4).

The hydrogeology in the Culebra dolomite was modeled in two steps: (1) steady-state modeling of the best estimate of the undisturbed hydraulic conditions, and (2) transient modeling of the hydrogeologic conditions resulting from excavating three shafts at the center of the

WIPP site and conducting several hydraulic tests. The study developed a Culebra ground-water flow model using the data base available as of approximately mid-1986. The transmissivities of the calibrated steady-state model, the model-calculated freshwater heads, the difference plot between calculated and observed freshwater heads, the model-calculated formation-water densities, and the difference plot between calculated and observed formation-water densities are shown in Figures 1.5, 1.6, 1.7, 1.8, and 1.9, respectively. The transient simulations provided good comparisons between model-calculated and observed freshwater-head histories using the transmissivity distribution for the calibrated steady-state model.

Haug et al.(1987) developed the following main conclusions:

(1) The steady-state model can be calibrated against the best estimate of the undisturbed heads.

(2) The hydraulic system (heads and flow directions) in the Culebra dolomite can be simulated as at steady-state considering a time period of several years.

(3) The calibrated transmissivity distribution is characterized by a large area of low transmissivities (less than 10^{-6} m^2/s) near the center of the site (including wells H-1, H-2, WIPP-12, WIPP-18, WIPP-19, WIPP-21, and WIPP-22, P-18, and H-5 and the WIPP-shaft area).

(4) Calibration of the model requires a higher transmissivity zone south of H-11/DOE-1.

(5) The calibrated model shows two main flow paths:

   (a) from north to south along the western boundary, and

   (b) across the WIPP site to the south-southeast (WIPP-13 to H-1 to H-3 to DOE-1 to H-11 to south)

(6) Calibration of the steady-state model against the best estimate of the ground-water densities is difficult. Regions of low salinity (1.0 to 1.02 g/cm^3) exist hydraulically down-gradient from regions of intermediate salinity (1.04 g/cm^3). The ground-water density distribution in the Culebra dolomite is probably not at steady state at present.

(7) The model-calculated ground-water density distribution is highly sensitive to vertical flux into the Culebra.

(8) The shaft excavations and subsequent leakage of ground water into the shafts caused significant hydraulic stress on the Culebra dolomite since 1981.

(9) The transient simulations for hydraulic stresses at the shafts and the H-2, H-3, and H-4 hydropads resulted in generally good agreement between model-calculated and observed freshwater-head histories.

(10) At the model scale, the implemented transient processes can be adequately simulated using a single-porosity approach (equivalent porous medium).

1.2.3 Other Recent Modeling Studies

Niou and Pietz (1987) presented a modeling study of the H-3 multipad pumping test using a two-dimensional ground-water inverse code known as INVERT. The model uses a maximum-likelihood framework coupled with a flow model based on finite-element techniques to calculate the formation parameters (transmissivity and storativity) from the observed transient responses in the observation wells. The objectives of their investigation were (Niou and Pietz, 1987):

(1) Characterize the Culebra dolomite to the extent the data permit by assigning regionalized values of transmissivity and storativity along with associated uncertainties;

(2) Compare model results with other modeling studies for the purpose of corroboration; and

(3) Judge the suitability of the approach for future work.

The model parameters were defined as constant over various subregions with best estimates determined as those that yield the best match between observed and calculated drawdowns during the H-3 multipad pumping test. The model utilized the transmissivity data base presented in Barr et al. (1983) to define the zoning patterns. The model area was 12 x 12 km centered on the H-3 hydropad.

The principal findings of this study may be summarized as follows (Niou and Pietz, 1987):

(1) The results show a high-transmissivity zone or fracture zone running from H-3 to DOE-1 and H-11, another high-transmissivity or fracture zone running south from H-3 to P-17, which may be an extension of the DOE-1/H-11 zone, and a zone of high transmissivity around the shafts that includes WIPP-21 to the north. The assignment of the latter zone is less certain because of the atypical recovery curves for WIPP-21 and WIPP-22.

(2) The transmissivity ranges calculated by INVERT generally agree with the modeling study by Haug et al. (1987) using SWIFT II, with the exception of the area between H-3 and the Waste Handling Shaft, where INVERT postulated a high-transmissivity zone on the basis of the responses at WIPP-21 and WIPP-22.

(3) Major difficulties in the utility of the inverse model were the lack of reliable estimates of the uncertainties in the prior

determinations (e.g., transmissivities) and the inability to assign uncertainties to the observed water-level data because of the complex prepumping trends.

Davies (1988) is preparing a report that will include modeling results for a region that is approximately 36 x 46 km around the WIPP site. The topics included are a driving-force analysis to evaluate the importance of variable fluid densities on flow directions and simulations of long-term brine-transport patterns. Analyses were also performed to determine the sensitivity of the calculated steady-state heads to the model boundary conditions, model dispersivity, steady-state variable density assumptions, and vertical flux. For the central part of his modeled region, he utilized an approximation of the calibrated transmissivity distribution presented in Haug et al. (1987). The conclusions of the modeling investigations are:

(1) The driving-force analysis and simulations indicate that a region with significant density-related effects on flow direction is present just south of the WIPP-site boundary.

(2) Most of the modeled region is insensitive to boundary conditions along the north and east.

(3) Flow velocities are high in Nash Draw, are very low east of WIPP, and are highly variable in the intermediate zone.

(4) Vertical flux is a possible source of fluid for the Culebra. The sensitivity of the calculated steady-state heads to vertical flux is higher in the eastern part of the model area than in the western.

1.3 Present Approach to Modeling of Ground-Water Flow in the Culebra Dolomite

The modeling studies presented in this report are a continuation of the work reported in Haug et al. (1987). However, the model area has been considerably enlarged in order to allow simulation of ground-water flow on a more regional scale and to evaluate the long-term pumping test at WIPP-13 (referred to as the northern multipad pumping test).

The enlarged model area is illustrated in Figure 1.2. The model boundaries were chosen at distances sufficiently far from both the H-3 hydropad and the WIPP-13 borehole so as not to be within the region affected by the pumping at both locations.

The modeling methodology consisted of the following steps:

(1) developing and documenting the hydrogeologic data base (i.e., Culebra thicknesses, elevations, transmissivities, storativities, equivalent freshwater heads, fluid densities, and hydrologic impacts of the shafts and hydraulic-testing activities);

(2) employing geostatistical techniques (e.g., kriging) to analyze and reconcile the field data as well as to support the implementation and calibration of the model;

(3) simulating steady-state flow under undisturbed hydrologic conditions (i.e., before excavation of the first shaft). Starting with the initial parameter distribution obtained by kriging techniques, the model is calibrated such that the difference between the calculated freshwater heads and the best estimate of the observed freshwater heads is less than the uncertainty associated with the observed values; and

(4) simulating the transient response in the Culebra dolomite, during the period 1981 to 1987, resulting from the excavation and sealing activities of the WIPP shafts and the major hydraulic and tracer-testing activities of the regional hydrologic characterization program. The transient model utilizes the pressures and brine concentrations of the calibrated steady-state model as initial conditions. The calculated transient freshwater heads are compared to the observed transient freshwater heads for selected boreholes.

This study is a second interim step towards a comprehensive modeling study characterizing the regional hydrogeology of the Culebra dolomite of the Rustler Formation at the WIPP site. The next step will incorporate the results of the transient effects due to the pumping during a tracer test at the H-11 hydropad and the transient effects due to the construction of the fourth shaft at the WIPP site. Improvement of the agreement between the observed and the calculated transient freshwater heads by additional calibration efforts is also planned. In addition, adjoint-sensitivity techniques will provide quantitative estimates of sensitivities of the model results to the spatial distribution of the model parameters and the boundary conditions. The final report is planned to be issued in early 1989.

2.0 SITE CHARACTERIZATION

2.1 General

The WIPP site lies within the geologic region known as the Delaware Basin and specifically within the geographic region known as Los Medaños. Both the Delaware Basin and Los Medaños region occur within the southern section of the Pecos River portion of the Great Plains Physiographic Province. Los Medaños is a region of gently sloping terrain which rises eastward from the Pecos River to the western caprock of the Llano Estacado, located approximately 40 km to the northeast of the WIPP site (Mercer, 1983).

2.2 Stratigraphy

The following stratigraphic summary is limited to a discussion of those sedimentary units which crop out in and around the WIPP site. These formations range in age from Permian to Quaternary as shown in the geologic column illustrated in Figure 2.1. The Delaware Mountain Group represents the Permian Guadalupian Series and is composed of a sequence of fine-grained clastic rocks. In the WIPP area, the Delaware Mountain Group consists of the Brushy Canyon, Cherry Canyon, and Bell Canyon Formations. The Bell Canyon consists of interbedded sandstone and shale which represent the fore-reef facies of a massive Permian reef known as the Capitan Limestone. The Ochoan Series rocks overlie the Guadalupian Series and contain a thick evaporitic sequence which accumulated in the Delaware Basin during Permian time. The Castile Formation is the basal formation of the Ochoan Series and is composed principally of anhydrite and halite with some carbonates and sandstones. Overlying the Castile is the Salado Formation, which is composed of thick beds of halite interbedded with anhydrite, polyhalite, dolomite, and clay. More complete descriptions of the Salado Formation are found in Jones (1973, 1975). Overlying the Salado Formation is the Rustler Formation, which is the most water-transmissive formation in the area (Mercer, 1983).

The Rustler Formation has been divided into five separate members based upon lithology (Vine, 1963). They are in ascending order: (1) the unnamed lower member composed of massive siltstone overlain by beds of halite, siltstone, and anhydrite; (2) the Culebra Dolomite Member; (3) the Tamarisk Member composed of two zones of massive to bedded anhydrite separated by a thick sequence of halite and siltstones; (4) the Magenta Dolomite Member; and (5) the Forty-niner Member composed of two thick anhydrite zones separated by a silty-halite unit, as in the Tamarisk. The Rustler Formation lithology presented above represents the lithological succession encountered in borehole P-18 which Snyder (1985) believes to be a complete unaltered section. The Rustler lithology varies across the model area. Further discussion of this variability is contained in Section 2.4. The Rustler Formation is conformably overlain by the Upper Permian Dewey Lake Red Beds, a series of interbedded siltstones and sandstones. These beds have prevalent vertical fractures which are generally gypsum filled.

In the eastern portion of the WIPP site, the Dewey Lake Red Beds are unconformably overlain by a Triassic clastic sequence deposited in a transitional depositional complex of fluvial, deltaic, and lacustrine environments. These units are collectively referred to as the Dockum Group.

Overlying the Dockum Group, where present, and the Dewey Lake Red Beds in the WIPP site area is a sequence of poorly sorted continental deposits of Quarternary Age. These are, in ascending order, the Gatuña Formation, the Mescalero caliche, and recent alluvium and other surficial deposits. The Gatuña Formation consists of a sequence of pale reddish-brown terrestrial sandstones and conglomerates which were laid down after a maximum cycle of erosion within the Pecos River Valley during a much more humid pluvial time (Bachman, 1980). Izette and Wilcox (1982) dated an ash bed in the upper portion of the Gatuña as middle Pleistocene (600,000 years before present (B.P.)) by mineralogy and fission-track dating.

Overlying the Gatuña Formation is the Mescalero caliche which is a pedogenic caliche formed in the C horizon of a paleosoil during a tectonically and climatically stable period following the deposition of the Gatuña Formation (Bachman, 1980). The Mescalero caliche has been dated as being Pleistocene (510,000-410,000 years B.P.) through uranium-series disequilibrium techniques (Bachman, 1980). Overlying the caliche is a series of Holocene surficial deposits which consist of sheetlike deposits of surface sand, sand soil, and sand dunes.

2.3 Regional Hydrogeology

In this report, the discussion of the regional hydrogeology will be limited to the Rustler Formation and the uppermost Salado Formation. The hydrogeology of the individual hydrostratigraphic units will be discussed in ascending order from the Rustler-Salado contact.

The Rustler-Salado contact residuum is transmissive in some areas around the WIPP site (Mercer, 1983). In Nash Draw and areas immediately west of the WIPP site, the contact exists as a dissolution residue capable of transmitting water. Robinson and Lang (1938) referred to this residuum making up the contact as the "brine aquifer". As one moves eastward from Nash Draw toward the Livingston Ridge surface, dissolution in the uppermost Salado, at the Rustler-Salado contact, and within the unnamed lower member of the Rustler Formation decreases and the transmissivity of this interval decreases. Transmissivities for the Rustler-Salado residuum range from 2×10^{-10} to 9×10^{-6} m^2/s in Nash Draw and from 3×10^{-11} to 5×10^{-8} m^2/s eastward from Livingston Ridge (Mercer, 1983). At well DOE-2, Beauheim (1986) attempted a slug test on the unnamed member and the Rustler-Salado contact and found that the permeability in this interval was too low to be tested effectively. In the waste-handling shaft, no water inflows from this interval were observed during excavation and shaft mapping (Holt and Powers, 1984). At H-16, Beauheim (1987b) performed drill-stem tests of a 34-m interval

including the unnamed-lower-member siltstone and the Rustler-Salado contact, and reported the transmissivity of this interval to be about 3×10^{-10} m^2/s.

The Culebra dolomite is considered to be the most transmissive hydrogeologic unit in the WIPP-site area. Mercer (1983) describes ground-water flow within the Culebra as being southerly in Nash Draw and south to southwesterly beneath the Livingston Ridge surface. Reported values for transmissivity in the Culebra in the Nash Draw area range from 2×10^{-5} to 1×10^{-3} m^2/s (Mercer, 1983). Within the model area, the transmissivities range from 1×10^{-9} to 1×10^{-3} m^2/s. Hydraulic gradients in the Culebra at the WIPP site generally range from 1×10^{-3} m/m to 4×10^{-3} m/m (Mercer, 1983). As a general trend, total dissolved solids in Culebra ground waters increase from west to east across the WIPP site and the model area.

The Tamarisk Member of the Rustler separates the Culebra dolomite from the Magenta, and is composed of a thick sequence of halite and siltstones sandwiched between an upper and lower anhydrite. The Tamarisk claystone sequence has been tested at wells H-14 and H-16 (Beauheim, 1987b) and at DOE-2 (Beauheim, 1986). In all cases the hydraulic testing failed due to the extremely low permeability of the unit. Mercer (1983) reported that in a few cases argillaceous zones within the Tamarisk Member have produced water at equivalent rates to the Magenta upon testing.

Ground water in the Magenta dolomite generally flows from the north toward the westsouthwest (Mercer, 1983). In most areas east of Nash Draw, and east and south of the H-6 hydropad, the Magenta exists as a confined system with very low transmissivity (less than or equal to 4×10^{-7} m^2/s). The difference between Magenta and Culebra hydraulic potentials generally increases eastward, with the Magenta having higher potentials. In areas of Nash Draw, the Magenta is generally at water-table conditions and may have a stronger hydraulic connection to other

units in the Rustler Formation. In other parts of Nash Draw, the Magenta is unsaturated. Magenta transmissivities range as high as 4×10^{-4} to 6×10^{-4} m^2/s immediately east of Nash Draw.

The uppermost member of the Rustler Formation, the Forty-niner Member, has claystones which are generally more transmissive than those in the Tamarisk Member. At well H-14, Beauheim (1987b) performed drill-stem tests upon the Forty-niner and determined that transmissivities were approximately an order of magnitude higher than in the Magenta at H-14. The average value of transmissivity calculated for the Forty-niner was 6×10^{-8} m^2/s as opposed to 6×10^{-9} m^2/s for the Magenta. Beauheim (1986) also tested the Forty-niner claystone in well DOE-2. Here again he calculated slightly higher transmissivities for the Forty-niner claystone than for the Magenta. The average of the two transmissivities of the Forty-niner reported by Beauheim (1986) for DOE-2 is 7.3×10^{-9} m^2/s. Drill-stem tests of the Forty-niner claystone at H-16 provided a transmissivity estimate of about 6×10^{-9} m^2/s, lower than that of the Magenta at H-16 (Beauheim, 1987b).

Although the Rustler-Salado residuum, the Culebra Dolomite Member, and the Magenta Dolomite Member are generally found to be the primary transmissive units within the Rustler, zones of relatively high transmissivity have been tested locally in the Rustler Formation outside of these horizons. In a few cases, discrete argillaceous zones within the Forty-niner Member and the Tamarisk Member have produced water at equivalent rates to the Culebra or the Magenta upon testing (Mercer and Orr, 1979; Beauheim, 1986).

2.4 Regional Dissolution in the Rustler Formation

Post-depositional dissolution within the Rustler Formation is observed both at the surface within Nash Draw, and in the subsurface at the WIPP site (Bachman, 1987). Nash Draw, located immediately west of the WIPP

site, is a depression resulting from both dissolution and erosion. In Nash Draw, members of the Rustler are actively undergoing dissolution and locally contain caves, sinks, and tunnels typical of karst morphology in evaporitic terrane. Lowenstein (1987) found evidence for significant post-depositional, late-stage dissolution of the Rustler at the WIPP site based on a detailed sedimentologic and petrologic core study.

Bachman (1980) identified three types of dissolution occurring in the Delaware Basin: local dissolution, regional dissolution, and deep-seated dissolution. Of these, regional dissolution is the type which has the most potential to dictate or alter the flow characteristics of the Rustler Formation underlying the WIPP site. Regional dissolution occurs when chemically unsaturated water penetrates to permeable beds, where it migrates laterally, dissolving the soluble units it contacts. On a regional scale, the consequence of such dissolution appears to be removal of highly soluble rock types, such as halite, combined with displacement and fracturing of overlying rocks.

Snyder (1985) found evidence for the presence of an eastward-migrating dissolution front within the Rustler Formation at the WIPP site. In his study, Snyder (1985) concluded that the regional dissolution was greatest in the west and decreased eastward evidenced by an increase in the number and thickness of halite beds and a corresponding thickening of the Rustler Formation (Figure 2.2). The stratigraphic level of the uppermost occurrence of salt is in the upper Rustler along the eastern margin of the WIPP site. As one moves westward toward Nash Draw, the uppermost salt is found in progressively deeper horizons of the Rustler. This implies that, as a general trend, the eastward advancement of the dissolution front is greatest in the upper Rustler and decreases as one gets nearer to the Rustler-Salado contact. As the halite units are dissolved, insoluble residues remain, forming beds of mudstones, siltstones, and chaotic breccia with a clay matrix. As can be seen in a

cross section taken between wells P-6, H-3, DOE-1, and P-18, (Figure 2.3), halite beds tend to thin and grade into residuum westward towards Nash Draw.

Although most investigators agree with the interpretation that a dissolution zone exists in the Rustler Formation at the WIPP site (Cooper and Glanzman, 1971; Powers et al., 1978; Mercer, 1983; Chaturvedi and Rehfeldt, 1984; Bachman, 1985; and Snyder, 1985), other investigators oppose this concept and believe that the westward decrease of halite within the Rustler simply represents depositional limits (Powers and Holt, 1984; and Holt and Powers, 1984). From detailed mapping of the Rustler in the waste-handling shaft, Holt and Powers (1984) reported no post-depositional dissolution features. Recently, Lowenstein (1987) conducted a detailed core analysis on core from wells DOE-2, WIPP-19, H-11, and H-12. The aim of the study was to distinguish between syndepositional features and post-depositional alteration features within the Rustler. Lowenstein (1987) could correlate structures, both syndepositional and post-depositional, over the study area and concluded that facies changes were not responsible for the westward decrease in halite within the Rustler in the study area. Lowenstein (1987) found evidence of late-stage alteration involving physical processes such as brecciation, slumping, fracturing, and faulting, as well as chemical processes such as rehydration of anhydrite to gypsum, precipitation of gypsum, and dissolution of halite, anhydrite, and gypsum. Thus, the study of Lowenstein supports the theory of a post-depositional dissolution of salt in the Rustler.

Based upon observations of outcrops, core, and detailed shaft mapping, the Culebra can be characterized, at least locally, as a fractured medium at the WIPP site (Chaturvedi and Rehfeldt, 1984; Holt and Powers, 1984). As the amount of fracturing and development of secondary porosity increases, the Culebra transmissivity generally increases (Chaturvedi and Channell, 1985). The fracturing and development of

secondary porosity is thought to be a product of late-stage alteration and dissolution of the Rustler Formation. In general, as the amount of the halite present in the Rustler decreases, the transmissivity of the dolomitic members increases as a result of halite removal and subsequent foundering and collapse of the more competent dolomitic members.

While it is commonly accepted that regional dissolution has been an active process within the Rustler in the past, there is some controversy over whether this dissolution front is still active. Within the last 1.8 million years (Pleistocene), the climate in southeastern New Mexico has varied between periods of cold, moist continental glaciation to relatively warm and arid periods (Bachman, 1987). In Middle Pleistocene time, approximately 500,000 years B.P., southeastern New Mexico received precipitation which well exceeded the evapotranspiration. This period was followed by several hundred thousand years of a drier climate. In late Pleistocene time (approximately 75,000 to 10,000 years B.P.) rainfall was more prevalent than today and temperatures were lower (Bachman, 1987). Bachman (1987) believes that most of the dissolution in the Rustler predates, or occurred during, Middle Pleistocene (Gatuña) time. However, he suggests that dissolution is ongoing in Nash Draw and areas very close to Livingston Ridge. Through the interpretation of radiocarbon data (Lambert, 1987) and stable isotopes (Lambert and Harvey, 1987), Lambert has suggested that recharge and subsequent dissolution of the Rustler ended after the more pluvial Late Pleistocene (10,000 to 20,000 years B.P.).

2.5 Implications of Rustler Ground-Water Isotopic Studies

Ground waters within the Rustler have been evaluated based upon stable isotopes, uranium isotopes, and radiocarbon (Lambert and Harvey, 1987; Chapman, 1986; Lambert and Carter, 1987; and Lambert, 1987). There has been debate over whether or not the Rustler, more specifically here the Culebra, is presently receiving significant recharge from meteoric

waters and if so, where the waters recharge and discharge. This section will give a brief summary of the four isotopic studies (cited above) in the context of their implications for a regional model of the Culebra dolomite. This summary is not meant to be a critique and therefore does not address the inherent assumptions or validity of these studies.

Lambert and Harvey (1987) used δD and $\delta^{18}O$ of waters from the Rustler and modern sources to determine if the Rustler ground water infiltrated under similar climatological conditions as are present today in Southeastern New Mexico. Figure 2.4 plots stable-isotope compositions for the Culebra and modern waters in $\delta D/\delta^{18}O$ space (Lambert and Harvey, 1987). In this diagram one can see that the modern surface waters and the majority of Culebra ground waters fall into two distinct and separate groups which lie within the meteoric field as it is defined by Epstein et al. (1965; 1970) and Craig (1961). The two outliers, Surprise Spring and WIPP-29, are thought to be contaminated from nearby potash-refining operations. Lambert and Harvey (1987) concluded that, because modern surface waters and Culebra ground waters are distinct and apparently not overlapping in $\delta D/\delta^{18}O$ space, the Rustler is not currently receiving significant modern recharge. They believe that the Rustler hydraulic system is currently in a transient state with discharge exceeding recharge.

Chapman (1986) interpreted stable-isotope data from the Rustler, the Roswell Basin, Carlsbad Caverns, the Ogallala, the Dewey Lake Red Beds, the Santa Rosa Sandstone, and the Capitan Limestone. Chapman (1986) concluded that waters in these formations in southeastern New Mexico were isotopically similar and that all were representative of recharge occurring under climatic conditions similar to those existing today. Contrary to Lambert and Harvey (1987), the study concludes that the Culebra does not contain "fossil water" and that the Culebra may be receiving present-day recharge. Chapman also states that the hydraulics of the Rustler cannot be determined based upon the interpretation of

stable isotopes alone and that many physical questions concerning physical hydrogeology of the Rustler must be answered before the problem of recharge can be defendably solved.

Lambert and Carter (1987) studied uranium-isotope systematics in ground waters from the Rustler Formation in the Northern Delaware Basin. They utilized uranium concentrations and $^{234}U/^{238}U$ activity ratios to try to determine residence times, isolation times, and travel times for waters within the Rustler aquifers. Lambert and Carter (1987) observed an increase in total carbon from east to west and a decrease in activity ratio from east to west. According to theory, high activity ratios evolve downgradient from areas of recharge. Lambert and Carter (1987) concluded that, in the last 30,000 years, the Culebra was not at steady-state conditions, neither hydraulically or geochemically, and that there were three general flow directions within the Culebra. The first flow direction was eastward and represented a recharge event from the west at least 10,000 to 30,000 years B.P. accounting for the eastward increase in activity ratio. The second flow direction was westward after the cessation of recharge and accounts for the present total-uranium systematics. The third flow direction is the present southward trend which is assumed to be recent and of short enough duration to not have altered the uranium systematics.

Lambert (1987) also studied the feasibility of the use of ^{14}C and other nuclides for their potential in geochronologic applications for ground waters in the Rustler Formation in southeastern New Mexico. From the samples taken, no ^{36}Cl or significant concentrations of ^{3}H were measured. He determined that the majority of the samples taken were contaminated with respect to ^{14}C by multiple sources (e.g., drilling fluid). For the wells which appeared to be least contaminated, percent modern carbon and $\delta^{13}C$ were used with the model of Evans et al. (1979) to calculate ^{14}C ages. The results were 16,100 years B.P. for H-4b, 12,100 years B.P. for H-6c, 14,900 years B.P. for H-9b, and 14,000 years

B.P. for Pocket Well. Because the conditions necessary for reliable age dating may not be satisfied for the available water samples, Lambert (1987) proposes to interpret these ages as minimum isolation times and considers this further evidence that the Rustler is not currently receiving significant recharge at the WIPP site.

3.0 MODEL CONCEPTUALIZATION

3.1 General Approach

For more than ten years, numerous field investigations at the WIPP site have focused on the Rustler Formation in general and the Culebra Dolomite Member in particular. The existing data for the Culebra include measurements of transmissivities, storativities, formation-fluid densities, depths to water, and pressures from the observation-well network. Construction activities at the WIPP site, such as the excavation of the shafts at the center of the site, have also provided hydrogeologic data. The majority of the hydrogeologic data are published in the following report series:

1) basic data reports (borehole-specific reports, e.g., Sandia National Laboratories and University of New Mexico, 1981);
2) hydrologic data reports (Hydro Geo Chem, 1985; INTERA and Hydro Geo Chem, 1985; INTERA, 1986; Saulnier et al., 1987; Stensrud et al., 1987 and 1988);
3) hydrogeologic interpretive reports (e.g., Mercer, 1983; Beauheim, 1986, 1987a,b,c; Saulnier, 1987); and
4) water-quality data and geochemical interpretive reports (e.g., Mercer, 1983; Uhland et al., 1987; Robinson, 1987).

The data base used for this modeling study and a complete listing of data sources are presented in Appendices A through G. The appendices include separate data bases for transmissivity, storativity, formation-fluid density, borehole locations, ground-surface and Culebra elevations, and freshwater heads. Each appendix has undergone significant internal review and is considered to represent the most current information about the site.

The data base was used in conjunction with geostatistical methods to assign the initial hydrogeologic parameters to each grid block in the model. These methods were also applied to the undisturbed freshwater heads to obtain the initial boundary conditions for the model. Calibration procedures also utilized geostatistical methods to update the spatial distribution of hydrogeologic parameters in order to reduce the difference between calculated and observed heads.

The following sections begin with a brief description of the computer code (SWIFT II) used in this modeling study. More detailed discussions of the data evaluation and analysis follow. A description of the basic model properties (e.g., boundaries, discretization, physical parameters, boundary conditions, etc.) is also included.

3.2 SWIFT II Code Description

The Sandia Waste-Isolation Flow and Transport code, SWIFT II, is a fully transient, three-dimensional, finite-difference code which solves the coupled equations for flow and transport in geologic media. The processes considered are:

- fluid flow
- heat transport
- dominant-species miscible displacement
- trace-species miscible displacement

Dominant-species miscible displacement refers to brine migration, whereas trace-species miscible displacement applies to the transport of solutes at concentrations not significantly affecting the fluid-flow parameters. This may include radionuclide-chain transport. The first three processes are coupled via porosity, fluid density, viscosity and enthalpy. Together they provide the velocity field on which the fourth process depends.

The SWIFT II code is designed to simulate flow and transport processes in both single- and double-porosity media. For fractured regions of a system to which dual porosity is to be applied, two sets of equations are solved, one for the fracture processes and the other for the matrix. The fracture-porosity equations describing flow and transport for the fractured regions are identical to the single-porosity equations for the nonfractured zone, except for sink terms giving the losses to the matrix. These equations are denoted as global equations. The equations describing the matrix processes, referred to as the local equations, differ somewhat from their global counterparts because they are one-dimensional.

SWIFT II provides a steady-state solution for fluid flow and brine migration. Because the matrix processes are assumed to be negligible at steady state, the state equations for the matrix porosity are not solved.

At high-level nuclear-waste repositories, heat transport is basically a transient process. Therefore, SWIFT II does not feature a steady-state solution for heat transport. However, the code will permit the transient solution of radionuclide transport (with or without dual porosity) in conjunction with the steady-state solution of fluid flow and brine migration. Although the model was originally developed for applications related to radionuclide transport, the algorithms used can handle the transport of any trace species undergoing sorption or first-order losses.

A comprehensive description of the theory and implementation of SWIFT II is presented in Reeves et al. (1986a). Two other documents related to the SWIFT II code have been published, namely a data input guide (Reeves et al., 1986b), and the verification-validation tests (Ward et al., 1984). The steady-state and transient simulations presented in this study will employ the steady-state and transient flow

equations with variable fluid density. Brine transport will not be calculated during the steady-state or transient simulations because the fluid densities will be fixed over space. The "time constant" to achieve steady-state conditions for fluid densities in the WIPP area is considered longer (several 1,000 years) than the time constant for flow (several years). Therefore, fixing the fluid densities will maintain the densities observed today and incorporate the density effects in the calculation of formation pressures and flow directions.

The double-porosity equations contained in SWIFT II will not be used in the steady-state or transient runs. Haug et al. (1987) demonstrated that double-porosity effects were negligible on the scale of the model.

3.3 Model Description

3.3.1 Model Area

The model area used in this study is shown in Figure 3.1. It encompasses an area extending 24 km in the east-west and 25 km in the north-south directions. The locations of the boundaries of the model were chosen to maximize the ability to determine appropriate boundary conditions and minimize the effect the boundaries may have on the transient modeling results for the H-3 and WIPP-13 multipad pumping tests. The western boundary lies within Nash Draw, which is assumed to be a major conduit for ground-water flow toward the south. The other boundaries of the model do not coincide with physical hydrologic boundaries. However, the uncertainty of the boundary conditions is minimized by utilizing hydrologic information from far-field wells (e.g., H-7b, H-10b, H-12, WIPP-26, WIPP-27, WIPP-28, and USGS-1).

3.3.2 Model-Grid Description

The finite-difference grid used in this modeling study (Figure 3.2)

was selected to facilitate the successful reproduction of both steady-state and transient heads by reducing the numerical problems associated with coarse gridding. The horizontal dimensions of the grid are listed in Table 3.1 along with the UTM coordinates of the corner points of the grid. The grid consists of 26 x 44 x 1 (x,y,z) grid blocks and has a much finer grid occurring in the central portion of the model in the vicinity of H-3, the shafts, and WIPP-13. The general "rule of thumb" used in developing the grid included not increasing adjacent grid-block sizes by more than a factor of two. This is to provide adequate resolution and numerical stability for transient flow modeling.

The vertical dimension of the finite-difference grid is taken from the thickness of the Culebra dolomite in the WIPP area. Several reports have documented the Culebra thicknesses observed in the WIPP-area boreholes (Jones, 1978; Sandia Laboratories and U.S. Geological Survey, 1979a,b,c,d,e,f, 1980a,b,c,d,e; Sandia National Laboratories, 1982; Sandia National Laboratories and D'Appolonia Consulting Engineers, 1982a,b,c, 1983a,b,c; Sandia National Laboratories and U.S. Geological Survey, 1980, 1981a,b, 1982, 1983a,b; Sandia National Laboratories and University of New Mexico, 1981; Mercer et al., 1987). The resulting thickness distribution is illustrated in Figure 3.3 and presented in Appendix B. A mean thickness of 7.7 m is assumed to be adequate for the vertical model dimension in this study and is therefore used for each grid block.

The elevation of the Culebra dolomite has been documented in the reports referenced above on the WIPP-area boreholes. Appendix B contains the ground-surface elevations and the depths to the Culebra. Based on that, the Culebra elevations at the borehole locations in the WIPP area were calculated. The elevations of the center of the Culebra range from 704.6 m above mean sea level (amsl) at H-10 to 900.5 m amsl at WIPP-26.

The Culebra-center elevations were estimated at each of the grid-block centers using AKRIP (Kafritsas and Bras, 1981), the MIT generalized kriging program (Figure 3.4). The kriged surface is consistent with the observed elevation data containing higher elevations in the western part of the model area and lower elevations in the east and southeast. Generally, the Culebra dips slightly to the southeast. However, the dip increases locally within sections of the model area (e.g., the northeast corner of the model area).

3.4 Physical Model Constants

SWIFT II requires the specification of a number of fluid and rock property constants that are used mainly in transient calculations. One of these parameters is the porosity of the rock. Matrix-porosity data of the Culebra dolomite were obtained from laboratory analyses on cores taken from several boreholes in the WIPP area (Core Laboratories, 1986). The resulting porosities range from 7 to 30%. A value of 16% was chosen as representative for the model area.

Other parameter constants that require specification include fluid viscosity, fluid and rock compressibilities, fluid thermal expansion, fluid and rock heat capacities, freshwater density, and brine fluid density. Table 3.2 lists the values assigned to each of these constants in this modeling study and the pertinent references from which these parameters were taken. A detailed justification for the selection of these values is presented in Haug et al. (1987). However, note that since isothermal conditions are assumed to exist in the modeled region, the specification of some of the above parameters (e.g., thermal expansion and heat capacity) is a mere formality as a model-input data requirement and has no impact on the model results.

3.5 Transmissivity of the Culebra Dolomite

3.5.1 Data Base

The transmissivity data base for the Culebra dolomite (Appendix C) is derived from numerous hydraulic tests performed at the WIPP site. Values have been obtained from drill-stem tests (DST's), slug tests, and local and regional-scale pumping or interference tests. Transmissivity values interpreted from these tests extend over a range of six orders of magnitude. Relative-frequency histograms were plotted in order to illustrate the range of values determined for each type of test (Figure 3.5). These histograms contain mean values for a given test type at a particular borehole. For example, if a borehole had ten pumping-test and two slug-test values in the data base, the pumping-test values are averaged to determine the mean pumping-test value for that well, and the two slug-test values are averaged to determine a mean slug-test value. The resulting numbers are then used in the respective histograms.

The histograms illustrate a range of six orders of magnitude for transmissivity values determined from pumping tests and a range of four orders of magnitude for those determined by regional interference tests. In both cases, the geometric mean of the distribution occurs between 1×10^{-5} m^2/s (log transmissivity of -5) and 1×10^{-6} m^2/s (log transmissivity of -6).

Transmissivity values determined from slug tests also range over several orders of magnitude. However, most of the values occur between 1×10^{-6} m^2/s (log transmissivity of -6) and 1×10^{-7} m^2/s (log transmissivity of -7). The DST distribution is very similar to the slug-test distribution with the largest number of log transmissivity values falling in the -6 to -7 log m^2/s interval. Thus, the mean log transmissivity values for these two distributions lie between -6 and -7 log m^2/s.

The large differences in the above transmissivity distributions result from the heterogeneous nature of the Culebra dolomite. This results in a wide range of possible transmissivity values present over the WIPP site. The area east of the WIPP site has, in general, lower permeabilities than regions west of the site.

The large differences in the transmissivity distributions also reflect the volume of rock stressed during a hydrogeologic test which is both test and site specific. For example, while at one location the permeability may facilitate different types of tests, the volume of rock actually hydraulically stressed in one test (e.g., slug) could be much smaller than the volume of rock stressed in another test (e.g., pumping). This difference in volume stressed may result in interpreted transmissivities that are representative of different spatial scales of the Culebra around the borehole. Therefore, the transmissivity data base has been evaluated in an attempt to determine representative values at a scale of tens of meters.

Appendix C describes the rationale used to assign transmissivity values at each borehole in the modeling study. The resulting transmissivity distribution is illustrated in Figure 3.6 and listed in Table 3.3. The distribution has the same general characteristics of the slug-test, DST, and pumping-test distributions. The large number of slug-test and DST values occurring between -6 and -7 log m^2/s generates the values on the lower end of the distribution and the pumping-test values are represented mostly at the high end. The regional interference values were not used in determining representative values at the boreholes, but were considered during model calibration.

3.5.2 Uncertainty of the Transmissivity Data

In order to evaluate the uncertainty associated with the transmissivity data, the variances and the standard deviations (σ) of

the transmissivity values at the hydropads or well locations were calculated (Appendix C, Table C.2). As discussed in Appendix C, a minimum standard deviation σ = 0.25 log m^2/s was assumed for pumping-test results. For the results of other hydraulic-testing data such as DST's or slug tests, a standard deviation σ = 0.5 log m^2/s was considered to be appropriate. Most hydropads or wells, where sufficient data are available to calculate reliable standard deviations, have values similar or higher than the assumed minimum standard deviations (e.g., at hydropads H-1, H-3, and H-5).

If one assumes that the hydraulic tests have tested a representative rock volume and that the measurement error is normally distributed, the standard deviations can be interpreted as uncertainty associated with the transmissivity data. In such a case, the mean transmissivity $\pm 2\sigma$ correspond to a 95% confidence interval. Thus, the assumed minimum uncertainty of the pumping-test results is half an order of magnitude (2σ = 0.5 log m^2/s), and for the other hydraulic tests it is one order of magnitude (2σ = 1.0 log m^2/s). The empirical uncertainties from the hydropads, where reliable standard deviations could be calculated, generally fall in between these two assumed values (e.g., at hydropad H-3, 2σ = 0.76 log m^2/s). These uncertainties were used as input to the kriging code K603 in the estimation of the transmissivity distribution of the model area (Section 3.5.3.1).

3.5.3 Estimation of Transmissivity Over the Model Region

Two geostatistical approaches were used in the estimation of the transmissivity field over the model region. This was done in order to determine the method which provided the more representative spatial distribution of the transmissivity values. Theoretically, both codes preserve the observed transmissivity data at the WIPP-area boreholes. A modified version of the USGS universal kriging code,

K603 (Skrivan and Karlinger, 1981), and the MIT generalized kriging code, AKRIP (Kafritsas and Bras, 1981), were the two codes used in this exercise. Both have specific advantages and disadvantages. Universal kriging requires the determination of a semi-variogram which provides the user with geostatistical parameters such as the correlation length (range) and sill. The uncertainty of the observed data may also be incorporated into the universal kriging results. Generalized kriging does not require a semi-variogram in its mathematical formulation and therefore does not provide the user with this information. The coefficients and order of a polynomial expression, referred to as a generalized covariance function (GCF), are determined and subsequently used in the estimation procedure. In addition, the uncertainty of the observed data cannot be accounted for in the generalized kriging program AKRIP. The following two sections describe the application of both kriging codes and present the essential results. A comparison of the results is contained in the third section.

3.5.3.1 Estimation of Transmissivity Field Using the Universal Kriging Code K603

The first step in estimating the transmissivity field using K603 consisted of calculating empirical semi-variograms based on the available transmissivity data (Table 3.3). Such empirical semi-variograms describe the spatial correlation between the observed data. Figure 3.7 shows a non-directional as well as two directional semi-variograms. The difference between the north-south and the east-west directional semi-variograms indicates a strong trend in the east-west direction. This is consistent with the fact that the transmissivities in the western part of the model area are generally higher than those in the eastern part (see also Section 2.4).

The second step of universal kriging is to determine the coefficients of a mathematical expression which describes the trend over the model area. The trend is then removed from the data which leaves the trend-corrected transmissivities as residuals. The removal of the trend from the data is considered successful when the difference between the directional semi-variograms of the residuals is a minimum. A non-directional semi-variogram of the residuals can then be used as the basis for the selection of the theoretical semi-variogram that is subsequently employed in the kriging procedure.

A detailed trend analysis using K603 confirmed that a linear east-west trend underlies the Culebra transmissivity data (Table 3.4). Higher order polynomials were investigated in the approximation of the east-west trend, but were insignificant compared to the linear trend. Trend analyses were also conducted to determine if minor trends occurred in other directions; however, no other significant trend could be detected. Therefore, only a linear east-west trend was used for the subsequent steps of the kriging analysis (Table 3.4).

The trend-corrected transmissivities, referred to as residuals, were used in the non-directional and directional semi-variograms in Figure 3.8. The agreement between the three curves demonstrates that all significant components of the regional trend underlying the transmissivity data have been removed. Based on a visual examination of Figure 3.8, a range or correlation length of about 3 km and a sill of about 1 log m^2/s should be used. There is no indication of a nugget.

A theoretical semi-variogram must be fitted to the non-directional semi-variogram (Figure 3.8) before the estimation of transmissivities can be performed. A spherical semi-variogram was

selected as the theoretical model to represent the trend-corrected transmissivities based on the shape of the non-directional curve (Figure 3.8). Theoretical models that are available include exponential, spherical, linear, and Gaussian (Skrivan and Karlinger, 1980). Having selected the type of the theoretical semi-variogram, the range (a) and sill (ω) parameters were systematically varied until a spherical semi-variogram was determined that was statistically consistent with the existing data base. A unique best-fit solution was found for the parameter combination a = 3.012 km and ω = 0.9355 log m^2/s (Table 3.4). These parameter values are close to the expected values (based on examination of Figure 3.8). The non-directional semi-variogram of the residuals and the selected spherical semi-variogram are plotted together in Figure 3.9. The two curves agree reasonably well.

The major differences of the results determined in this semi-variogram analysis to those reported in the previous modeling study of Haug et al. (1987) are:

1. When the previous modeling study was conducted, the available transmissivity data base was much smaller, i.e., data from only 24 hydropads or well locations were available as compared to data from 38 locations in this study. In addition, some of the previously existing data were considerably less reliable. Because of the small data base, statistically significant trends could not be identified, and therefore, trend-corrected transmissivities were not used in the previous study.

2. The non-directional semi-variogram in the previous modeling study characterized the spatial correlation of the transmissivity data excluding the existance of a trend. A larger correlation length (about 4 km), a larger sill (ω = 2.05 log m^2/s) and an exponential semi-variogram had to be

used in order to characterize the previous transmissivity data base in a statistically consistent manner.

3. The semi-variogram analysis of the present modeling study resulted in the estimation of a linear east-west trend and the use of a spherical semi-variogram with a shorter correlation length (about 3 km) and a smaller sill ($\omega = 0.9335$ log m^2/s). In general terms, the overall uncertainty of the transmissivity field appears to be reduced by 50% on log scale because of the smaller sill value. The shorter correlation length indicates a larger heterogeneity on a scale of several kilometers than one would expect based on the previous study.

The transmissivity data and the selected spherical semi-variogram (Tables 3.3 and 3.4) were used to estimate the transmissivity distribution within the model area. Figure 3.10 shows a contour map generated using the logarithms of the estimated transmissivities as well as a contour map of the associated estimation errors (expressed as single standard deviations). The log transmissivity estimate is assumed to represent the arithmetic mean of a Gaussian distribution having a standard deviation equal to the estimation error.

The kriged transmissivity distribution illustrated in Figure 3.10 is clearly influenced by the identified linear east-west trend, especially in areas at distances greater than the correlation length from the transmissivity data points. Obvious aberrations from the regional trend exist in the areas of increased transmissivities at WIPP-25, H-6, and DOE-2 as well as in the area of high transmissivities at DOE-1 and H-11. Relatively low transmissivities are shown in the area of P-15, H-4, CB-1, and P-17.

For the calculation of the estimation error displayed in Figure 3.10, a zero uncertainty was assumed for the existing transmissivity data. This simplification results in estimation errors which are likely too low. Nevertheless, they were calculated because they can be directly compared to the estimation errors calculated by AKRIP which does not account for the uncertainties associated with the data (Section 3.5.3.2).

The contour maps shown in Figure 3.11 were generated subsequent to assigning uncertainties to the observed transmissivities (Section 3.5.2). The estimated transmissivity field shows no significant differences compared to that displayed in Figure 3.10. The distribution of the estimation error is characterized by low values in the central part of the model area and higher values along the eastern and western model boundary. In the immediate neighborhood of the hydropads and wells, the estimation errors are generally 0.5 log m^2/s or less. This corresponds to an uncertainty (i.e., two standard deviations) of approximately +/- one order of magnitude on a linear scale. In large parts of the central model area defined by the WIPP-site boundary, the estimation error is between 0.5 and 0.75 log m^2/s.

3.5.3.2 Estimation of Transmissivity Field Using the Generalized Kriging Code AKRIP

The estimation of the transmissivity field using AKRIP required the determination of a theoretical generalized covariance function (GCF) consistent with the logarithms of the Culebra transmissivity data. The GCF is the theoretical "model" used to estimate the transmissivities of the model area. The coefficients of the GCF are determined by an iterative procedure in which the GCF is fitted to local "neighborhoods" defined by subsets of the observed transmissivity data. In this study, a neighborhood is defined by

the ten nearest observed data points surrounding a particular estimation point in the model area. As the estimation point changes, the data points defining the neighborhood also changes. Because the transmissivity data within a given neighborhood may contain a local trend, changing the data defining a neighborhood may result in changes to the local trend. In addition, as the number of observed points defining a neighborhood increases, the scale of the trend also increases and the ability to adequately represent local trends in the data decreases. The neighborhood used to define a trend in the K603 code consists of all of the observed data resulting in the determination of a single regional trend over the model region. The neighborhood used in AKRIP (ten points) is more representative of the local trends present in the transmissivities of the Culebra dolomite.

The zero-order GCF used in this study is listed in Equation (3.1):

$$K(h) = -1.794E\text{-}04\ |h| \qquad (3.1)$$

where K(h) is the generalized covariance and h is distance between the estimation point and an observed data point. A consistency check is normally performed on the theoretical GCF to verify that it is statistically consistent with the input data. A GCF that is consistent with the input data should provide a reduced mean square error near 1.0 (see de Marsily, 1986). The GCF listed in Equation (3.1) gave a reduced mean square error of 1.5 which is a little high. However, Equation (3.1) preserves the input data at the observed points better than other GCF models that were investigated.

The initial log transmissivity estimates and the corresponding estimation errors calculated using the above GCF are shown in Figures 3.12a and 3.12b, respectively. These figures depict the

higher transmissivity values in the western part (log transmissivity from -3.0 to -3.5) of the model region and the lower values (log transmissivity from -6.0 to -8.0) in the east. The lowest values of transmissivity occur along the eastern boundary and reflect the projection of the underlying local trends determined by AKRIP. The log transmissivity values within the WIPP-site boundary vary from -4.1 at H-6 to -7.0 at P-15. A local high occurs near the H-11 and DOE-1 boreholes. Here the log transmissivity values are between -4.5 and -5.0. This area is considered to be a local high because of the surrounding lower log transmissivity values.

The estimation errors (as defined by one standard deviation) within the model region are highest near the northeast boundary due to the lack of data in the area. Here the errors have log values of 1.5. Within the central portion of the model area, the errors of the estimate are between 0.5 and 0.75 log m^2/s. A three-dimensional representation of the initial log transmissivity field is presented in Figure 3.13. The log transmissivity field is presented in terms of negative log transmissivity or log hydraulic resistivity. Note the low-resistivity region to the west and the high resistivities in the east. The local high-transmissivity zone around H-11 appears as a small "crater" of low resistivities surrounded by the higher resistivities defined by P-15, P-17, and H-17.

3.5.3.3 Comparison Between the Results of Universal Kriging and the Results of Generalized Kriging

A comparison between the results of the two different geostatistical methods, universal kriging (Figures 3.10 and 3.11) and generalized kriging (Figure 3.12), shows both interesting similarities and differences.

The transmissivities estimated by both methods are consistent in areas where field data are available. Both methods show a regional east-west trend as well as increased transmissivities in the area of WIPP-25, H-6, and DOE-2. Also, the increased transmissivities at DOE-1 and H-11 and the relatively low transmissivities in the area of P-15, H-4, CB-1, and P-17 are shown on both contour maps.

In areas further away from the data points, the differences between the results are larger. In general, universal kriging (K603) emphasizes the east-west trend more, which results in relatively simple, straight contour lines in the outer parts of the model area. This is because universal kriging assumes a single linear east-west trend. Deviations from the general trend are present in the contour map only within the correlation length of about 3 km of the hydropads and wells. In contrast, generalized kriging (AKRIP) uses the local trend defined by the ten closest data points when estimating the transmissivity at a given location. As a result, the local trends in Figure 3.12 may have a different east-west component than the single trend surface illustrated in Figures 3.10 and 3.11. However, the differences between the K603 and AKRIP results in most parts of the model area are less than 0.5 log m^2/s. Thus, the differences are not larger than the estimation errors calculated by either program.

A comparison between the estimation errors obtained from the two geostatistical methods shows a similarity in the western and central part of the model area. Generally, the estimation errors provided by AKRIP (Figure 3.12) are 0.25 log m^2/s lower than the estimation errors calculated by K603 (Figure 3.10). The lower estimation errors originate from the GCF used in the generalized kriging procedure (Section 3.5.3.2) which has a higher reduced mean square error (RMSE of 1.5) than that determined for the semi-variogram used in K603 (RMSE of 1.0). The RMSE value, defined as

the average ratio of the theoretical to the calculated variance, tends to be larger than 1.0 if the variance of the estimated values is lower than the variance of the observed values.

Major differences between the estimation errors from the two kriging methods exist mainly in the north-eastern corner of the model area. No measured data exist in this area. K603 calculated estimation errors in this area between 1.00 and 1.25 log m^2/s. The corresponding values calculated by AKRIP are as high as 1.75 log m^2/s. The reason for this large difference lies in the different methods by which the two codes incorporate trends. K603 assumes that in such areas the regional trend is the best estimate. Although the code accounts to some extent for the uncertainty associated with the estimated trend, the uncertainty is essentially governed by the sill of the theoretical semi-variogram. In comparison, the generalized covariance function (GCF) used by AKRIP does not reach a maximum value like a sill at a given separation distance. Therefore, the estimation errors calculated in AKRIP may steadily increase with distance away from the nearest data point. Thus, the different estimation errors in the north-eastern model area reveal one of the fundamental differences between the universal and the generalized kriging approaches.

In summary, K603 represents a flexible method allowing the user to utilize his expertise and judgment; however, this may add a degree of subjectivity to the results. AKRIP can be characterized as a "black-box method" with a restrictive underlying mathematical formulation which excludes the subjectivity of the user to a large degree. In principle, both codes can be used to estimate the initial model transmissivities and the transmissivity distributions used during the model calibration. In areas without data, the results differ somewhat because K603 uses a

single trend surface and AKRIP uses several local trends defined by the nearest data points. Since local trends are probably more consistent with the observed data than one single trend over the entire model region, AKRIP was selected to estimate the initial transmissivity field and the modified transmissivity distributions during the model calibration.

3.6 Storativity of the Culebra Dolomite

3.6.1 Data Base

The storativity data base (Appendix D) was evaluated to determine representative values at a scale of tens of meters. The rationale used in the evaluation is discussed in Appendix D. The final values assigned to borehole locations are listed in Table 3.3. The total number of storativity values is much less than the number of transmissivity values. The storativity values have a mean which lies between 5×10^{-4} and 1×10^{-5} and a range that extends over 3 orders of magnitude.

3.6.2 Correlation Between Storativity and Transmissivity

Because the number of storativity values is much smaller than the number of transmissivity values, it is interesting to assess whether or not the two hydrogeologic parameters are statistically correlated. If they are statistically correlated, the transmissivity distributions could be used to infer additional storativity values.

One widely used method to determine whether two parameters are correlated is linear-regression analysis (LRA). LRA uses a least-squares calculation to determine the best-fit line to two variables (one dependent and one independent) plotted in x-y (parameter 1 vs parameter 2) format. The slope and y-intercept of the best-fit line

and a parameter referred to as the r^2 value are calculated in LRA. The r^2 parameter, which ranges in value from zero to one, is a measure of the goodness of fit of the fitted line to the data. The higher the r^2 value, the better the fit of the line to the data. Thus, the r^2 value derived from LRA of two highly correlated parameters should be approximately equal to one.

The Culebra transmissivity and storativity data discussed in Sections 3.5.1 and 3.6.1 were analyzed with LRA to determine whether or not any correlation between the parameters exists. Initially, the analysis used all data from those hydrologic tests from which both transmissivity and storativity values were determined. The r^2 value calculated using this data was 0.07. If the data set is filtered to include only those values of transmissivity and storativity determined from interference tests, the r^2 value decreases to 0.003. These results therefore provide quantitative evidence for dismissing correlation between the storativity and transmissivity of the Culebra.

This does not exclude the possibility that geostatistical parameters determined for the transmissivity (e.g., semi-variogram model, correlation distance, and sill) are similar to the geostatistical parameters characteristic of the storativity. A parameter such as correlation distance could be the same for several hydrogeologic parameters without those actual parameters displaying a strong correlation. Regional structural or diagenetic events could provide the mechanisms to produce geostatistical similarities for several hydrogeologic parameters.

3.6.3 Initial Model Storativities

The storativity value chosen for the transient modeling in this study is 2×10^{-5}, the same value used in Haug et al. (1987). Future modeling studies, which will include the hydraulic stresses due to

construction of a fourth shaft and pumping during a tracer test at the H-11 hydropad, will utilize a spatial distribution for storativity during model calibration and sensitivity analyses.

3.7 Hydraulic Conditions in the Culebra Dolomite

3.7.1 Data Base

Data from the observation-well network in the Culebra were evaluated in this study to characterize the hydraulic conditions in the Culebra. Appendix E presents the hydrographs plotted as equivalent freshwater head versus time. (The term "freshwater head" is utilized in this report and is equivalent to the term "freshwater elevation above mean sea level" because the head values are always related to mean sea level. It refers to the elevation of a column of fresh water with a fluid density of 1 g/cm^3 that would exert a pressure at the elevation of the Culebra equal to the formation pressure.)

The freshwater-head data are calculated from either depth-to-water or downhole-pressure-transducer measurements. The procedure used and the information necessary to calculate the freshwater heads is also presented in Appendix E. In addition to the monitoring wells, transducers installed in the lining of the three shafts at the WIPP site have monitored pressures at the Culebra-liner interface in the three shafts. From these hydrographs, estimates of the undisturbed hydraulic conditions and the transient responses due to shaft and site-characterization activities in the Culebra dolomite were assessed.

The calculation of the equivalent freshwater heads from depth-to-water and transducer measurements requires knowledge of the average borehole-fluid density. The estimation of the uncertainty in the borehole-fluid-density estimates and the corresponding uncertainty in the equivalent freshwater heads are discussed in Appendix E. In

addition to the fluid-density uncertainty, water-level variations exhibited in a well's hydrograph may result from long-term natural head changes (trends) or, in some cases, changes of unknown origin. Appendix E lists the estimates of these individual uncertainties for each undisturbed freshwater-head estimate and combines these for a total uncertainty at each well, which is qualitatively meant to correspond to one standard deviation of the freshwater head measurements.

The term "observed freshwater heads" is used in this report to refer to equivalent freshwater heads that are determined from the depth-to-water and transducer measurements. The term "calculated freshwater heads" refers to heads calculated using SWIFT II.

3.7.2 Abridged Transient Data

The hydrographs of equivalent freshwater head versus time are utilized in the transient modeling activities. Because the data base is very large, the equivalent freshwater-head data were abridged to make the hydrograph plots of observed and simulated freshwater heads easier to read. The data were scanned on a seven-day interval to obtain the minimum, maximum, and mean values corresponding to that week. This technique preserves the complexity of the data and minimizes the number of points to be plotted. The transient head data also have uncertainty introduced by the uncertainty in the borehole-fluid density. To illustrate this uncertainty in graphical presentations, these uncertainties (tabulated in Appendix E), expressed in terms of meters of head, are added to the minimum and maximum observed freshwater heads. The transient-data hydrographs used for comparing observed and model-calculated freshwater heads plot the mean observed head value for each week with a vertical bar depicting the minimum and maximum observed freshwater heads plus uncertainties. For the case of a single measured value during a particular week, this value is plotted as the mean and a vertical bar depicting the uncertainties is added to it (see Section 5.1 to 5.3).

3.7.3 Estimation of the Undisturbed Hydrologic Conditions over the Modeled Region

The undisturbed freshwater heads are assumed to be representative of a steady-state system. Haug et al. (1987) found that leakage from the Culebra into the WIPP shafts has occurred since the excavation of the first shaft (the construction and salt-handling shaft, 7/4/81-10/23/81). This leakage has caused drawdown responses at many of the observations wells at the WIPP site. For this reason, undisturbed freshwater heads are best determined from data collected before mid 1981. For wells in close proximity to the shafts for which no water-level data were recorded before the summer of 1981, undisturbed freshwater heads could not be estimated.

The determination of long-term mean formation pressures referred to as undisturbed pressures involved evaluating the hydrographs for the WIPP-site boreholes (Appendix E). We assume that the undisturbed pressures represent the quasi-steady-state pressure field that was present before the excavation of the shafts. Table 3.5 summarizes the estimates of undisturbed freshwater head for each of the wells and also lists the uncertainty associated with that value.

The estimation of the undisturbed pressures expressed in terms of equivalent freshwater heads over the model region was performed using the AKRIP code with the observed undisturbed freshwater heads at the well locations. The estimated heads and the errors of the estimation are illustrated in Figures 3.14a and 3.14b. The freshwater heads reveal a predominantly southerly flow direction across the WIPP site. The heads within the southeastern portion of the modeled area reflect an approximately western flow direction.

Figure 3.14a depicts low hydraulic gradients (1×10^{-4} m/m) north and south of the WIPP site. The low gradient north of the WIPP site is defined by minor head differences between the WIPP-28, WIPP-27,

WIPP-30, DOE-2, H-5, and H-6 boreholes. The low gradient south of the WIPP site is defined by the minor head differences between the H-11, H-17, P-17, H-4, CB-1, H-12, and H-7 boreholes. Hydraulic gradients are higher (4×10^{-3} m/m) in the north-central and central portions of the site. These higher gradients appear consistent with the lower transmissivities within this region. However, the initial transmissivity distribution with low transmissivities in the area of H-4, CB-1, P-17, and H-17 does not seem to be consistent with the observed low gradients immediately south of the southern site boundary. This implies that the estimated transmissivity field in this region does not adequately represent the actual transmissivities and will have to be modified during the calibration of the model in order to reproduce the observed heads.

The estimation errors (Figure 3.14b) are highest beyond the edges of the areas defined by observed data (i.e., west of WIPP-27 and east of WIPP-28, WIPP-30, and H-5). The errors only reflect one standard deviation of the kriged undisturbed freshwater-head estimates and do not incorporate the uncertainty in the observed-head data. However, estimates of the uncertainty of the observed heads will be used to determine when the steady-state model is considered calibrated. That is, the difference between the calculated and observed heads at a given borehole will be compared to the uncertainty (expressed as one standard deviation) of the observed head. If the difference between the calculated and observed heads is less than or equal to the uncertainty associated with the observed head, then the match at that given location will be considered adequate. In doing this, the amount of changes to the initial transmissivity field required to match observed heads having relatively high uncertainty will be reduced. A more detailed description of the approach used during calibration is discussed in Section 4.3.1.

3.7.4 Hydraulic Stresses Since 1981

Since the summer of 1981, the freshwater-head distribution in the Culebra dolomite has been influenced by drilling and excavating three shafts (waste-handling shaft, construction and salt-handling shaft, and exhaust shaft) at the center of the WIPP site (see chronology and discussion of shaft-construction activities in Appendix G). In addition, several wells have been drilled or re-completed in the model area and numerous well-testing activities, some of very long durations (e.g., H-4 tracer test), have been conducted since 1981 (Appendix E). Consequently, the hydrologic conditions at the beginning of or during the H-3 and WIPP-13 multipad pumping tests cannot be considered to be undisturbed. Haug et al. (1987) illustrated the large drawdown cone caused by the different activities at the WIPP site since 1981. The center of the drawdown cone coincides with the location of the shafts. The diameter of the drawdown cone was about 7 km and the depth was about 33 m at the shaft location. The drawdowns at wells H-1 and H-2 reached maxima of 12.2 m and 7.1 m, respectively (Haug et al., 1987).

The implementation of these disturbances at the WIPP site, which are transient by their nature, was achieved using the wellbore submodel of SWIFT II (Reeves et al., 1986a). This submodel allows injection or withdrawal of water from the model at specified locations (i.e., at the well locations). Details of the implementation are discussed in Chapter 5. Similarly, the H-3 multipad and WIPP-13 multipad pumping tests were implemented using the above-mentioned wellbore submodel. This implementation is also discussed in detail in Chapter 5.

3.7.5 Initial Boundary Conditions

The Culebra dolomite along the eastern boundary of the model area is characterized by extremely low transmissivities and negligible flow. The eastern boundary was therefore considered to be reasonably

represented as a no-flow boundary. Prescribed-pressure boundaries with prescribed formation-water densities were applied to the northern, southern, and western boundaries. Freshwater heads were estimated at the outer edges of all grid blocks along the north, south, and western model boundaries using AKRIP with the best estimates of the undisturbed freshwater heads (Table 3.5) at observation wells. These grid-block-edge values were then used to calculate the formation pressures at grid-block-center elevations along the model boundaries. During the simulation, the prescribed pressures are maintained along the outer edges of the model area.

3.8 Formation-Fluid Densities

3.8.1 Data Base

The formation-fluid-density data base (Appendix F) was compiled and evaluated to determine the most recent and most reliable fluid-density information available for the Culebra dolomite. The principal sources used in compiling the data base include (the reader is referred to Appendix F for the complete listing of data sources):

1) hydrogeologic and hydrologic data reports (Mercer, 1983; INTERA and Hydro Geo Chem, 1985; INTERA, 1986; Saulnier et al., 1987; Stensrud et al., 1987);
2) geochemistry reports (Robinson, 1987; Uhland and Randall, 1986; Uhland et al., 1987); and
3) unpublished INTERA and Hydro Geo Chem notes from field logbooks.

The Robinson (1987) report provides a good analysis of the fluid-density data available before 1987. She discusses the integrity of previous formation-fluid samples and suggests which values can be considered representative of the formation. However, since publication of her report, new density data have been published in

Uhland et al. (1987). These authors present fluid-density data from the WIPP Water Quality Sampling Program being performed to expand the geochemical data base and to establish background values for various geochemical constituents in Rustler ground waters.

The present study has attempted to integrate the data contained in the above reports and field notes to determine which formation-fluid-density values are most representative of in-situ formation fluids. Unfortunately, several WIPP-area boreholes have not had sufficient pumping to remove drilling fluids still present in the formation around the boreholes. Thus, we have evaluated the fluid-density data base and determined formation-fluid-density values we believe are most representative of in-situ ground waters (Table 3.6). A detailed description of the methodology used in the evaluation of the representativeness of the fluid-density values is discussed in Haug et al. (1987).

3.8.2 Estimation of Formation-Fluid Densities Over Modeled Region

The fluid-density data deemed representative of the Culebra were used to estimate the formation-fluid densities over the model region. The generalized kriging code, AKRIP, calculated the estimates of fluid densities which were assigned to the model grid blocks. Densities ranging from 1.00 to 1.06 g/cm^3 occur in a wide region extending from boreholes WIPP-28 to H-7b (Figure 3.15). Higher fluid densities were estimated east of this region with values ranging from 1.08 to 1.16 g/cm^3 along the eastern boundary. The area of the model with the highest uncertainty in fluid-density values occurs along the eastern boundary. Data in this area were estimated from the west-east trend in the observed values. Fluid-density values in the central region of the model area have lower uncertainties due to the larger number of boreholes located there.

At this point, several remarks should be made regarding the use of the estimated formation densities in the model. Geochemical evidence (Section 2.5) suggests that the chemical constituents within the Culebra dolomite may not be at steady state with the present flow field. Therefore, using the observed formation-fluid densities as a calibration parameter during steady-state flow simulation would not be valid. For this reason, the formation-fluid densities estimated for each of the grid blocks were held constant for all model simulations. This allowed inclusion of the observed density distribution and the effects that variable densities have on the present-day flow field.

4.0 SIMULATION OF FLOW UNDER UNDISTURBED HYDROLOGIC CONDITIONS (PRE-SHAFT)

The simulation of ground-water flow in the Culebra dolomite was performed using the following approach. Initially, the boundary conditions of the conceptual model and the system parameters (such as storativity, transmissivity, and various system constants, Table 3.3) were defined based on the documented data base. Using these data, a simulation was performed to assess how well the initial estimates of the system parameters reproduced the observed, undisturbed freshwater heads.* Subsequent changes to the initial estimates of the boundary conditions and transmissivity field were implemented as required to minimize the difference between the calculated and observed heads. The model was considered calibrated when the difference between the calculated and observed freshwater heads was less than the uncertainty (as defined by one standard deviation) assigned to each observed freshwater head. Because some observed values are more uncertain than others, assigning one overall "threshold" value (i.e., one or two meters) within which the differences should lie did not seem adequate. The results of the initial and final calibrated simulations and a more detailed explanation of the technical approach are presented in the following sections.

4.1 Initial Conditions

The system parameters which comprise the components of the initial model conditions have been previously described in Section 3. The conceptual model, described in Sections 1 and 3, is a two-dimensional steady-state flow system with variable fluid densities and formation elevations. The current fluid-density distribution is assumed to have been created by a flow system different from the one existing today, with little modification as yet by the current flow system. Therefore, the fluid

* As discussed in Section 3.7.1, "observed freshwater heads" refer to equivalent freshwater heads calculated from depth-to-water and transducer-pressure measurements.

densities were simulated as spatially fixed, i.e., no transport of brine is calculated in the steady-state model. Furthermore, no sources, sinks, or vertical flux are considered in this conceptual model for the undisturbed hydrologic conditions.

The initial model parameters are described in Sections 3.3 through 3.8. The initial transmissivities assigned to each model grid block are the generalized kriged estimates obtained using the code AKRIP (Section 3.5.3.2). The initial boundary conditions (Table 4.1) were estimated from the observed freshwater-head distribution and the kriged density distribution (Sections 3.7.3 and 3.8.2). The transmissivities and the initial boundary conditions are the calibration parameters used in the simulations. However, because the boundary conditions are constrained by the observed freshwater-head data, the transmissivity distribution is the more important calibration parameter.

4.2 Initial Steady-State Simulation

After establishing the initial boundary conditions and the initial model parameters described above, the initial simulation of steady-state flow in the Culebra was performed. The results of this initial run are summarized in Figures 4.1 and 4.2. Figure 4.1 illustrates the calculated freshwater heads derived from the calculated formation pressures and assigned fluid densities. The difference between the calculated and observed heads is shown in Figure 4.2.

Figure 4.2 demonstrates that the calculated heads in the initial simulation do not reproduce the observed heads. The differences between the calculated and the observed heads have high negative values (more than -10 m) in the north-central part of the modeled region and relatively small positive values in the southern part of the modeled region (Table 4.2). The high negative values reflect the difference between the low calculated values and the high observed values in the

northern region. The differences of -6.0 m and -3.2 m at WIPP-27 and WIPP-28, respectively, imply that the heads specified for northern boundary conditions are likely too low. High negative differences indicate that the transmissivities in the area north of H-6, DOE-2, and H-5 are too low. Positive differences occur around H-11, DOE-1, H-4, P-15, P-17, CB-1, and H-17, indicating that the calculated heads at these wells are too high. The highest positive difference occurs at H-11 where the calculated head is 4.6 meters higher than the observed head.

Changes to the initial transmissivity distribution and boundary conditions can be used to improve the agreement between calculated and observed heads. Unfortunately, changes to improve the agreement in the northern region will generate a poorer agreement in the southern region, i.e., higher, positive head differences south of the WIPP site. Thus, changes in the initial transmissivity field are needed at several locations in the modeled region. The justification and methodology for the implementation of changes in the boundary conditions and transmissivity distributions is described in Section 4.3.

4.3 Calibration of the Steady-State Model

4.3.1 General Approach

The calibration approach used to improve the agreement between the initial calculated heads and the observed heads has previously been described in Haug et al. (1987). The technique employs "pilot points" or additional transmissivity data points which are added to the set of observed transmissivity data and used to alter the transmissivities within the model region through kriging. This approach greatly enhances one's ability to adjust the transmissivity within areas of a model with the minimum amount of effort and is derived from a technique discussed in de Marsily, (1983). In principle, universal kriging (K603) or generalized kriging (AKRIP) could be used for the

model calibration. As discussed in Section 3.5.3.3, AKRIP was selected because of its capability to incorporate local trends in the observed transmissivity data into the kriged transmissivity estimates.

The locations and values of the pilot points are determined by the head differences of the previous simulation. That is, after each simulation, new information on the response of the model to changes in the transmissivity field is obtained. At that time, the effect of the altered transmissivity field in minimizing the head differences is evaluated. A criterion has been devised to determine whether or not large-scale transmissivity features should be added to match the observed head values. If the difference between the calculated and observed heads at a given location is greater than twice the uncertainty of the observed value (i.e., two standard deviations), then introducing large-scale transmissivity features, such as increasing the transmissivity up or down gradient of a particular area, is considered justified.

Table 4.2 lists the differences between the initial calculated and observed freshwater heads and the values equivalent to the uncertainty (1σ) of the observed head for each borehole. The head differences in the northern part of the modeled region are larger than twice the uncertainty of the observed heads. The large negative differences are due to a lack of sufficient ground-water flux from the northern boundary of the model. Therefore, assigning higher heads along the northern boundary and higher transmissivities upgradient from the wells with large negative differences is justified.

Once a sufficient number of transmissivity pilot points were added to reduce the head differences below 2σ at each borehole, local-scale transmissivity features were used to reduce the head differences to below 1σ at each borehole. The model was considered calibrated when the head difference at each borehole was less than or equal to the uncertainty of the observed head.

4.3.2 The Steady-State Calibrated Transmissivity Field

The transmissivity field that is considered to reproduce the observed freshwater-head distribution adequately, hereafter referred to as the steady-state calibrated transmissivity field, is shown in Figures 4.3 and 4.4. The steady-state calibrated transmissivity field contains the same broad features as the initial transmissivity field (Figure 3.12a); namely, increasing transmissivity from east to west and locally high transmissivity around H-11 and DOE-1.

The calibration of the model generally proceeded from the northern part to the southern part of the model area. However, to reduce the number of simulations during calibration, several changes were often implemented in one step. The first step during calibration involved increasing the heads along the northern boundary, increasing the hydraulic gradient along the western boundary, and increasing the transmissivities in the northern region of the model. These changes resulted in a higher ground-water flux entering the central part of the model, which increased the heads in the H-11 area because of the low transmissivities south of H-11. Therefore, the transmissivities in the southern part of the model were increased to "drain" the additional flux entering the central part of the model area.

The individual changes to the initial transmissivity field are as follows:

1. Four pilot points with transmissivity values ranging from 2×10^{-4} to 3×10^{-5} m^2/s were placed between the northern model boundary and the WIPP-site boundary (Figure 4.3). These pilot points increased the transmissivities just west of WIPP-28 and WIPP-30 which increased the ground-water flux to the north-central region of the modeled area. In addition, five pilot points were added (between P-17 and H-17) south of H-11 which increased the

transmissivities south of H-11 by one order of magnitude to approximately 6 x 10^{-6} m^2/s. These changes significantly reduced the differences between the calculated and observed heads at most of the wells north of the WIPP site. The head differences at H-1, H-2, and H-3 were also reduced below the uncertainty of the observed values. However, negative differences were still present at P-14 (-4.1 m), WIPP-18 (-2.6 m), and WIPP-25 (-6.2 m) and positive differences were still present (2 to 3 m) in the H-11, DOE-1, and H-14 area.

2. The second step during the calibration of the model was to reduce the negative head differences at WIPP-25 and P-14. This required an increase in the transmissivities in the northwestern area of the model to increase the ground-water flow into the system. Pilot points were added to increase the transmissivities slightly in this area to 6 x 10^{-4} m^2/s. In addition, a low-transmissivity region was introduced south of WIPP-25 and north of P-14 to reduce the flux leaving the WIPP-25 area (Figure 4.3). The transmissivities in this low-transmissivity zone are a factor of 4 less than those in the initial kriged transmissivity field. The low transmissivities caused a damming effect which increased the heads at WIPP-25, P-14, and WIPP-18 such that the differences between the calculated and observed heads were less than the uncertainties of the observed heads. However, because the calculated head at WIPP-26 was already 1 m higher than the observed head, the transmissivities south of WIPP-26 were increased by a factor of 5 to drain the additional flux of ground water that was expected based on the above changes in the vicinity of WIPP-25 and P-14.

3. The third step during calibration was to reduce the 2- to 3-m head differences at DOE-1, H-11, and H-14. The pilot points in the area south of H-11 were adjusted several times. The head differences were finally reduced below the uncertainties of the observed heads when the transmissivities south of H-11 were

increased to approximately 3×10^{-5} m^2/s. Figure 4.3 illustrates the area south of H-11 that has the higher transmissivity values. The transmissivity is depicted by a contour of -4.5 log m^2/s (3×10^{-5} m^2/s) occurring west of H-17 and east of P-17. This feature is less transmissive than the one proposed in Haug et al. (1987).

Figure 4.4 also illustrates the high-transmissivity feature between H-17 and P-17. In the initial kriged transmissivity field, expressed in terms of negative log transmissivity (Figure 3.13), the area between P-17 and H-17 formed a highly resistive barrier south of H-11. This highly resistive barrier has now been reduced to allow ground water to flow south from the area between H-11 and DOE-1. A more detailed discussion of the sensitivity of the calculated heads at H-11, DOE-1, and H-14 to this high-transmissivity feature is presented in Section 4.3.4.

4.3.3 The Calibrated Steady-State Heads

The calibrated steady-state heads were calculated using the boundary conditions listed in Table 4.3 and the calibrated transmissivity field described in Section 4.3.2. Figure 4.5a shows the calibrated steady-state heads over the model region. The calculated head distribution is quite similar to the observed distribution (Figure 3.14a). The gradients in the calibrated head distribution agree with the gradients defined by the undisturbed heads, i.e., low gradients north and south of the WIPP-site boundary and an increased gradient within the WIPP-site boundary. The largest flux of ground water enters the system along the northern model boundary west of WIPP-28 and flows predominantly south toward WIPP-25 (Figure 4.5b) Flow in the northern part of the WIPP site is generally from north to south. A large portion of the ground water within the WIPP-site boundaries enters the high-transmissivity zone south of H-11 and exits the modeled region from the central part of the southern boundary east of H-7.

The Darcy velocities of the calibrated steady-state model were calculated by SWIFT II using the transmissivity distribution (Figure 4.3), the steady-state pressure field (Note: the calibrated equivalent freshwater head distribution (Figure 4.5) is determined from calculated pressures at formation depth), the prescribed fluid-density distribution (Figure 3.15), and the center-of-Culebra elevations (Figure 3.4). The Darcy velocities are defined as the specific discharge per unit cross-sectional area normal to the direction of the flow. In a porous medium, estimates of the mean pore-water velocity are calculated as the Darcy velocity divided by the effective porosity. However, a spatially-constant porosity assigned for the entire model area is unrealistic. Therefore, only Darcy velocities are shown in Figure 4.5b. Such velocities should be interpreted as indicators for the flow directions and the relative importance of the different flow paths.

Within the modeled region, the Darcy-velocity vectors range in value over six orders of magnitude. The lowest velocities occur east of the WIPP site, where the magnitude of the velocity vectors is approximately 1×10^{-12} m/s (Figure 4.5b). The highest velocities occur in the southern portion of Nash Draw along the western boundary of the model, where the velocities are between 1×10^{-7} to 1×10^{-6} m/s. South of WIPP-12, toward the WIPP shafts, the Darcy-velocity magnitudes are approximately 2.5×10^{-10} to 7.5×10^{-10} m/s. The velocities increase to approximately 2.5×10^{-9} m/s in the high-transmissivity zone south of H-11. The increase in velocity is lower than expected from the 1 to 2 orders of magnitude increase in the transmissivities because the gradient within the area south of H-11 is much lower than that to the north at the WIPP-site center. The velocity vectors in the vicinity of DOE-2 and in the northeast quadrant of the model area are misleading because of the Culebra elevation changes that occur in these areas. Section 4.3.6 discusses the velocities in these areas in detail.

The head differences (the calculated heads minus the observed heads) for the calibrated model are illustrated in Figure 4.6. The uncertainties of the observed heads and the head differences are listed on Table 4.4. All the head differences are less than the uncertainties of the observed heads except at H-7.

The differences between the calculated and observed heads at boreholes in the vicinity of H-11 are small and positive. The maximum positive head difference in this area occurs at H-11, where the calculated head is 1.5 m higher than the observed head. The head differences at P-17 and H-17 are -1.2 m and +0.9 m, respectively. This contrast between negative and positive values implies that the high-transmissivity zone extending southward from H-11 should probably be located further east of P-17 towards H-17 than it is in the calibrated transmissivity field presented in Figure 4.3. However, the differences at both P-17 and H-17 are less than the uncertainties of the respective observed heads. The sensitivity of the calculated heads in this vicinity to the high-transmissivity zone was investigated and is presented in detail in Section 4.3.4.

Several small changes to the calibrated transmissivity field could be introduced in future modeling studies to reduce the head differences listed in Table 4.3. For example, the head difference at H-7 could be reduced by implementing higher transmissivities between Nash Draw and H-7. This would channel flow from Nash Draw toward H-7 and increase the calculated head. Adjusting the southern boundary conditions would also affect the heads in the H-7 area. This was performed and is discussed in Section 4.3.5. In general, an increase in the specified heads along the southern boundary reduces the head differences at H-7 and increases the differences between the calculated and observed heads at H-11, DOE-1, and H-14. Therefore, even higher transmissivities than are present in the calibrated model south of H-11 (5×10^{-5} m^2/s) would be required in order to reproduce the observed heads at these boreholes adequately.

4.3.4 Sensitivity of the Calculated Heads to the High-Transmissivity Zone South of H-11

During the drilling of H-17, a halite bed was found in the Tamarisk Member of the Rustler formation, an indicator that the Culebra transmissivities near H-17 are low. A slug test in the Culebra suggested the transmissivity was approximately 2×10^{-7} m^2/s, Beauheim (1987b). This value is obviously much less than the transmissivity proposed for the high-transmissivity zone (Figure 4.3). However, the low transmissivity at H-17 does not exclude the possibility that some type of high-transmissivity feature exists that provides a conduit for flow from the H-11 area.

During the calibration of the model in this study, the calculated heads were consistently too high in the vicinity of H-11. The assumption of no vertical ground-water flux from the Culebra necessitated a higher transmissivity feature between P-17 and H-17 to reduce the differences between the calculated and observed heads at H-11 and DOE-1.

Two additional simulations were performed to demonstrate the need for a higher transmissivity feature south of H-11. The first simulation, case 1, used the calibrated model described in Section 4.3.3 without the pilot points used to generate the high-transmissivity zone. The second simulation, case 2, employed the calibrated model with an intermediate-transmissivity zone south of H-11 in place of the high-transmissivity zone in the calibrated model.

In case 1, only one pilot point, located southwest of H-12, was included in the southern part of the model (Figure 4.7). In the initial transmissivity field (Figure 3.12a), the transmissivities between H-17 and P-17 were approximately 6×10^{-7} m^2/s (log transmissivity of -6.2) and in Figure 4.7, the transmissivities in this area are about three times greater or approximately 2×10^{-6} m^2/s (log transmissivity of -5.75).

The transmissivity distribution used in case 1 (Figure 4.7) is very similar to the calibrated transmissivity distribution (Figure 4.3). Small changes occur because the pilot points used to generate the high-transmissivity zone influenced the transmissivity estimates over the southern portion of the model region.

The calculated heads for case 1 are illustrated in Figure 4.8. The calculated heads in the northern and western parts of the model are very close to the observed heads (Figure 3.14a). However, the calculated heads in the area between H-15 and H-17 are significantly higher (6 to 8 m) than the observed heads. In addition, the calculated gradients in this region of the model are not the same as those observed (Figure 3.14a). Figure 4.9 illustrates the head differences over the model region for case 1. These differences are also listed in Table 4.5. The major differences between the observed heads and those calculated for case 1 occur in the southern part of the WIPP site. The calculated heads range from three to five meters higher than the observed heads in the vicinity of H-1 (Table 4.4) to a maximum difference of 8.7 m at H-11. The head differences south of H-11 range from 5.5 m at H-17 to 1.1 m at H-12. The head differences determined in case 1 imply that a change more dramatic than the three-fold increase in the transmissivity values between P-17 and H-17 is necessary to reduce the calculated heads in this southern region of the model area.

Case 2 was performed to determine the effect of intermediate transmissivities (6×10^{-6} m^2/s) south of H-11 on the calculated heads. This value is an order of magnitude greater than the initial transmissivities, a factor of three increase greater than the case 1 values, and an order of magnitude less than the calibrated transmissivity in this area. Figure 4.10 shows the transmissivity distribution used for case 2. As in case 1, the transmissivities are very similar to the calibrated transmissivities except in the area

south of H-11. The calculated heads for this simulation are illustrated in Figure 4.11. The calculated heads north and west of the WIPP site agree well with the observed heads (Figure 3.14a). Figure 4.12 shows that as in case 1, the differences between the calculated and observed heads increases significantly between H-15 and H-11. The magnitudes of the head differences (Table 4.6) are less than those calculated for case 1, but the 3- to 5-meter differences in the vicinity of H-11 are still relatively high. Therefore, as expected, even higher transmissivities than used in case 2 are required south of H-11 to reduce the head differences at H-11, DOE-1, and H-14.

In summary, two simulations, case 1 and case 2, were performed to demonstrate the need for the high-transmissivity zone between P-17 and H-17 which was introduced while calibrating the model to reduce the differences between the calculated and observed heads at H-14, DOE-1, and H-11. The calibrated transmissivities between P-17 and H-17 are approximately 5×10^{-5} m^2/s, or approximately 1.5 orders of magnitude higher than the transmissivities used in case 1 (2×10^{-6} m^2/s), and one order of magnitude higher than the transmissivities used in case 2 (6×10^{-6} m^2/s). The head differences for case 1 in the vicinity of H-11 ranged from 5.3 to 8.7 m. In case 2, the head differences were reduced by approximately 3.5 m from those in case 1. In conclusion, with the present data base, the increase in the transmissivity between P-17 and H-17 is necessary to reduce the head difference at H-11 below the +/- 2-m uncertainty of the observed H-11 head.

4.3.5 Sensitivity of the Calculated Heads to the Southwestern Boundary Conditions

A third simulation, case 3, was performed to determine the effect that changing the heads along the southwestern boundaries of the model would have on the calculated heads at H-7 and in the vicinity of H-11.

The calibrated transmissivity distribution (Figure 4.3) was used for this simulation. The specified hydraulic gradient along the lower half of the western boundary was lowered to approximately 7.5×10^{-4} m/m, slightly less than the calibrated model's gradient of 9×10^{-4} m/m. The change in gradient raised the specified head at the southwest corner of the model area from 910 m amsl in the calibrated model to 911 m amsl for case 3. Also, the specified heads along the western half of the southern boundary were raised by 2 m. This increase in the specified heads in the southwest part of the model area essentially lowered the regional hydraulic gradient between the northern and southern boundaries.

The calculated heads for the case 3 simulation are shown in Figure 4.13. In the northern part of the WIPP site, the calculated heads at DOE-2, WIPP-13, and H-6 are slightly greater (0.2 to 0.4 m) than the heads for the calibrated model. The increase in the heads becomes greater in the southern half of the WIPP site where heads at the H-3, H-14, and H-15 boreholes were increased by an average of 1.6 m. The increase in calculated heads south of H-14 was approximately the same as at H-11 and H-7, which had increases of 1.9 m.

Figure 4.14 shows the difference between the calculated and observed heads for case 3. The difference at H-7 was reduced below its 1 m uncertainty value. However, the head differences in the vicinity of H-11 were increased to values above the observed-head uncertainties (Table 4.7). Therefore, higher transmissivities south of H-11 than those used in the calibrated model would be required to reduce the head differences in this portion of the model area. Future modeling efforts would require continuation of these calibrations with a variable transmissivity distribution and changes to the specified heads along the western and southern boundaries.

4.3.6 Apparent Local Maxima and Minima in the Calculated Freshwater Heads

Equivalent freshwater heads are a common unit used to represent formation pressures over a given area or at a borehole location. For this reason, the formation pressures in this study are presented in equivalent freshwater heads. However, freshwater heads are limited in their use as a direct indicator of ground-water flow direction because the equivalent-freshwater-head equation (Appendix E) ignores the gravity-related pressure that is generated in a variable elevation, saline ground-water system. This condition can lead to local maxima or minima in the equivalent-freshwater heads. For example, the calculated freshwater heads in Figures 4.5, 4.8, 4.11, and 4.13 have two local highs occurring along the eastern no-flow boundary. A local low also occurs between WIPP-30 and H-5 (the 935-m contour line). The following paragraphs explain the reasons for these local highs and lows in the calculated freshwater-head distribution.

A detailed illustration of the center-of-Culebra elevations (m amsl) in the northeast quadrant of the model is shown in Figure 4.15. Three minima occur in the Culebra elevation map. Two of these minima are located along the eastern boundary of the model area, one along the northern part of the boundary and one in the central part of the eastern boundary directly east of the WIPP site. The third elevation low occurs in the area between DOE-2 and WIPP-11. Each of these low-elevation areas forms a trough or local depression within areas of relatively significant elevation changes. The elevation low occurring along the northern part of the eastern boundary is based on a Culebra elevation from Davies (1988). The elevations defining the low occurring in the central part of the eastern model-area boundary are estimated by AKRIP based on the local trends observed in the nearby data inside the modeled area. The low area between DOE-2 and WIPP-11 is defined by stratigraphic data from the logs of those two wells (Mercer et al., 1987; and Sandia National Laboratories and U.S. Geological Survey, 1982).

A detailed representation of the model-calculated freshwater heads in the northeast quadrant of the model area is illustrated in Figure 4.16. Local maxima coincide with the three minima in the Culebra elevations shown in Figure 4.15. The local extremes in freshwater heads in this part of the model area are due to gravity-induced pressures generated by the rapid changes in adjacent grid-block elevations. Significant elevation changes between adjacent grid blocks increase the pressure in the lower-elevation grid block by the weight of the column of water assumed to exist between the two grid blocks. The equation used to convert this pressure to equivalent freshwater head assumes that this column of water has a density equal to 1.0 g/cm^3. In the northeast quadrant of the model area, however, the fluid densities range from 1.05 g/cm^3 to 1.16 g/cm^3. This range of fluid densities coupled with the variation in the Culebra elevations in the WIPP area can generate local freshwater-head anomalies of up to 5 m.

The Darcy-velocity equation is:

$$\text{Velocity} = \frac{k}{\mu}\left[\frac{\Delta P}{d} - \left(\bar{\rho} * g * \frac{\Delta z}{d}\right)\right] \qquad (4.1)$$

where k is the harmonic-mean permeability between adjacent grid blocks, μ is fluid viscosity, ΔP is the pressure difference between adjacent grid blocks, d is the distance along one of the principal axes, x, y, or z between adjacent grid blocks, $\bar{\rho}$ is the mean fluid density of adjacent grid blocks, g is gravity, and Δz is the difference of adjacent grid-block center elevations. The first term accounts for the driving force due to pressure differences between two adjacent grid blocks, and the second term accounts for the gravity-induced pressures generated by elevation and fluid-density effects. Velocities are calculated in the x and y directions because of the assumption used for modeling the Culebra as a confined aquifer with no vertical flux.

The calculated Darcy velocities (Figure 4.5b) are accurate representations of the flow directions given the assumption of porous-medium flow and the boundary conditions used in the model. The y-components of the velocity vectors over the model region are generally oriented south, even in the areas where the local freshwater highs occur. One exception occurs in the northeastern corner of the model area where the two terms on the right-hand side of Equation (4.1) are the same within the limits of discretization and the accuracy of the algorithm. These terms are also approximately the same in the vicinity of DOE-2. This results in unreliable velocity magnitudes and directions.

The importance of accounting for the gravity-induced pressure or gravity-related driving force in the WIPP area has also been described by Davies (1987). He presents a modified form of Darcy's law incorporating the variable density and elevation effects and investigates changes in the flow directions generated by incorporating gravity-related driving forces. In summary, the local freshwater-head maxima or minima illustrated in Figures 4.5, 4.8, 4.11, and 4.13 are derived from the choice of presenting the data in the unit of equivalent freshwater head. The velocity vectors illustrated in Figure 4.5b are accurate representations of the flow direction except in areas where the difference between the two components of the velocity equation (Equation 4.1) is small, such as in the northeast corner of the model area.

4.4 Calculated Particle Travel Times in the Model Region

In a steady-state flow field, particle travel times calculated using mean pore-water velocities are good indicators of the travel times due strictly to the changes in permeability and hydraulic gradient over a particular area, but should be interpreted relative to the spatially-constant porosity used in the calculation of mean pore-water velocities. The particle travel times should also be interpreted

relative to the uncertainties associated with the permeabilities and the hydraulic gradients. Uncertainties in the permeabilities and the calculated pressures used in the calculation of the hydraulic gradient generate variations in the particle travel paths and times from a given release point, whereas uncertainties in the porosities directly affect the variations in the particle travel time along a given path. In Andrews et al. (1987), the importance of considering both particle travel-path uncertainty and particle travel-time uncertainty is demonstrated using a statistical sampling approach from distributions of the hydrogeologic parameters at the bedded salt site in Deaf Smith County, Texas.

In this study, a significant portion of the uncertainties of the permeabilities in the WIPP-site area can be derived from the estimation errors of the transmissivity field (Figure 3.12b). The uncertainties of the observed transmissivity values must also be considered. The uncertainties of the observed heads (Table 3.5) originates from the uncertainties in the borehole-fluid densities and the trends observed in the hydrographs for the WIPP-area boreholes (Appendix E). Given the uncertainties associated with the hydrologic data from the boreholes at the WIPP-site, the particle travel times presented in this section should be considered uncertain. They are presented to illustrate the range in particle travel times in the calibrated steady-state model using the steady-state calibrated transmissivities and a spatially-constant porosity of 16 percent.

Calculations were performed for the release of seven particles in the flow field defined by the steady-state calibrated heads. Of these seven, three were released along the western half of the northern boundary to determine the travel times within the model area representing Nash Draw. The four other particles were released within the WIPP-site boundary at locations coincident with H-5, H-6, H-18, and a point corresponding to the centroid of the underlying repository which

was considered the base-case release point in Reeves et al. (1987). Figure 4.17 illustrates the particle travel paths for all seven particles. The paths are consistent with the velocity vectors illustrated in Figure 4.5b. The shortest travel times occur in the western part of the model area where particles A and B have values of approximately 450 and 975 years, respectively. Both of these particles traveled directly south in the area representing Nash Draw where the Darcy velocities range from 1×10^{-7} m/s to 1×10^{-6} m/s. Particle C initially travels southward but is redirected toward the area representing Nash Draw where the majority of the ground water entering the model along the northern boundary eventually flows. Particle C has a travel time of 2.8×10^{3} years which is less than one order of magnitude greater than the travel times for particles A and B.

The travel path of particle D, originating at H-6, is oriented southwest because the ground-water flow in this area is oriented away from the relatively low transmissivities south of H-6. The travel path is eventually redirected southeast toward H-7 and exits the southern model boundary with a total particle travel time of 1.6×10^{4} years. Particle E was released from a location coincident with H-5 and exits the model area from the southern boundary in 1.4×10^{6} years. The calculated travel time for Particle E is very long because of the low calculated Darcy velocities (1×10^{-11} to 1×10^{-10} m/s) near the eastern WIPP-site boundary and because Particle E does not enter the high-velocity zone between H-17 and P-17 which is generated by the high-transmissivity zone described in Section 4.3.2.

Particles F and G were released in the central part of the WIPP site. The release point for Particle F is slightly south of H-18. The particle then travels southeast toward H-3, enters the high-velocity zone between H-17 and P-17 and reaches the southern model boundary in 5.8×10^{4} years. Particle G was released in the Culebra from a point coincident with the centroid of the underlying repository area. This

release point was used as the base-case release point in Reeves et al. (1987). The calculated particle travel time for Particle G to reach the southern WIPP-site boundary is approximately 1.3×10^4 years, which is about one-third of the total travel time to the southern model boundary (3.6×10^4 years). Assuming a porous-medium equivalent porosity of 0.16 and the southern WIPP-site boundary as the accessible environment, the particle travel time to the accessible environment determined for particle G in this study is approximately 2.5 times longer than the travel time to the accessible environment (southern WIPP-site boundary) presented in Reeves et al. (1987). The increase in particle travel time in this study is primarily due to the lower ground-water velocities south of H-3 generated by the lower transmissivities in the vicinity of H-11. This increase in travel time should be considered qualitative since additional model calibration is yet to be completed (see Section 5).

5.0 SIMULATION OF TRANSIENT RESPONSES RESULTING FROM SHAFT ACTIVITIES AND WELL TESTS

The focus of this modeling study is to simulate the undisturbed hydrologic conditions and the transient behavior of the Culebra dolomite in response to the H-3 and WIPP-13 multipad pumping tests. The simulation of these tests was conducted to assess how well the steady-state calibrated model reproduces the transient tests performed in the Culebra. The following Sections 5.1, 5.2, and 5.3 describe the five transient simulations performed in this study.

All of the simulations utilize the calculated heads of the calibrated steady-state model (Figure 4.5) as the initial condition. The initial or base-case transient simulation also used the transmissivities of the calibrated steady-state model. The other four transient simulations were conducted to evaluate the effect the model transmissivities and storativities have on the calculated transient freshwater heads. The first two sensitivity simulations used the base-case storativity but had different transmissivity distributions than the base case. A factor-of-two increase in the calibrated transmissivities was used in the first case and a factor-of-two decrease in the calibrated transmissivities was used in the second case. The other two sensitivity simulations used the base-case transmissivity distribution but changed the base-case model storativity values by factors of 2.5 and 0.5.

The transient simulations include the hydraulic tests and other activities that caused significant hydraulic stresses on the Culebra. The most important disturbance of the hydrologic system during recent years was caused by excavating the shafts at the center of the WIPP site (Appendix G). The transient simulations in this modeling study includes the entire shaft history extending from its beginning in July 1981 to the present (late 1987). For convenience, January 1, 1981 was selected as the beginning of the simulation time scale. The time-step size selection criteria for the simulations are described in Appendix G.

Well tests at H-2, H-3, H-4, and WIPP-13 were also included in the transient simulations. Descriptions of these tests are also contained in Appendix G. Many other well-testing and water-quality-sampling activities have been conducted at the WIPP site and could be implemented in the transient simulation. In general, most of these are of short duration with relatively small impacts on the hydrologic conditions in the Culebra. We have selected tests of longer duration which have significantly stressed the Culebra in the vicinity of H-3 or WIPP-13. This was done to incorporate the hydrologic stresses present during the beginning of the H-3 and WIPP-13 multipad pumping tests.

The observed transient data are presented in terms of freshwater heads which required knowledge of representative borehole-fluid densities (Appendix E). Because borehole-fluid density is an uncertain parameter, a specific symbol has been used in the figures showing the plotted transient hydrographs to express the uncertainty in the transient freshwater heads calculated from the densities in Table E.2. The symbol used is a vertical line, indicating the uncertainty associated with the freshwater-head value, with a horizontal tic mark which corresponds to the best estimate of the freshwater-head value (Section 3.7.2).

5.1 Initial Transient Simulation Using the Steady-State Calibrated Model

The details of the shaft activities which hydraulically stressed the Culebra and the tests performed at the WIPP-area boreholes which were used in the transient simulation are presented in Appendix G. Sections 5.1.1 to 5.1.9 describe the initial transient simulation performed using the transmissivity distribution and boundary conditions of the steady-state calibrated model. The initial simulation is also referred to as the base-case transient simulation in later sections. Additional calibration was not performed to improve the results determined in the initial simulation. Transient calibration requires an

iterative procedure which includes changing local transmissivities and storativities to improve the calculated transient results while maintaining the calibrated steady-state fit to the observed heads. This type of procedure will be done in the transient simulations included in future modeling studies.

5.1.1 Simulation of the Early Shaft Pressure History

The effects of the early shaft pressure history in 1981 and 1982 were observed at H-1, H-2, and to a lesser extent at H-3 (Stevens and Beyeler, 1985) (Figure 5.1a). At H-1, the calculated drawdown resulting from the first exposure of the construction and salt handling (C & SH) shaft to atmospheric pressure is greater than the observed drawdown. The subsequent increase in calculated head at H-1, generated from the simulation of the filling of the C & SH shaft with brine, is higher than the observed head. The lack of agreement between the simulated and observed heads implies that (1) the model transmissivities between the C & SH shaft and H-1 are too high, and/or (2) the model storativity (2×10^{-5}) between the C & SH shaft and H-1 is too low.

The magnitude of calculated drawdown at H-2 and H-3 during the early-shaft-history time period is approximately the same as the observed drawdown at both boreholes. However, the calculated heads at H-2 are generally 5 m lower than the observed heads. This head difference implies that the model transmissivities between the C & SH shaft and H-2 are too high, or that the model storativity is too low. The calculated freshwater heads at H-3 generally agree with the observed heads during this period, indicating that the model parameters between the shaft location and the H-3 hydropad have approximately representative values.

The early shaft pressure history probably caused very strong head changes at WIPP-21 and WIPP-22, and to a lesser extent at WIPP-19 and WIPP-18. However, because these wells were not completed as Culebra observation wells until the summer of 1985, no observed data exist from these wells for the years 1981 and 1982.

5.1.2 Simulation of the Open-Shaft Period

The drawdown cone caused by ground-water leakage into the open shafts during 1982 through 1985 (Appendix G, Section G.2.2) has been observed at H-1, H-2, and to a lesser extent at H-3. The drawdown caused by the open shafts would also have been observed at the wells WIPP-21, WIPP-22, WIPP-19, and WIPP-18 if they had been recompleted in the Culebra before 1985. In general, the calculated transient heads are about 10 m lower than the observed heads (Figure 5.1a) indicating that the transmissivity and/or storativity distribution in the vicinity of the shafts must be modified to obtain a better agreement between the observed and the calculated transient head data. The effect of adjusting the model transmissivities and storativities on the calculated transient heads is demonstrated and discussed in Sections 5.2 and 5.3.

5.1.3 Simulation of the Shaft Leakage After Shaft Sealing

In summer 1985, the exhaust shaft was sealed (Appendix G). This reduced considerably the leakage of ground water from the Culebra into the shafts (Figure 5.2). The observed freshwater-head increase caused by the exhaust-shaft sealing is shown on the plot of calculated and measured transient freshwater heads for the shaft location (Figure 5.1g). The fluid-pressure recovery due to the sealing of the exhaust shaft can also be recognized at H-1 and H-2 (Figure 5.1a), but the head response is complicated by the recovery from the H-3 step-drawdown test. Thus, it is difficult to quantify the specific

response at H-1 and H-2 due to the shaft sealing in summer 1985. A response to the sealing of the exhaust shaft may have occurred at the DOE-1 and H-11 boreholes (Figures 5.1b and 5.1c). However, pumping at H-11 during the same period of the shaft sealing has made the identification of a shaft-sealing response in the observed transient data difficult. The recovery could have probably been identified at the WIPP wells north of the shaft locations if these wells had not been undergoing recompletion or recovering from recompletion.

5.1.4 Simulation of the H-2 Well Tests

The response to the hydrologic and tracer tests at H-2 during 1983 and 1984 were incorporated into the model as described in Appendix G, Section G.3.1. The production rates during the tests are shown in Figure 5.3. Compared to the other well tests incorporated into the transient simulation (Appendix G), these tests were only minor hydrologic stresses on the Culebra dolomite. Thus, the effects of the H-2 well tests are not pronounced at H-1 and H-3 (Figure 5.1a). The head data for H-2 display considerable scatter apparently as a result of both testing at H-2 and activities at the shafts and other hydropads. H-2 has also had a complicated density history which adds further scatter to the data. Therefore, it is difficult to assess whether or not the calculated response to the H-2 well tests adequately represents the actual response.

5.1.5 Simulation of the H-3 Convergent-Flow Tracer Test

The H-3 convergent-flow tracer test performed from April to June 1984 is discussed in Appendix G, Section G.3.2. The production rates during the H-3 convergent-flow tracer test are shown in Figure 5.3. The calculated drawdown at the H-3 hydropad in response to this test (Figure 5.1a) is twice the observed drawdown. This implies that 1) the calibrated transmissivity in the H-3 hydropad area is too low,

and/or 2) the storativity in the vicinity of the H-3 hydropad is greater than the storativity of 2×10^{-5} used in the model.

The calculated drawdowns in the spring of 1984 at H-1 and H-2 (Figure 5.1a) are approximately 6 m and 4 m, respectively. Because the observed drawdowns at those wells due to the H-3 convergent-flow tracer test cannot be easily identified due to the considerable scatter in the observed data, it is difficult to compare the calculated and observed responses. At H-11, the calculated drawdown cannot easily be compared against the observed because the observed heads are influenced by a prior pumping test conducted at the H-11 hydropad which was not included in the simulation (Figure 5.1b). At DOE-1, the calculated freshwater heads agree well with the observed data (Figure 5.1c).

5.1.6 Simulation of the H-3 Step-Drawdown Test

The H-3 step-drawdown test conducted in June and July 1985 is described in Appendix G, Section G.3.3. The production rates for the test are shown in Figure 5.3. Similar to the response observed for the convergent-flow tracer test, the calculated drawdown at the H-3 hydropad (Figure 5.1a) is twice the observed drawdown. The magnitude of the observed and calculated drawdowns at H-1 and H-2 are approximately the same (Figure 5.1a).

As with the convergent-flow tracer test, the step-drawdown test caused small responses at DOE-1 and H-11. In both wells, the calculated and observed drawdowns are in good agreement. However, the calculated recovery is much slower than the observed. This indicates that the model transmissivities between H-3 and DOE-1 and between H-3 and H-11 are probably adequate and that other factors are causing the differences.

5.1.7 Simulation of the H-3 Multipad Pumping Test

The H-3 multipad pumping test conducted from October through December 1985 is discussed in Appendix G, Section G.3.4. The pumping rates are shown in Figure 5.3 and the calculated and observed transient responses at the H-1, H-2, and H-3 locations are illustrated in Figure 5.1a. The calculated drawdown at the H-3 hydropad is again two times greater than the observed drawdown in the pumping well H-3b2 (lowermost values of the H-3 hydrograph in Figure 5.1a). The observed data at H-1 and H-2 exhibit drawdown and recovery in response to the H-3 multipad test. At H-1, the observed and calculated drawdowns have about the same magnitude relative to the pretest fluid levels, while at H-2 the observed drawdown is somewhat larger than the calculated drawdown. In both wells, the observed recovery is slower than the calculated recovery. Unfortunately, reliable observed data for these wells are not available for the periods during the H-3 convergent-flow tracer test and the H-3 step-drawdown test. Therefore, it is difficult to identify whether the disagreement between H-1 and H-2 calculated and observed data from the H-3 multipad pumping test is caused by using non-representative model parameters such as transmissivity or by other hydrologic disturbances such as pressure changes in the shafts.

A response to the H-3 multipad pumping test was also observed at H-11 and DOE-1. The calculated drawdowns match the observed drawdowns quite well. However, as in the previous responses to H-3 testing, the calculated recovery at both wells is slower than the observed recovery.

The maximum drawdown observed during the H-3 multipad pumping test at WIPP-21 was 10 m (Figure 5.1e). The other WIPP wells in the vicinity of the shafts had drawdowns less than WIPP-21. Slow recoveries were also observed. The fluid densities in the WIPP wells in the vicinity of the shafts during the pumping and recovery periods of the H-3

multipad test are not well known. Therefore, in the following discussion only the relative changes in freshwater head are considered, rather than the absolute magnitudes of the freshwater heads.

A comparison of the relative changes in the calculated drawdowns and the observed changes in heads at WIPP-21, WIPP-22, and WIPP-19 shows that the responses to the H-3 multipad test calculated by the model were much smaller than those observed. The disagreement between the calculated and the observed data implies that either the model transmissivities used are not representative of the actual transmissivities, or that some other event caused the extent of drawdown at WIPP-21, WIPP-22, WIPP-19, and WIPP-18 to the north of the WIPP shafts. Considering that the observed drawdown at WIPP-21 is larger than that observed at H-1, a rather high permeability feature would be required between H-3 and WIPP-21 to produce such a response. At present, no data exist to support a postulated high-transmissivity feature between WIPP-21 and H-3. An alternative explanation of the WIPP-21 response is presented in the following paragraph.

Transducer measurements in the Culebra in the waste-handling shaft (Figure 5.1g) showed a sudden pressure drop during the H-3 multipad pumping test, similar to the observed water-level response at WIPP-21. The equivalent-freshwater-head drawdown at the waste-handling shaft is more than twice as large as the observed drawdown at H-1. Haug et al. (1987) proposed that during the H-3 multipad pumping test, additional leakage of ground water from the Culebra occurred in one of the shafts, thus causing the sudden pressure drop. This scenario was simulated in Haug et al. (1987) and was shown to improve the reproduction of the responses at the WIPP wells during the H-3 pumping test. Haug et al. (1987) concluded that the proposed additional leakage at one of the shafts could explain the observed responses in

WIPP-21, WIPP-22, and WIPP-19, and that it could account for the smaller calculated drawdowns and slower observed recoveries of H-1 and H-2. Implementation and further investigation of this hypothesis was not performed in the present modeling study.

5.1.8 Simulation of the H-4 Convergent-Flow Tracer Test

The convergent-flow tracer test at the H-4 hydropad conducted between October 1982 and October 1984 is described in Appendix G, Section G.3.5, and the pumping rates during the test are graphically shown in Figure 5.3. The calculated and the observed transient heads at the H-4 hydropad are illustrated in Figure 5.1b. The calculated drawdown during the H-4 convergent-flow tracer test is approximately two times greater than the observed drawdown in the observation wells (H-4a, H-4b), while the observed drawdown in the pumped well (H-4c) was much larger. The calculated rate of recovery, however, appears to agree with the observed. This comparison of calculated and observed responses to the H-4 tracer test indicates that the model transmissivities employed in the area of the H-4 hydropad are generally lower than the actual transmissivities. Because of the low transmissivities in the vicinity of H-4, the H-4 hydropad was the only location that responded to the pumping during the H-4 convergent-flow tracer test.

5.1.9 Simulation of the WIPP-13 Multipad Pumping Test

The WIPP-13 pumping test conducted from January to February 1987 is described in Appendix G, Section G.3.6. The pumping rates used in the model are illustrated in Figure 5.3. The calculated and observed drawdowns at WIPP-13 are shown in Figure 5.1d. The calculated drawdown is approximately twice the observed drawdown, implying that the steady-state calibrated transmissivity at WIPP-13 is probably too low.

The calculated drawdowns at the H-6, DOE-2, and P-14 boreholes are illustrated in Figures 5.1b and 5.1c. The relative magnitudes and timing of the calculated drawdowns and recoveries compare well with the observed transient freshwater heads at these locations. This implies that the calibrated transmissivities between these boreholes and WIPP-13 are probably close to the actual transmissivities.

Wells WIPP-12, WIPP-18, WIPP-19, WIPP-21, WIPP-22, WIPP-30, and ERDA-9 also responded to the pumping at WIPP-13. The calculated and observed transient freshwater heads at these locations are shown in Figures 5.1d and 5.1e. The calculated drawdowns are generally much lower than the observed drawdowns at these locations. For example, the maximum observed drawdowns at WIPP-12 and ERDA-9 are approximately 8 m and 1 m, respectively. The calculated drawdown at WIPP-12, however, is about 2 m and there was no identifiable calculated drawdown at ERDA-9, implying that the actual transmissivity and storativity distributions between WIPP-13 and the other WIPP wells are different from those used in the model. The calibrated steady-state model transmissivities surrounding the WIPP wells nearest to the shafts are approximately 5×10^{-7} m^2/s. These relatively low transmissivities form a barrier to flow which reduces the magnitude of the responses at these wells due to pumping at WIPP-13. This causes the calculated responses to be lower than the observed responses. It is also possible that a local feature with transmissivities similar to those at WIPP-13 with a storativity lower than 2×10^{-5} exists between WIPP-13 and the WIPP wells just north of the shafts.

5.2 Sensitivity of the Transient Calculated Freshwater Heads to Transmissivity

A detailed calibration of the model to the observed transient freshwater-head data was not possible due to time constraints. Section 5.1 indicates that adjustments to the transmissivities and

storativity used in the steady-state calibrated model are needed to reproduce the transient responses. To determine the effect that general changes in the transmissivity or storativity have on the calculated transient freshwater heads, several additional transient simulations were performed. The sensitivity of the calculated freshwater heads to model transmissivities is presented in this section, while the sensitivity of the calculated transient freshwater heads to changes in model storativities is presented in Section 5.3.

Two simulations were performed in which the steady-state calibrated transmissivities were changed by a constant factor over the entire model area. The fit of the steady-state calibrated model to the undisturbed heads was maintained because the calculated head distribution for the steady-state model remains the same when the boundary conditions are fixed and the transmissivities are globally changed by a constant factor. In the first simulation, hereafter referred to as T-case 1, a global multiplier of 2 was applied to the grid-block transmissivities of the calibrated steady-state model. This increases the ability of the model to transmit flow from one grid block to another. The second simulation, T-case 2, used a global transmissivity factor of 0.5 which reduced the ability of the model to transmit flow.

Both of these global changes in the model transmissivities caused changes in the hydraulic connection in the area around the shaft which affected the flux of ground water draining from the Culebra into the shaft. To maintain the Culebra pressure observed at the shaft, the flux must increase if the transmissivity increases. Conversely, the flux into the shaft will decrease if the global model transmissivity decreases. The calculated transient freshwater heads determined in T-case 1 and T-case 2 are shown in Figures 5.4a through 5.4k. These sensitivity simulations show, in general, that doubling the transmissivity over the entire model improved the fit between the calculated and observed drawdown at the various pumping wells included

in the transient simulation (H-2, H-3, H-4, and WIPP-13). Conversely, a 50% decrease in the transmissivities (T-case 2) resulted in a poorer fit between the calculated and observed drawdowns at the pumping wells.

5.2.1 Sensitivity of the Shaft-Induced Responses to Transmissivity

The simulation of the shaft pressure history during construction showed that the filling of the C & SH shaft with brine produced greater drawdowns and higher recoveries than calculated by the steady-state model at boreholes H-1, H-2, and H-3 (Figures 5.4a, 5.4b, and 5.4c) when the transmissivities between the shaft and these wells were increased, and lower drawdowns and recoveries when the transmissivities were reduced. The response of the shafts' grid block during this time period was determined by a series of pressure-controlled events which are different from rate-controlled events (Appendix G).

During the early shaft history, the higher transmissivities used in T-case 1 resulted in a larger flux of ground water entering the shaft from the formation and an increase in the hydraulic connection between the shaft and H-1, H-2, and H-3. This increase in hydraulic connection increased the distance to which the pressures prescribed at the shaft were transmitted. When the global transmissivities were decreased, the flux and the hydraulic connection between H-1, H-2, and H-3 and the shaft were also decreased, thus reducing the calculated responses. The calculated response at H-1 to the shaft pressure history using lower transmissivities, T-case 2, was much closer to the observed response. However, the calculated response at H-2 and H-3 in the initial or "base-case" transient simulation is better than the results determined in T-case 1 or T-case 2.

The open-shaft period (1982-1985) and the recovery period after the sealing of the exhaust shaft (July 1985) also proved to be sensitive to global changes in transmissivity. The calculated responses

determined in T-case 1 produce a better fit to the observed data. More adjustments to the hydrogeologic parameters of the model will be needed to reduce the differences between the calculated and observed responses in the vicinity of the shaft and extending to H-1, H-2, and H-3.

5.2.2 Sensitivity of the Calculated Responses from the H-3 Tests to Transmissivity

The calculated and observed transient freshwater heads for the base-case transient simulation and the two sensitivity simulations, T-case 1 and T-case 2, at the H-3 hydropad are shown in Figure 5.4c. The calculated drawdown at H-3 for T-case 1 agrees well with the observed drawdown during the H-3 convergent-flow tracer test and the H-3 step-drawdown test but is slightly less than the observed drawdown during the H-3 multipad pumping test. There is good agreement between the calculated responses and the observed responses during the recovery period of both of these tests. Conversely, lower global transmissivities produced a poorer agreement between calculated and observed responses than was determined for the base-case transient simulation.

The calculated responses at the H-1 and H-2 boreholes to the H-3 tests were significantly altered by variations in the assigned transmissivities. The absolute magnitudes of the drawdowns at H-1 and H-2 were increased when the transmissivities were lowered and reduced when the transmissivities were raised. For H-1 and H-2, the best fit to the observed relative drawdown and recovery rate was generally obtained in the base-case simulation. This implies that the calibrated transmissivities between H-1, H-2, and H-3 are probably representative and that the calculated responses at the H-1 and H-2 boreholes can be improved by reducing the large drawdown caused by the shafts.

The calculated responses for the base-case and sensitivity simulations for the H-11 and DOE-1 boreholes are shown in Figures 5.4f and 5.4g. At both locations, a factor of two increase in the global transmissivities improved both the calculated drawdown and the calculated recovery for the time period after April 1984 in response to the H-3 tests. Therefore, the model transmissivities between H-3, DOE-1, and H-11 are slightly lower than necessary to reproduce the observed transient responses.

5.2.3 Sensitivity of the Calculated Responses from the H-4 Test to Transmissivity

The calculated and observed responses during the H-4 convergent-flow tracer test for the base-case transient simulation and the two sensitivity simulations are shown in Figure 5.4d. The best fit of the calculated responses to the observed responses occurred when the global transmissivities were two times the base-case transmissivities. The calculated freshwater head values are also much closer to the observed head values than for the base case. Thus, the model transmissivities in the H-4 area are slightly lower than necessary to reproduce the observed transient responses.

5.2.4 Sensitivity of the Calculated Responses from the WIPP-13 Pumping Test to Transmissivity

In the base-case transient simulation, the calculated drawdown at WIPP-13 during the WIPP-13 multipad pumping test was approximately twice the observed drawdown. An increase in the global model transmissivities by a factor of two significantly reduced the difference between the calculated and the observed drawdowns as shown on Figure 5.4j. Alternatively, in the T-case 2 simulation, Figure 5.4j shows that multiplying the global transmissivity by 0.5 created a greater calculated drawdown and delayed recovery at WIPP-13.

The calculated drawdown of H-6 best represents the observed drawdown when the global transmissivities are decreased by 50 percent (Figure 5.4e). The calculated drawdown at DOE-2 was improved from the base case when the global transmissivities were decreased by a factor of two (Figure 5.4h). However, the calculated recovery at DOE-2 is closer to the observed recovery using the base-case transmissivities.

The calculated responses at WIPP-12, WIPP-18, WIPP-19, WIPP-21, and WIPP-22 were not significantly improved by either of the global changes to the transmissivity field. Figures 5.4i and 5.4k show the calculated responses at WIPP-12 and WIPP-22 as examples of the simulations at these wells. At both wells, the difference between the calculated and observed freshwater heads is reduced by increasing the global transmissivity. Because drawdowns during the WIPP-13 pumping test were not adequately simulated at these wells, future modeling studies will require additional local changes to the hydrogeologic parameters to improve the simulated responses at these locations.

5.3 Sensitivity of the Transient Calculated Freshwater Heads to Storativity

The storativity used in the initial or base-case transient simulation was 2×10^{-5}. Two transient simulations were performed to determine the sensitivity of the calculated freshwater heads to storativity. In these simulations, the transmissivity distribution was the same as for the base-case or calibrated steady-state model. In the first simulation, S-case 1, the storativity was increased to 5×10^{-5}. The storativity used in the second simulation, S-case 2, is 1×10^{-5}. The magnitude of the global changes in the storativity are approximately the same as the global changes to the transmissivities used in the sensitivity analysis of transmissivity described in Section 5.2.

5.3.1 Sensitivity of the Shaft-Induced Responses to Storativity

Reducing the storativity by one-half yielded approximately the same pressure response at the shaft grid block as increasing the transmissivity by a factor of two. The differences between the calculated and observed responses at H-1, H-2, and H-3 due to shaft events (Figures 5.5a, 5.5b, and 5.5c) in the S-case 1 and S-case 2 simulations are not significantly different than the results determined in the T-case 2 and T-case 1 simulations, respectively. Therefore, local changes to both the transmissivity and storativity will have to be made to reduce the differences between the calculated and observed responses.

5.3.2 Sensitivity of the Calculated Responses from the H-3 Tests to Storativity

The calculated and observed freshwater heads for the sensitivity simulations, S-case 1 and S-case 2, at the H-3 hydropad are illustrated in Figure 5.5c. As expected, the changes in storativity did not affect the results as much as the changes in the transmissivity. Generally, using a higher storativity reduced the drawdowns determined in the base-case simulation by approximately 6 to 10 m during the various tests at H-3. Alternatively, using a lower storativity increased the calculated drawdowns in the base-case simulations by 4 m to 6 m. In general, the higher storativity improved the comparison between the calculated and observed responses to post-1984 testing activities at H-3.

Figures 5.5a and 5.5b show the S-case 1 and S-case 2 simulations for the H-1 and H-2 boreholes. The base-case storativity produced the best relative drawdown at H-1. However, a lower storativity reduced the difference between the calculated and observed drawdowns at H-2. Using a storativity of 1.5×10^{-5} between H-3 and H-2 will probably

reproduce the observed relative drawdown given the same base-case transmissivity between these boreholes (approximately 1×10^{-6} m^2/s). This storativity value is slightly lower than the value of 3×10^{-5} that was determined by Beauheim (1987a) in interpreting the response at H-2 due to pumping at H-3. This is partly because the model transmissivities between H-2 and H-3 are slightly different than the average value he reported.

The calculated responses at H-11 and DOE-1 to the tests at H-3 in the S-case 2 storativity simulation contain slightly higher calculated drawdowns than the base-case simulations as shown on Figures 5.5f and 5.5g. The results indicate that a storativity between the S-case 2 and the base-case storativity in the vicinity of the 2 wells is probably necessary to simulate the observed drawdowns at these wells. The simulation using the higher global transmissivity, T-case 1, provided the best match to the recovery data at both of these locations (Figures 5.4f and 5.4g).

5.3.3 Sensitivity of the Calculated Responses from the H-4 Test to Storativity

Adjustments to the global storativity did not significantly reduce the differences between the calculated and observed transient freshwater heads in the vicinity of the H-4 hydropad. An increase in storativity (Figure 5.5d) did reduce the drawdown during the H-4 convergent-flow tracer test, but the reduction in calculated drawdown was not as great as that calculated using an increased global transmissivity (Figure 5.4d). Increases in both the transmissivity and the storativity may be needed to reproduce the transient heads at the H-4 hydropad adequately.

5.3.4 Sensitivity of the Calculated Responses from the WIPP-13 Pumping Test to Storativity

In the base-case simulation, the maximum calculated drawdown at WIPP-13 was approximately 20 m greater than the observed drawdown. Increasing the global storativity to 5×10^{-5} lowered this difference to approximately 15 m, whereas decreasing the global storativity increased the difference to about 22 m (Figure 5.5j). In contrast, a decrease in the global storativity improved the calculated results at H-6, DOE-2, WIPP-12, WIPP-18, WIPP-19, WIPP-21, and WIPP-22.

Figures 5.5e, 5.5h, 5.5i, and 5.5k show the calculated and observed transient responses at H-6, DOE-2, WIPP-12, and WIPP-22. Significant reductions in the differences between the calculated and observed responses are obtained at these locations using a lower storativity. In the T-case 1 and T-case 2 simulations (Section 5.2), the changes to the global transmissivities did not significantly improve the results at these boreholes. Only minor improvements resulted when the transmissivity was increased by a factor of two. Therefore, in order to reproduce the observed drawdowns during the WIPP-13 pumping test at these boreholes, the transmissivity should be further increased and the storativity should be decreased.

5.4 Summary of Transient Simulations

In the base-case transient simulations, the calculated drawdowns at the pumping wells H-2, H-3, H-4, and WIPP-13, are a factor of two greater than the observed drawdowns. The calculated drawdowns at H-1, H-2, and H-3, due to the hydraulic stresses caused by shaft events, are also a factor of two greater than the observed drawdown. The calculated drawdowns at P-14, DOE-2, and H-6 in response to the WIPP-13 pumping test adequately reproduce the observed drawdowns. The calculated drawdowns at H-11 and DOE-1 due to the H-3 pumping test are also similar to the observed drawdowns at these boreholes.

Sensitivity simulations were performed to determine the effect of the magnitude of the model transmissivities and storativity on the calculated transient freshwater heads. The simulations demonstrate that higher transmissivities are needed at H-2, H-3, H-4, and WIPP-13. In addition, lower transmissivities are necessary between the shafts and H-1, H-2, and H-3, and a higher transmissivity, low-storativity zone is required between WIPP-13 and the WIPP wells in the vicinity of the shafts to reproduce the observed transient responses.

6.0 CONCLUSIONS

The advent of new hydrogeologic data from testing at the WIPP-site boreholes has enlarged the hydrogeologic data base used in hydrologic-characterization studies of the WIPP-site area. The purpose of this second interim modeling report is to provide an updated numerical simulation of the ground-water flow in the Culebra dolomite based on the hydrogeologic data base as of November 1987. The main conclusions are presented below.

(1) The calibrated transmissivity distribution contains the same general trend over the model area as the observed transmissivities with predominantly lower transmissivities ($<1 \times 10^{-7}$ m^2/s) east of the WIPP-site boundary, intermediate transmissitivities in the central part of the model area (1×10^{-6} to 1×10^{-4} m^2/s) and high transmissivities ($>1 \times 10^{-3}$ m^2/s) in the western part of the model area representing Nash Draw. Local differences to the general trend are present west of WIPP-30 and WIPP-26 and between H-17 and P-17. The transmissivities in these areas were increased to reduce the differences between the calculated and observed heads below the uncertainties of the observed heads. The high-transmissivity feature between H-17 and P-17 is less transmissive than a similar feature proposed in Haug et al. (1987).

(2) The steady-state calibrated freshwater heads illustrate low hydraulic gradients (1×10^{-4} m/m) north of the WIPP-site boundary between WIPP-28 and DOE-2 and south of the WIPP-site boundary between H-17 and H-7. Higher gradients (4×10^{-3} m/m) occur in the central part of the model area.

(3) The model-calculated ground-water-flow directions are predominantly south to southwest. The largest volume of ground water enters the model area through the northern model boundary

and enters the high-transmissivity area along the western part of the model representing Nash Draw. A significant portion of the ground water within the WIPP-site boundaries passes through the high-transmissivity zone south of H-11 and exits the southern boundary of the model area east of H-7. The model-calculated flow directions support conclusions from previous modeling and isotopic studies that the ground-water chemistry is not at steady state with respect to ground-water flow.

(4) The calculated Darcy velocities range over six orders of magnitude in the model area. The highest velocities (1×10^{-7} to 1×10^{-6} m/s) occur in the western portion of the model area representing Nash Draw. Darcy velocities within the WIPP-site boundary range from approximately 5×10^{-10} m/s in the vicinity of the shafts to 1×10^{-9} m/s in the high-transmissivity zone south of H-11. Darcy velocities of 1×10^{-12} m/s occur east of the WIPP-site boundary.

(5) A sensitivity analysis of the calculated freshwater heads to the high-transmissivity zone between H-17 and P-17 determined that differences between the calculated and observed heads in the vicinity of H-11 ranged from 3 to 8 m with transmissivity values between H-17 and P-17 (2×10^{-6} m^2/s) three times higher than those in the initial kriged estimates (6×10^{-7} m^2/s). The differences were reduced to less than six meters when the transmissivity values between H-17 and P-17 were increased to 6×10^{-6} m^2/s, one order of magnitude higher than the initial kriged estimates. The differences were ultimately reduced below the uncertainties of the observed heads when the transmissivities between H-17 and P-17 were increased to 5×10^{-5} m^2/s.

(6) The steady-state calibrated transmissivities adequately reproduce the observed drawdowns at P-14, DOE-2, and H-6 during the WIPP-13 multipad pumping test. The calculated drawdowns at H-11 and DOE-1

during the simulation of the H-3 multipad pumping test are also similar to the observed drawdowns. The steady-state calibrated transmissivities do not adequately reproduce the observed transient responses generated from the shaft events or the observed drawdowns at the pumping wells used in the simulation, H-2, H-3, H-4, and WIPP-13. Generally, the calculated drawdown at these wells is a factor of two greater than the observed drawdown. Similarly, the calculated drawdown due to the shaft events is a factor of two greater than the observed drawdown at H-1, H-2, and H-3.

(7) Sensitivity analyses performed to determine the effects of the model transmissivities and storativity upon the calculated transient heads indicate that adjustments to the steady-state calibrated transmissivities are necessary to reduce the differences between the calculated and observed transient data. These analyses indicate (1) lower transmissivities are required between the shafts and H-1, H-2, H-3, and the WIPP wells in the vicinity of the shafts; (2) higher transmissivities are necessary in the vicinity of H-2, H-3, H-4, and WIPP-13; and (3) a higher transmissivity, low-storativity zone between WIPP-13 and the WIPP wells in the vicinity of the shafts is necessary to reproduce the observed transient responses.

7.0 BIBLIOGRAPHY

Andrews, R.W., A.M. LaVenue, B.M. Thompson, and J.E. Campbell, 1987. Application of Uncertainty Analysis Techniques to Address NRC Travel Time Performance Measures at a Potential HLW Disposal Site in Deaf Smith County, Texas. NWWA Proceedings from Solving Ground Water Problems with Models, Vol. 1., February, 1987. Denver, Colorado.

Bachman, G.O., 1980. Regional Geology and Cenozoic History of Pecos Region, South-eastern, New Mexico. U.S. Dept. of the Interior Geological Survey, Open-File Report 80-1099, 116 p.

Bachman, G.O., 1985. Assessment of Near-Surface Dissolution at and Near the Waste Isolation Pilot Plant (WIPP), Southeastern New Mexico. Sandia National Laboratories, Contractor Report SAND84-7178, 33 p.

Bachman, G.O., 1987. Karst Evaporites in Southwestern New Mexico. Sandia National Laboratories, SAND86-7078, 82 p.

Barr, G.E., W.B. Miller, and D.D. Gonzalez, 1983. Interim Report on the Modeling of the Regional Hydraulics of the Rustler Formation. Sandia National Laboratories, SAND83-0391, 58 p.

Bear, J., and C. Braester, 1972. Simultaneous flow of immiscible liquids in a fractured medium, in Fundamentals of Transport Phenomena in Porous Media, Developments in Soil Sciences, 2, International Association for Hydraulic Research, Elsevier Publishing Company, Amsterdam, p. 177-202.

Beauheim, R.L., 1986. Hydraulic-Test Interpretations for Well DOE-2 at the Waste Isolation Pilot Plant (WIPP) Site. Sandia National Laboratories, SAND86-1364, 89 p.

Beauheim, R.L., 1987a. Analysis of Pumping Tests of the Culebra Dolomite Conducted at the H-3 Hydropad at the Waste Isolation Pilot Plant (WIPP) Site. Sandia National Laboratories, SAND86-2311, 154 p.

Beauheim, R.L., 1987b. Interpretations of Single-Well Hydraulic Tests Conducted at and Near the Waste Isolation Pilot Plant (WIPP) Site, 1983-1987. Sandia National Laboratories, SAND87-0039.

Beauheim, R.L., 1987c. Interpretation of the WIPP-13 Multipad Pumping Test of the Culebra Dolomite at the Waste Isolation Pilot Plant (WIPP) Site. Sandia National Laboratories, SAND87-2456.

Chapman, J.B., 1986. Stable Isotopes in the Southeastern New Mexico Groundwater: Implications for Dating Recharge in the WIPP Area. New Mexico Environmental Evaluation Group, EEG-35, 76 p.

Chaturvedi, L. and K. Rehfeldt, 1984. Groundwater occurrence and the dissolution of salt at the WIPP radioactive waste repository site. American Geophysical Union, EOS, July 3, 1984, p. 457-459.

Chaturvedi, L. and J.K. Channell, 1985. The Rustler Formation as a Transport Medium for Contaminated Groundwater. New Mexico Environmental Evaluation Group, EEG-32, 85 p.

Cole, C.R. and F.W. Bond, 1980. Assessment of Effectiveness of Geologic Isolation Systems: Comparison of INTERA and WISAP Consequence Model Application. Report prepared by Pacific Northwest Laboratory for Office of Nuclear Waste Isolation under contract to U.S. Department of Energy, PNL-3070, UC-70, 50 p.

Cooper, J.B., 1962. Ground-Water Investigations of the Project Gnome Area, Eddy and Lea Counties, New Mexico. U.S. Geological Survey TEI-802, Open-File Report, 67 p., 17 Figures.

Cooper, J.B. and V.M. Glanzman, 1971. Geohydrology of Project Gnome Site, Eddy County, New Mexico. U.S. Geological Survey, Professional Paper 712-A, 28 p.

Core Laboratories, Inc., 1986. Special Core Analysis Study for INTERA Technologies, WIPP Site, File Number: SCAL 203-850073, Core Laboratories Inc., Aurora, Colorado.

Craig, H., 1961. Standard for reporting concentrations of deuterium and oxygen-18 in natural waters. Science, V. 133, p. 1833-1834.

Crawley, M.E., 1987. Second Data Release Report for the Pressure-Density Survey Program. Prepared by IT Corporation. DRAFT.

Crawley, M.E., in preparation. Third Data Release Report for the Pressure-Density Survey Program. Prepared by IT Corporation. DRAFT.

D'Appolonia Consulting Engineers, Inc., 1980. Modeling Verification Studies: Long-Term Waste Isolation Assessment. Report prepared for Westinghouse Electric Corporation under contract to U.S. Department of Energy.

Davies, P.B., 1987. Modeling Areal, Variable-Density, Ground-Water Flow Using Equivalent Freshwater Head -- Analysis of Potentially Significant Errors. NWWA Proceedings from Solving Ground Water Problems with Models, Vol. 2., February, 1987. Denver, Colorado.

Davies, P.B., 1988. Variable-Density Ground-Water Flow and Paleohydrology in the Region Surrounding the Waste Isolation Pilot Plant (WIPP), Southeastern New Mexico. U.S. Geological Survey, Water-Resources Investigations.

de Marsily, G., 1983. Interpretation of Interference Tests in a Well Field Using Geostatistical Techniques to Fit the Permeability Distribution in a Reservoir Model. Second NATO Advanced Study Inst., GEOSTAT 1983 - Tahoe, CA.

de Marsily, G., 1986. Quantitative Hydrogeology. Academic Press, Inc., Orlando, Florida, 440 p.

Dennehy, K.F., 1982. Results of Hydrologic Tests and Water-Chemistry Analysis, Wells H-6a, H-6b, and H-6c at the Proposed Waste Isolation Pilot Plant Site, Southeastern New Mexico. U.S. Geological Survey, Water-Resources Investigations 82-8, 68 p.

Dennehy, K.F. and J.W. Mercer, 1982. Results of Hydrologic Tests and Water-Chemistry Analysis, Wells H-5a, H-5b, and H-5c at the Proposed Waste Isolation Pilot Plant Site, Southeastern New Mexico. U.S. Geological Survey, Water-Resources Investigations 82-19, 83 p.

Epstein, S., R.P. Sharp, and A.J. Gow, 1965. Six-year record of oxygen and hydrogen isotope variations in South Pole firn. Jour. Geophys. Res., V. 70, p. 1809-1814.

Epstein, S., R.P. Sharp, and A.J. Gow, 1970. Antarctic ice sheet: Stable isotope analyses of Byrd station cores and interhemispheric climatic implications. Science, V. 168, p. 1570-1572.

Evans, G.V., R.L. Otlet, R.A. Downing, R.A. Monkhouse, and G. Rae, 1979. Some problems in the interpretation of isotope measurements in United Kingdom aquifers, in Proceedings of the International Symposium of Isotope Hydrology, STI/PUB/493, V. 2.

Fenix and Scisson, Inc., 1982. SPDV Exploratory Shaft Hole History; Albuquerque, New Mexico. Consultants report prepared for the U.S. Department of Energy, 37 p.

Freeze, R.A., and J.A. Cherry, 1979. Groundwater. Prentice-Hall, Inc., Englewood Cliffs, New Jersey, 604 p.

Gonzalez, D.D., 1983a. Groundwater Flow in the Rustler Formation, Waste Isolation Pilot Plant (WIPP), Southeast New Mexico (SENM): Interim Report. Sandia National Laboratories, SAND82-1012, 39 p.

Gonzalez, D.D., 1983b. Hydrogeochemical Parameters of Fluid-Bearing Zones in the Rustler and Bell Canyon Formations: Waste Isolation Pilot Plant (WIPP) Southeastern New Mexico (SENM). Sandia National Laboratories, SAND83-0210, 37 p.

Haug, A., V.A. Kelley, A.M. LaVenue, and J.F. Pickens, 1987. Modeling of Ground-Water Flow in the Culebra Dolomite at the Waste Isolation Pilot Plant (WIPP) Site: Interim Report, Sandia National Laboratories, Contractor Report SAND86-7167.

Holt, R.M. and D.W. Powers, 1984. Geotechnical Activities in the Waste Handling Shaft, Waste Isolation Pilot Plant (WIPP) Project Southeastern New Mexico. U.S. Department of Energy, WTSD-TME-038.

Hydro Geo Chem, Inc., 1985. WIPP Hydrology Program, Waste Isolation Pilot Plant, SENM, Hydrologic Data Report #1. Sandia National Laboratories, Contractor Report SAND85-7206, 710 p.

INTERA Technologies, Inc., 1986. WIPP Hydrology Program, Waste Isolation Pilot Plant, SENM, Hydrologic Data Report #3. Sandia National Laboratories, Contractor Report SAND86-7109.

INTERA Technologies, Inc. and Hydro Geo Chem, Inc., 1985. WIPP Hydrology Program, Waste Isolation Pilot Plant, SENM, Hydrologic Data Report #2. Sandia National Laboratories, Contractor Report SAND85-7263.

IT Corporation, 1987. Initial Data Release Report for the Pressure-Density Survey Program. Prepared by IT Corporation. DRAFT.

Izette, G.A. and R.E. Wilcox, 1982. Map Showing Localities and Inferred Distributions of the Huckleberry Ridge, Mesa Falls and Lava Creek Ash Beds (Pearlette Family Ash Beds) of Pliocene and Pleistocene Age in the Western United States and Southern Canada. U.S. Geological Survey, Miscellaneous Investigations Series Map I-1325.

Jarolimek, L., M.J. Timmer, and D.W. Powers, 1983. Correlation of Drillhole and Shaft Logs, Waste Isolation Pilot Plant (WIPP) Project, Southeastern New Mexico. U.S. Department of Energy, TME 3179.

Jones, C.L., 1973. Salt Deposits of Los Medanos Area, Eddy and Lea Counties, New Mexico. U.S. Geological Survey, Open-File Report 4339-7, 67 p.

Jones, C.L., 1975. Potash Resources in Part of Los Medanos Area of Eddy and Lea Counties, New Mexico. U.S. Geological Survey, Open-File Report 75-407, 37 p.

Jones, C.L., 1978. Test Drilling for Potash Resources: Waste Isolation Pilot Plant Site, Eddy County, New Mexico. U.S. Geological Survey, Open-File Report 78-592, V. 1 & 2, 431 p.

Kafritsas, J. and R.L. Bras, 1981. The practice of kriging, Technical Report 263, Ralph M. Parsons Lab., Mass, Inst. of Technol., Cambridge, 107 p.

Kelley, V.A. and J.F. Pickens, 1986. Interpretation of the Convergent-Flow Tracer Tests Conducted in the Culebra Dolomite at the H-3 and H-4 Hydropads at the Waste Isolation Pilot (WIPP) Site. Sandia National Laboratories, Contractor Report SAND86-7161.

Kuchling, H., 1982. Taschenbuch der Physik. Verlag Harri Deutsch, Thun und Frankfurt, 678 p.

Lambert, S.J., 1987. Feasibility Study: Applicability of Geochronologic Methods Involving Radiocarbon and Other Nuclides to the Groundwater Hydrology of the Rustler Formation. Sandia National Laboratories, SAND86-1054.

Lambert, S.J. and J.A. Carter, 1987. Uranium-Isotope Systematics in Groundwaters of the Rustler Formation, Northern Delaware Basin, Southeastern New Mexico. Sandia National Laboratories, SAND87-0388.

Lambert, S.J. and D.M. Harvey, 1987. Stable Isotope Geochemistry of Groundwaters in the Delaware Basin of Southeastern New Mexico. Sandia National Laboratories, SAND87-0138.

Langguth, H.-R., and Voigt, R., 1980. Hydrogeologische Methoden, Springer-Verlag, New York, 486 p.

Lerman, A., 1979. Geochemical Processes. John Wiley and Sons, New York, 481 p.

Lowenstein, T.K., 1987. Post Burial Alteration of the Permian Rustler Formation Evaporites, WIPP Site, New Mexico: Textural, Stratigraphic and Chemical Evidence. New Mexico Environmental Evaluation Group, EEG-36, 56 p.

Mercer, J.W., 1983. Geohydrology of the Proposed Waste Isolation Pilot Plant Site, Los Medanos Area, Southeastern New Mexico. U.S. Geological Survey, Water-Resources Investigations 83-4016, 113 p.

Mercer, J.W., R.L. Beauheim, R.P. Snyder, and G.M. Fairer, 1987. Basic Data Report for Drilling and Hydrologic Testing of Drillhole DOE-2 at the Waste Isolation Pilot Plant (WIPP) Site. Sandia National Laboratories, SAND86-0611.

Mercer, J.W., P. Davis, K.F. Dennehy, and C.L. Goetz, 1981. Results of Hydrologic Tests and Water-Chemistry Analyses, Wells H-4a, H-4b, and H-4c at the Proposed Waste Isolation Pilot Plant Site, Southeastern New Mexico. U.S. Geological Survey, Water-Resources Investigations 79-98, 178 p.

Mercer, J.W. and B.R. Orr, 1977. Review and Analysis of Hydrogeologic Conditions Near the Site of a Potential Nuclear-Waste Repository, Eddy and Lea Counties, New Mexico. U.S. Geological Survey, Open-File Report 77-123, 35 p.

Mercer, J.W. and B.R. Orr, 1979. Interim Data Report on the Geohydrology of the Proposed Waste Isolation Pilot Plant Site Southeast New Mexico. U.S. Geological Survey, Water-Resources Investigations 79-98, 178 p.

Niou, S. and J. Pietz, 1987. A Statistical Inverse Analysis of the H-3 Hydropad Pumping Test. Report prepared by IT Corporation, Inc. for Westinghouse Electric Corporation.

Powers, D.W., S.J. Lambert, S.E. Shaffer, L.R. Hill, and W.D. Weart, editors, 1978. Geologic Characterization Report, Waste Isolation Pilot Plant (WIPP) Site, Southeastern New Mexico. Volumes I and II. Sandia National Laboratories, SAND78-1596.

Powers, D.W., and R.M. Holt, 1984. Depositional environments and dissolution in the Rustler Formation (Permian), southeastern New Mexico. (Abs.) Geol. Soc. Amer., 97th Annual Meeting Abstracts with Program, V. 16, No. 6, p. 627.

Reeves, M. V.A. Kelley, and J.F. Pickens, 1987. Regional Double-Porosity Solute Transport in the Culebra Dolomite: An Analysis of Parameter Sensitivity and Importance at the Waste Isolation Pilot Plant (WIPP) Site. Sandia National Laboratories, SAND87-7105, 68 p.

Reeves, M., D.S. Ward, N.D. Johns, and R.M. Cranwell, 1986a. Theory and Implementation for SWIFT II, the Sandia Waste-Isolation Flow and Transport Model, Release 4.84. Sandia National Laboratories, NUREG/CR-3328 and SAND83-1159, 189 p.

Reeves, M., D.S. Ward, N.D. Johns, and R.M. Cranwell, 1986b. Data Input Guide for SWIFT II, the Sandia Waste-Isolation Flow and Transport Model for Fractured Media, Release 4.84. Sandia National Laboratories, NUREG/CR-3162 and SAND83-0242, 144 p.

Richey, S.F., 1987. Water-Level Data From Wells in the Vicinity of the Waste Isolation Pilot Plant, Southeastern New Mexico. U.S. Department of Energy, U.S. Geological Survey Open-File Report 87-120, 107 p.

Robinson, K.L., 1987. Analysis of Solutes in Groundwaters from the Rustler Formation at and Near the WIPP Site. Sandia National Laboratories, SAND86-0917.

Robinson, T.W. and W.B. Lang, 1938. Geology and Ground-Water Conditions of the Pecos River Valley in the Vicinity of Laguna Grande de la Sal, New Mexico. New Mexico State Engineer, 12th & 13th Biennial Reports, p. 77-100.

Sandia Laboratories and U.S. Geological Survey, 1979a. Basic Data Report for Drillhole WIPP 13 (Waste Isolation Pilot Plant - WIPP). Sandia Laboratories, SAND79-0273, 16 p.

Sandia Laboratories and U.S. Geological Survey, 1979b. Basic Data Report for Drillhole WIPP 25 (Waste Isolation Pilot Plant - WIPP). Sandia Laboratories,SAND79-0279, 26 p.

Sandia Laboratories and U.S. Geological Survey, 1979c. Basic Data Report for Drillhole WIPP 26 (Waste Isolation Pilot Plant - WIPP). Sandia Laboratories, SAND79-0280, 31 p.

Sandia Laboratories and U.S. Geological Survey, 1979d. Basic Data Report for Drillhole WIPP 27 (Waste Isolation Pilot Plant - WIPP). Sandia Laboratories, SAND79-0281, 20 p.

Sandia Laboratories and U.S. Geological Survey, 1979e. Basic Data Report for Drillhole WIPP 28 (Waste Isolation Pilot Plant - WIPP). Sandia Laboratories, SAND79-0282, 33 p.

Sandia Laboratories and U.S. Geological Survey, 1979f. Basic Data Report for Drillhole WIPP 29 (Waste Isolation Pilot Plant - WIPP). Sandia Laboratories, SAND79-0283, 19 p.

Sandia Laboratories and U.S. Geological Survey, 1980a. Basic Data Report for Drillhole WIPP 18 (Waste Isolation Pilot Plant - WIPP). Sandia Laboratories, SAND79-0275, 18 p.

Sandia Laboratories and U.S. Geological Survey, 1980b. Basic Data Report for Drillhole WIPP 19 (Waste Isolation Pilot Plant - WIPP). Sandia Laboratories, SAND79-0276, 27 p.

Sandia Laboratories and U.S. Geological Survey, 1980c. Basic Data Report for Drillhole WIPP 21 (Waste Isolation Pilot Plant - WIPP). Sandia Laboratories, SAND79-0277, 18 p.

Sandia Laboratories and U.S. Geological Survey, 1980d. Basic Data Report for Drillhole WIPP 22 (Waste Isolation Pilot Plant - WIPP). Sandia Laboratories, SAND79-0278, 21 p.

Sandia Laboratories and U.S. Geological Survey, 1980e. Basic Data Report for Drillhole WIPP 30 (Waste Isolation Pilot Plant - WIPP). Sandia Laboratories, SAND79-0284, 19 p.

Sandia National Laboratories, 1982. Simulated-Waste Experiments Planned for the Waste Isolation Pilot Plant (WIPP). Sandia National Laboratories, SAND82-0547, 62 p.

Sandia National Laboratories and D'Appolonia Consulting Engineers, 1982a. Basic Data Report for Drillhole WIPP 12 (Waste Isolation Pilot Plant - WIPP). Sandia National Laboratories, SAND82-2336, 62 p.

Sandia National Laboratories and D'Appolonia Consulting Engineers, 1982b. Basic Data Report for Deepening of Drillhole WIPP 13 (Waste Isolation Pilot Plant - WIPP). Sandia National Laboratories, SAND82-1880, 54 p.

Sandia National Laboratories and D'Appolonia Consulting Engineers, 1982c. Basic Data Report for Drillhole WIPP 14 (Waste Isolation Pilot Plant - WIPP). Sandia National Laboratories, SAND82-1783, 36 p.

Sandia National Laboratories and D'Appolonia Consulting Engineers, 1983a. Basic Data Report for Drillhole AEC 7 (Waste Isolation Pilot Plant - WIPP). Sandia National Laboratories, SAND79-0268, 96 p.

Sandia National Laboratories and D'Appolonia Consulting Engineers, 1983b. Basic Data Report for Drillhole AEC 8 (Waste Isolation Pilot Plant - WIPP). Sandia National Laboratories, SAND79-0269, 100 p.

Sandia National Laboratories and D'Appolonia Consulting Engineers, 1983c. Basic Data Report for Drillhole ERDA 10 (Waste Isolation Pilot Plant - WIPP). Sandia National Laboratories, SAND79-0271, 78 p.

Sandia National Laboratories and U.S. Geological Survey, 1980. Basic Data Report for Drillhole WIPP 32 (Waste Isolation Pilot Plant - WIPP). Sandia National Laboratories, SAND80-1102, 25 p.

Sandia National Laboratories and U.S. Geological Survey, 1981a. Basic Data Report for Drillhole WIPP 33 (Waste Isolation Pilot Plant - WIPP). Sandia National Laboratories, SAND80-2011, 27 p.

Sandia National Laboratories and U.S. Geological Survey, 1981b. Basic Data Report for Drillhole WIPP 34 (Waste Isolation Pilot Plant - WIPP). Sandia National Laboratories, SAND81-2643, 52 p.

Sandia National Laboratories and U.S. Geological Survey, 1982. Basic Data Report for Drillhole WIPP 11 (Waste Isolation Pilot Plant - WIPP). Sandia National Laboratories, SAND79-0272, 28 p.

Sandia National Laboratories and U.S. Geological Survey, 1983a. Basic Data Report for Drillhole ERDA 6 (Waste Isolation Pilot Plant - WIPP). Sandia National Laboratories, SAND79-0267, 64 p.

Sandia National Laboratories and U.S. Geological Survey, 1983b. Basic Data Report for Drillhole ERDA 9 (Waste Isolation Pilot Plant - WIPP). Sandia National Laboratories, SAND79-0270, 54 p.

Sandia National Laboratories and University of New Mexico, 1981. Basic Data Report for Drillhole WIPP 15 (Waste Isolation Pilot Plant - WIPP). Sandia National Laboratories, SAND79-0274, 31 p.

Saulnier, G.J., Jr., 1987. Analysis of Pumping Test of the Culebra Dolomite Conducted at the H-11 Hydropad at the Waste Isolation Pilot Plant (WIPP) Site. Sandia National Laboratories, Contractor Report SAND87-7124.

Saulnier, G.J., Jr., G.A. Freeze, and W.A. Stensrud, 1987. WIPP Hydrology Program, Waste Isolation Pilot Plant, Southeastern New Mexico, Hydrologic Data Report #4. Sandia National Laboratories, Contractor Report SAND86-7166.

Seward, P.D., 1982. Abridged Borehole Histories for the Waste Isolation Pilot Plant (WIPP) Studies. Sandia National Laboratories, SAND82-0080, 79 p.

Skrivan, J. and M. Karlinger, 1980. Semi-Variogram Estimation and Universal Kriging Program, U.S. Geological Survey Technical Report PB81-120560, 98 p.

Snyder, R.P., 1985. Dissolution of Halite and Gypsum, and Hydration of Anhydrite to Gypsum, Rustler Formation in the Vicinity of the Waste-Isolation Pilot Plant, Southeastern New Mexico. U.S. Geological Survey, Open-File Report 85-229, 11 p.

Stensrud, W.A., M.A. Bame, K.D. Lantz, A.M. LaVenue, J.B. Palmer, and G.J. Saulnier, Jr., 1987. WIPP Hydrology Program, Waste Isolation Pilot Plant, Southeastern New Mexico, Hydrologic Data Report #5. Sandia National Laboratories, Contractor Report SAND87-7125.

Stensrud, W.A., M.A. Bame, K.D. Lantz, T.L. Caufman, J.B. Palmer, and G.J. Saulnier, Jr., 1988. WIPP Hydrology Program, Waste Isolation Pilot Plant, Southeastern New Mexico, Hydrologic Data Report #6. Sandia National Laboratories, Contractor Report SAND87-7166.

Stevens, K. and W. Beyeler, 1985. Determination of Diffusivities in the Rustler Formation from Exploratory Shaft Construction at the Waste Isolation Pilot Plant in Southeastern New Mexico. U.S. Geological Survey Water-Resources Investigations Report 85-4020, 32 p.

Uhland, D.W., and W.S. Randall, 1986. 1986 Annual Water Quality Data Report for the Waste Isolation Pilot Plant, Westinghouse Electric Corporation Report DOE-WIPP-86-006.

Uhland, D.W., W.S. Randall, and R.C. Carrasco, 1987. 1987 Annual Water Quality Data Report for the Waste Isolation Pilot Plant, Westinghouse Electric Corporation Report DOE-WIPP-87-006.

U.S. Department of Energy, 1980. Final Environmental Impact Statement, Waste Isolation Pilot Plant, DOE/EIS-0026, UC-70, Volume 2.

U.S. Department of Energy, 1981. Waste Isolation Pilot Plant, Safety Analysis Report. Five Volumes.

Vine, J.D., 1963. Surface Geology of the Nash Draw Quadrangle, Eddy County, New Mexico. U.S. Geological Survey, Bulletine 1141-B, 46 p.

Ward, D.S., M. Reeves, and L.E. Duda, 1984. Verification and Field Comparison of the Sandia Waste-Isolation Flow and Transport Model (SWIFT), Sandia National Laboratories, NUREG/CR-3316 and SAND83-1154, 155 p.

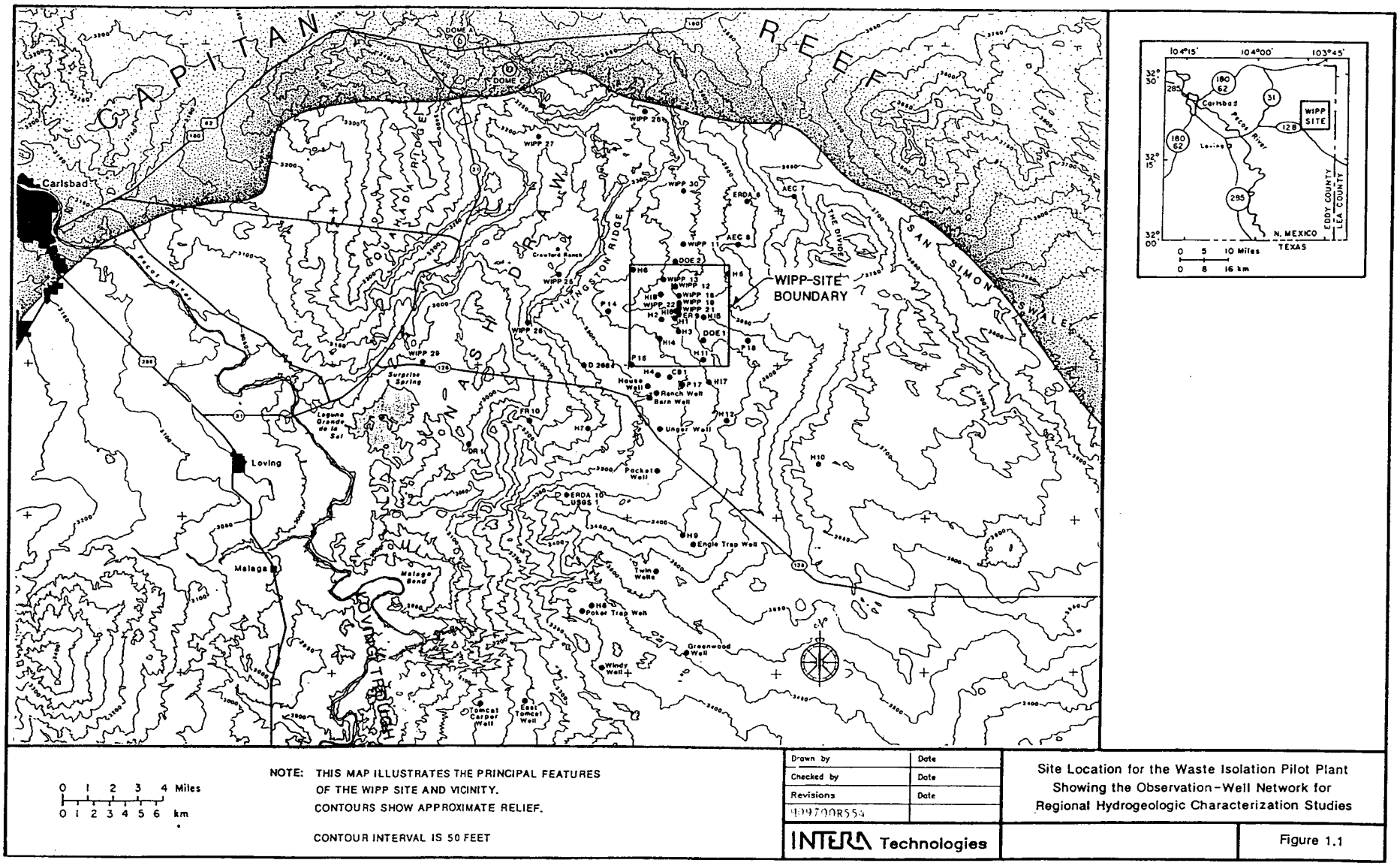

NOTE: THIS MAP ILLUSTRATES THE PRINCIPAL FEATURES OF THE WIPP SITE AND VICINITY.
CONTOURS SHOW APPROXIMATE RELIEF.

CONTOUR INTERVAL IS 50 FEET

Drawn by	Date
Checked by	Date
Revisions	Date
9109200R554	

INTERA Technologies

Site Location for the Waste Isolation Pilot Plant Showing the Observation-Well Network for Regional Hydrogeologic Characterization Studies

Figure 1.1

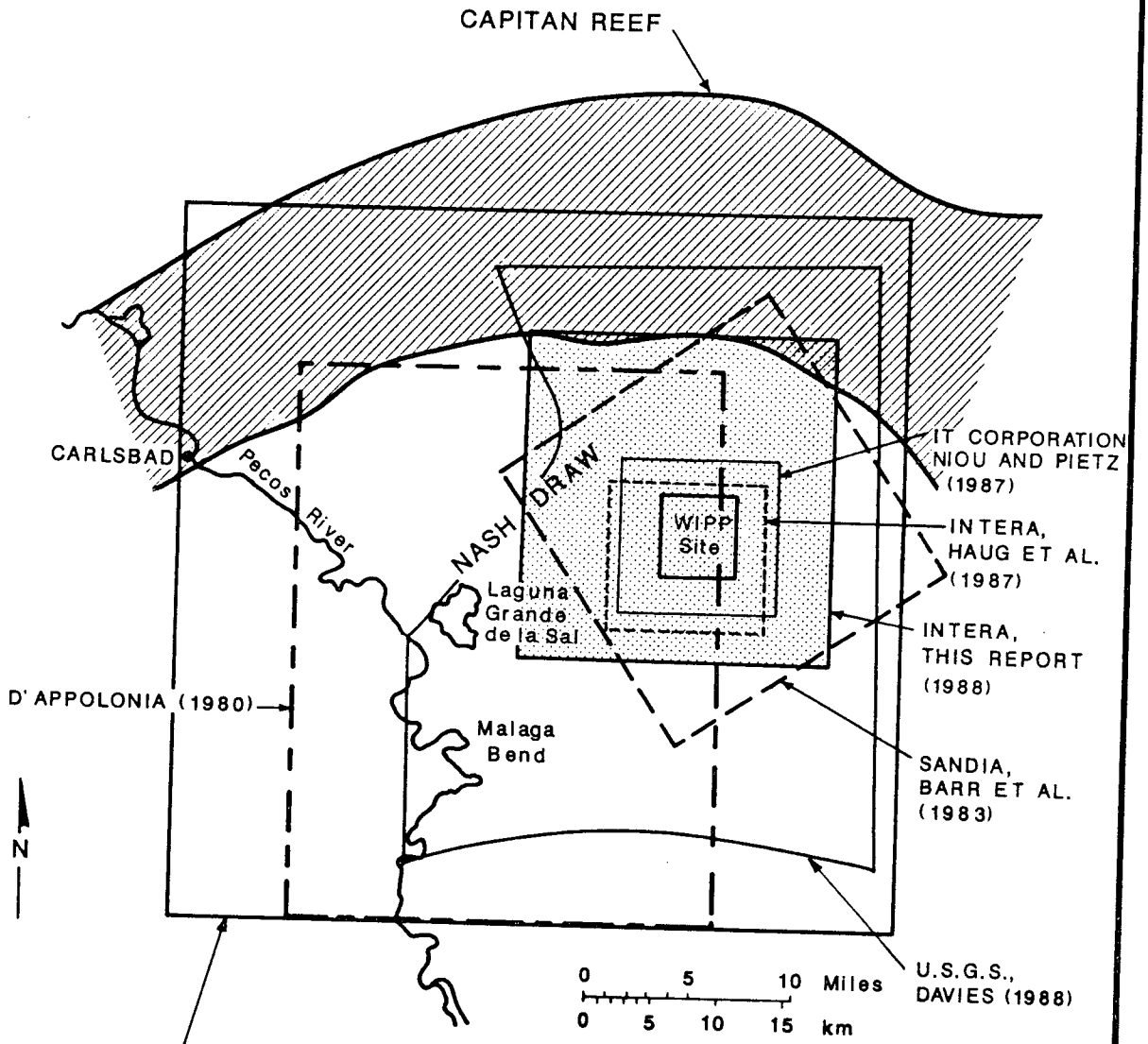

Drawn by	Date	Comparison of Regional-Model Areas for Simulating Ground-Water Flow in the Rustler Formation and/or the Culebra Dolomite Member at the WIPP Site
Checked by	Date	
Revisions	Date	
H09700R554		
INTERA Technologies		Figure 1.2

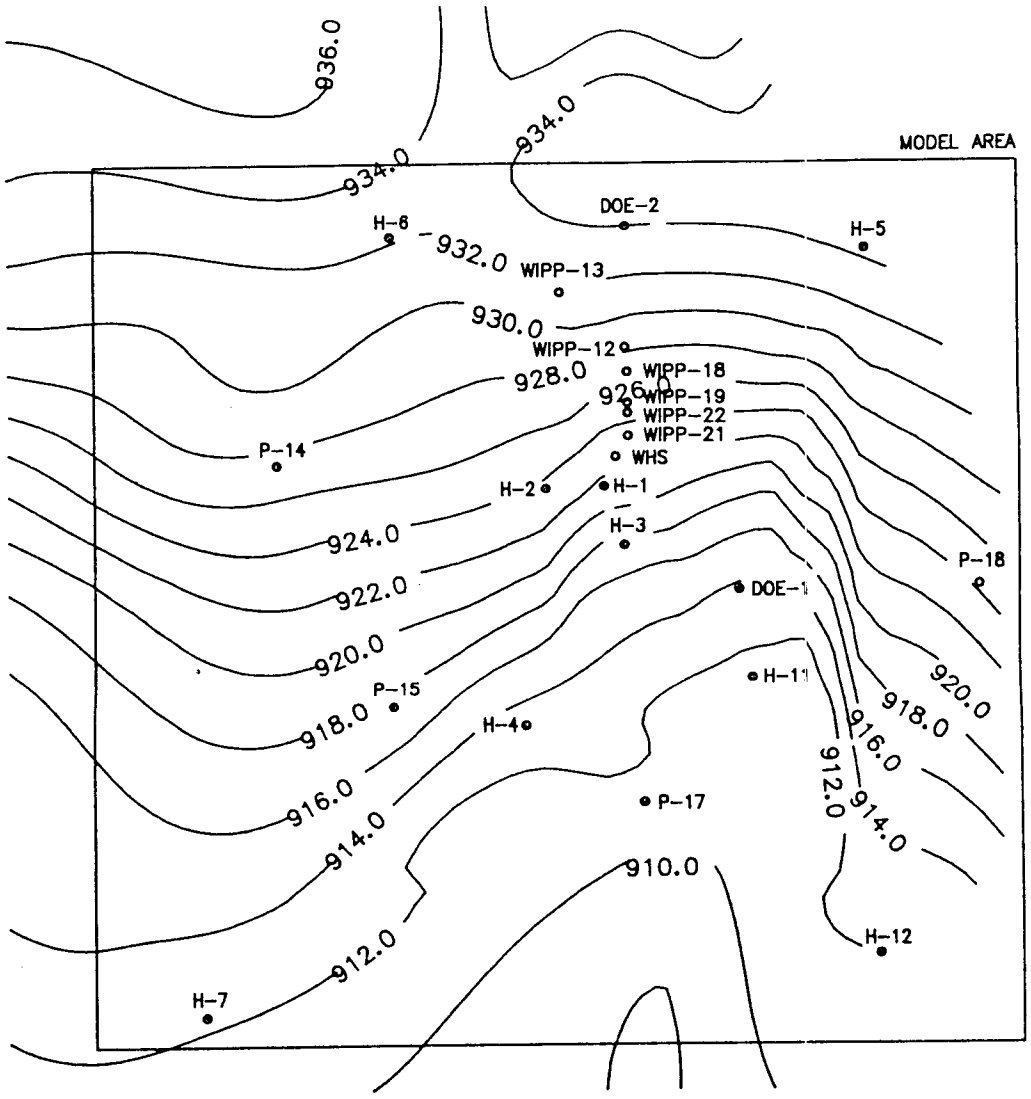

Drawn by	Date
Checked by	Date
Revisions	Date
HD9700R554	

Best Estimate of the Undisturbed Freshwater Heads in the Culebra (From Haug et al., 1987)

INTERA Technologies

Figure 1.3

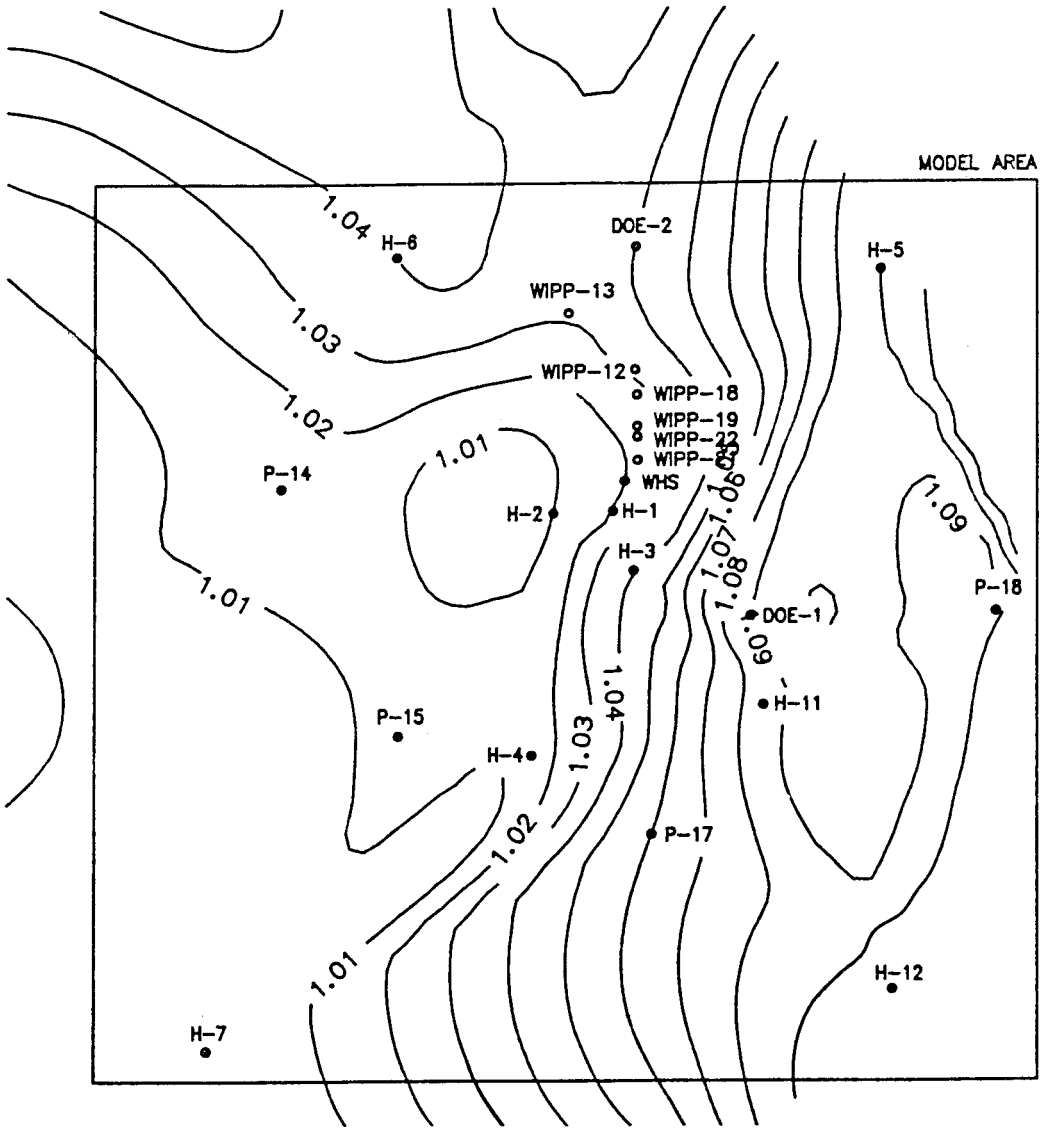

Drawn by	Date
Checked by	Date
Revisions	Date
HD9700R554	

Best Estimate of Undisturbed Formation-Water Densities in the Culebra (From Haug et al., 1987)

INTERA Technologies

Figure 1.4

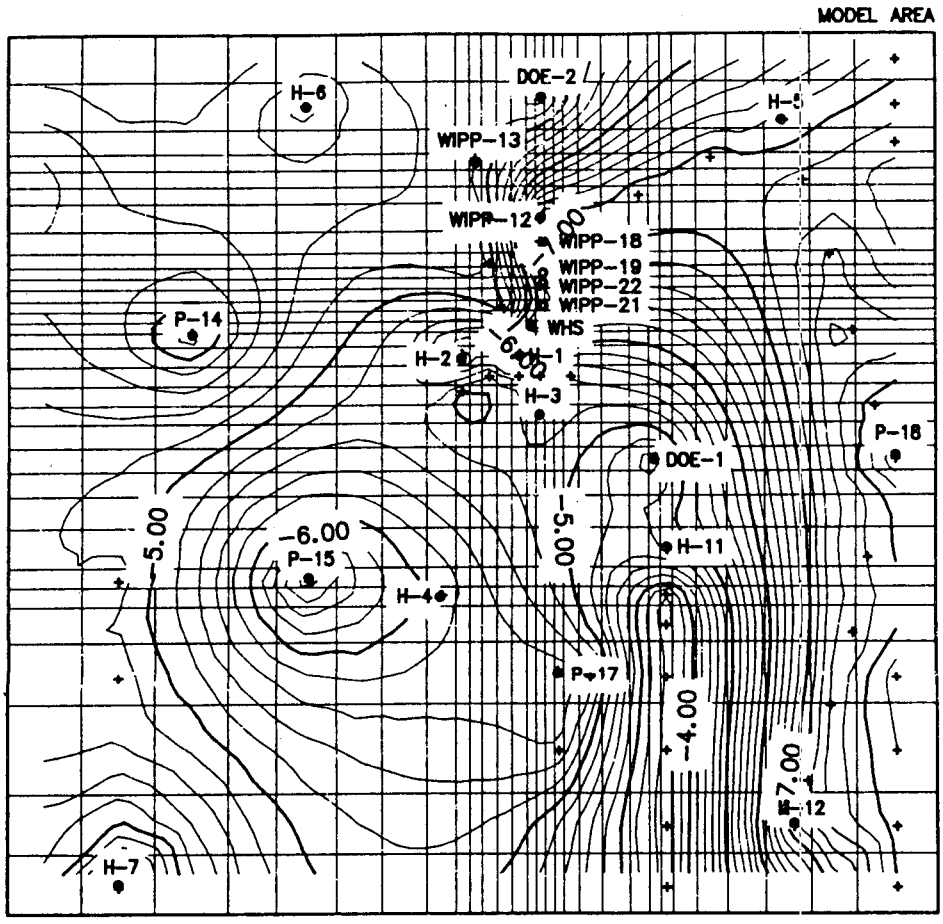

Drawn by	Date
Checked by	Date
Revisions	Date
H09700R554	

Transmissivities of the Calibrated Steady-State Model (From Haug et al., 1987)

INTERA Technologies

Figure 1.5

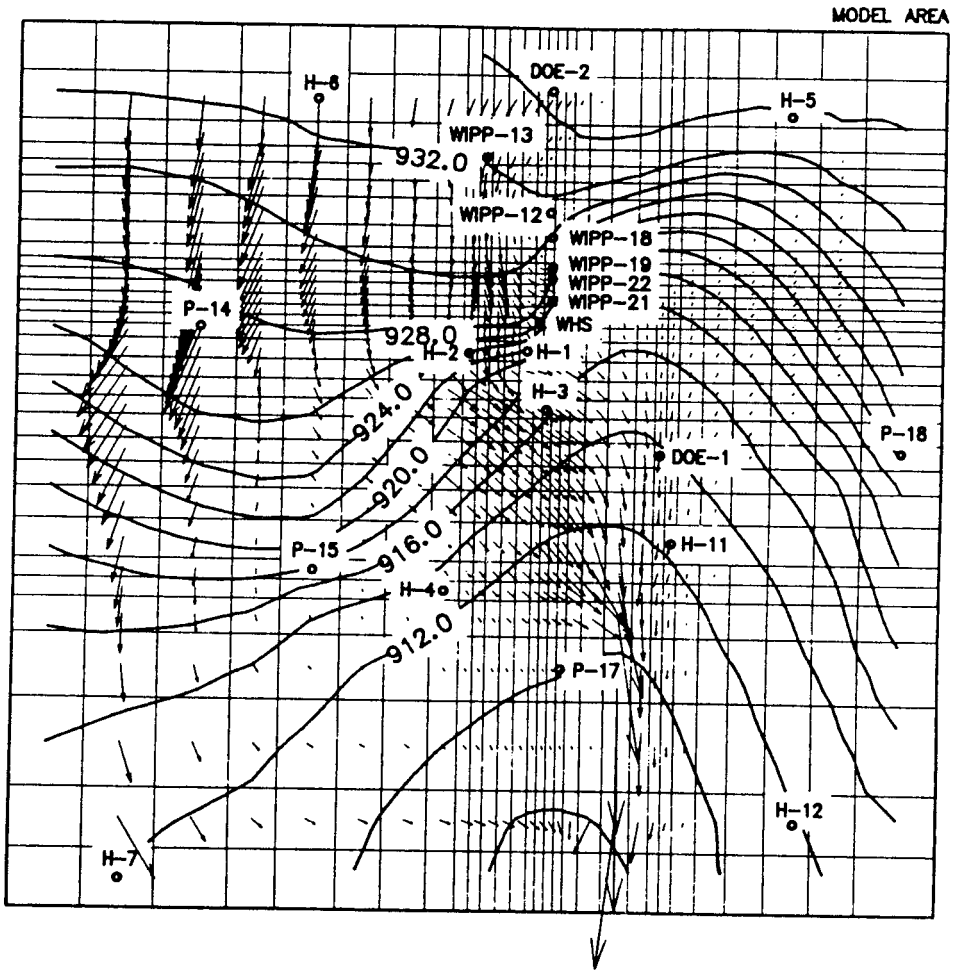

Drawn by	Date
Checked by	Date
Revisions	Date
H09700R554	

Calibrated Steady-State Model:Freshwater Heads and Darcy Velocities (From Haug et al., 1987)

INTERA Technologies

Figure 1.6

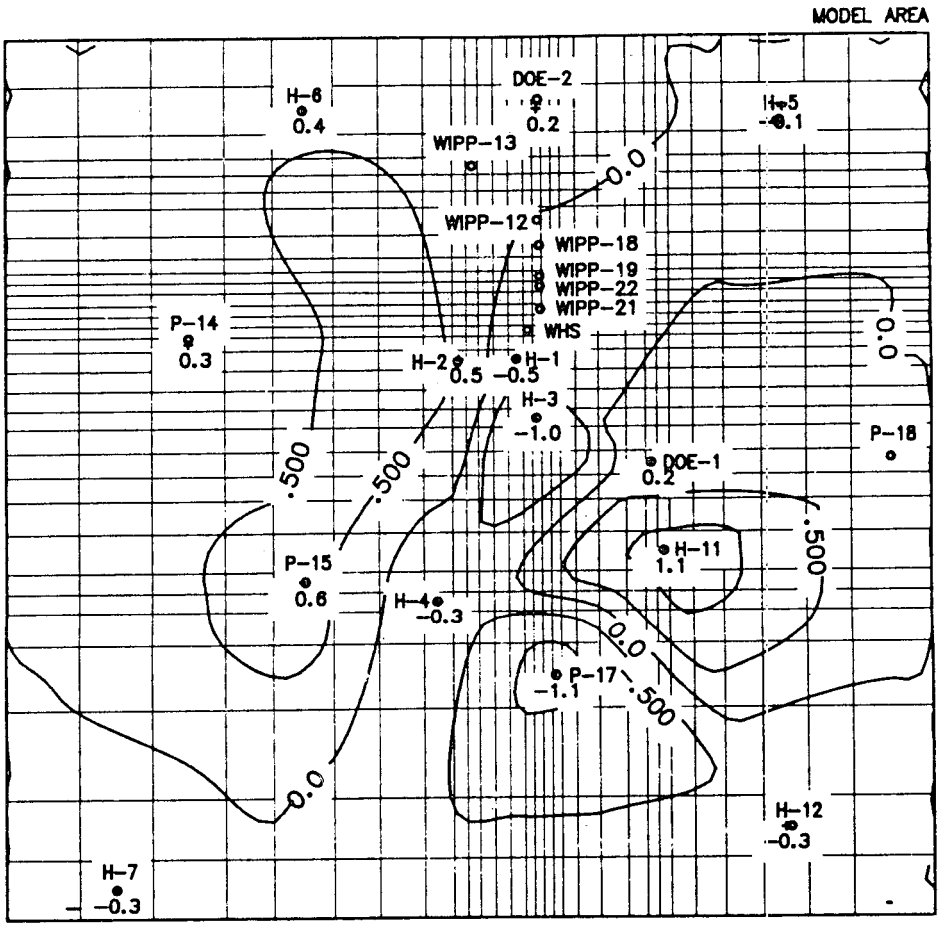

Drawn by	Date
Checked by	Date
Revisions	Date
HO9700R554	

Calibrated Steady-State Model: Differences Between the Calculated and the Observed Freshwater Heads (From Haug et al., 1987)

INTERA Technologies

Figure 1.7

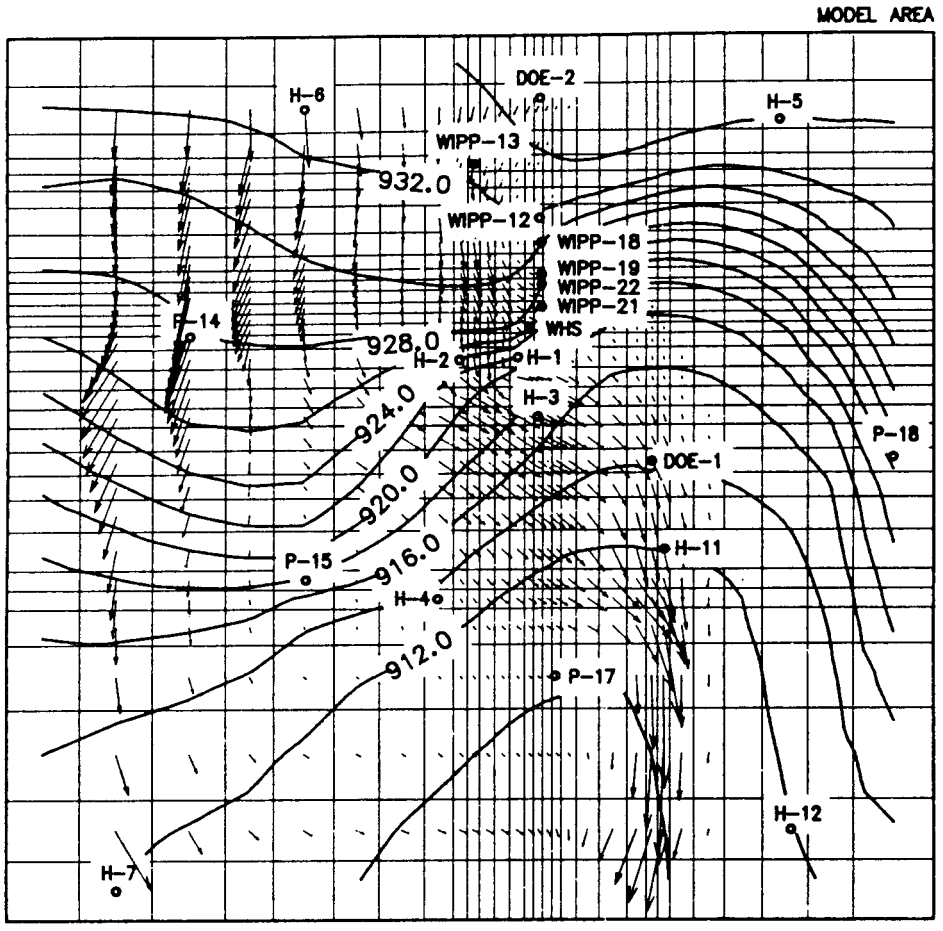

DARCY VELOCITY VECTOR: 1.E-8 m/s
(Linear Scale)

0 1 2 Miles

0 1 2 3 km

o Observation Well

Freshwater Heads in m amsl
Contour Scale: Linear
Contour Interval: 2 m

Drawn by	Date
Checked by	Date
Revisions	Date
HD9700R554	

Calibrated Steady-State Model: Formation-Water Densities and Darcy Velocities (From Haug et al., 1987)

INTERA Technologies

Figure 1.8

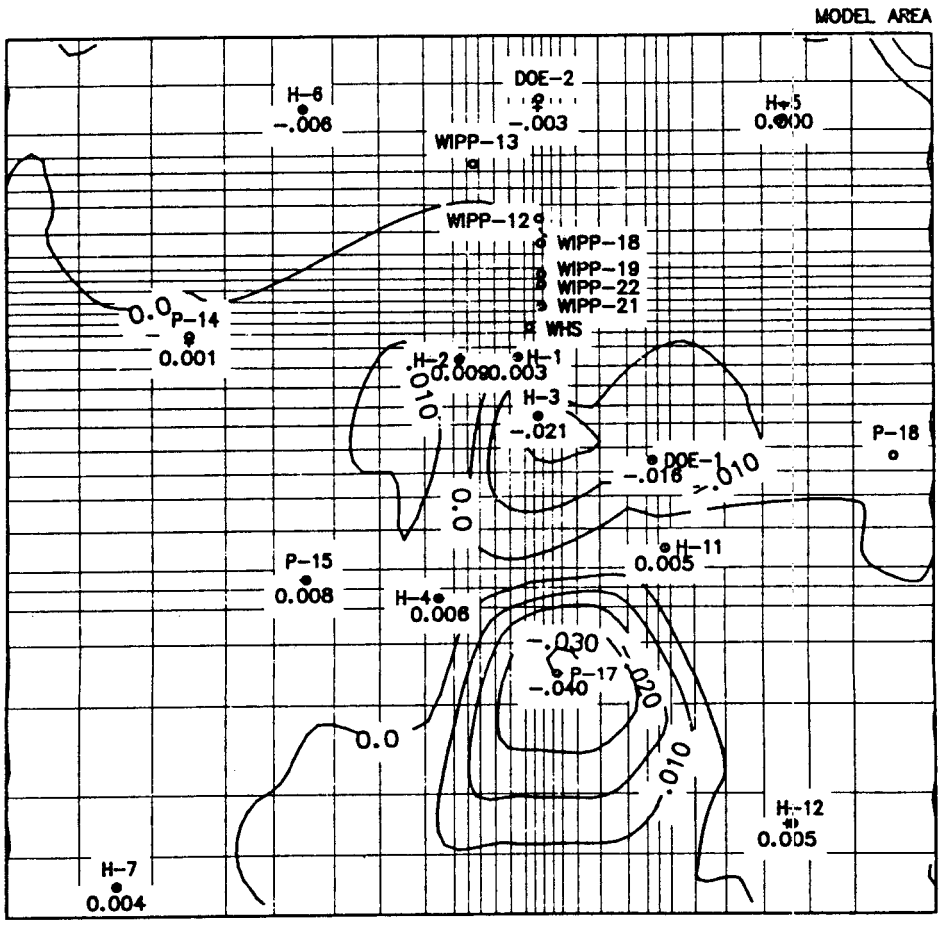

Drawn by	Date
Checked by	Date
Revisions	Date
HD9700R554	

Calibrated Steady-State Model: Differences Between the Calculated and the Observed Formation-Water Densities (From Haug et al., 1987)

INTERA Technologies

Figure 1.9

SYSTEM	SERIES	GROUP	FORMATION	MEMBER
RECENT	RECENT		SURFICIAL DEPOSITS	
QUATERN-ARY	PLEISTO-CENE		MESCALERO CALICHE	
			GATUÑA	
TRIASSIC		DOCKUM	UNDIVIDED	
PERMIAN	OCHOAN		DEWEY LAKE RED BEDS	
			RUSTLER	Forty-niner
				Magenta
				Tamarisk
				Culebra
				Unnamed
			SALADO	Upper
				McNutt
				Lower
			CASTILE	
	GUADALUPIAN	DELAWARE MOUNTAIN	BELL CANYON	
			CHERRY CANYON	
			BRUSHY CANYON	

Drawn by	Date	Geologic Column Representative of WIPP Area (After Powers et al., 1978)
Checked by	Date	
Revisions	Date	
H09700R554		
INTERA Technologies		Figure 2.1

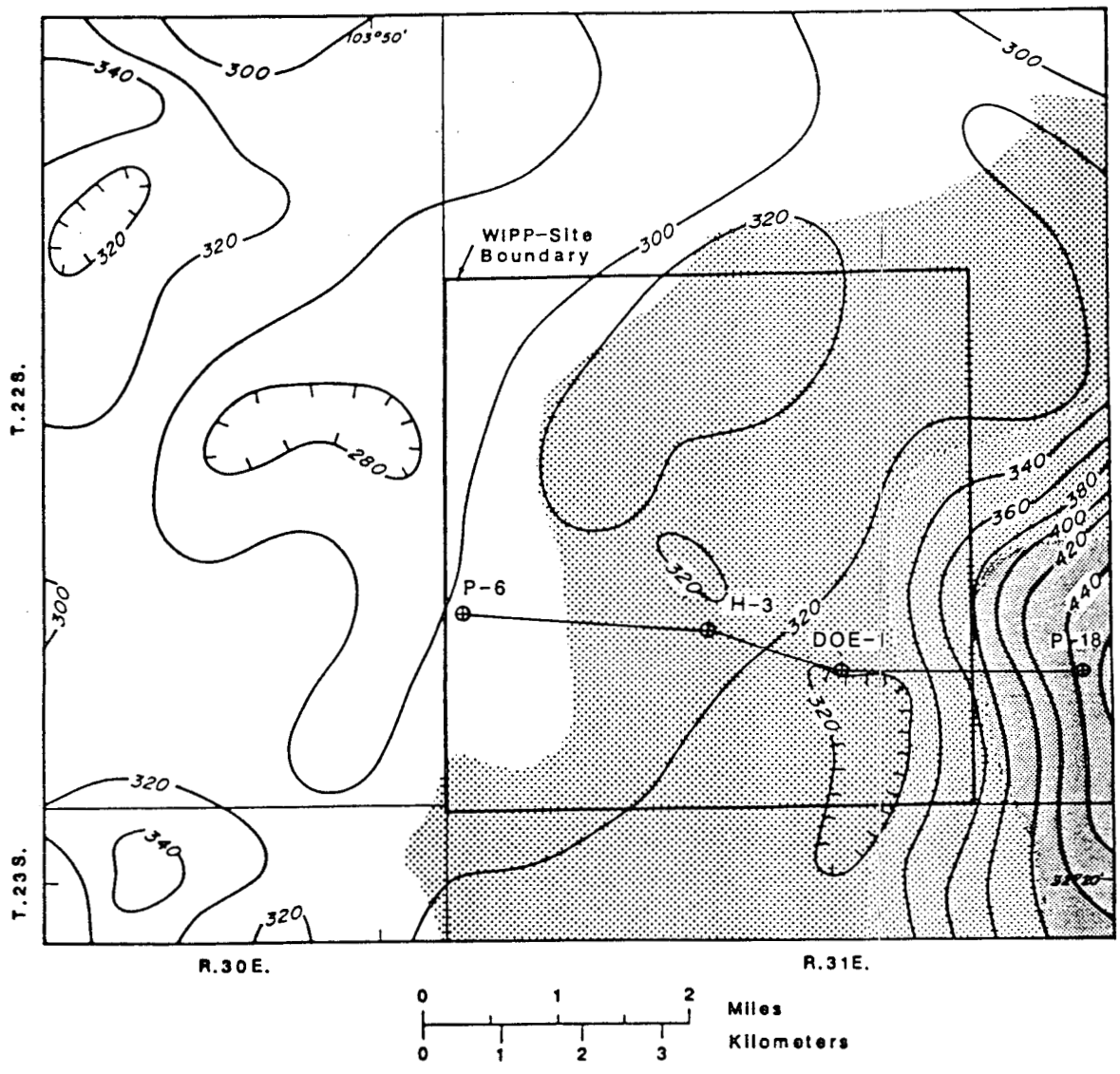

Drawn by	Date
Checked by	Date
Revisions	Date
H09700R554	

The Occurrence of Halite Beds Within the Rustler Formation (After Snyder, 1985)

INTERA Technologies

Figure 2.2

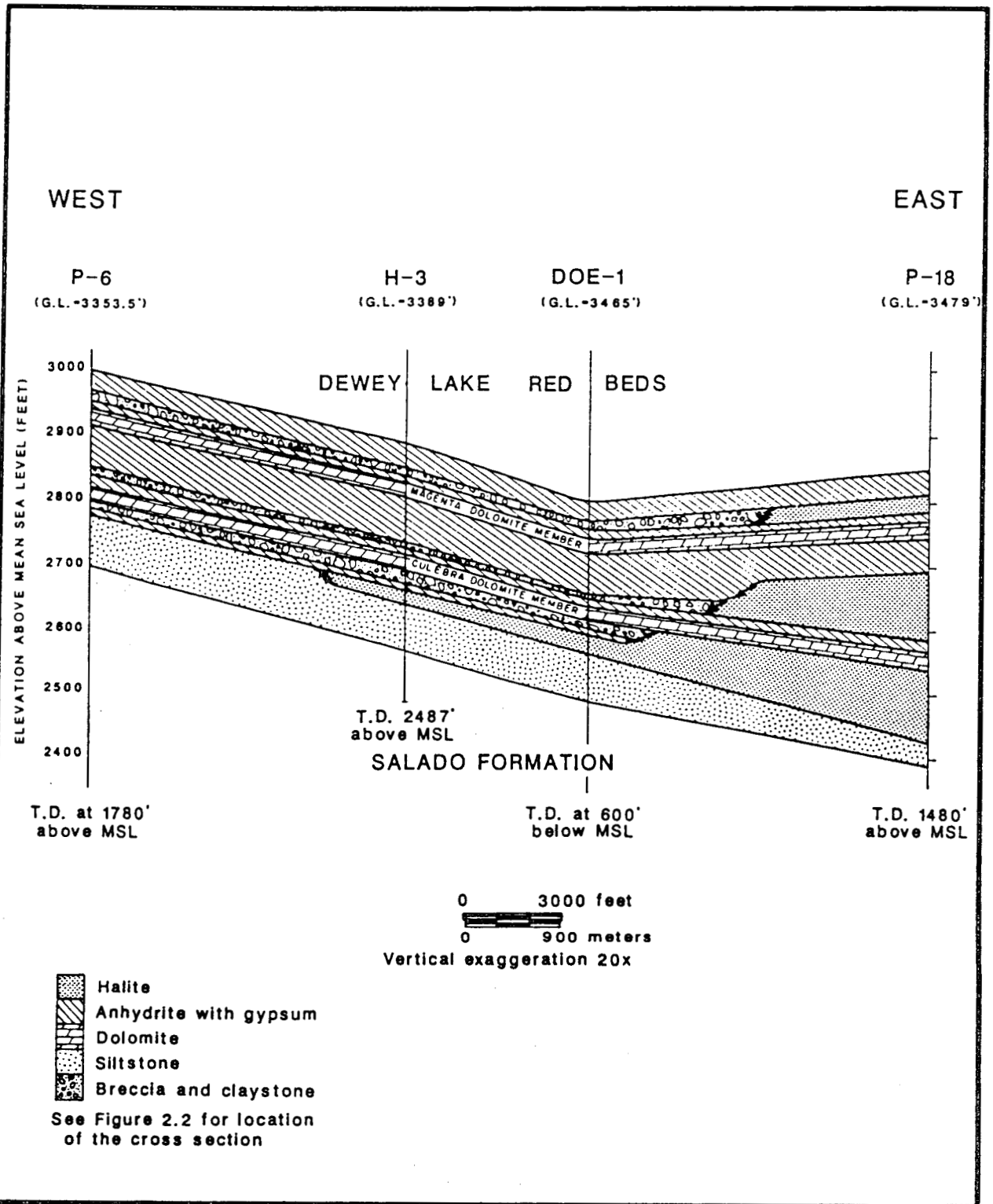

Drawn by	Date
Checked by	Date
Revisions	Date
H09700R554	

Stratigraphic Cross Section of the Rustler Formation West to East Across the WIPP Site (After Chaturvedi and Channell, 1985)

INTERA Technologies

Figure 2.3

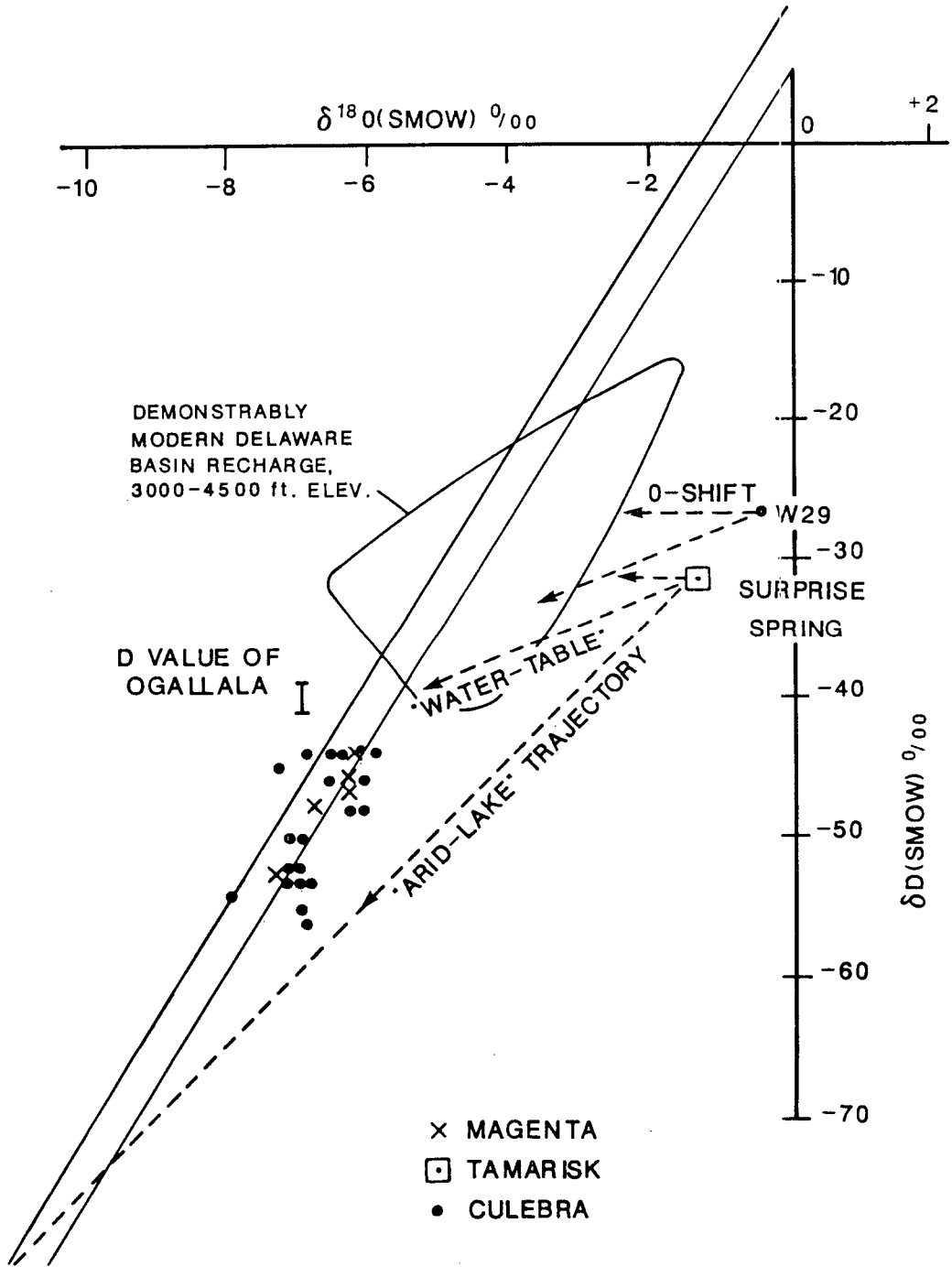

Drawn by	Date
Checked by	Date
Revisions	Date
HD9700R554	

Stable-Isotope Compositions of Ground Waters from the Rustler Formation (After Lambert and Harvey, 1987)

INTERA Technologies

Figure 2.4

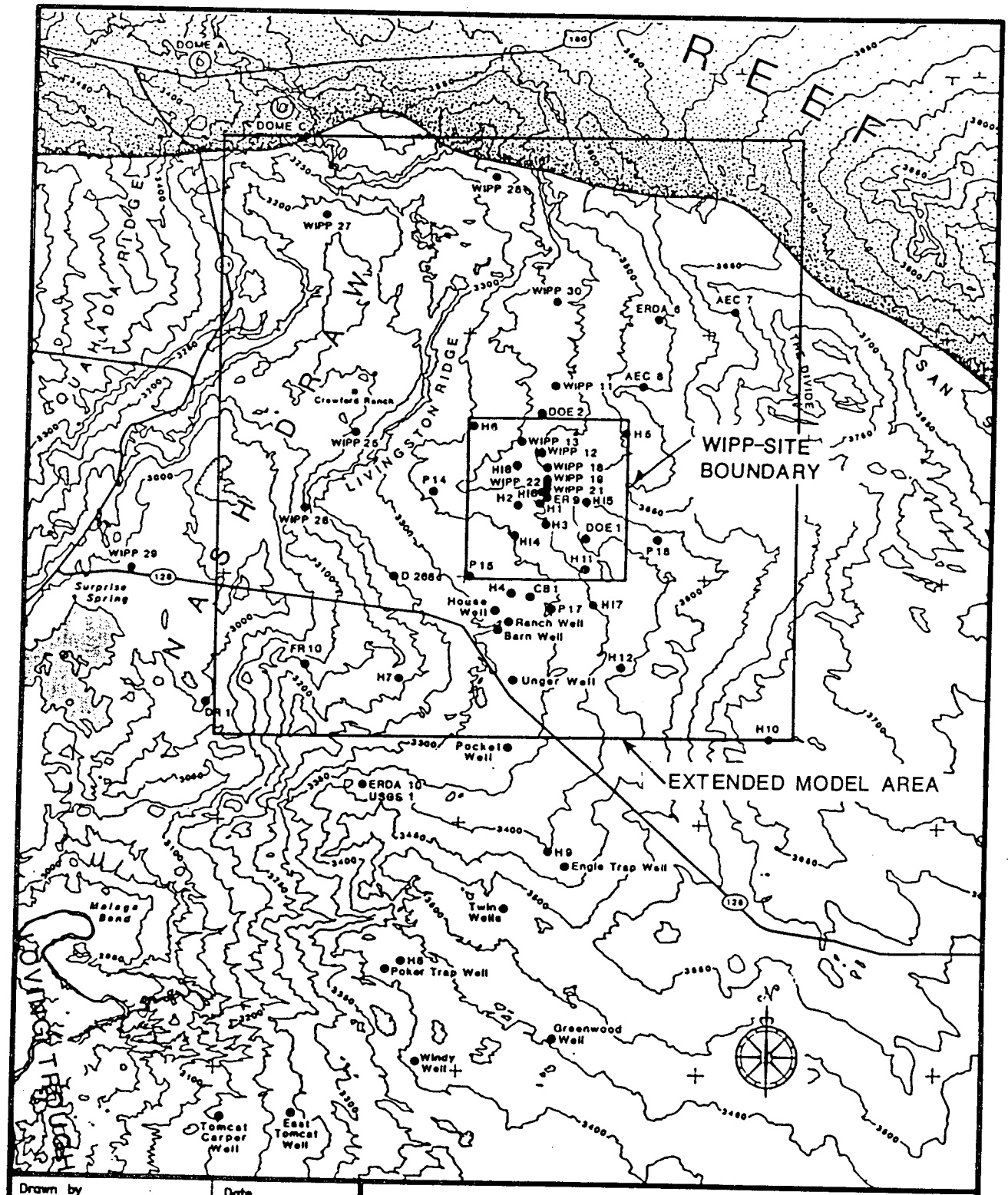

Drawn by	Date
Checked by	Date
Revisions	Date
HD9700R554	

WIPP–Area and Model Boundaries

INTERA Technologies

Figure 3.1

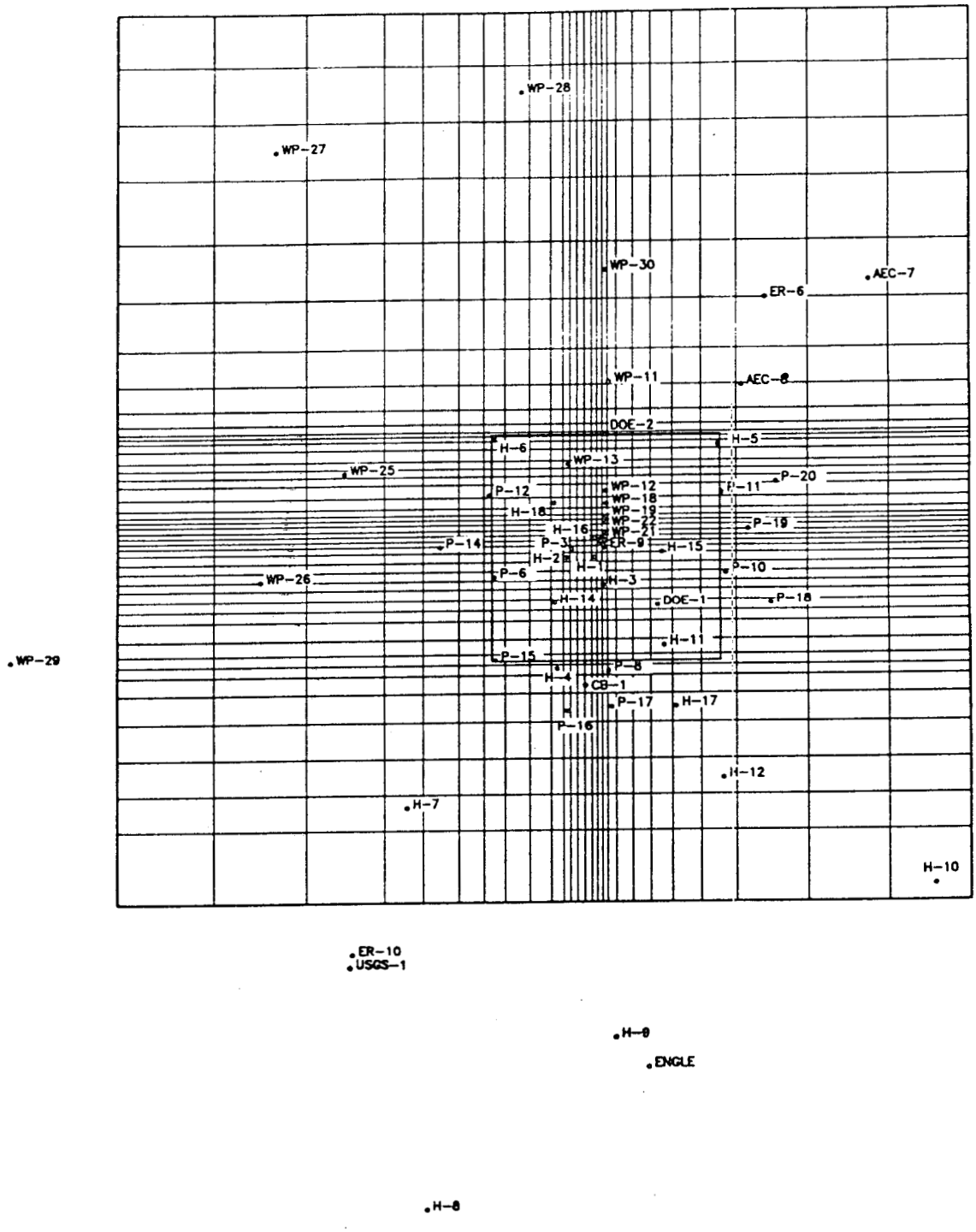

Drawn by	Date
Checked by	Date
Revisions	Date
H09700R554	

WIPP-Area Boreholes and Model Grid

INTERA Technologies

Figure 3.2

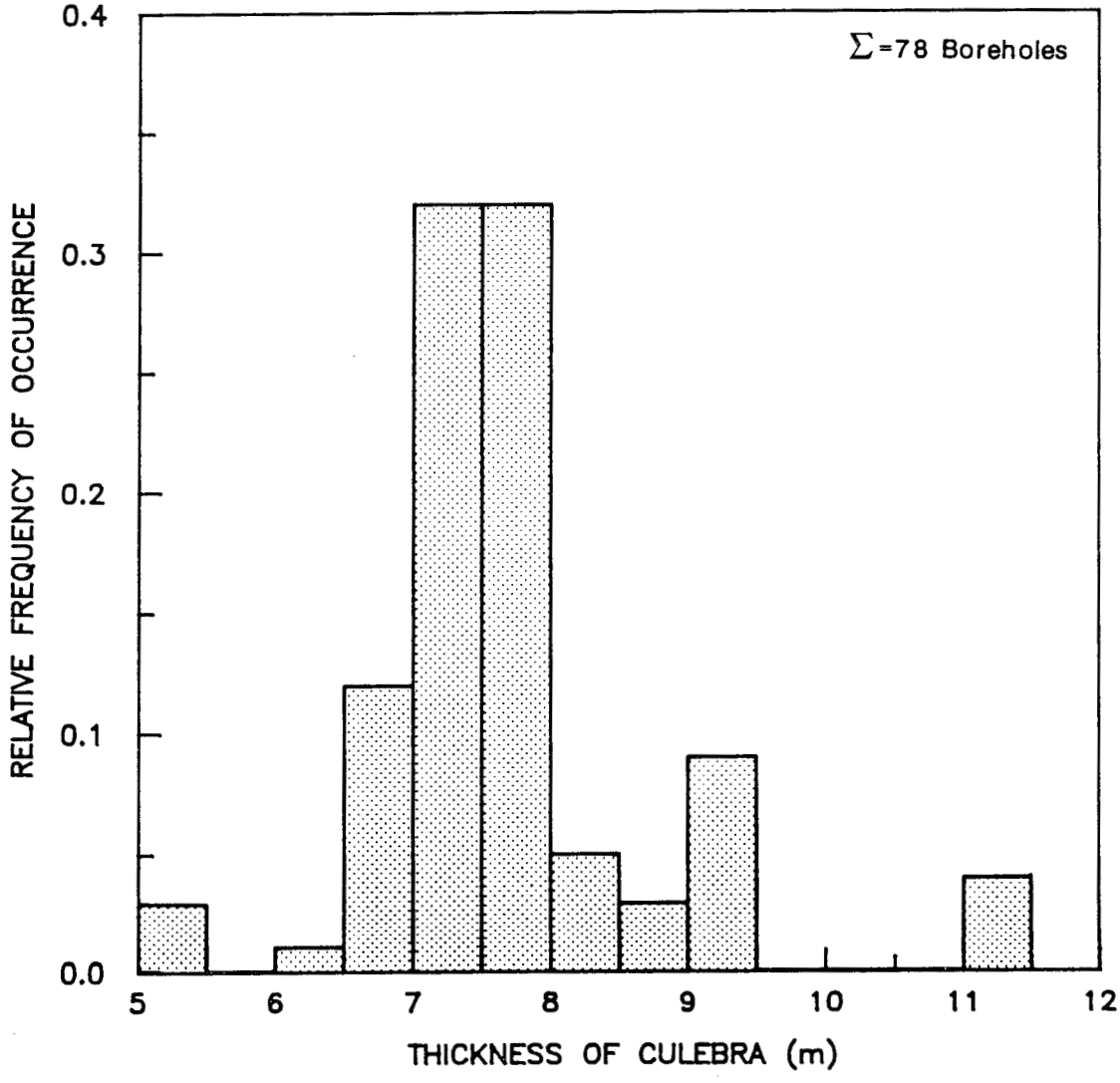

Drawn by	Date
Checked by	Date
Revisions	Date
HD9700R554	

Thickness Distribution of the Culebra Dolomite

INTERA Technologies

Figure 3.3

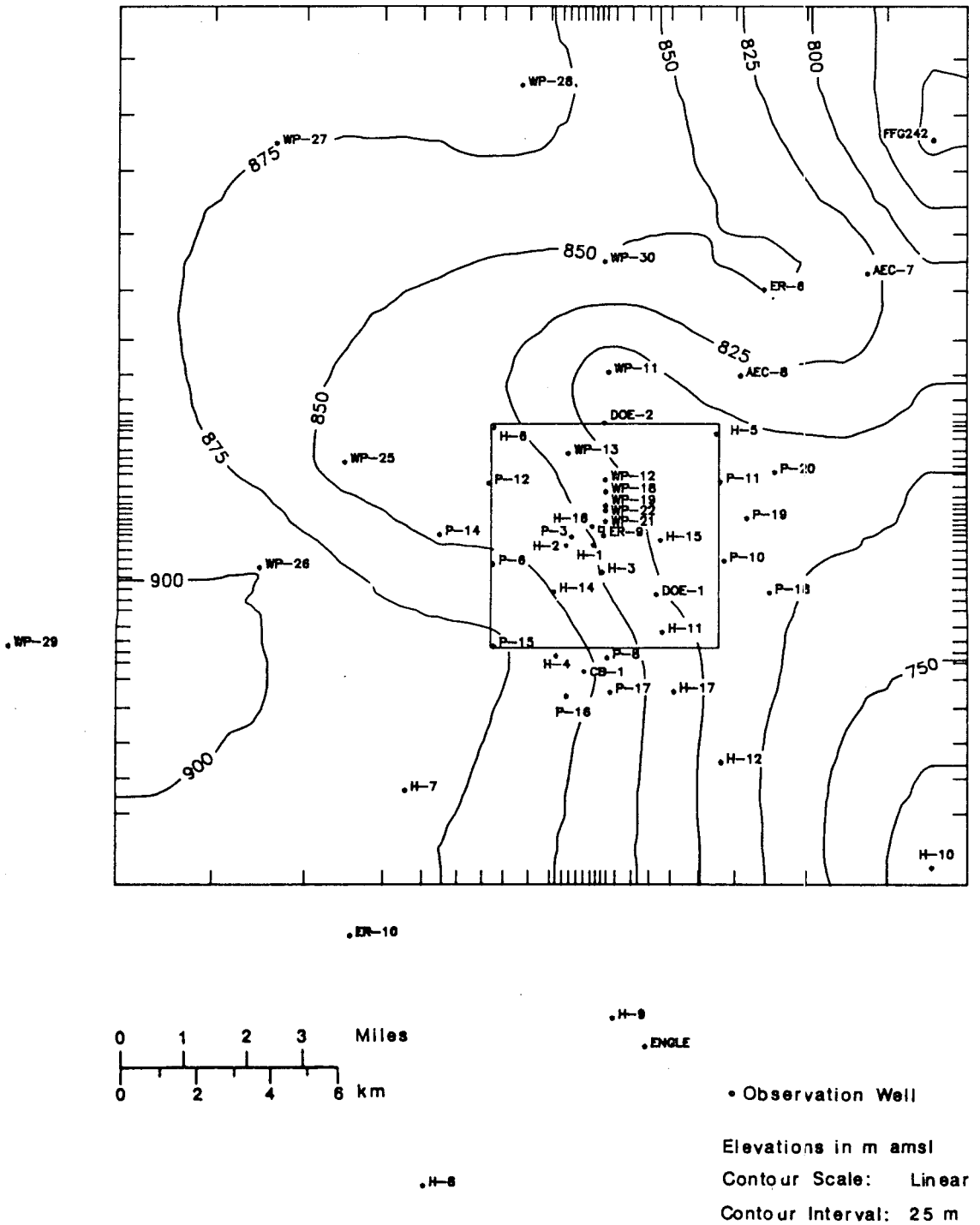

Drawn by	Date
Checked by	Date
Revisions	Date
H09700R554	

Center-of-Culebra Elevations Over Modeled Region

INTERA Technologies

Figure 3.4

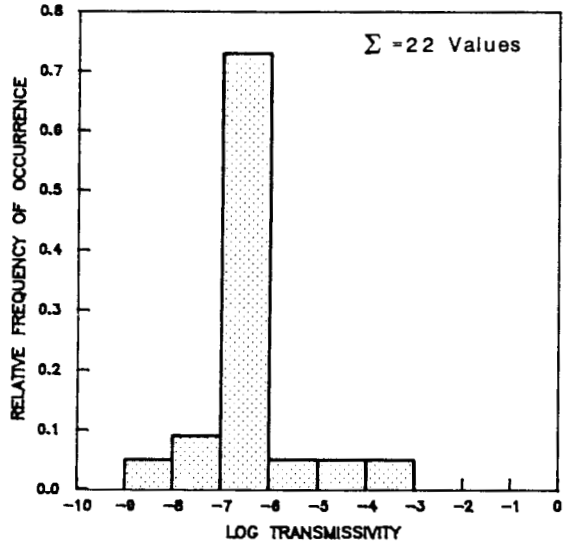

Log Transmissivity Distribution of Slug Test Values

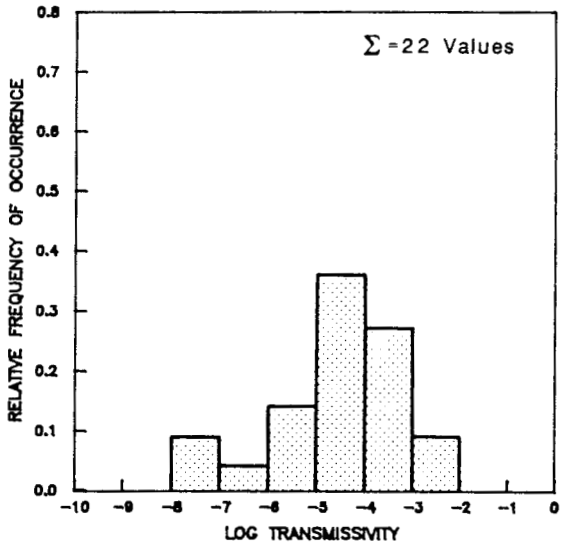

Log Transmissivity Distribution of Pumping Test Values

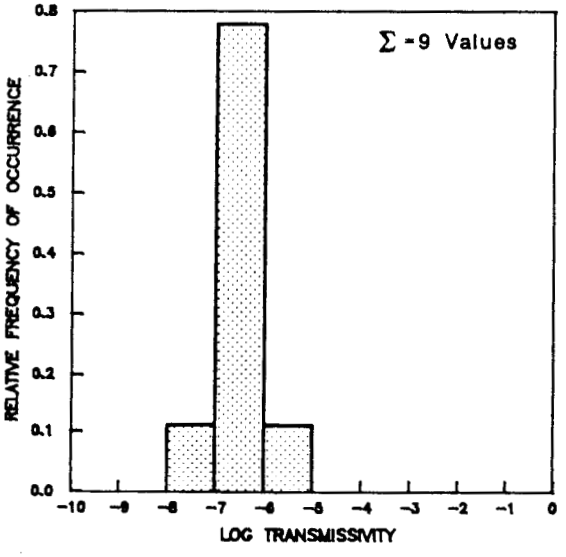

Log Transmissivity Distribution of DST Values

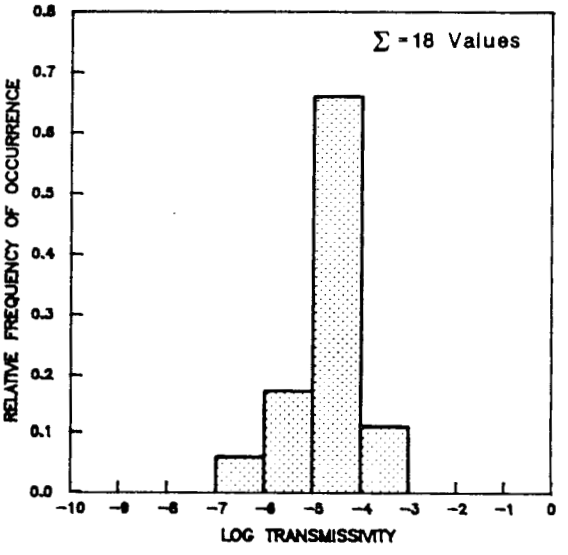

Log Transmissivity Distribution of Interference Values

Drawn by	Date
Checked by	Date
Revisions	Date
H09700R554	

Frequency Histograms of Log Transmissivities (m^2/s) Representative of Selected Hydrogeologic Tests in the Culebra Dolomite

INTERA Technologies

Figure 3.5

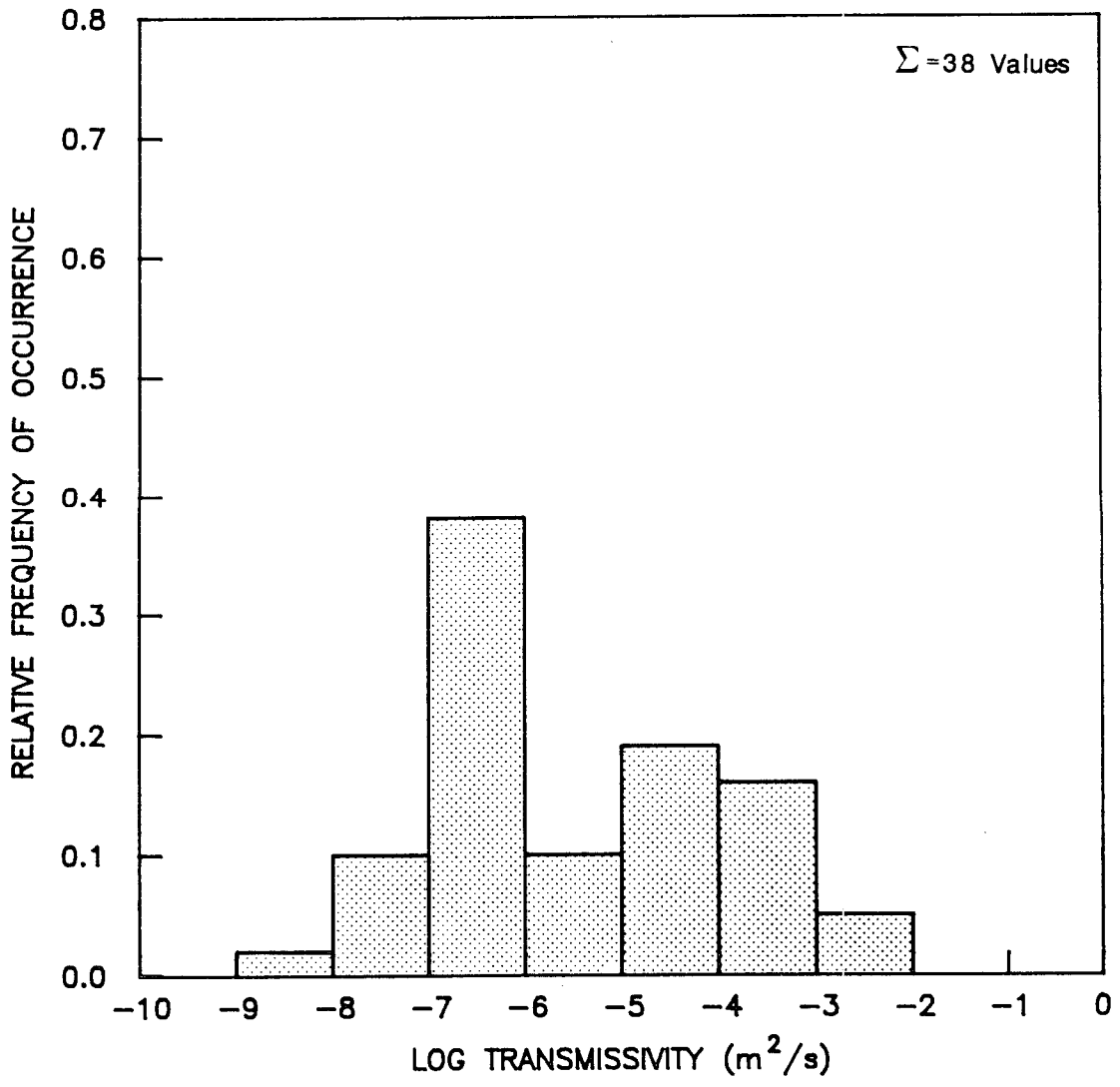

Drawn by	Date
Checked by	Date
Revisions	Date
H09700R554	

Log Transmissivity Distribution of Final Transmissivity Values

INTERA Technologies

Figure 3.6

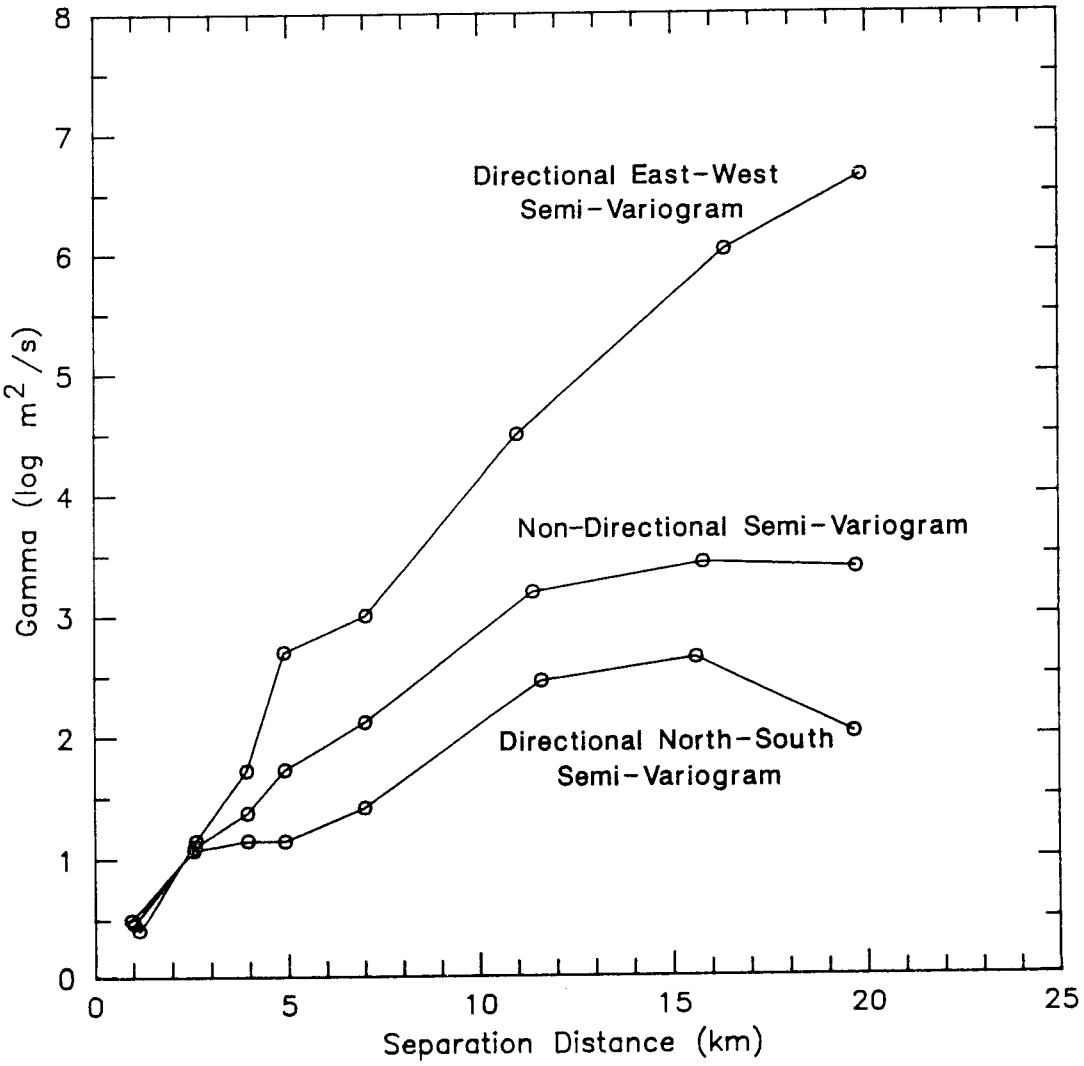

Drawn by	Date	Raw Semi-Variograms of Culebra Transmissivities
Checked by	Date	
Revisions M.L.	Date 1/25/88	
H09700R554	1/27/88	
INTERA Technologies		Figure 3.7

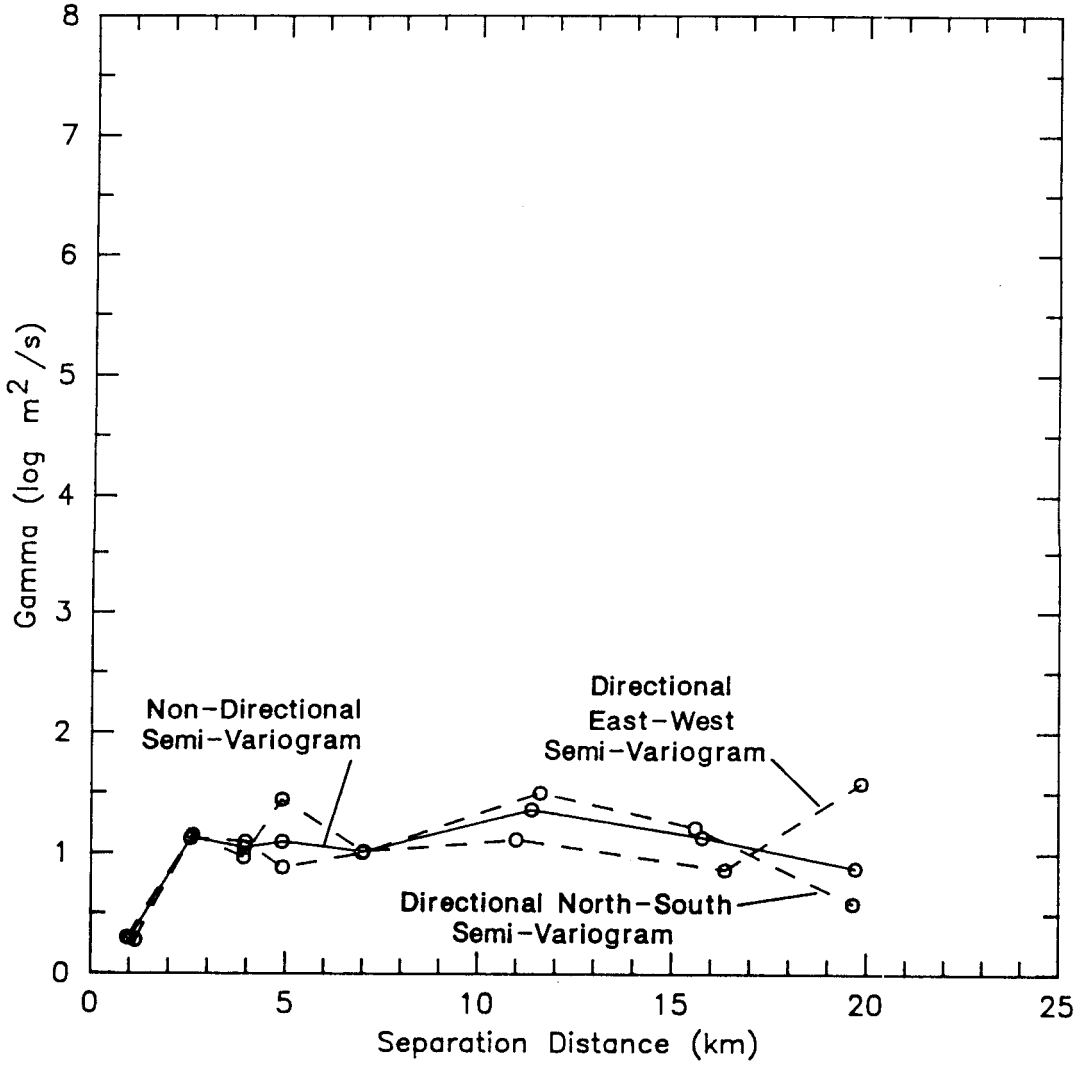

Drawn by	Date
Checked by	Date
Revisions M.L.	Date 1/25/88
H09700R554	1/27/88

Raw Semi-Variograms of Residuals

INTERA Technologies

Figure 3.8

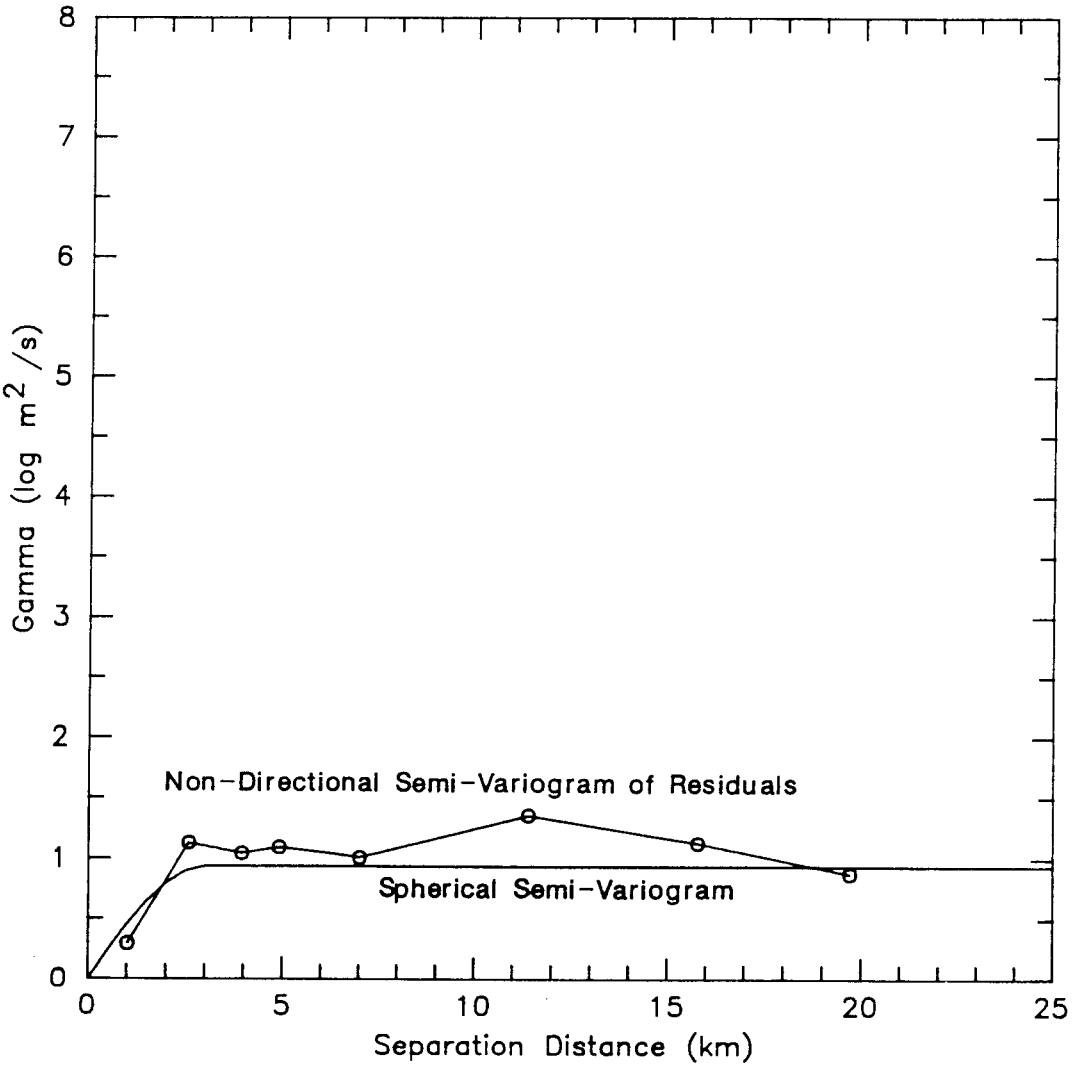

Drawn by	Date	Raw and Theoretical Semi-Variograms	
Checked by	Date		
Revisions M.L.	Date 1/25/88		
H09700554	1/27/88		
INTERA Technologies			Figure 3.9

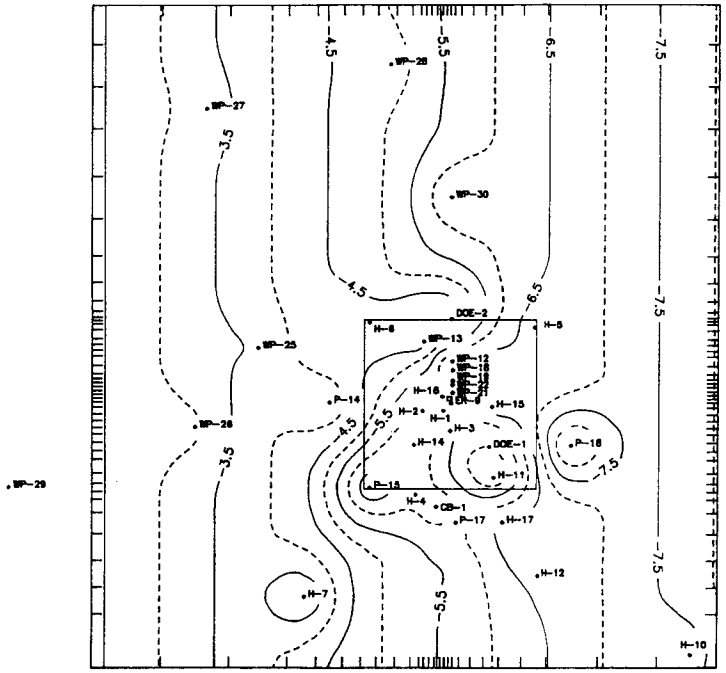

A. KRIGED TRANSMISSIVITIES

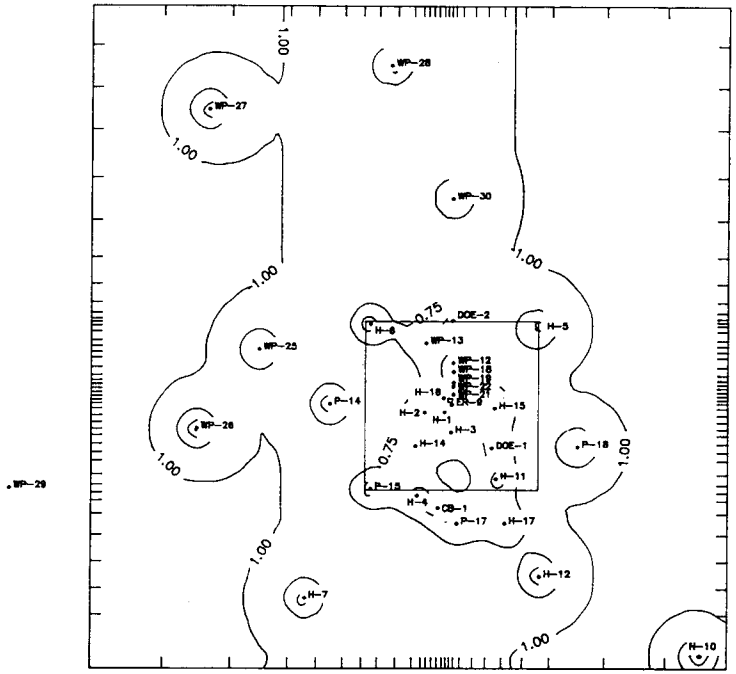

B. ESTIMATION ERRORS

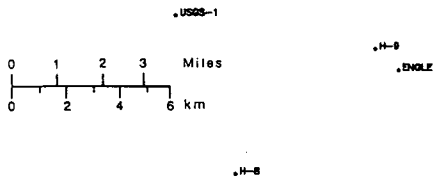

• Observation Well

Transmissivities in m^2/s

Contour Scale: Logarithmic

Contour Interval: 0.5 log m^2/s

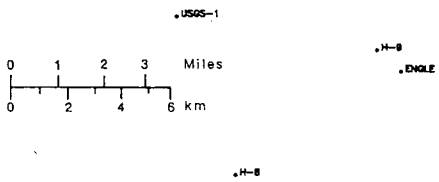

• Observation Well

Transmissivities in m^2/s

Contour Scale: Logarithmic

Contour Interval: 0.5 log m^2/s

Drawn by	Date	K603 Transmissivity Estimates and Estimation Errors Without Data Uncertainty
Checked by	Date	
Revisions M.L.	Date 1/25/88	
8092903554	1/27/88	
INTERA Technologies		Figure 3.10

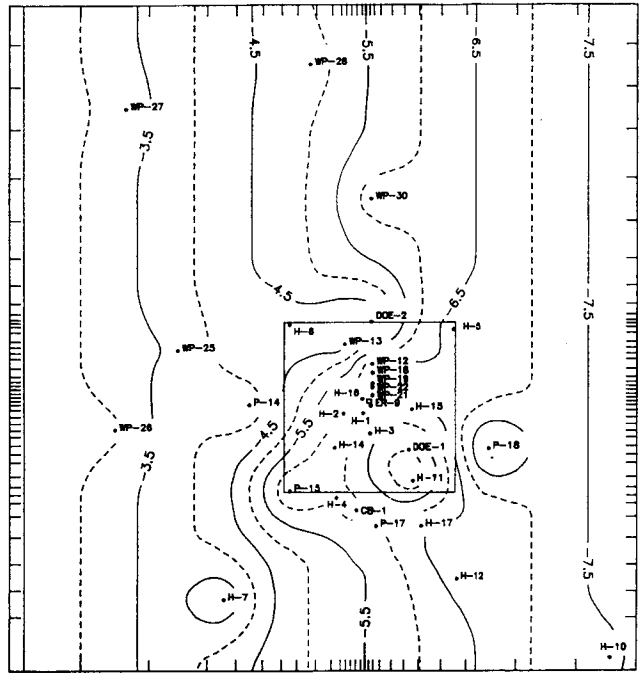

A. KRIGED TRANSMISSIVITIES

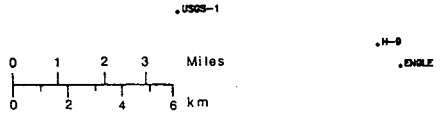

• Observation Well

Transmissivities in m^2/s

Contour Scale: Logarithmic

Contour Interval: 0.5 log m^2/s

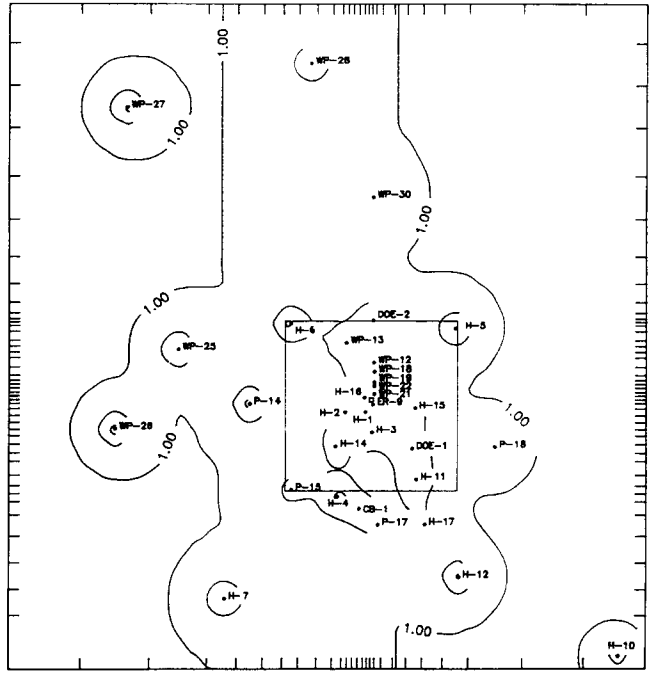

B. ESTIMATION ERRORS

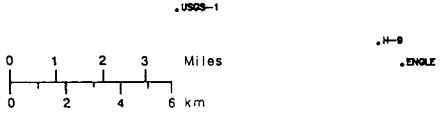

• Observation Well

Transmissivities in m^2/s

Contour Scale: Logarithmic

Contour Interval: 0.5 log m^2/s

Drawn by	Date
Checked by	Date
Revisions	Date
3009300554	

K603 Transmissivity Estimates and Estimation Errors With Data Uncertainty

INTERA Technologies

Figure 3.11

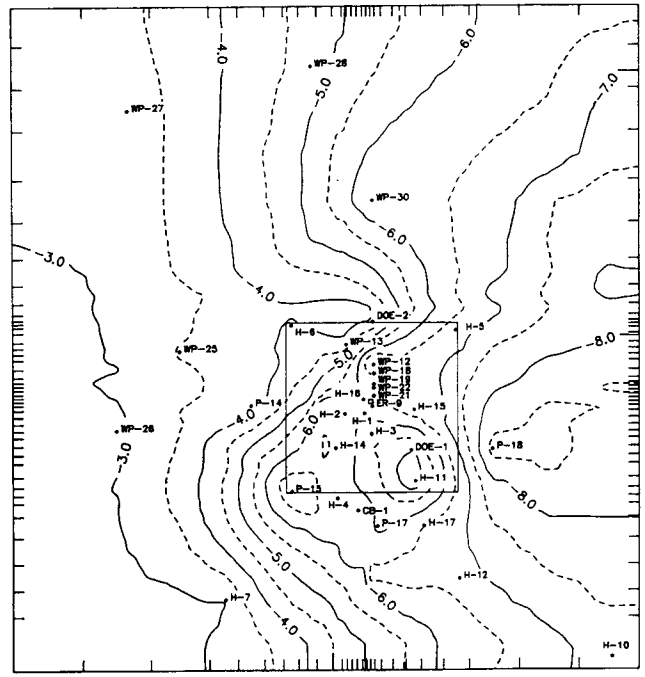

A. KRIGED TRANSMISSIVITIES

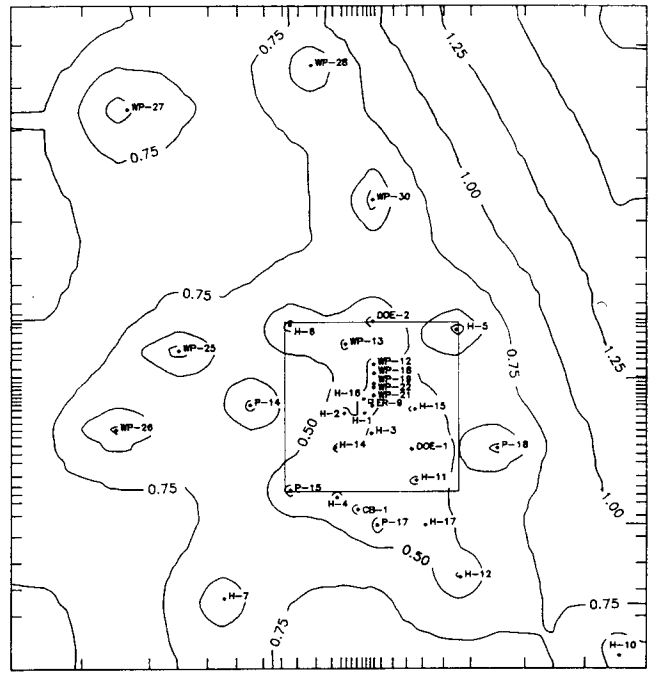

B. ESTIMATION ERRORS

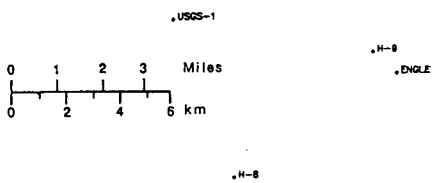

• Observation Well

Transmissivities in m^2/s

Contour Scale: Logarithmic

Contour Interval: 0.5 log m^2/s

• Observation Well

Transmissivities in m^2/s

Contour Scale: Logarithmic

Contour Interval: 0.25 log m^2/s

Drawn by	Date
Checked by	Date
Revisions	Date
EDT 253004	

Initial Kriged Transmissivities and Estimation Errors (Using AKRIP)

INTERA Technologies

Figure 3.12

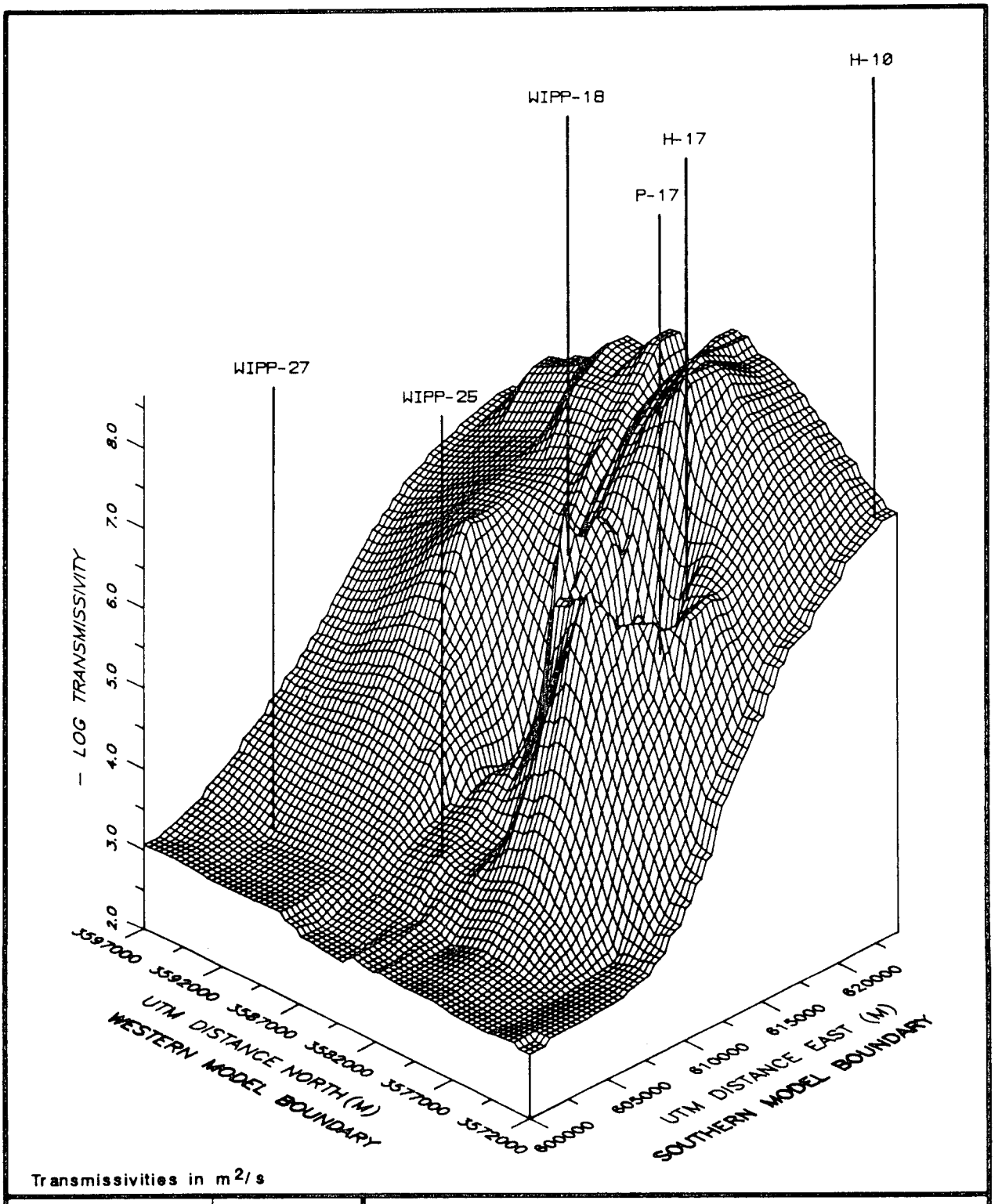

Transmissivities in m^2/s

Drawn by	Date
Checked by	Date
Revisions	Date
H09700R554	

The Initial Negative Log Transmissivities (Using AKRIP)

INTERA Technologies

Figure 3.13

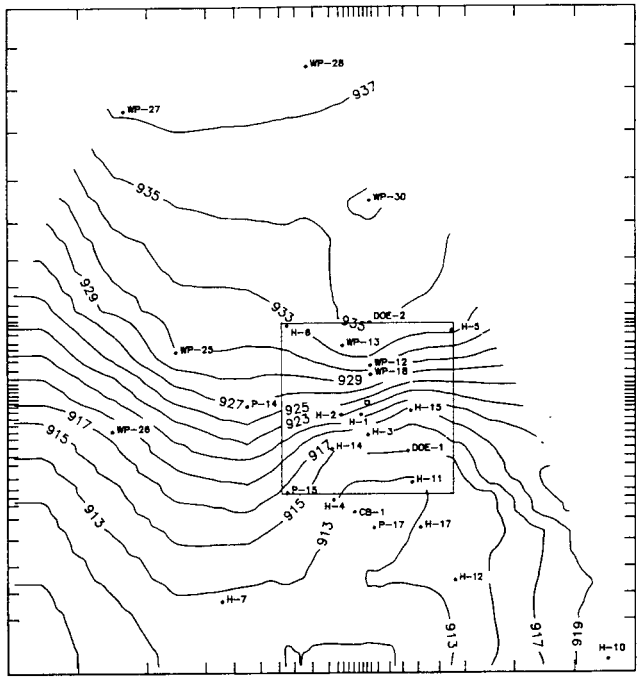

A. KRIGED FRESHWATER HEADS

0 1 2 3 Miles
0 2 4 6 km

• Observation Well

Freshwater Heads in m a.s.l.
Contour Scale: Linear
Contour Interval: 2 m

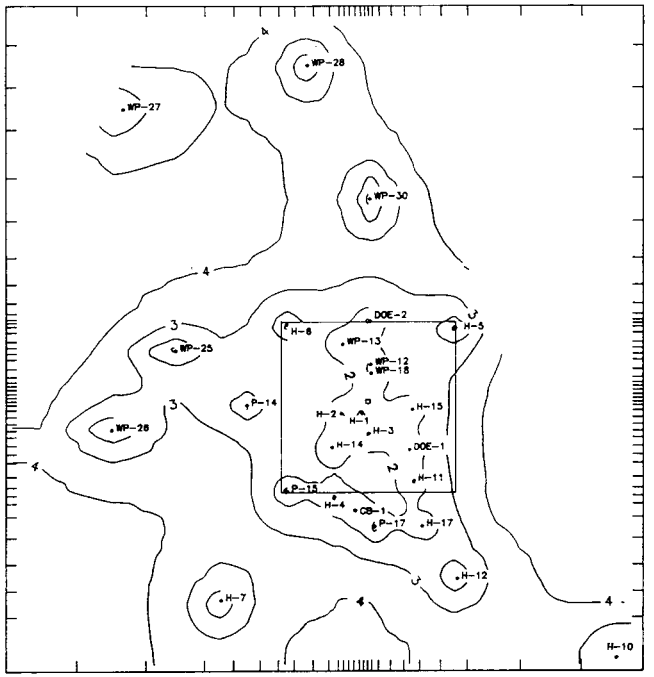

B. ESTIMATION ERRORS

0 1 2 3 Miles
0 2 4 6 km

• Observation Well

Freshwater Heads in m a.s.l.
Contour Scale: Linear
Contour Interval: 1 m

Drawn by	Date
Checked by	Date
Revisions	Date
A09700R554	

INTERA Technologies

Kriged Freshwater Heads and Estimation Errors (Using AKRIP)

Figure 3.14

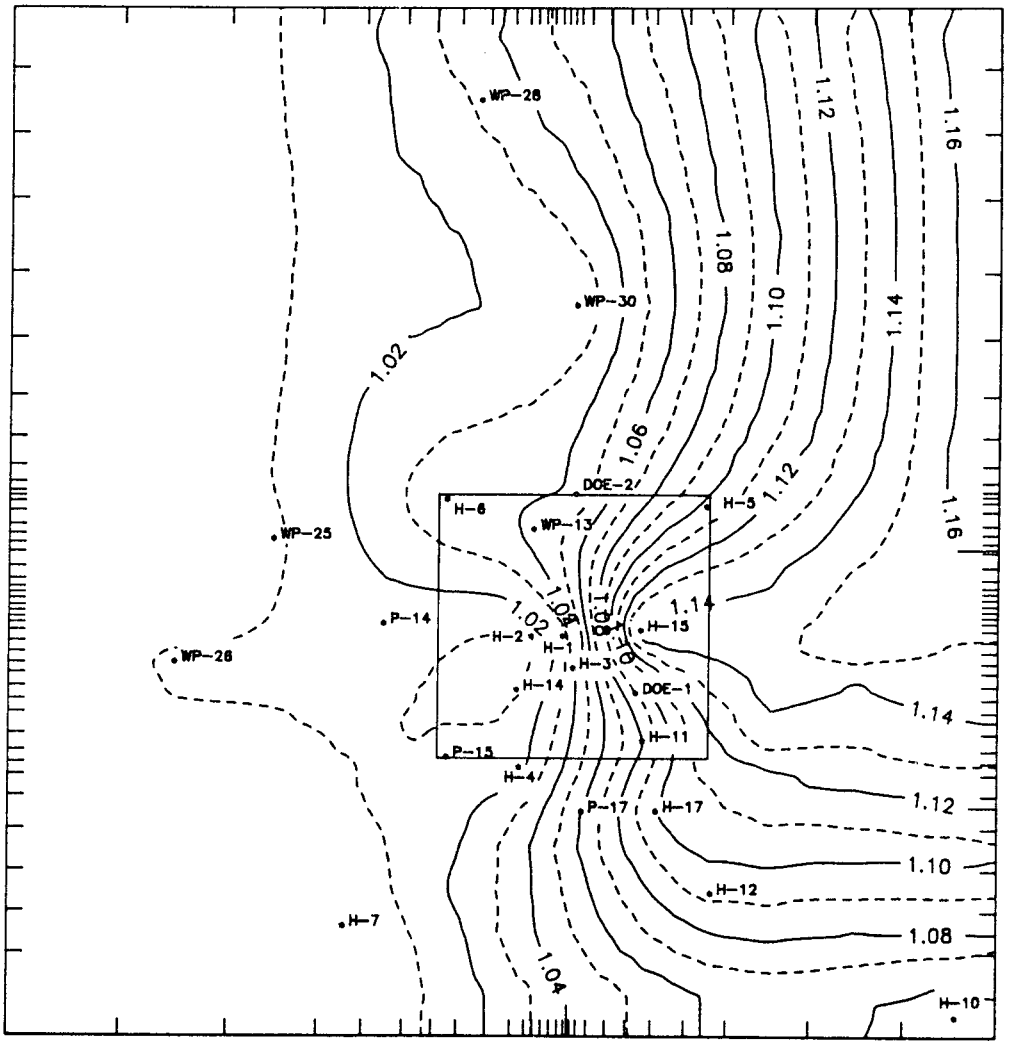

0 1 2 3 Miles

0 2 4 6 km

H-9

ENGLE

H-8

• Observation Well

Formation-Water Densities in g/cm^3

Contour Scale: Linear

Contour Interval: 0.01 g/cm^3

Drawn by	Date	Kriged Formation-Fluid Densities Used in Model (Using AKRIP)
Checked by	Date	
Revisions M.L.	Date 1/25/88	
HD9700R554	1/27/88	
INTERA Technologies		Figure 3.15

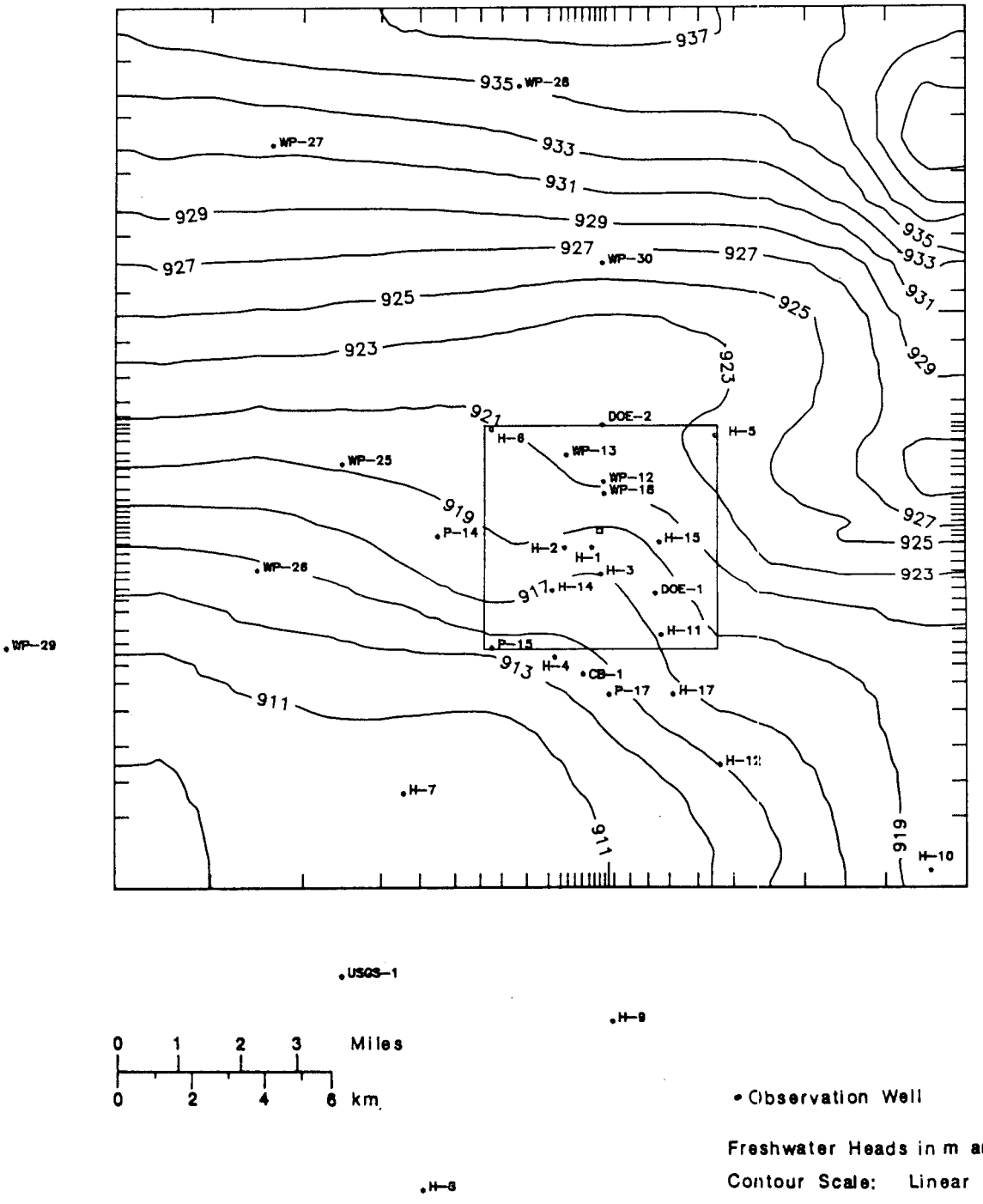

Drawn by	Date
Checked by	Date
Revisions	Date
H09700R554	

The Calculated Freshwater Heads of the Initial Simulation (Using AKRIP Initial Transmissivities and the Initial Boundary Conditions)

INTERA Technologies

Figure 4.1

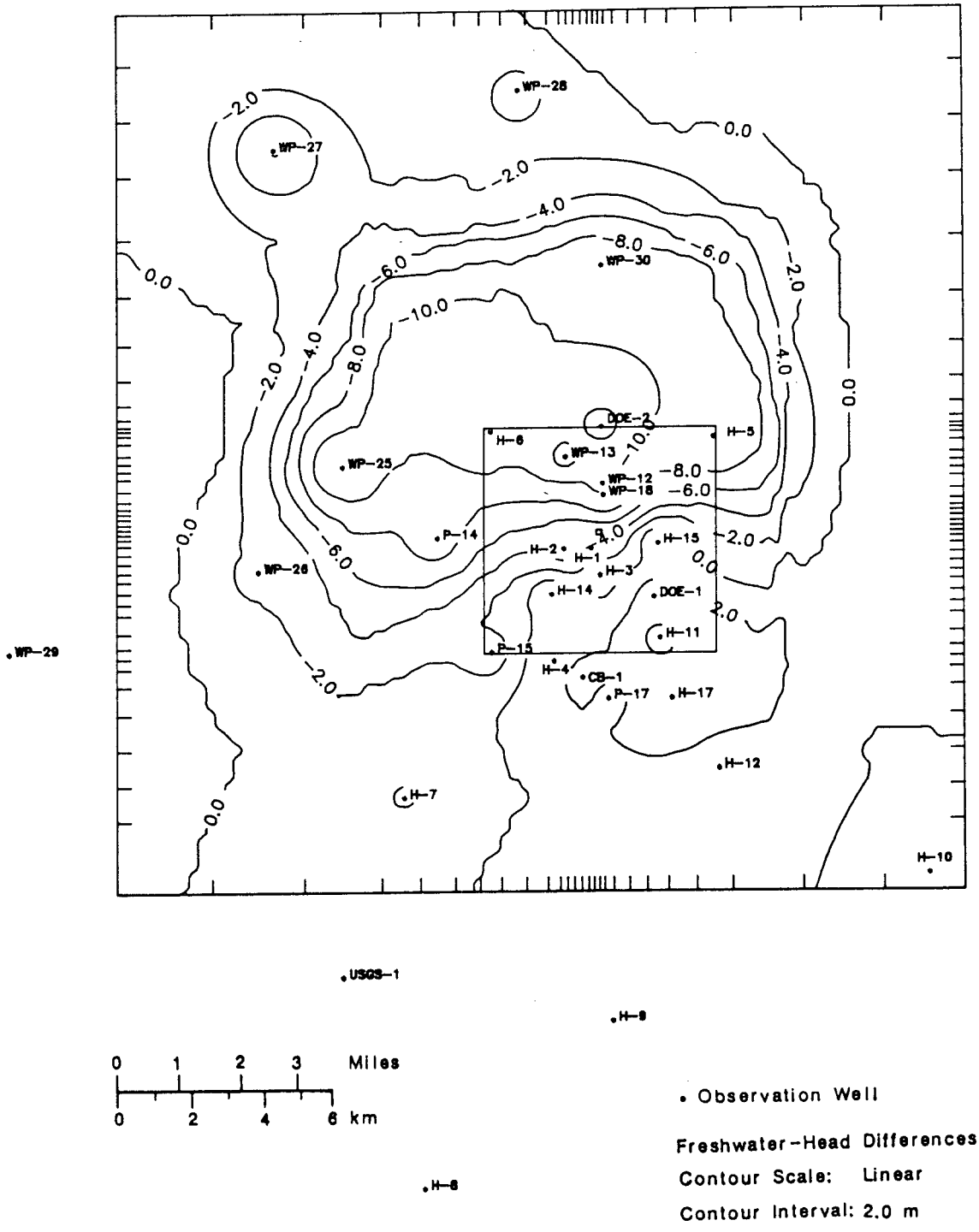

Drawn by	Date
Checked by	Date
Revisions	Date
H09700R554	

The Differences Between the Calculated and the Observed Freshwater Heads of the Initial Simulation

INTERA Technologies

Figure 4.2

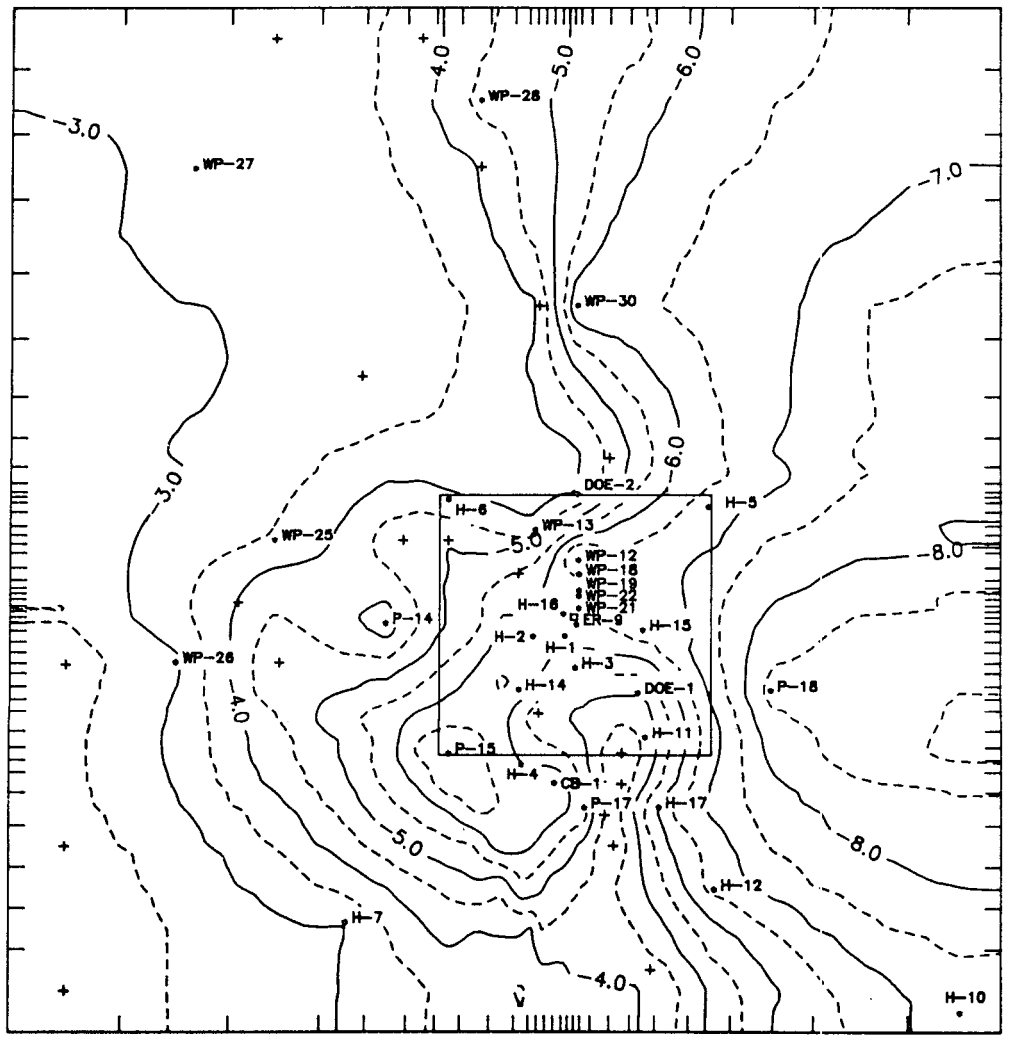

Drawn by	Date
Checked by	Date
Revisions	Date
HD9700R554	

The Steady-State Calibrated Log Transmissivities (Using AKRIP)

INTERA Technologies

Figure 4.3

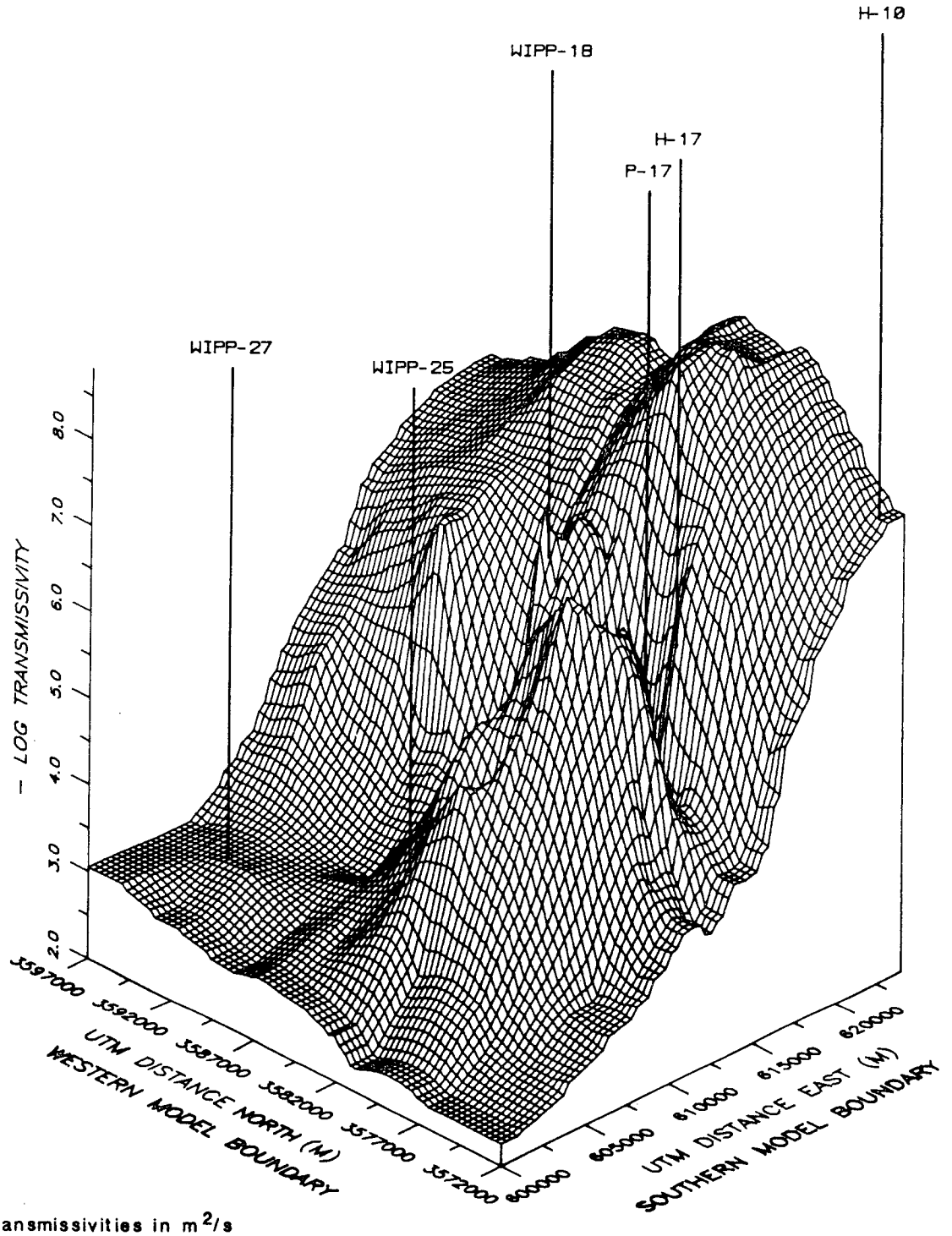

Transmissivities in m^2/s

Drawn by	Date
Checked by	Date
Revisions	Date
H09700R554	

The Steady-State Calibrated Negative Log Transmissivities

INTERA Technologies

Figure 4.4

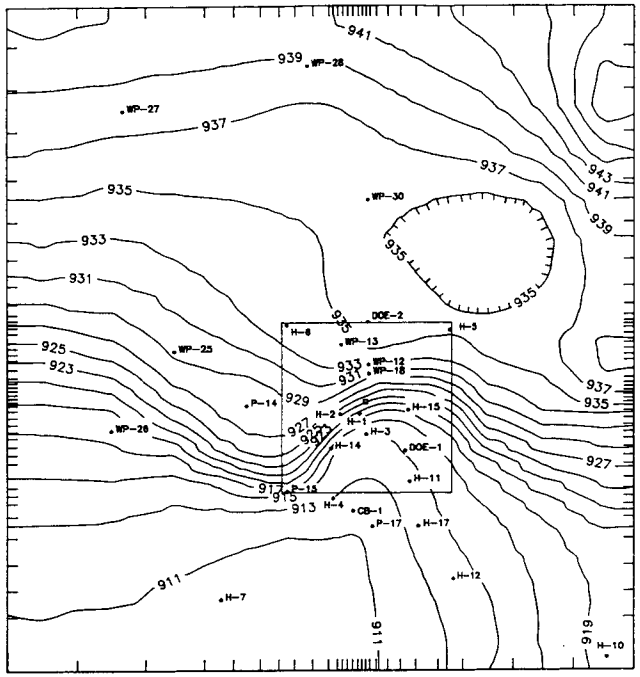

A. STEADY-STATE CALIBRATED HEADS

• Observation Well

Freshwater Heads in m a.s.l.

Contour Scale: Linear

Contour Interval: 2 m

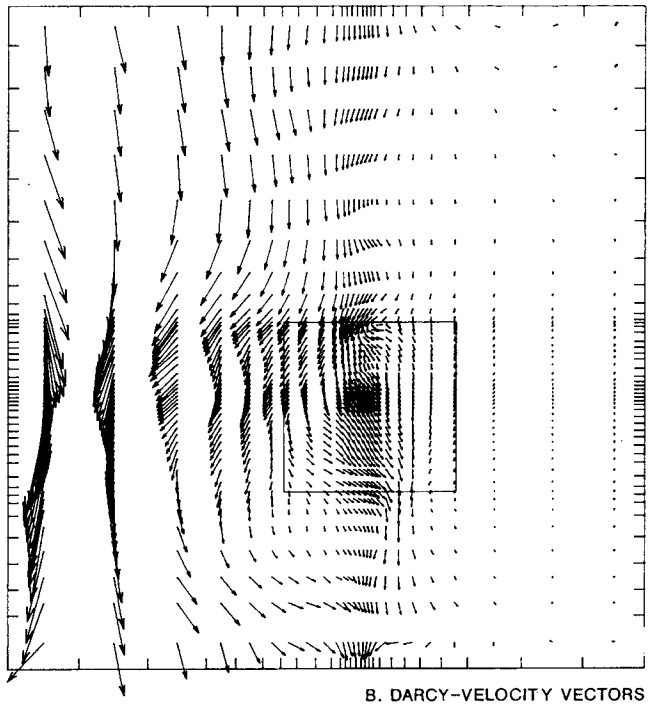

B. DARCY-VELOCITY VECTORS

Drawn by	Date
Checked by	Date
Revisions	Date
H09700R554	

Steady-State Calibrated Heads and Darcy-Velocity Vectors

INTERA Technologies

Figure 4.5

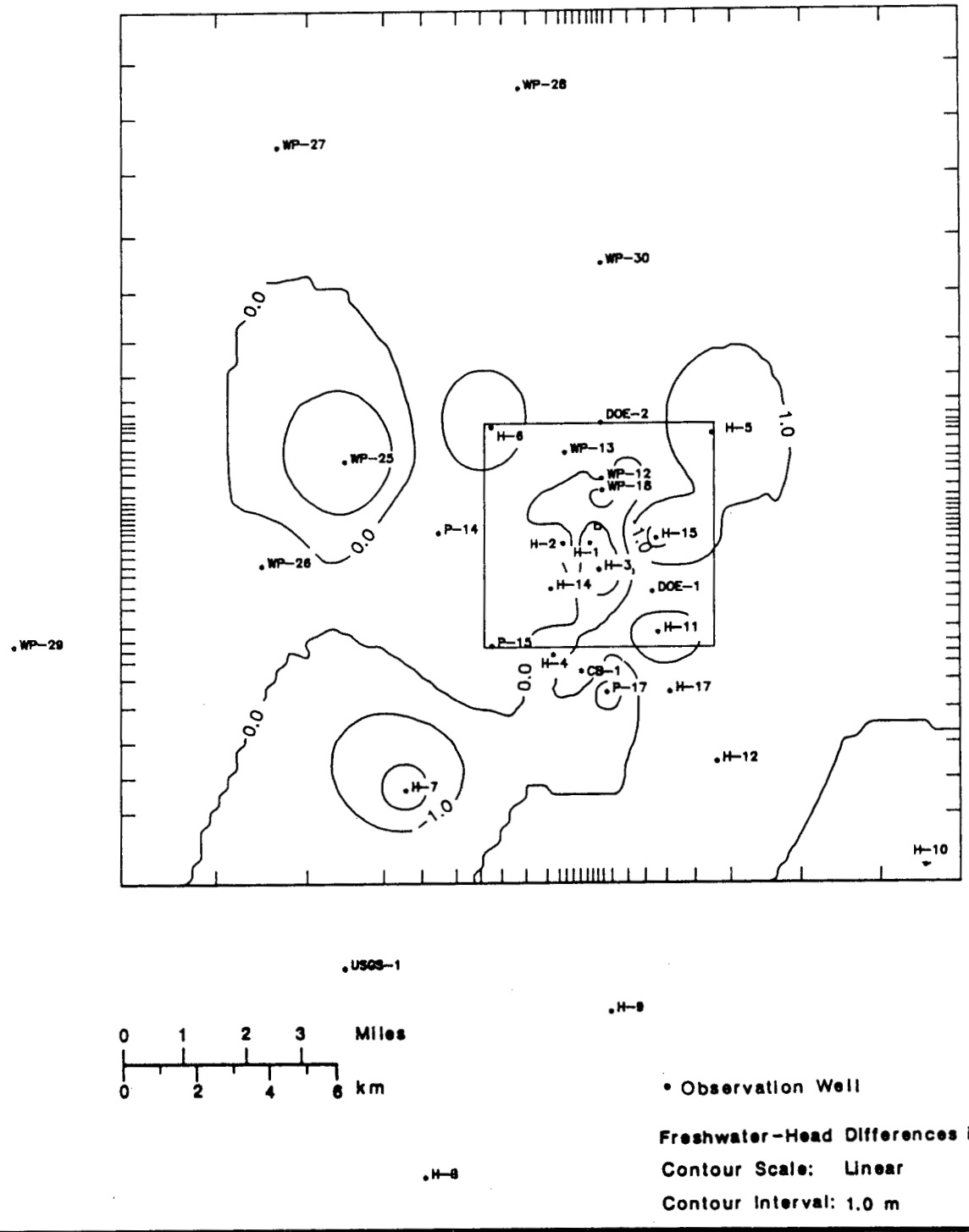

Drawn by	Date
Checked by	Date
Revisions	Date
H09700R554	

Differences Between the Calibrated Steady-State and Observed Freshwater Heads

INTERA Technologies

Figure 4.6

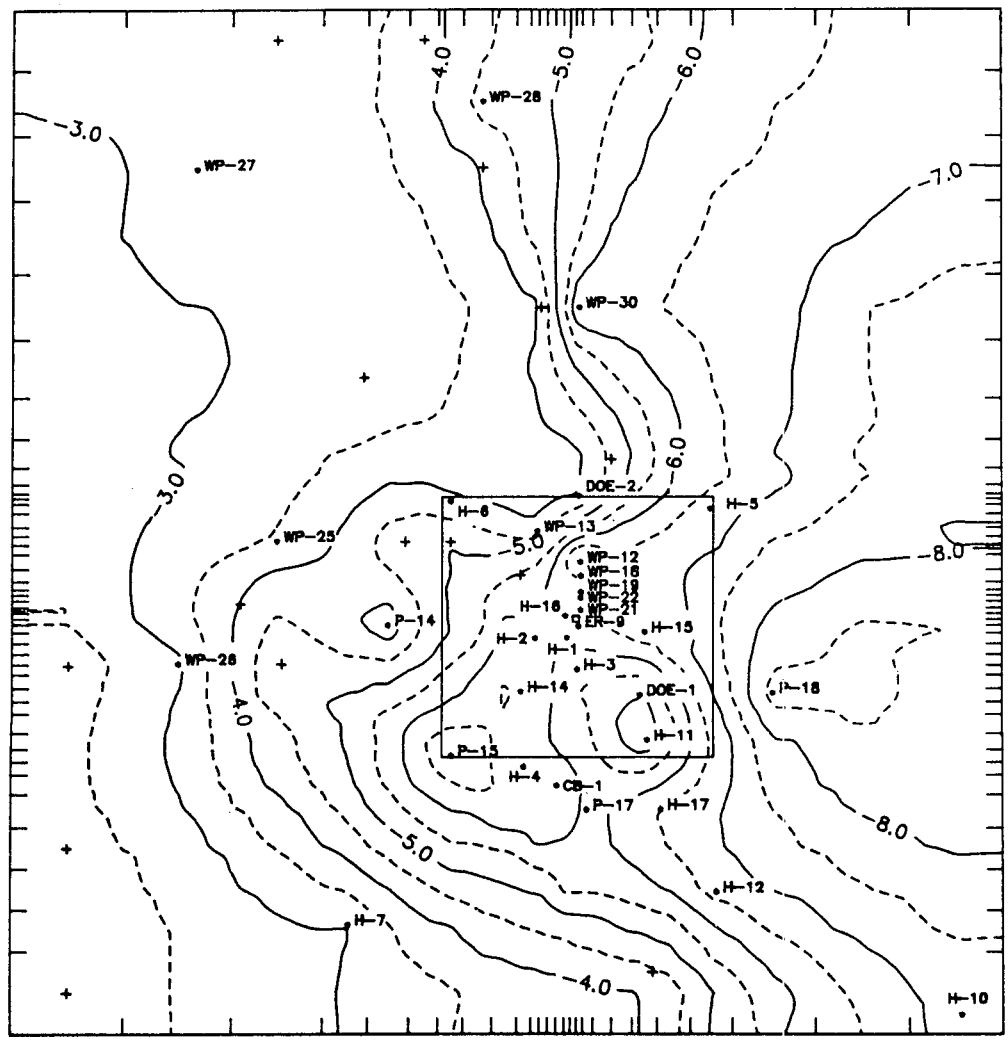

Drawn by	Date
Checked by	Date
Revisions	Date
H09700R554	

Log Transmissivities Without a High-Transmissivity Zone South of H-11

INTERA Technologies

Figure 4.7

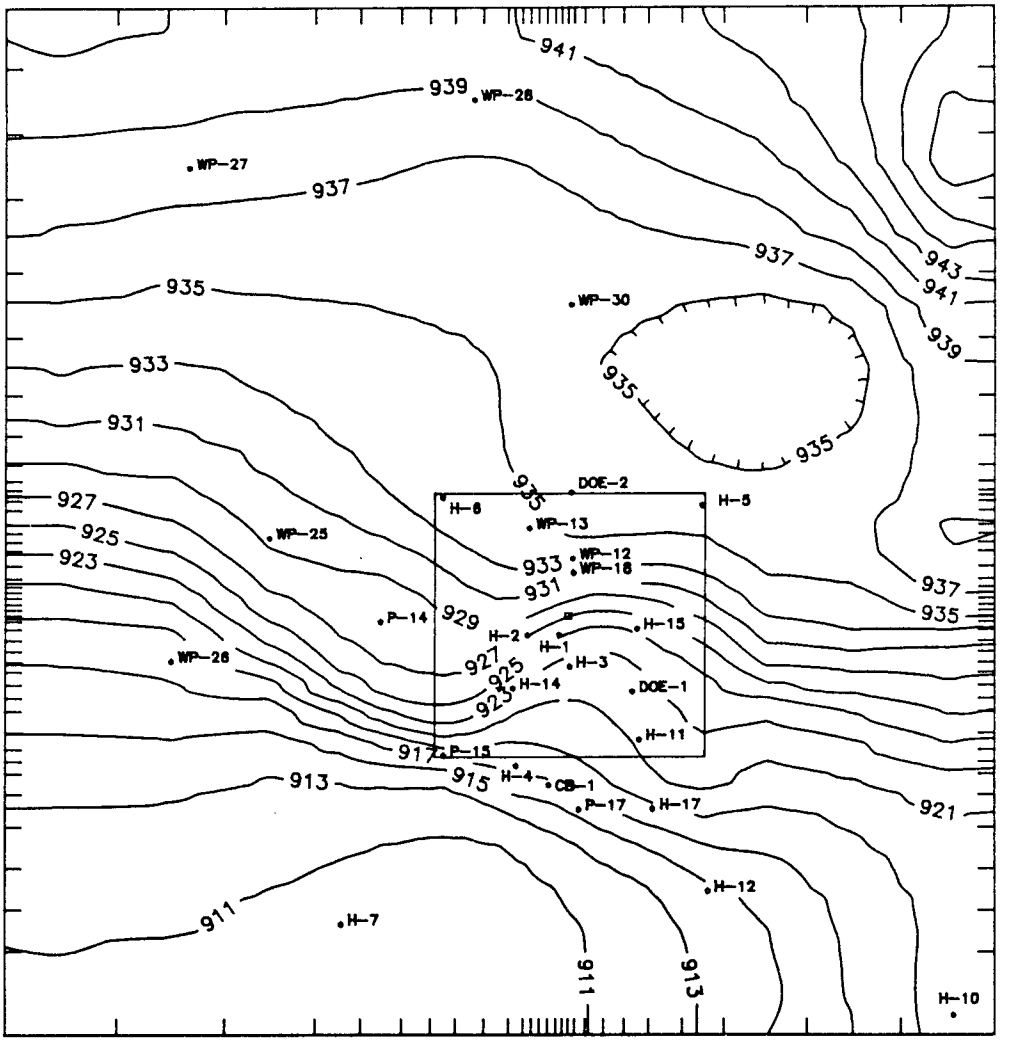

Drawn by	Date
Checked by	Date
Revisions	Date
H09700R554	

The Calculated Freshwater Heads Without a High-Transmissivity Zone South of H-11

INTERA Technologies

Figure 4.8

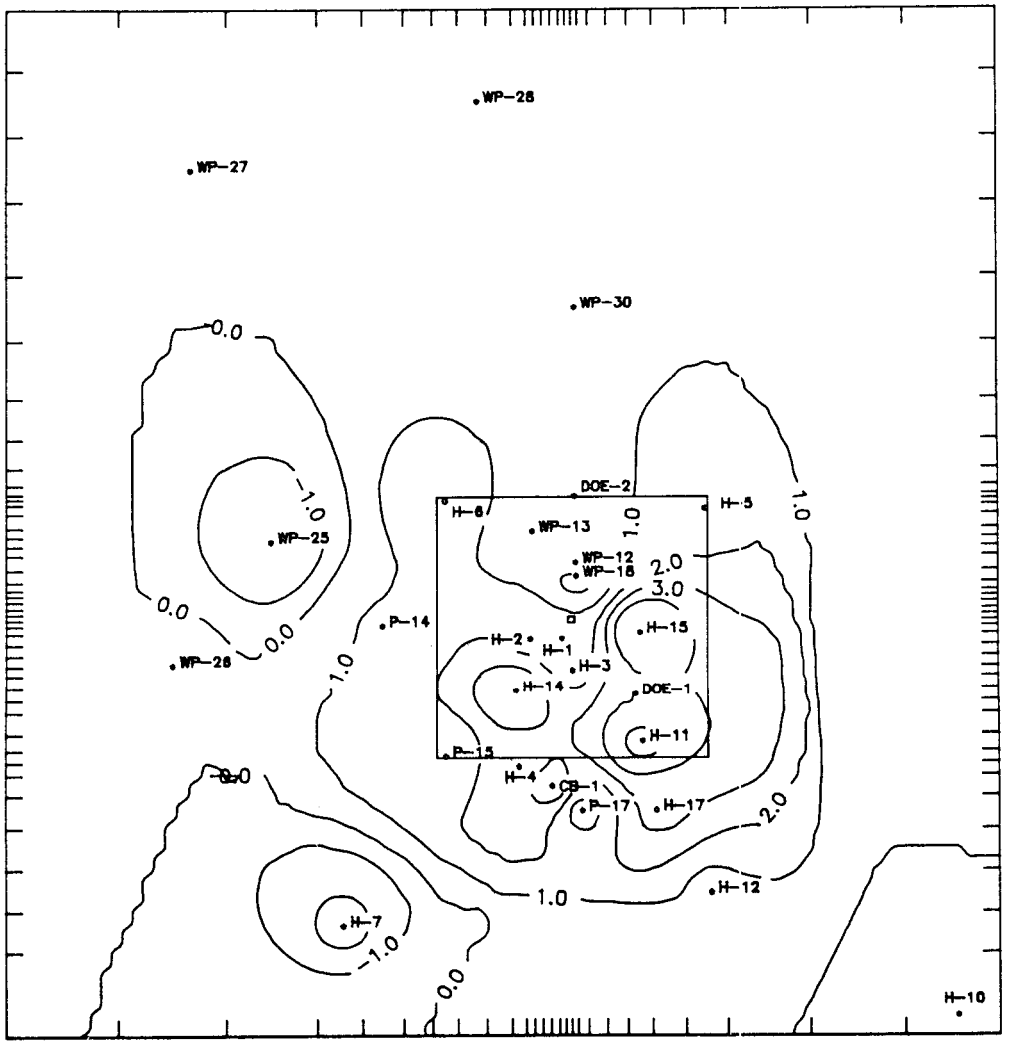

Drawn by	Date
Checked by	Date
Revisions	Date
H09700R554	

Differences Between the Calculated and Observed Freshwater Heads Without a High-Transmissivity Zone South of H-11

INTERA Technologies

Figure 4.9

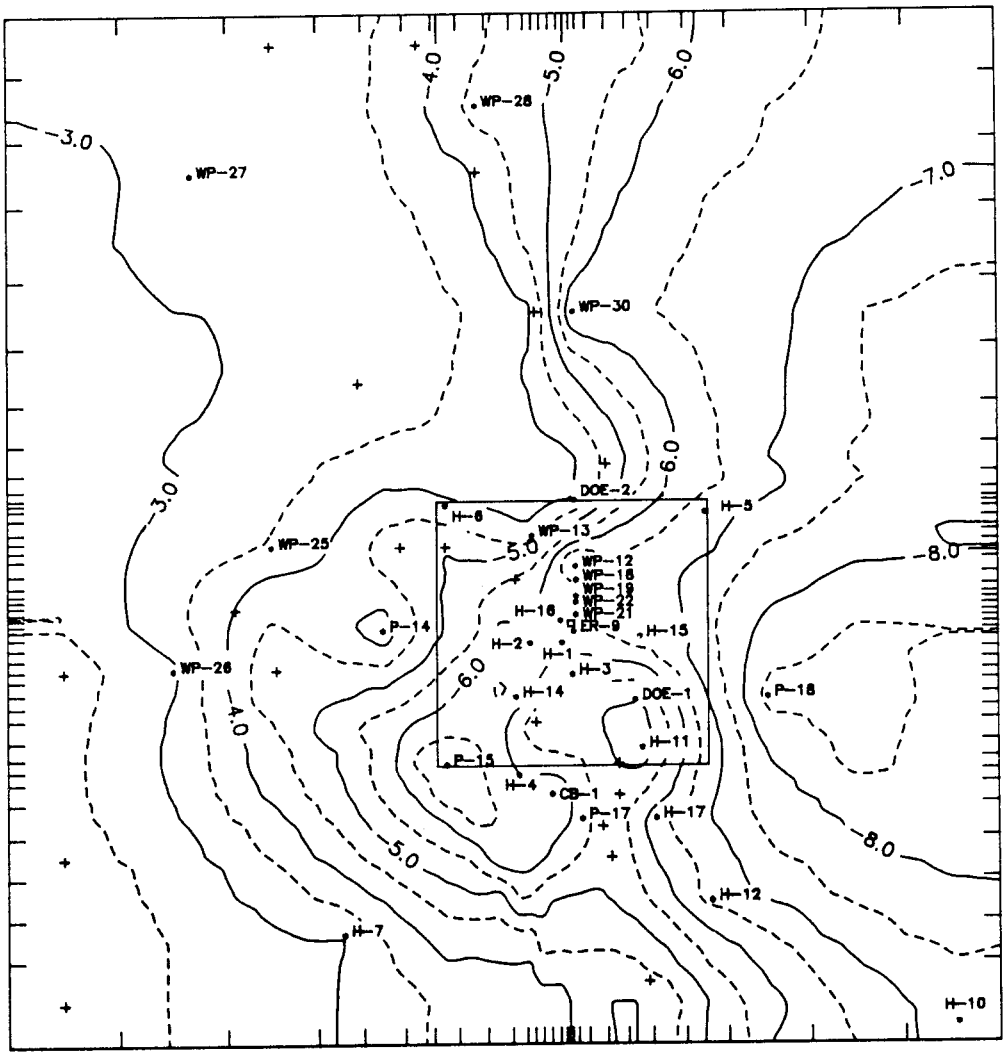

Drawn by	Date
Checked by	Date
Revisions	Date
H09700R554	

Log Transmissivities With a Moderate-Transmissivity Zone South of H-11

INTERA Technologies

Figure 4.10

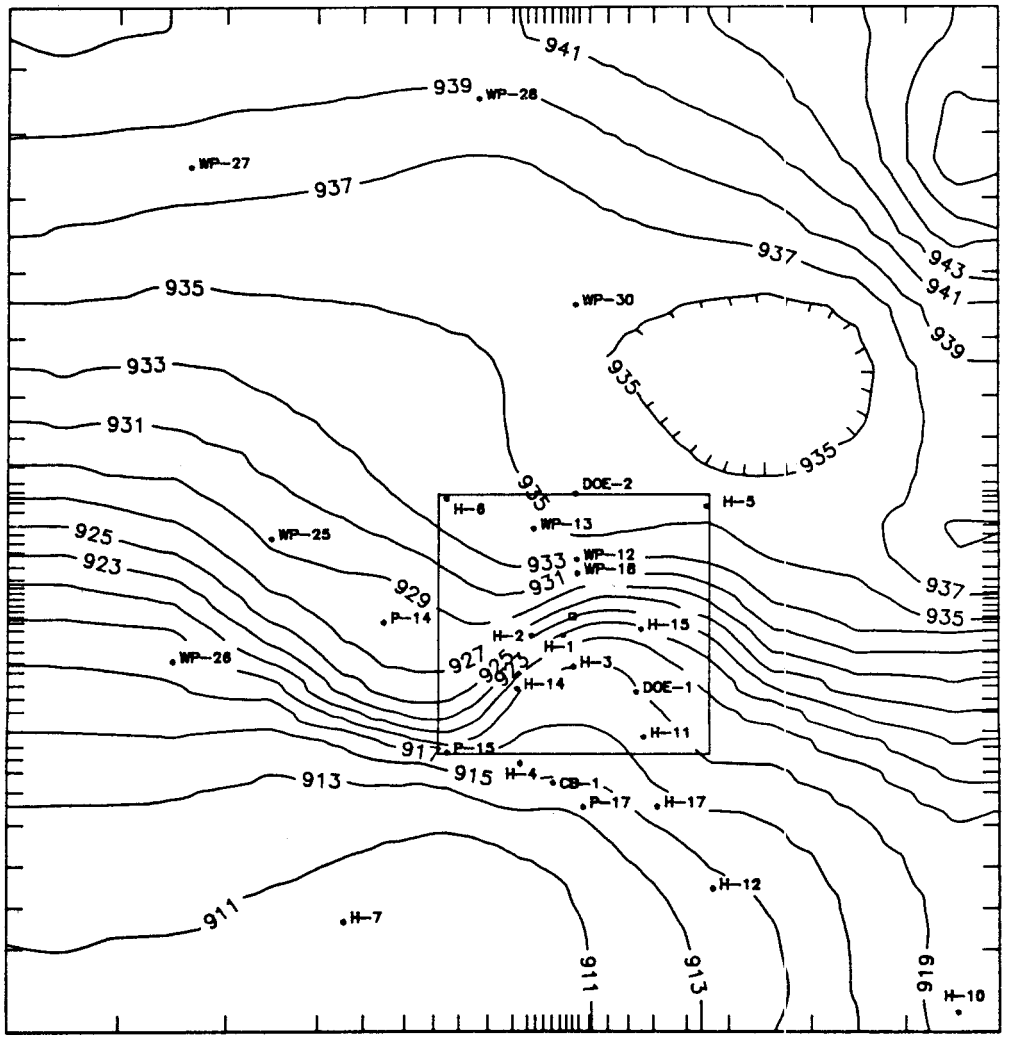

Drawn by	Date
Checked by	Date
Revisions	Date
H09700R554	

The Calculated Freshwater Heads With a Moderate-Transmissivity Zone South of H-11

INTERA Technologies

Figure 4.11

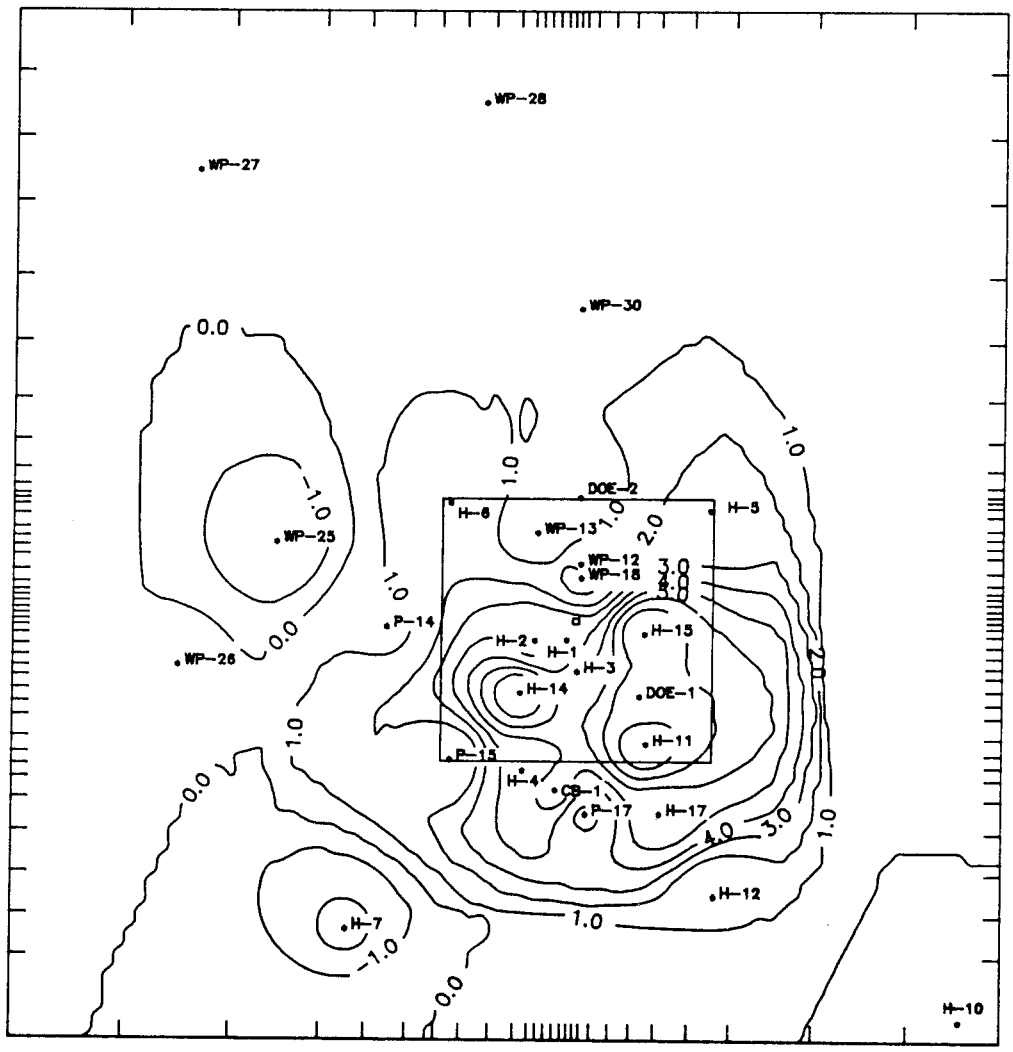

Drawn by	Date
Checked by	Date
Revisions	Date
HD9700R554	

Differences Between the Calculated and Observed Freshwater Heads With a Moderate-Transmissivity Zone South of H-11

INTERA Technologies

Figure 4.12

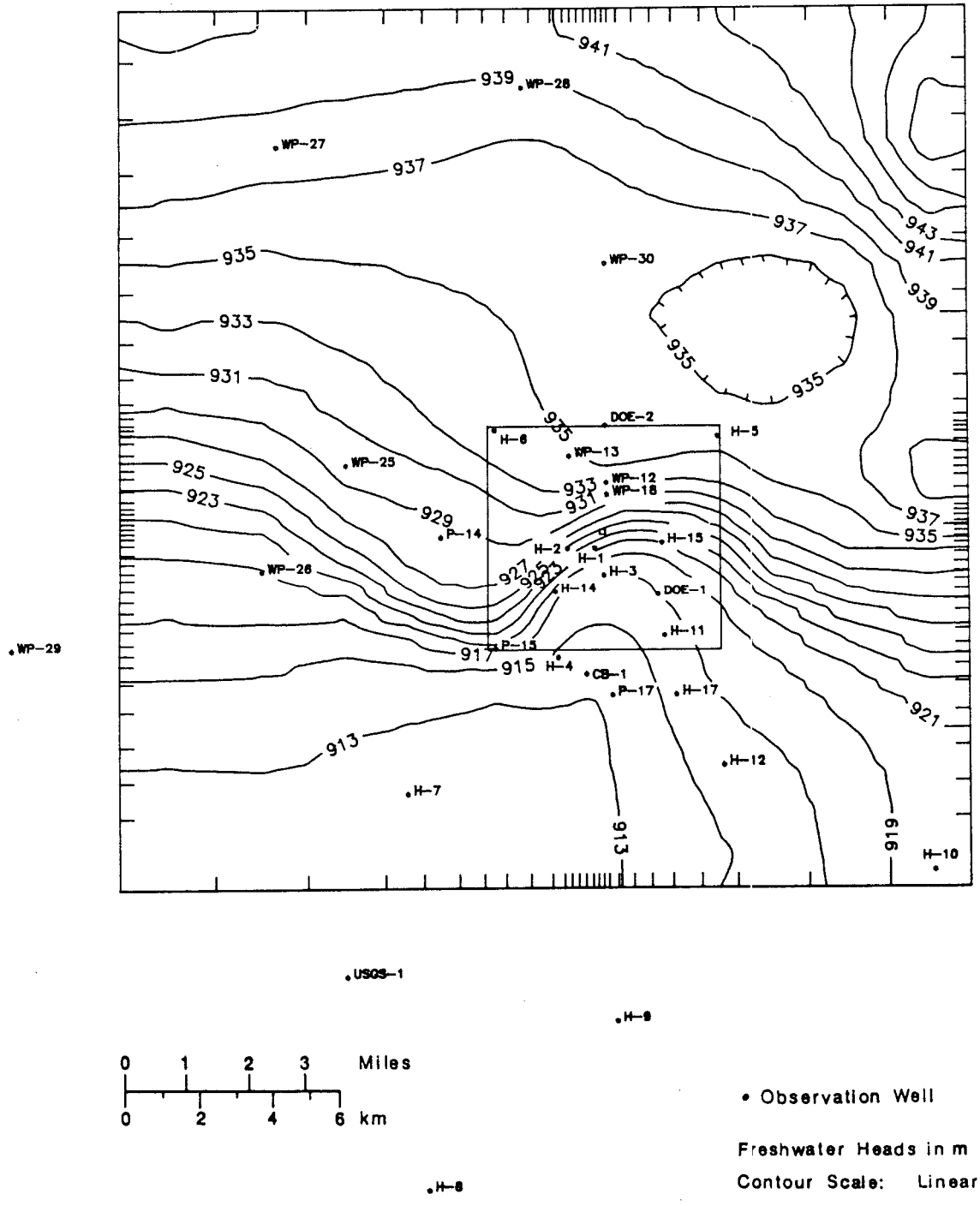

Drawn by	Date
Checked by	Date
Revisions	Date
HD9700R554	

The Calculated Freshwater Heads using Increased Heads at Southwestern Model Boundaries

INTERA Technologies

Figure 4.13

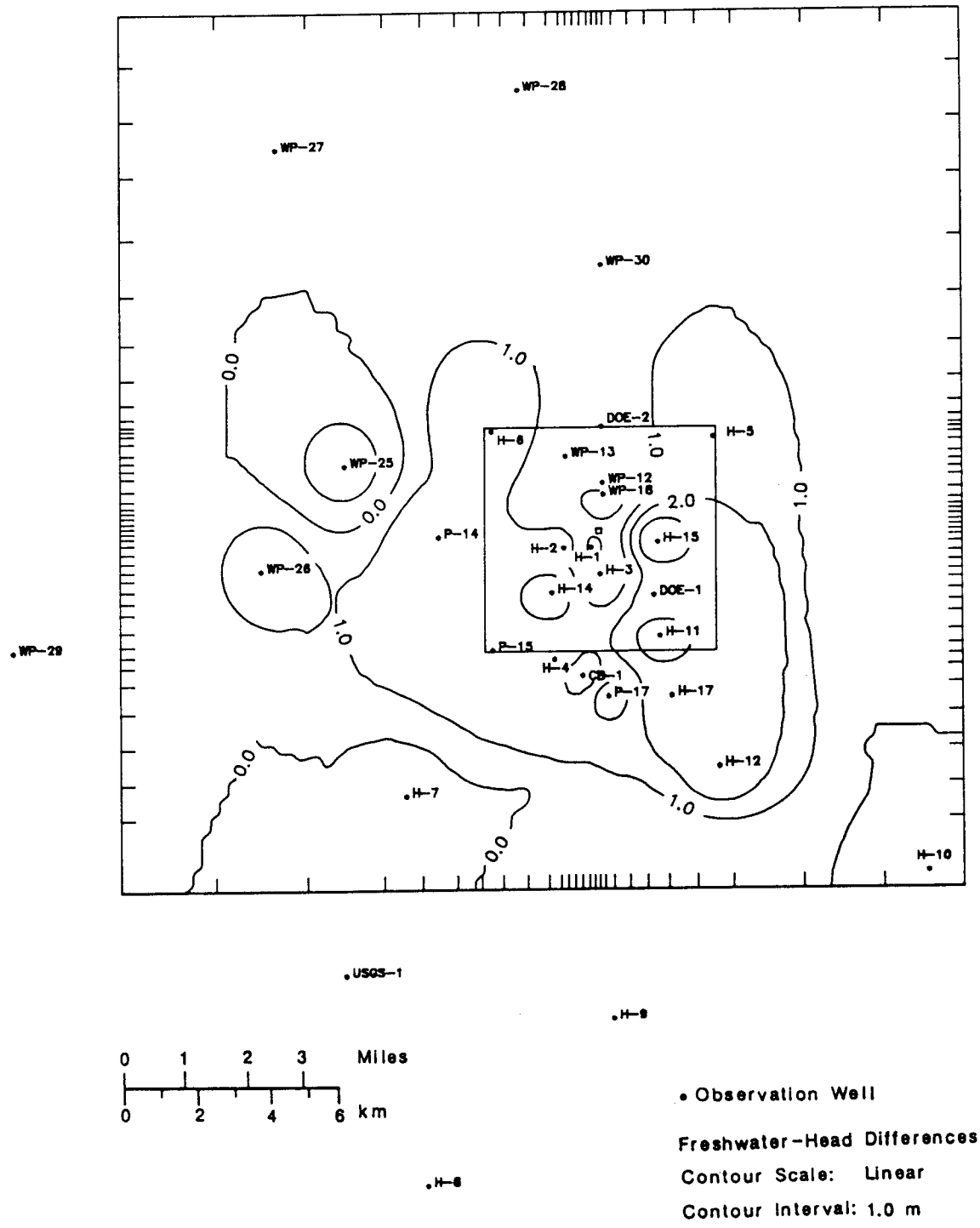

Drawn by	Date
Checked by	Date
Revisions	Date
H09700R554	

Differences Between the Calculated and the Observed Freshwater Heads Using Increased Heads at Southwestern Model Boundaries

INTERA Technologies

Figure 4.14

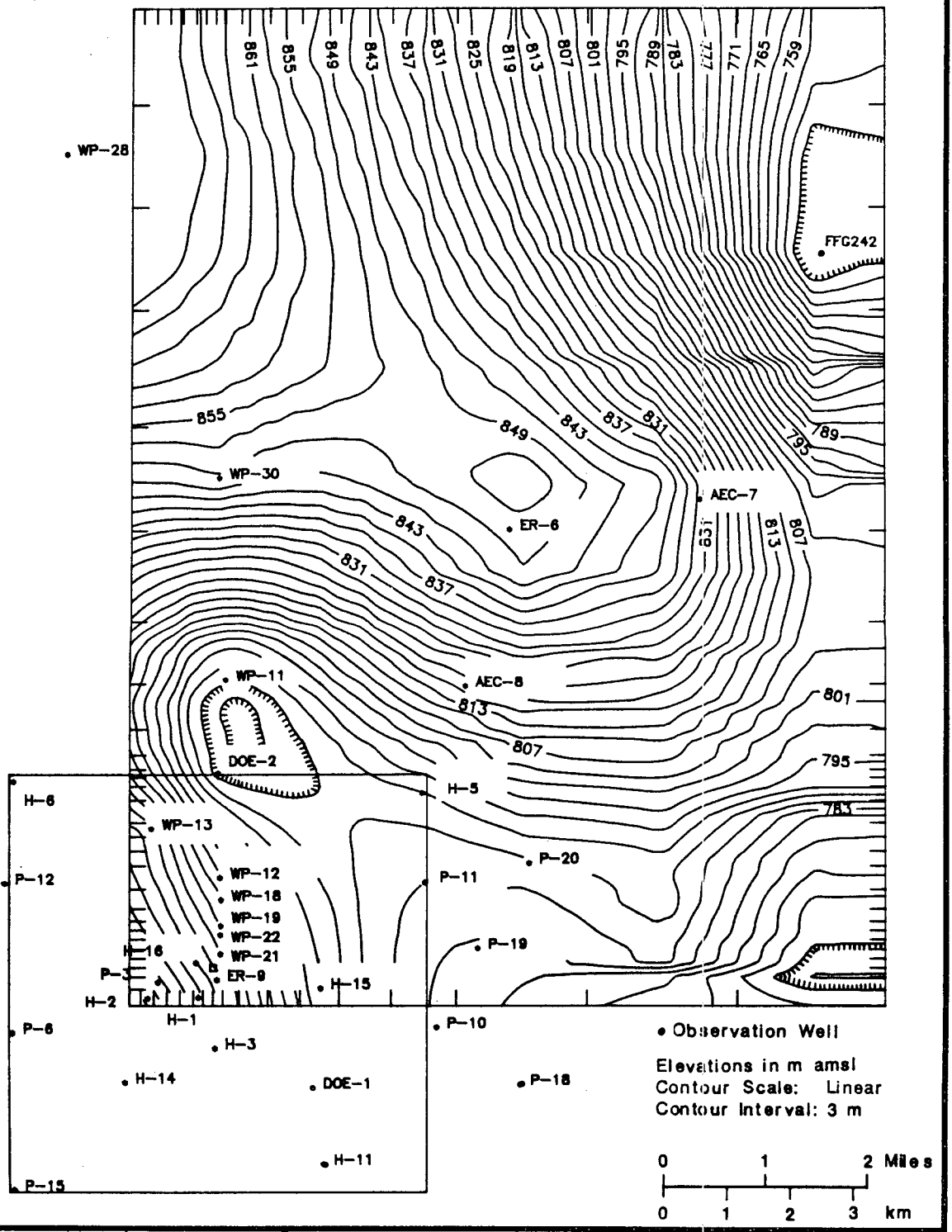

Drawn by	Date
Checked by	Date
Revisions	Date
H09700R554	

Center-of-Grid-Block Elevations in Northeast Quadrant of Modeled Area

INTERA Technologies

Figure 4.15

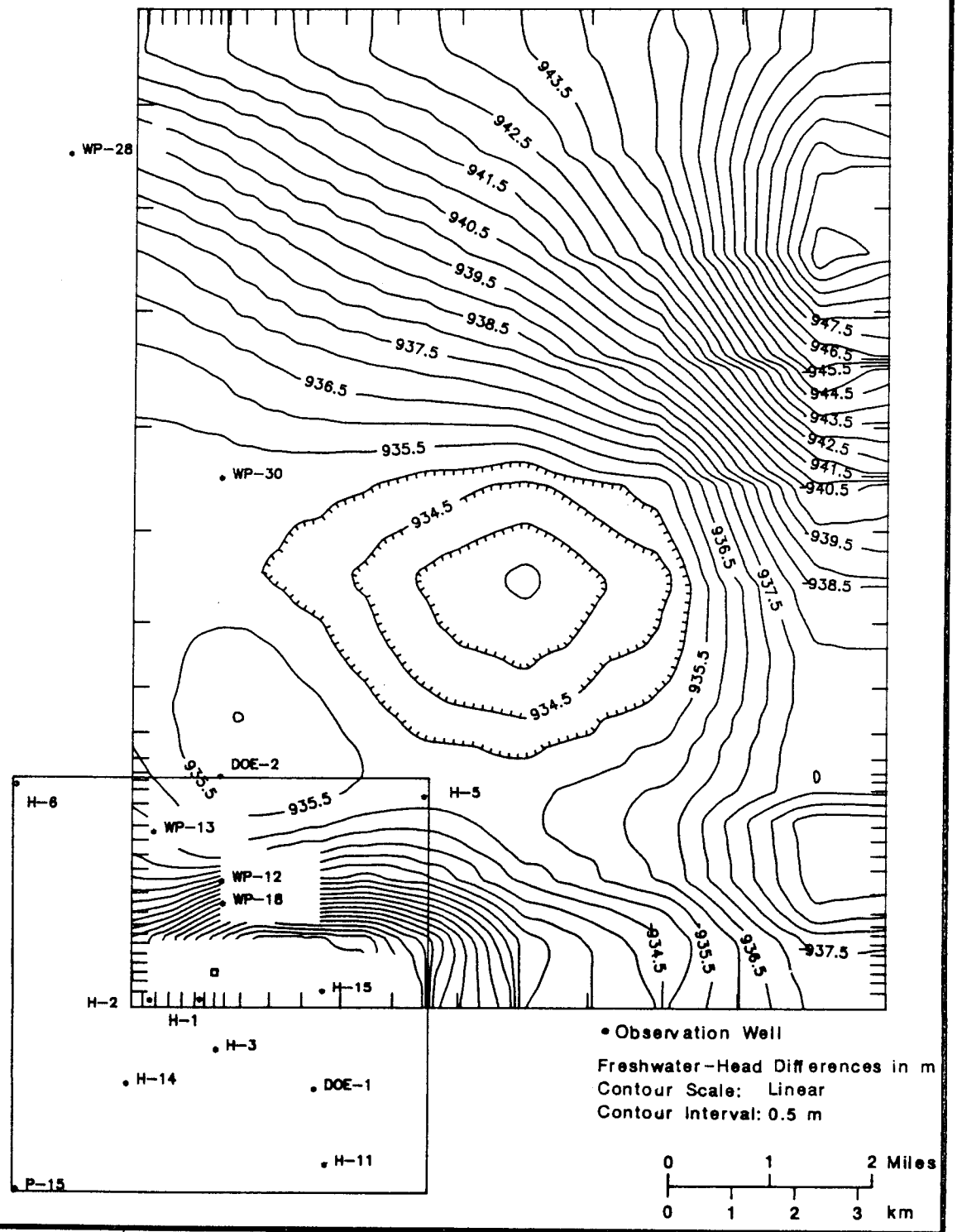

Drawn by	Date
Checked by	Date
Revisions	Date
HD9700R554	

Model-Calculated Freshwater Heads in Northeast Quadrant of Modeled Region

INTERA Technologies

Figure 4.16

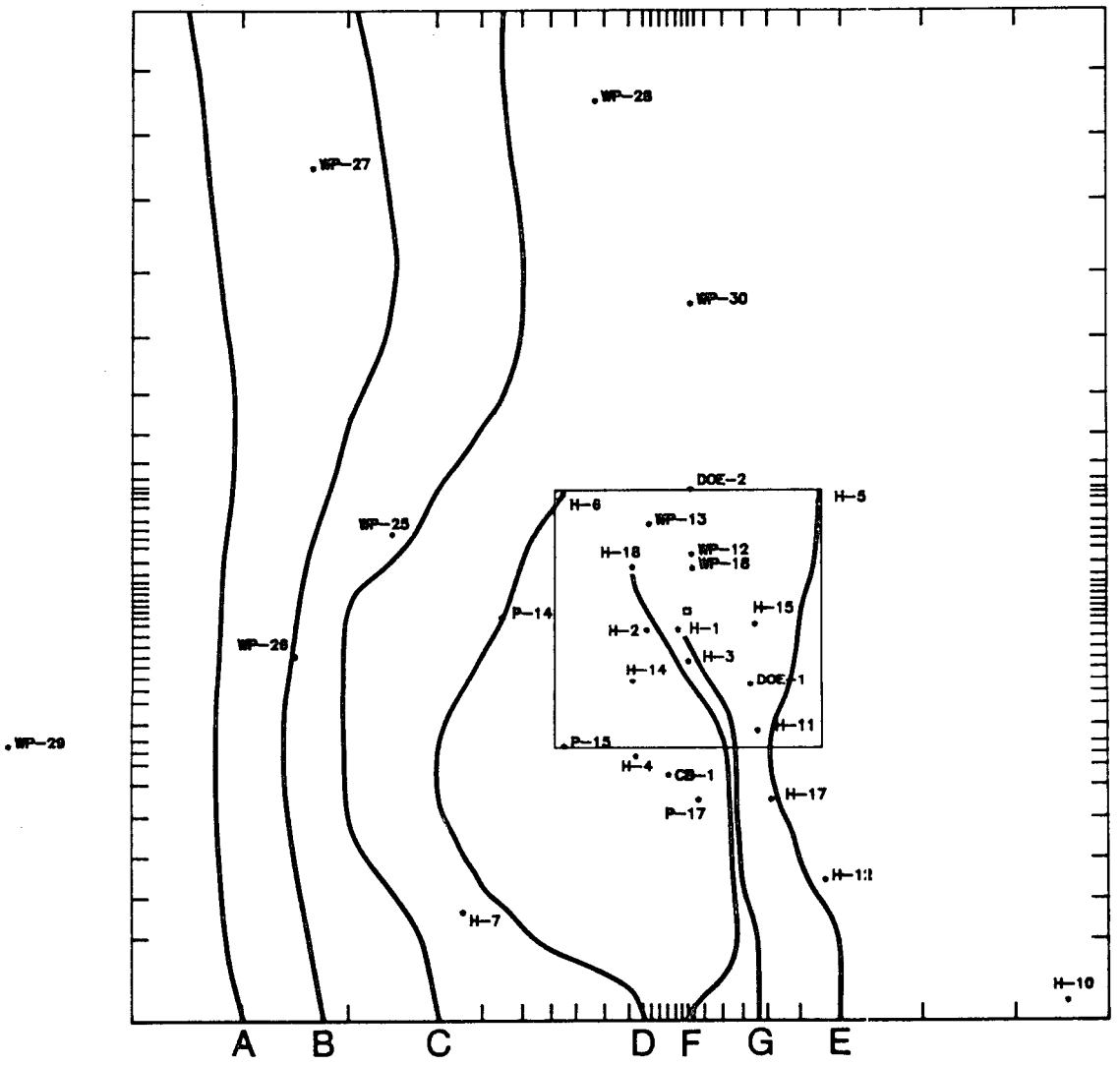

Calculated Particle Travel Times

Particle A = 4.5×10^2 years
Particle B = 9.8×10^2 years
Particle C = 2.8×10^3 years
Particle D = 1.6×10^4 years
Particle E = 1.4×10^6 years
Particle F = 5.8×10^4 years
Particle G = 3.6×10^4 years

Drawn by	Date	Calculated Particle Travel Times In the Model Region	
Checked by	Date		
Revisions	Date		
INTERA Technologies			Figure 4.17

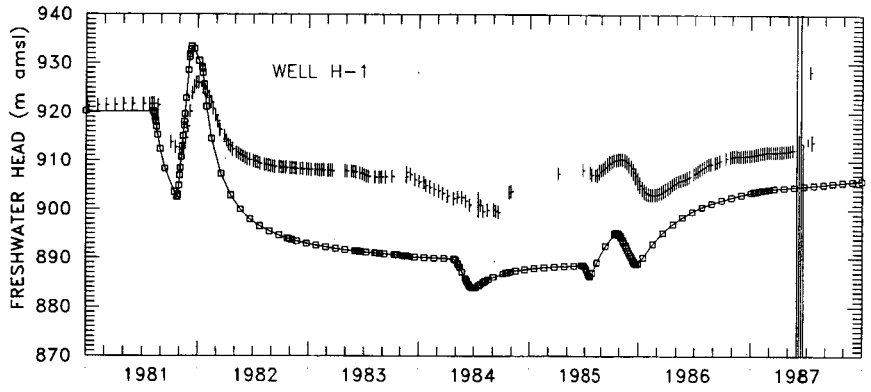

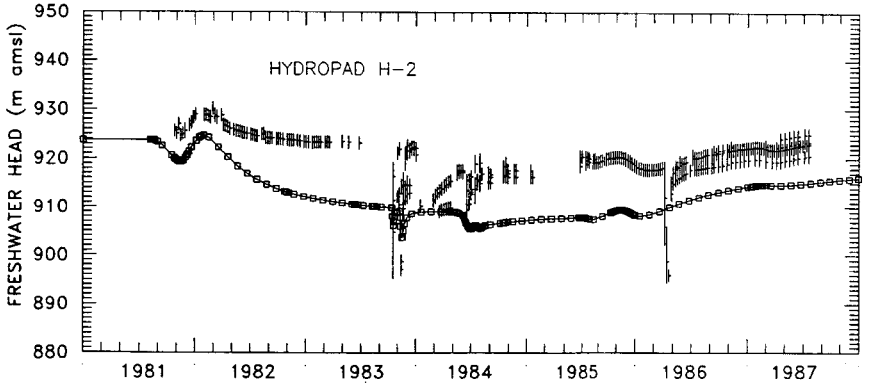

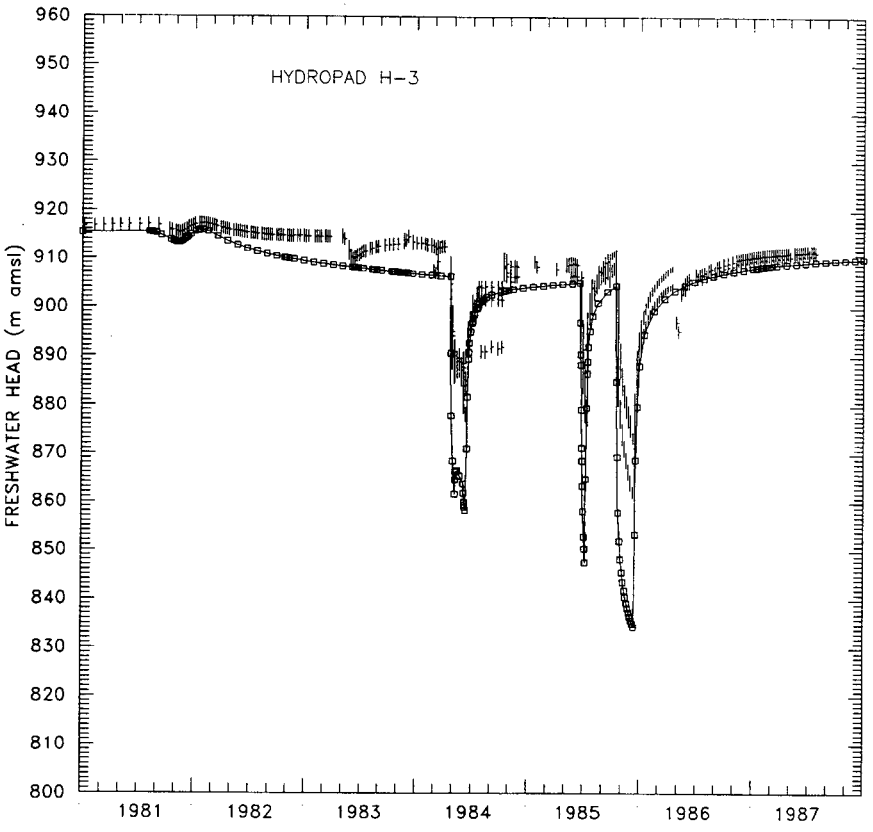

LEGEND: Calculated Freshwater Heads

Observed Freshwater Heads (Water Level Data)

Observed Freshwater Heads (Transducer Data)

Drawn by	Date
Checked by	Date
Revisions	Date
H09700554	

INTERA Technologies

Calculated and Observed Transient Freshwater Heads at H-1, H-2, and H-3 Using the Steady-State Calibrated Transmissivity Distribution

Figure 5.1a

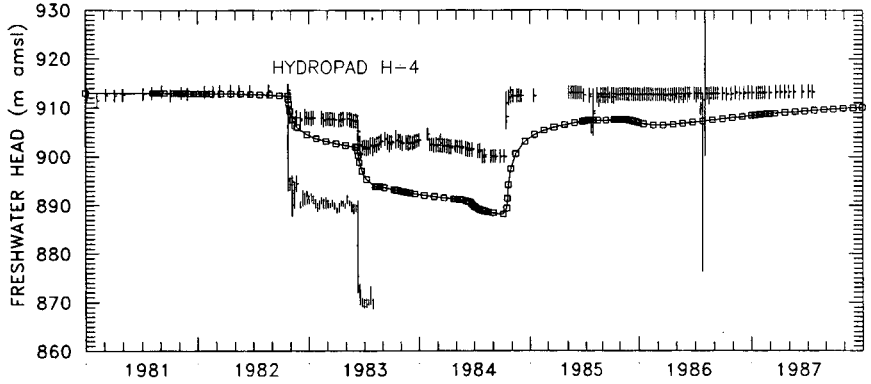

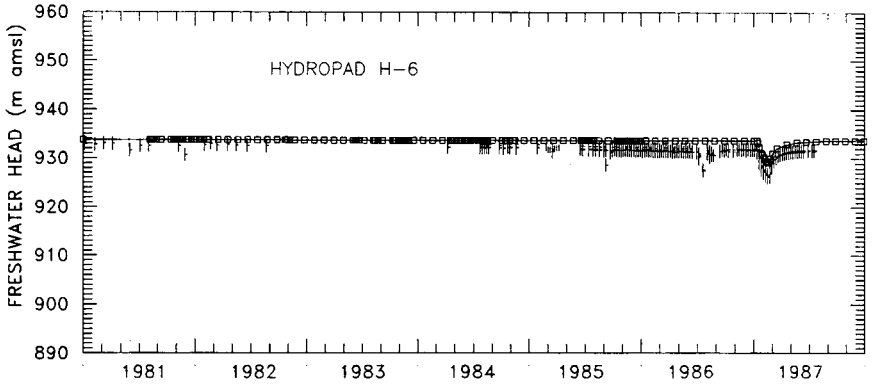

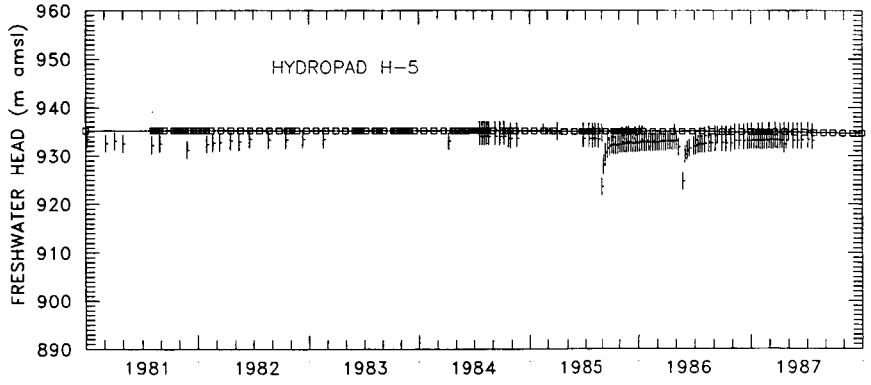

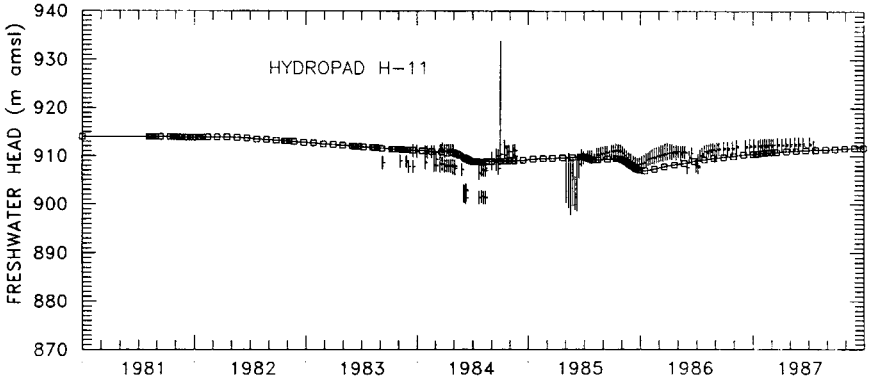

LEGEND: Calculated Freshwater Heads

Observed Freshwater Heads (Water Level Data)

Observed Freshwater Heads (Transducer Data)

Drawn by	Date
Checked by	Date
Revisions	Date
H09700R554	

INTERA Technologies

Calculated and Observed Transient Freshwater Heads at H-4, H-5, H-6, and H-11 Using the Steady-State Calibrated Transmissivity Distribution

Figure 5.1b

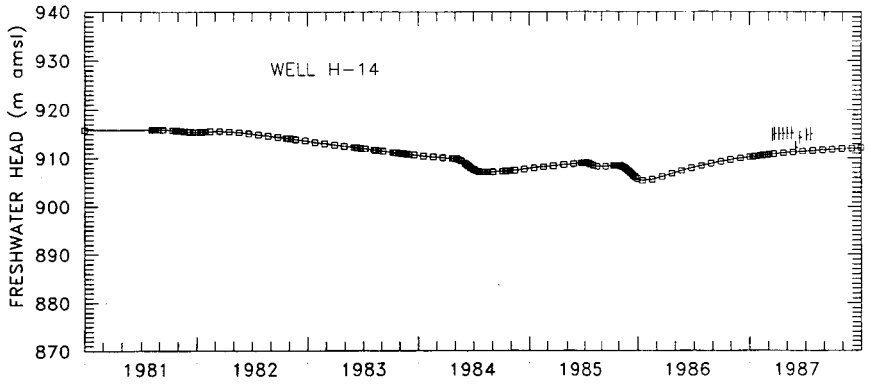

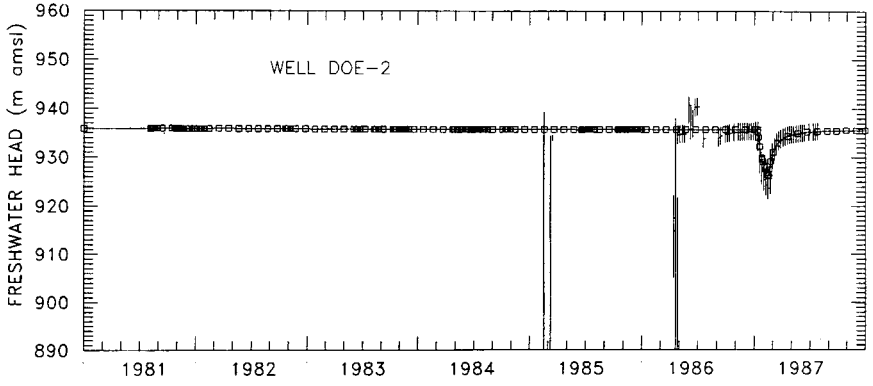

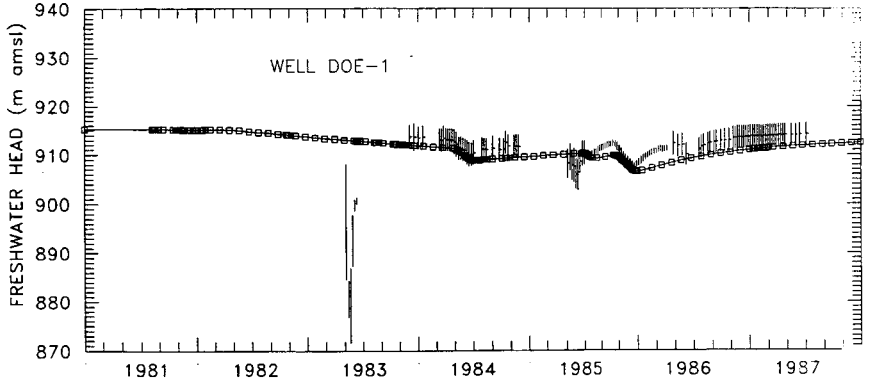

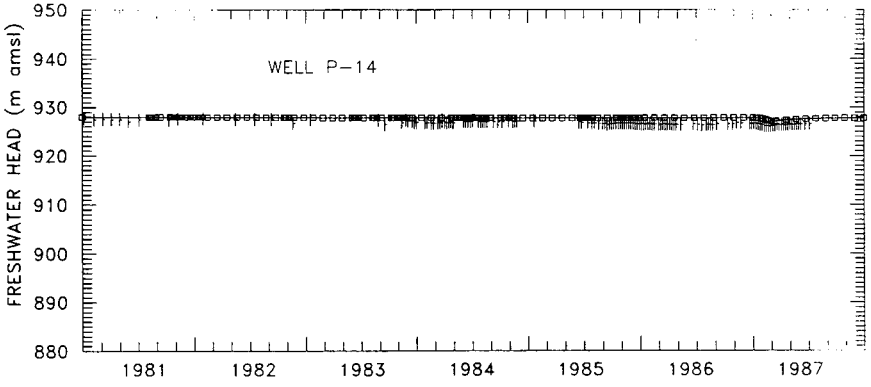

LEGEND: Calculated Freshwater Heads

Observed Freshwater Heads (Water Level Data)

Observed Freshwater Heads (Transducer Data)

Drawn by	Date
Checked by	Date
Revisions	Date
H09700R554	

Calculated and Observed Transient Freshwater Heads at H-14, DOE-1, DOE-2, and P-14 Using the Steady-State Calibrated Transmissivity Distribution

INTERA Technologies

Figure 5.1c

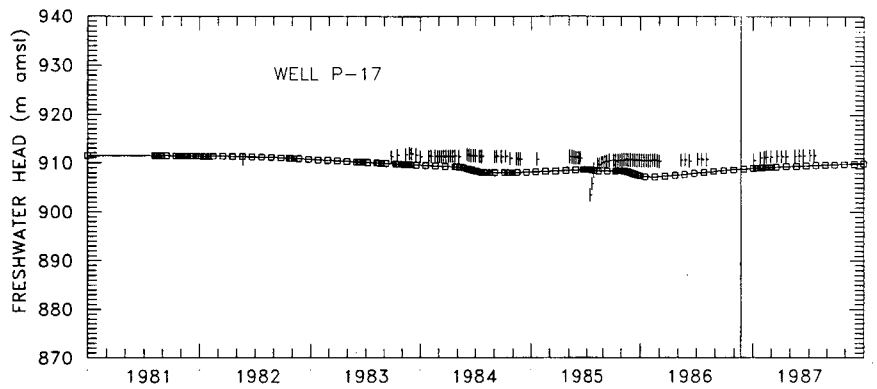

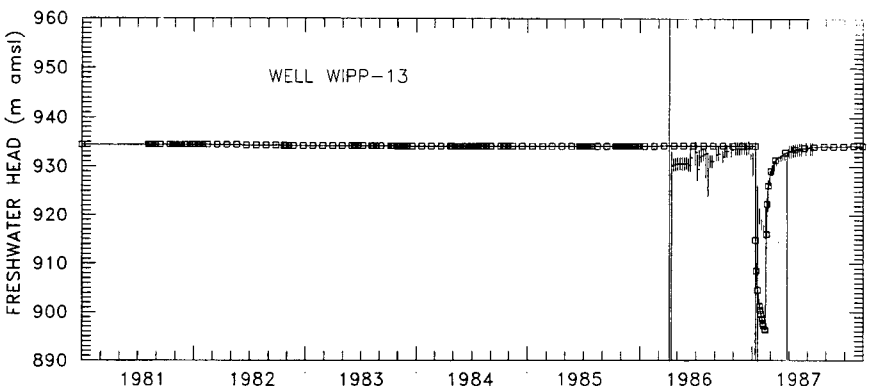

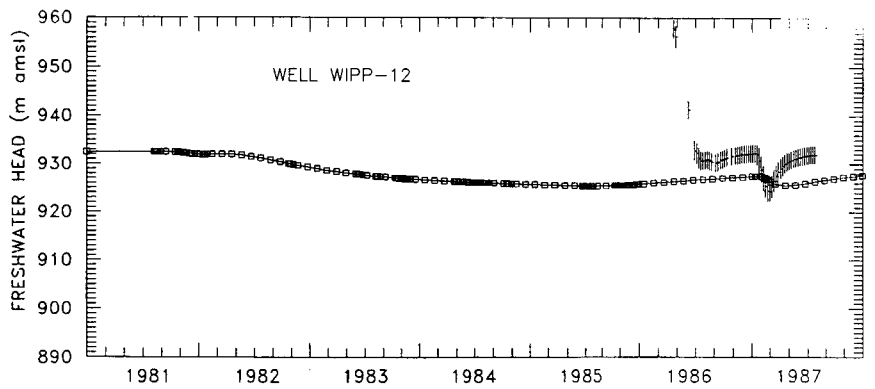

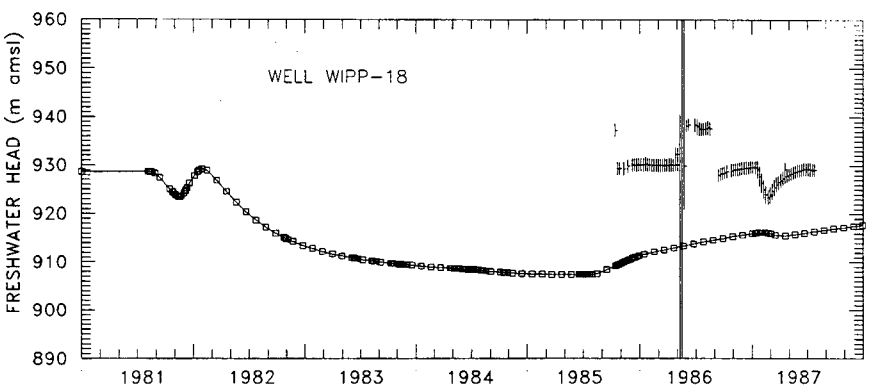

LEGEND: Calculated Freshwater Heads

Observed Freshwater Heads (Water Level Data)

Observed Freshwater Heads (Transducer Data)

Drawn by	Date
Checked by	Date
Revisions	Date
H09700R554	

INTERA Technologies

Calculated and Observed Transient Freshwater Heads at P-17, WIPP-12, WIPP-13,and WIPP-18 Using the Steady-State Calibrated Transmissivity Distribution

Figure 5.1d

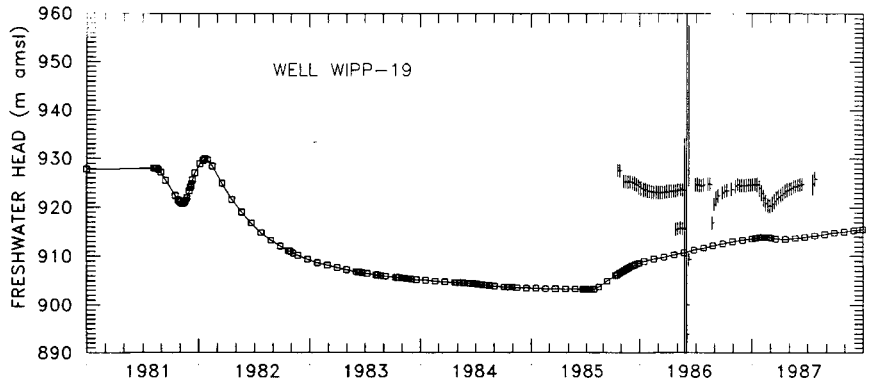

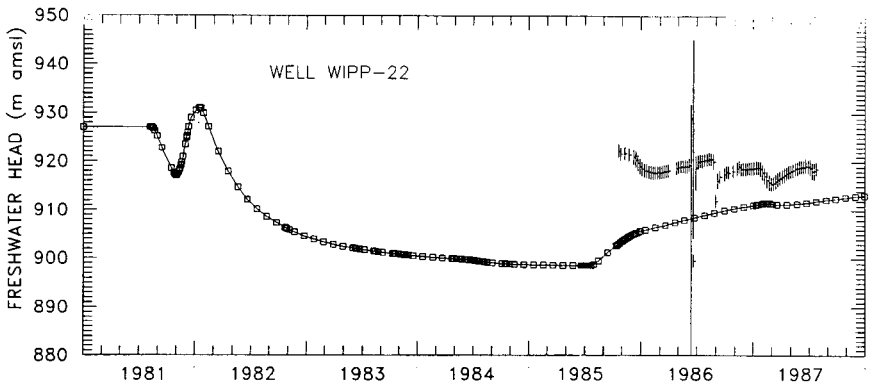

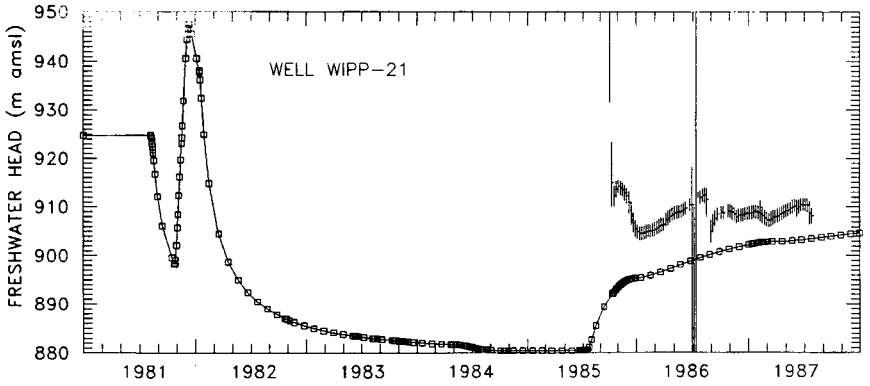

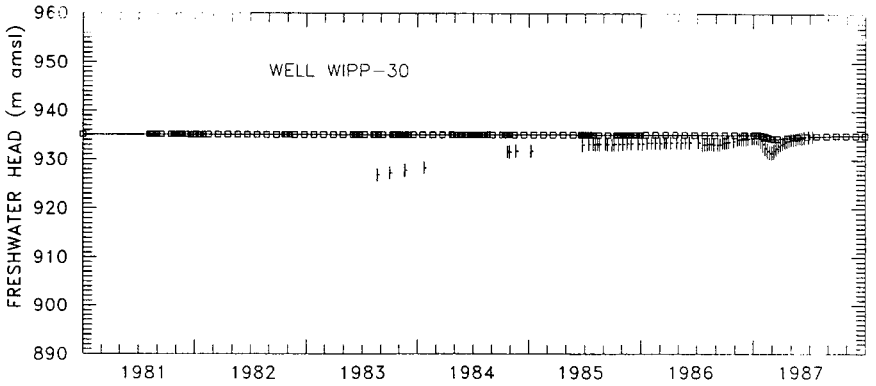

LEGEND: Calculated Freshwater Heads

Observed Freshwater Heads (Water Level Data)

Observed Freshwater Heads (Transducer Data)

Drawn by	Date
Checked by	Date
Revisions	Date
H09700R554	

Calculated and Observed Transient Freshwater Heads at WIPP-19, WIPP-21, WIPP-22, and WIPP-30 Using the Steady-State Calibrated Transmissivity Distribution

INTERA Technologies

Figure 5.1e

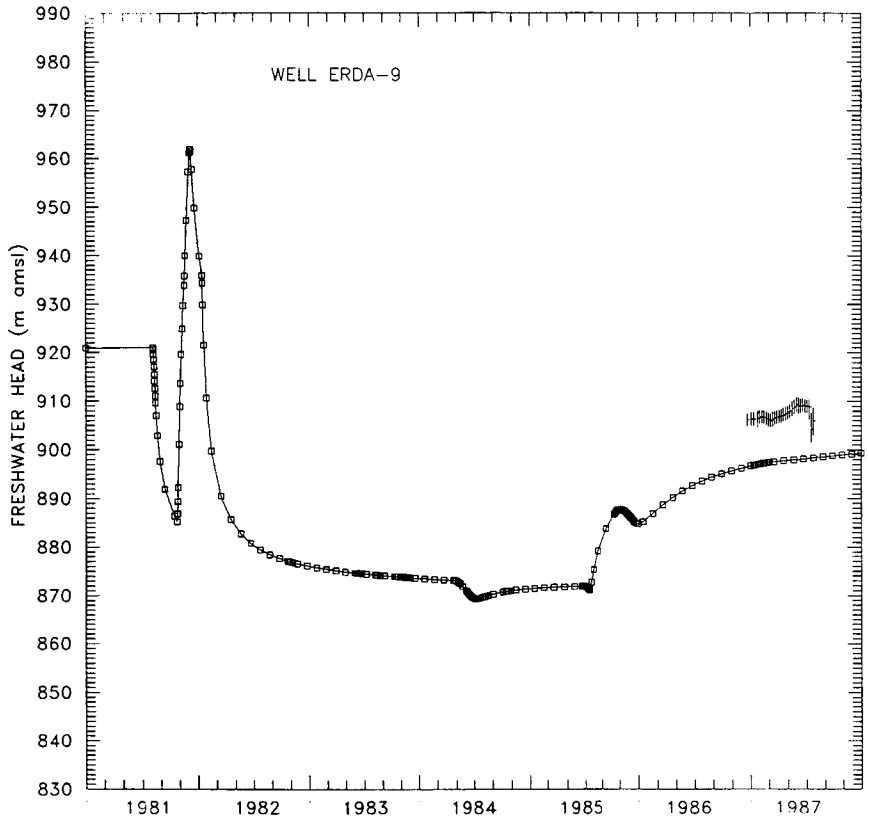

LEGEND: Calculated Freshwater Heads

Observed Freshwater Heads (Water Level Data)

Observed Freshwater Heads (Transducer Data)

Drawn by	Date
Checked by	Date
Revisions	Date
H09700R554	

INTERA Technologies

Calculated and Observed Transient Freshwater Heads at ERDA-9 Using the Steady-State Calibrated Transmissivity Distribution

Figure 5.1f

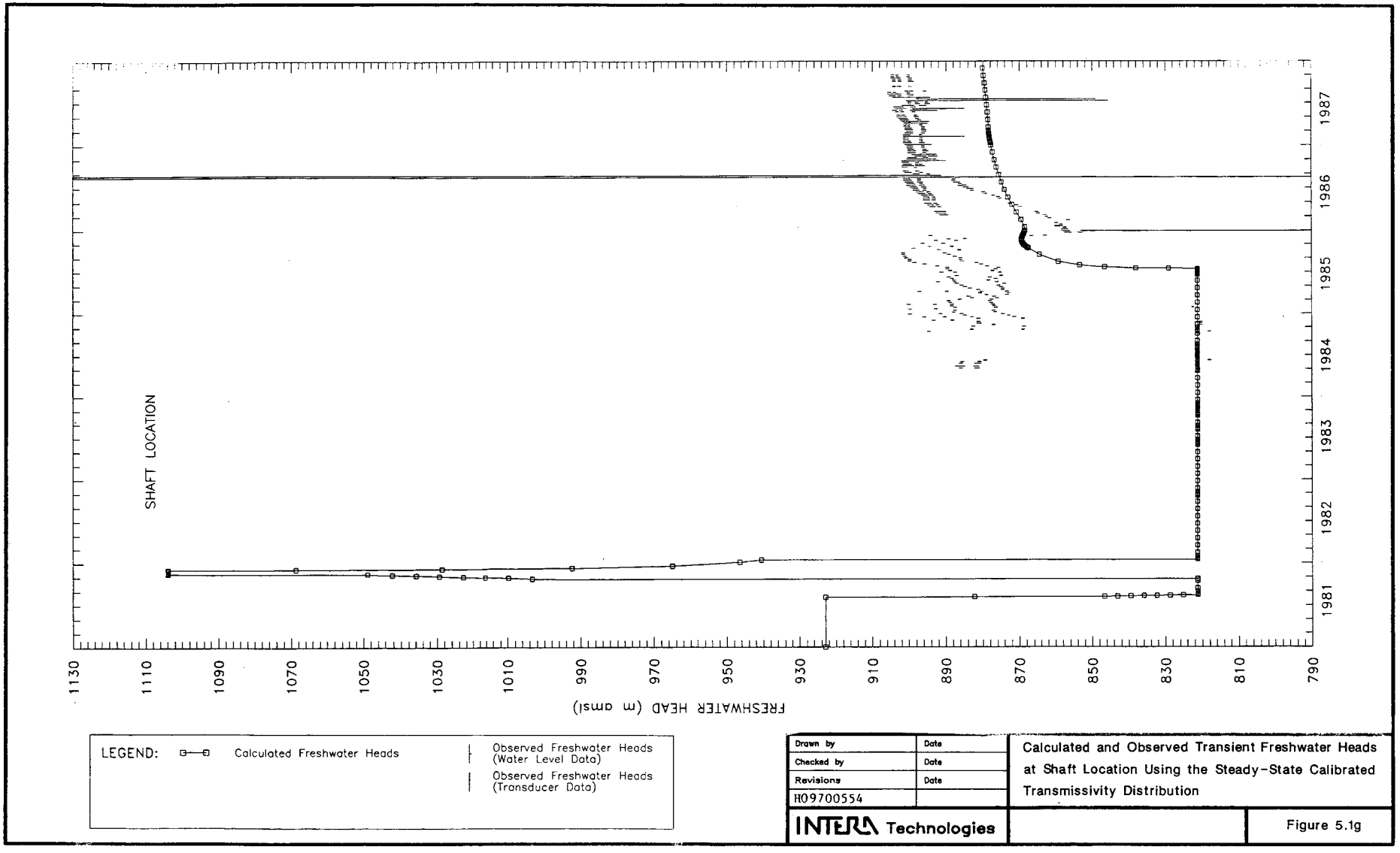

Drawn by	Date
Checked by	Date
Revisions	Date
H09700554	

INTERA Technologies

Calculated and Observed Transient Freshwater Heads at Shaft Location Using the Steady-State Calibrated Transmissivity Distribution

Figure 5.1g

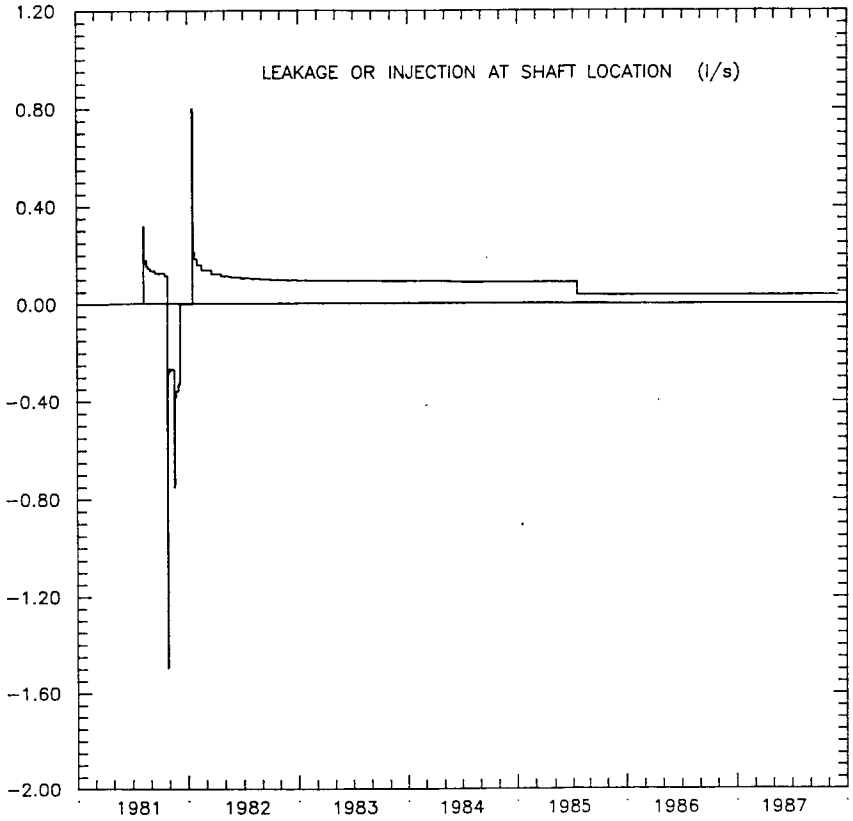

Drawn by	Date
Checked by	Date
Revisions	Date
409700R554	

INTERA Technologies

Leakage or Injection Rates at the Shaft Location Used in the Base-Case Transient Simulation

Figure 5.2

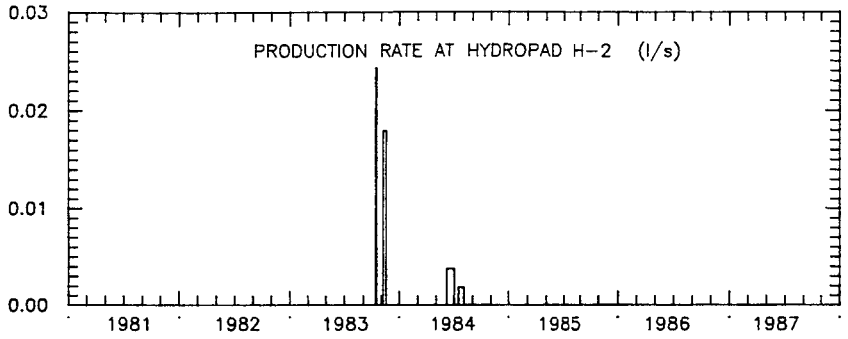

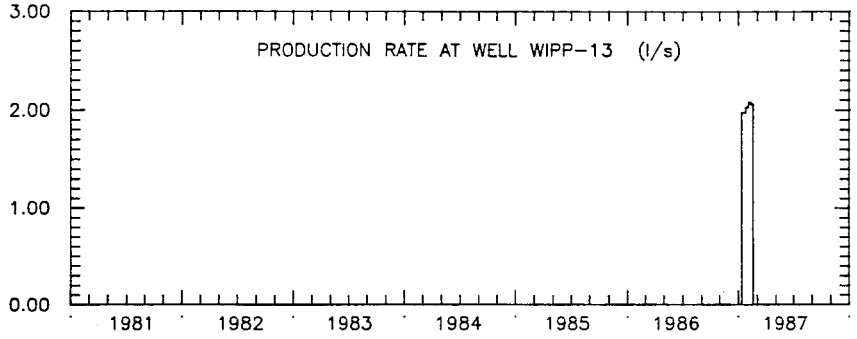

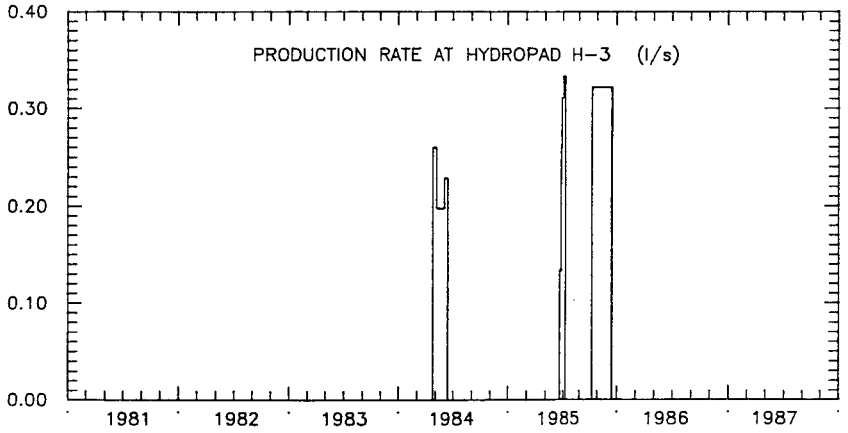

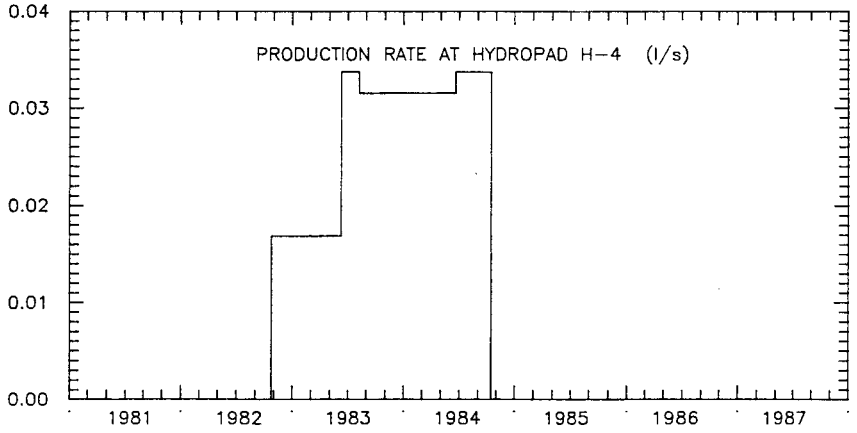

Drawn by	Date
Checked by	Date
Revisions	Date
929700R554	

INTERA Technologies

Well-Test Pumping Rates Used in the Transient Simulations

Figure 5.3

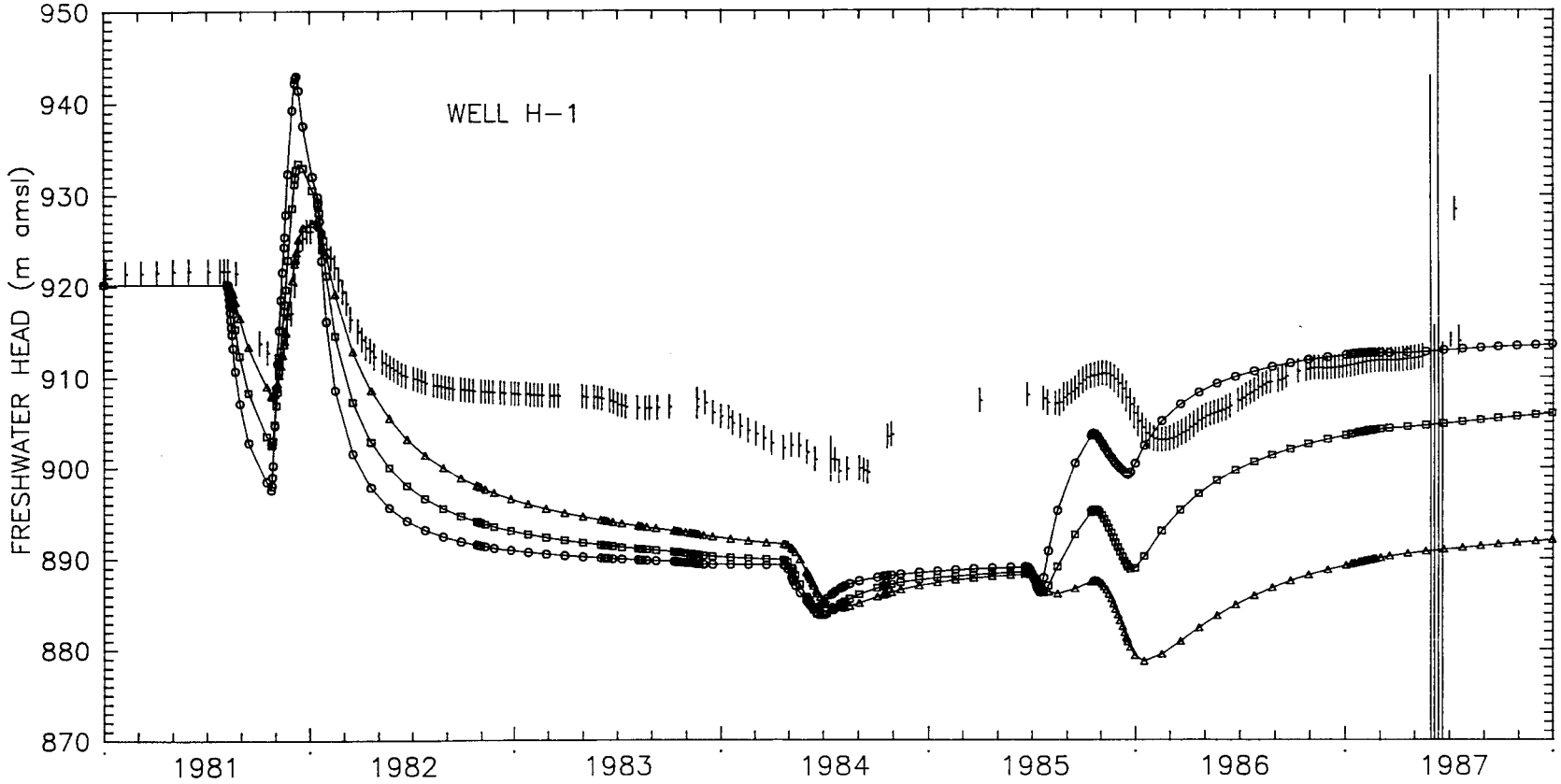

LEGEND:

- Calculated Freshwater Heads Using T=0.5 x TSS
- Calculated Freshwater Heads Using T=1 x TSS
- Calculated Freshwater Heads Using T=2 x TSS
- Observed Freshwater Heads (Water Level Data)
- Observed Freshwater Heads (Transducer Data)

TSS = Transmissivities of the Calibrated Steady-State Model

Drawn by	Date
Checked by	Date
Revisions	Date
H097008554	

INTERA Technologies

Sensitivity of Calculated Transient Freshwater Heads at H-1 to Transmissivity

Figure 5.4a

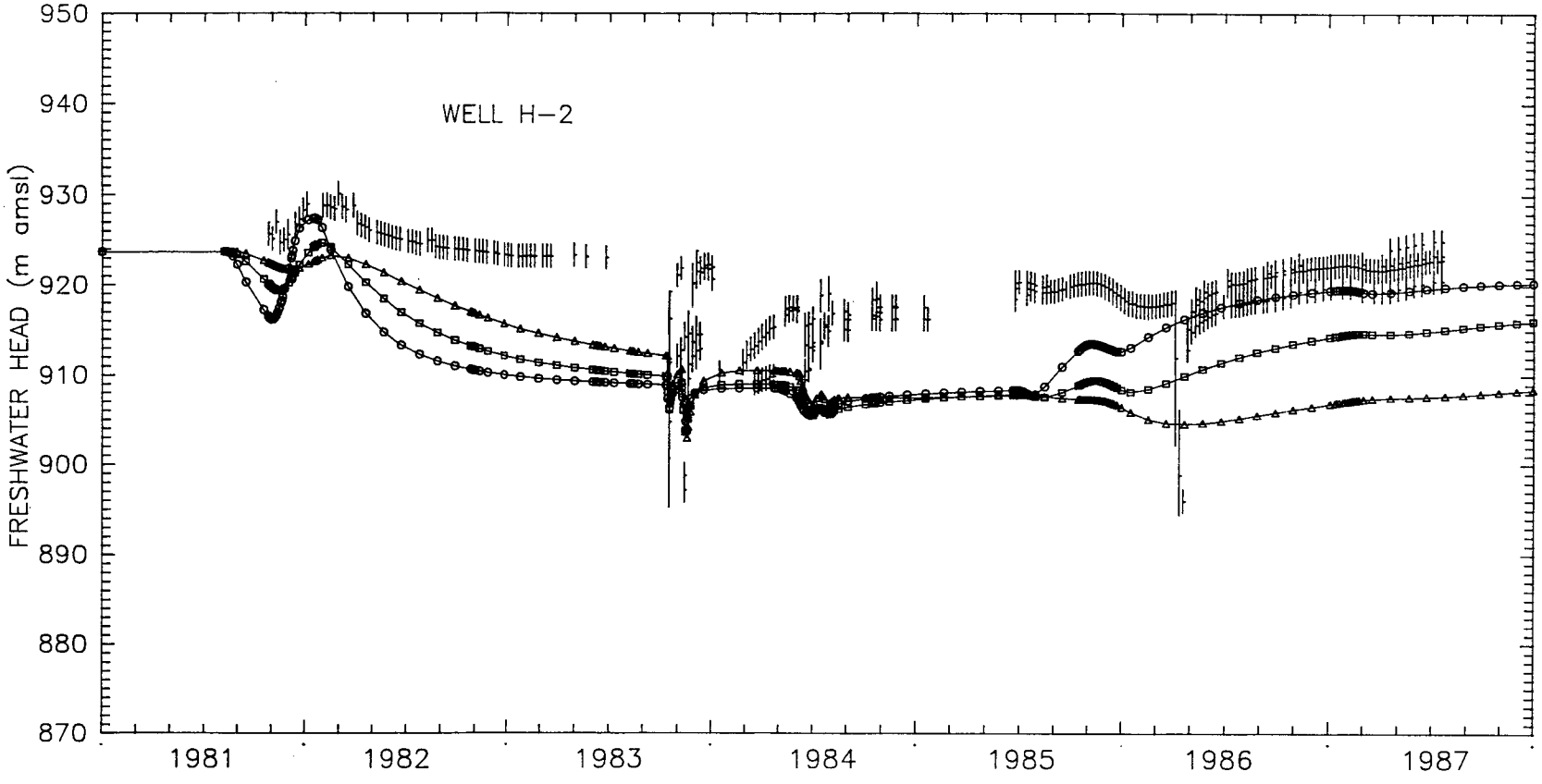

LEGEND:

- Calculated Freshwater Heads Using T=0.5 x TSS
- Calculated Freshwater Heads Using T=1 x TSS
- Calculated Freshwater Heads Using T=2 x TSS
- Observed Freshwater Heads (Water Level Data)
- Observed Freshwater Heads (Transducer Data)

TSS = Transmissivities of the Calibrated Steady-State Model

Drawn by	Date
Checked by	Date
Revisions	Date
H09700554	

INTERA Technologies

Sensitivity of Calculated Transient Freshwater Heads at H-2 to Transmissivity

Figure 5.4b

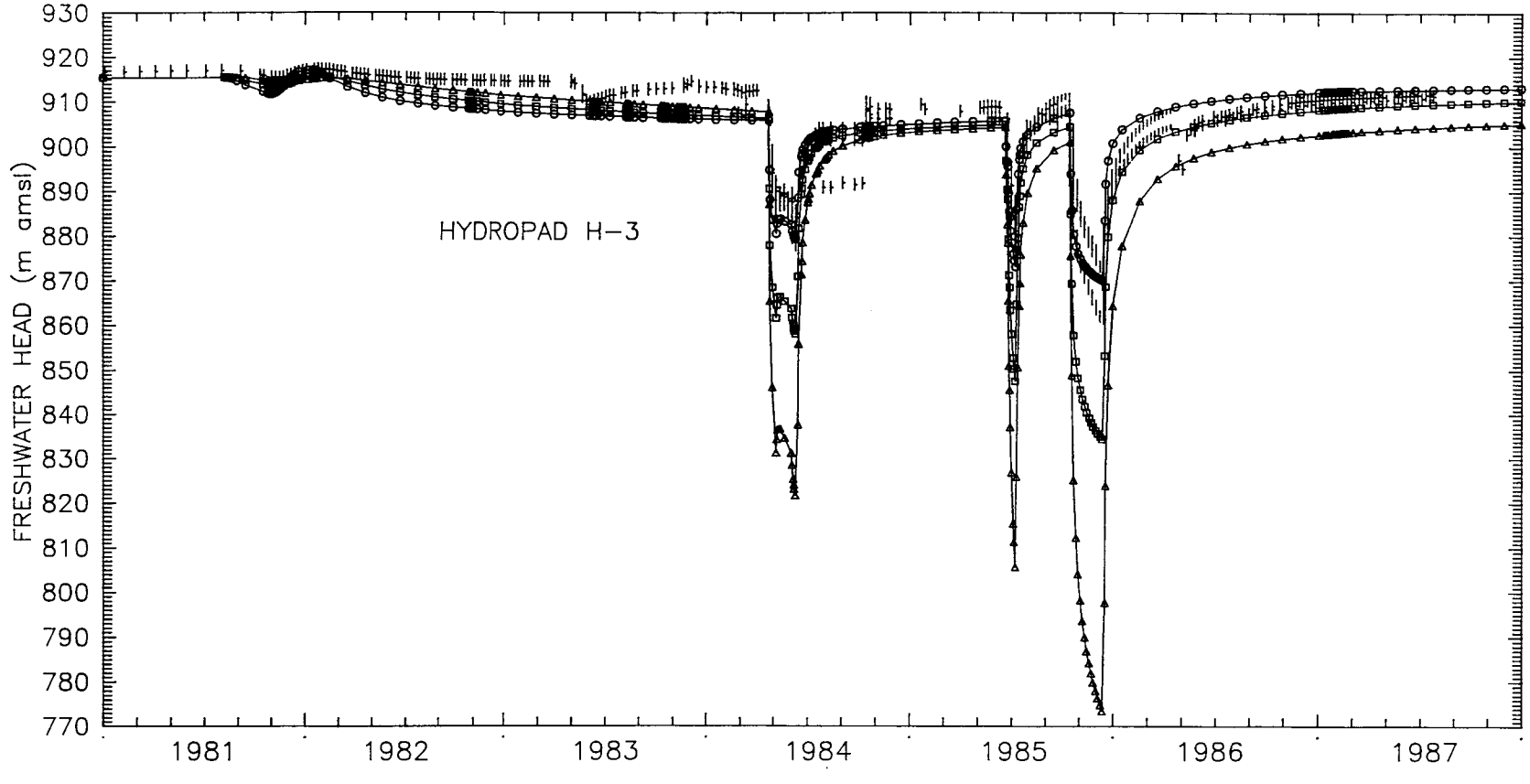

LEGEND:

- Calculated Freshwater Heads Using T=0.5 x TSS
- Calculated Freshwater Heads Using T=1 x TSS
- Calculated Freshwater Heads Using T=2 x TSS
- Observed Freshwater Heads (Water Level Data)
- Observed Freshwater Heads (Transducer Data)

TSS = Transmissivities of the Calibrated Steady-State Model

Drawn by	Date
Checked by	Date
Revisions	Date
H29700B554	

INTERA Technologies

Sensitivity of Calculated Transient Freshwater Heads at H-3 to Transmissivity

Figure 5.4c

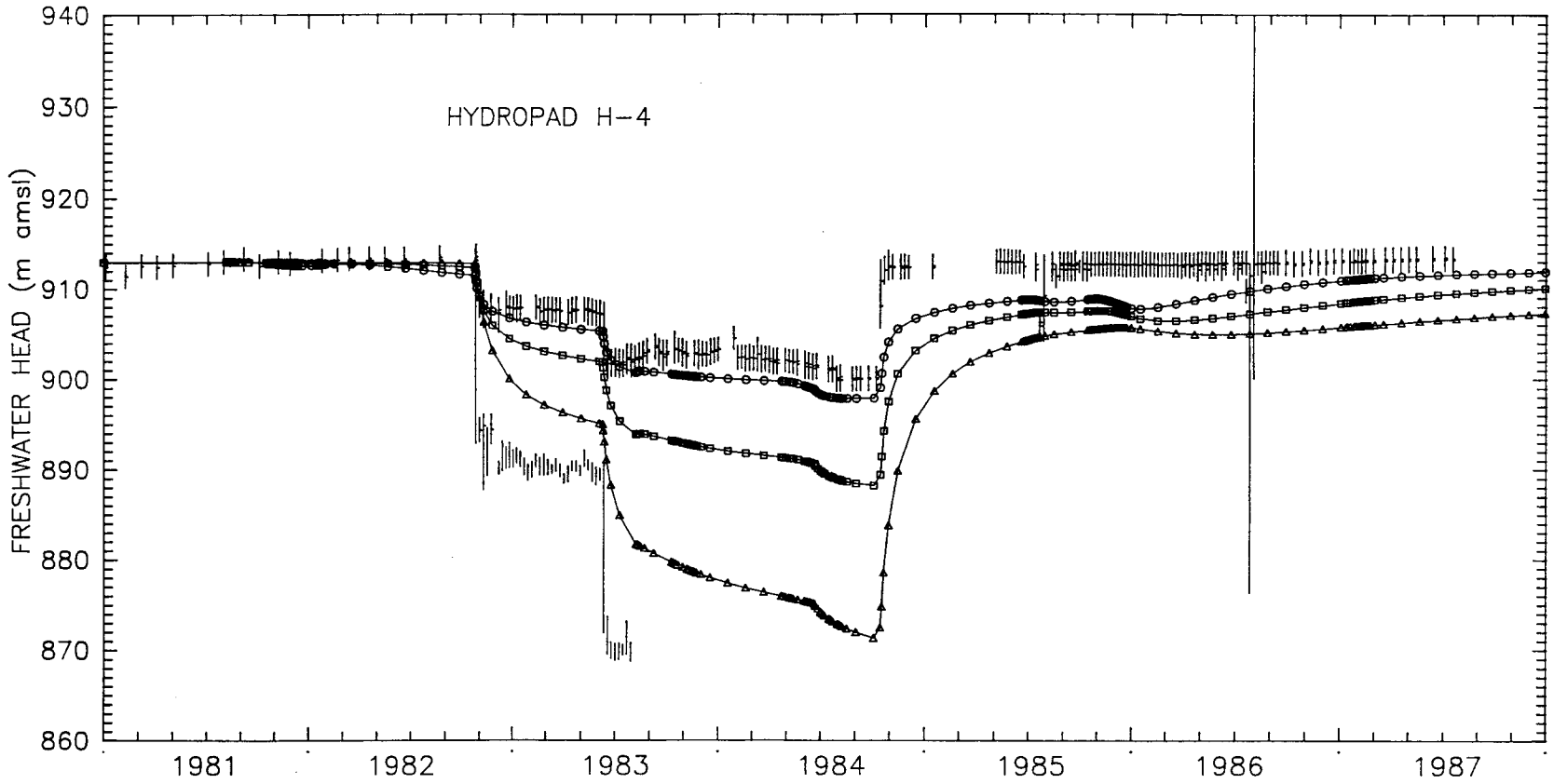

LEGEND:

- Calculated Freshwater Heads Using T=0.5 x TSS
- Calculated Freshwater Heads Using T=1 x TSS
- Calculated Freshwater Heads Using T=2 x TSS
- Observed Freshwater Heads (Water Level Data)
- Observed Freshwater Heads (Transducer Data)

TSS = Transmissivities of the Calibrated Steady-State Model

Drawn by	Date
Checked by	Date
Revisions	Date
4097008554	

INTERA Technologies

Sensitivity of Calculated Transient Freshwater Heads at H-4 to Transmissivity

Figure 5.4d

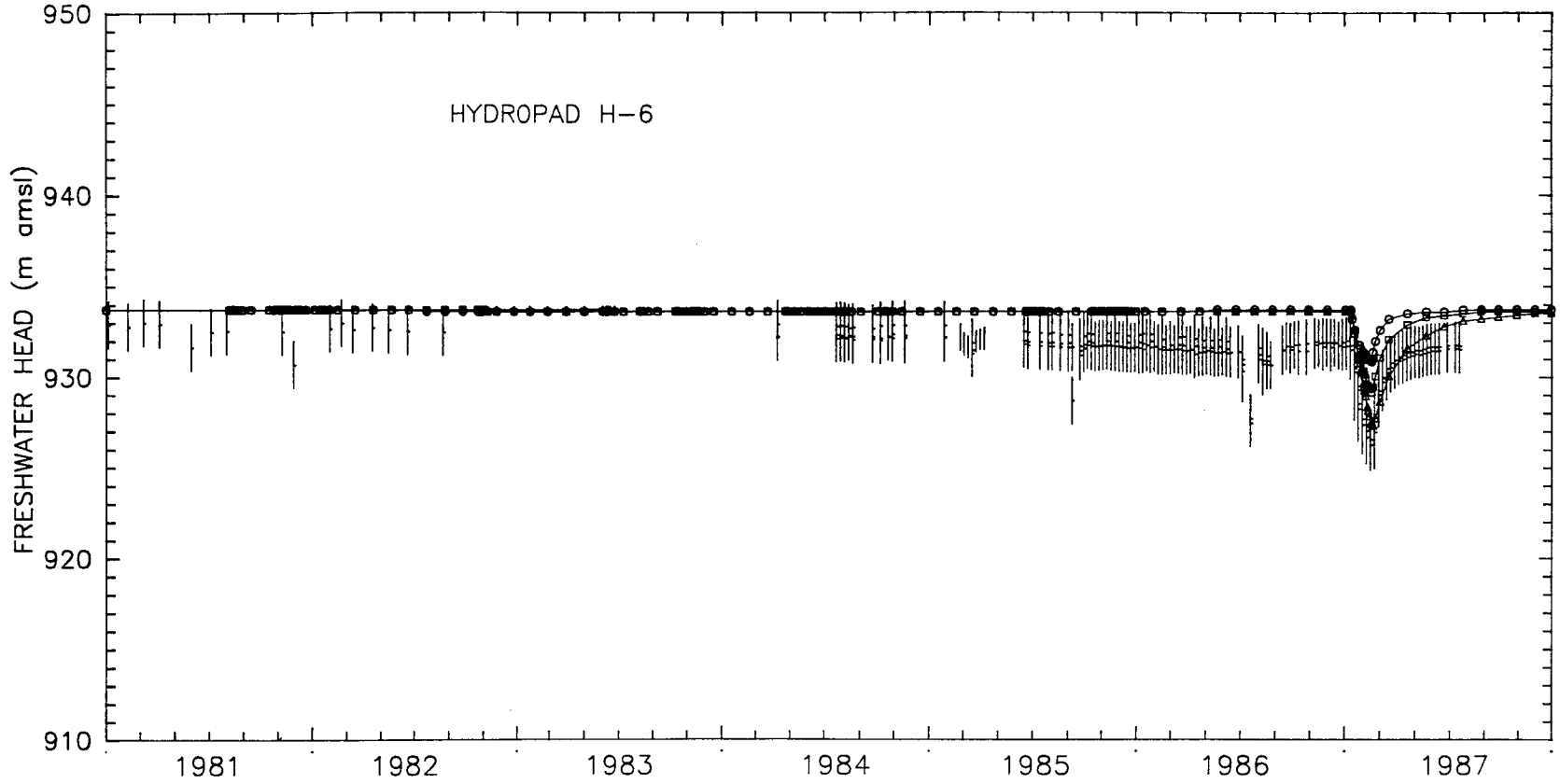

LEGEND:

- Calculated Freshwater Heads Using T=0.5 x TSS
- Calculated Freshwater Heads Using T=1 x TSS
- Calculated Freshwater Heads Using T=2 x TSS
- Observed Freshwater Heads (Water Level Data)
- Observed Freshwater Heads (Transducer Data)

TSS = Transmissivities of the Calibrated Steady-State Model

Drawn by	Date
Checked by	Date
Revisions	Date
H09700552	

INTERA Technologies

Sensitivity of Calculated Transient Freshwater Heads at H-6 to Transmissivity

Figure 5.4e

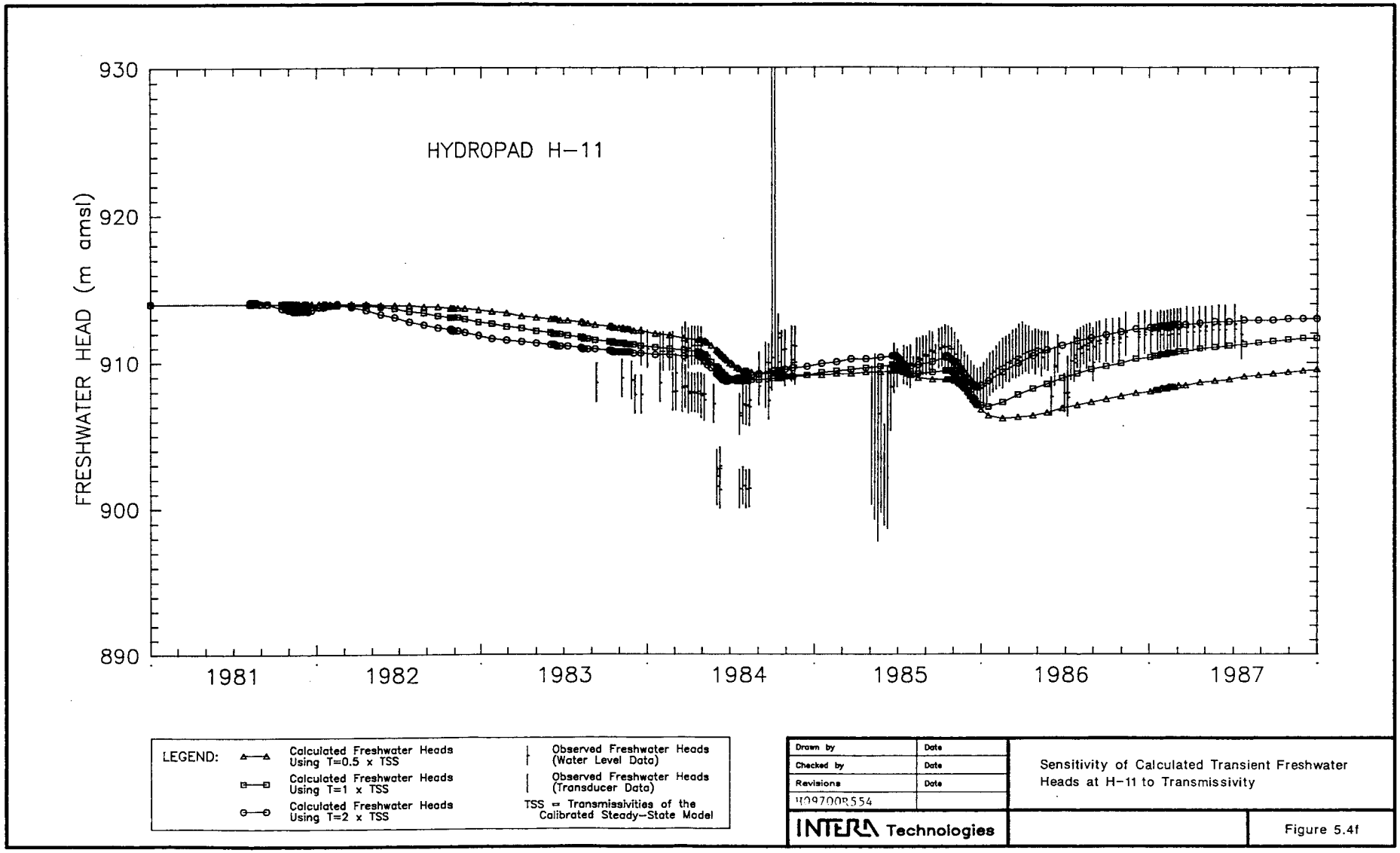
HYDROPAD H-11
FRESHWATER HEAD (m amsl)
930
920
910
900
890
1981
1982
1983
1984
1985
1986
1987
LEGEND:
Calculated Freshwater Heads Using T=0.5 x TSS
Calculated Freshwater Heads Using T=1 x TSS
Calculated Freshwater Heads Using T=2 x TSS
Observed Freshwater Heads (Water Level Data)
Observed Freshwater Heads (Transducer Data)
TSS = Transmissivities of the Calibrated Steady-State Model
Drawn by
Date
Checked by
Date
Revisions
Date
H09700R554
INTERA Technologies
Sensitivity of Calculated Transient Freshwater Heads at H-11 to Transmissivity
Figure 5.4f

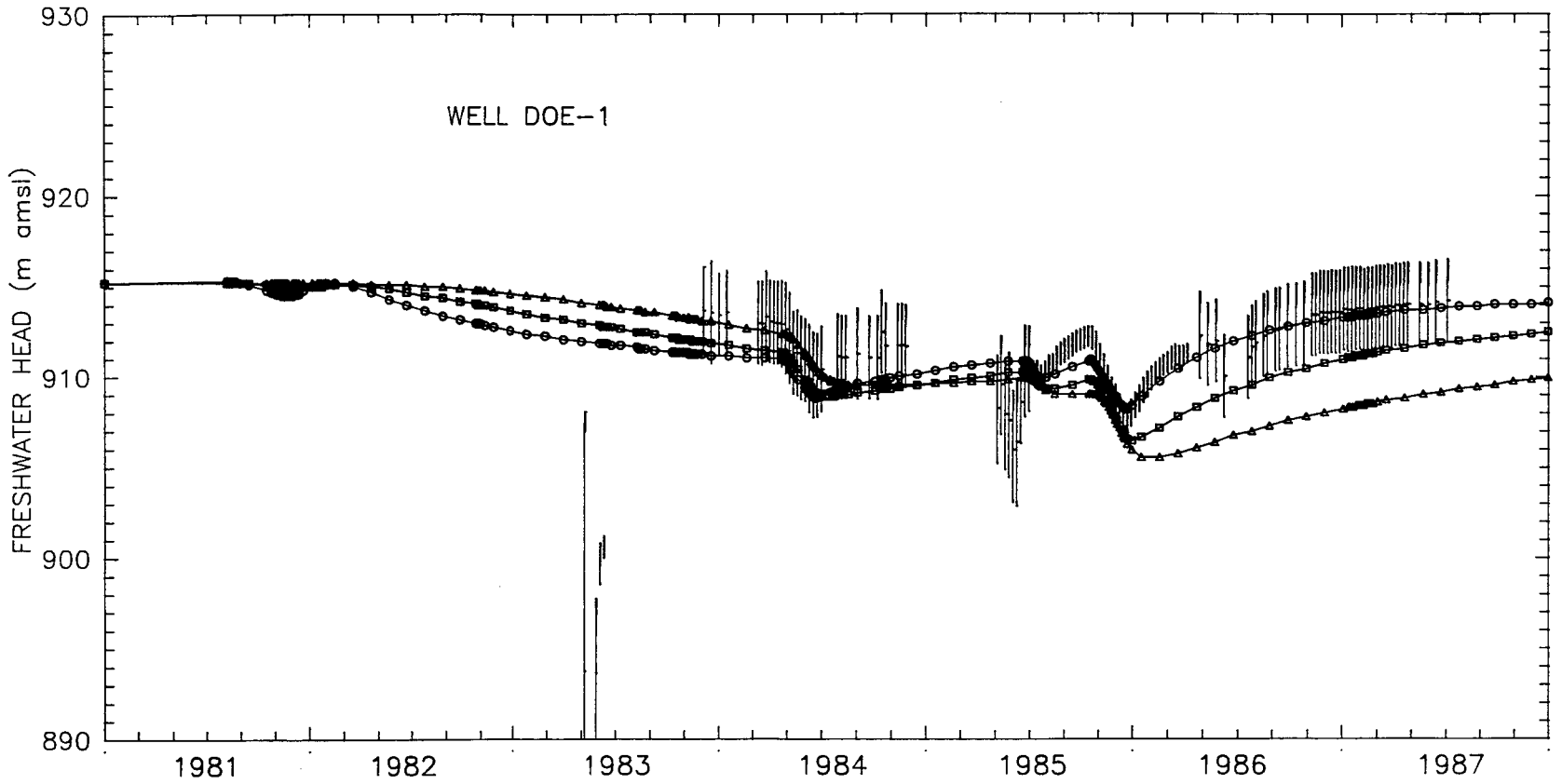

LEGEND:

- Calculated Freshwater Heads Using T=0.5 x TSS
- Calculated Freshwater Heads Using T=1 x TSS
- Calculated Freshwater Heads Using T=2 x TSS
- Observed Freshwater Heads (Water Level Data)
- Observed Freshwater Heads (Transducer Data)

TSS = Transmissivities of the Calibrated Steady-State Model

Drawn by	Date
Checked by	Date
Revisions	Date
H09700R554	

INTERA Technologies

Sensitivity of Calculated Transient Freshwater Heads at DOE-1 to Transmissivity

Figure 5.4g

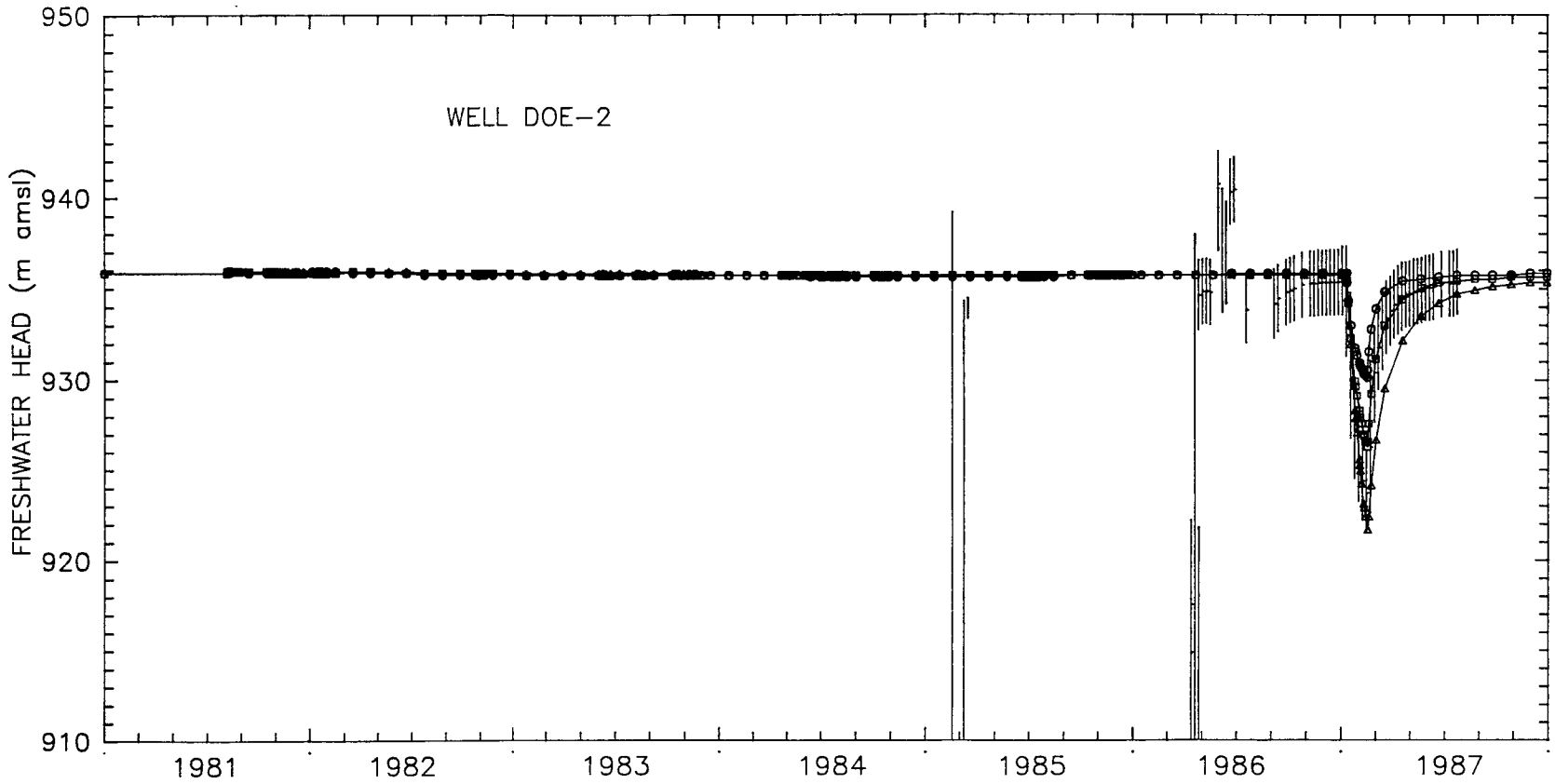

LEGEND:

- Calculated Freshwater Heads Using T=0.5 x TSS
- Calculated Freshwater Heads Using T=1 x TSS
- Calculated Freshwater Heads Using T=2 x TSS
- Observed Freshwater Heads (Water Level Data)
- Observed Freshwater Heads (Transducer Data)

TSS = Transmissivities of the Calibrated Steady-State Model

Drawn by	Date
Checked by	Date
Revisions	Date
H09700554	

INTERA Technologies

Sensitivity of Calculated Transient Freshwater Heads at DOE-2 to Transmissivity

Figure 5.4h

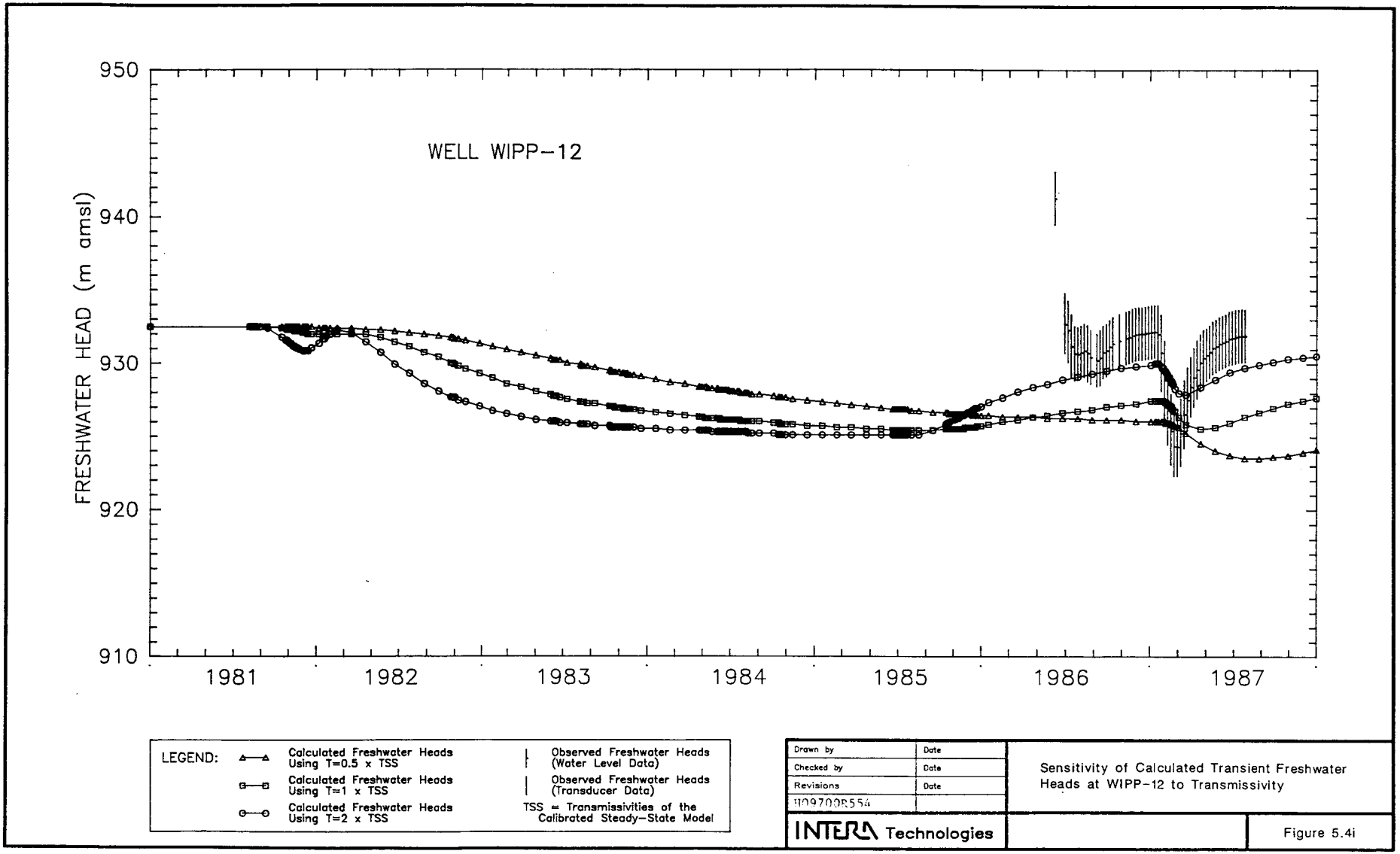

Drawn by	Date
Checked by	Date
Revisions	Date
9109700R554	

INTERA Technologies

Sensitivity of Calculated Transient Freshwater Heads at WIPP-12 to Transmissivity

Figure 5.4i

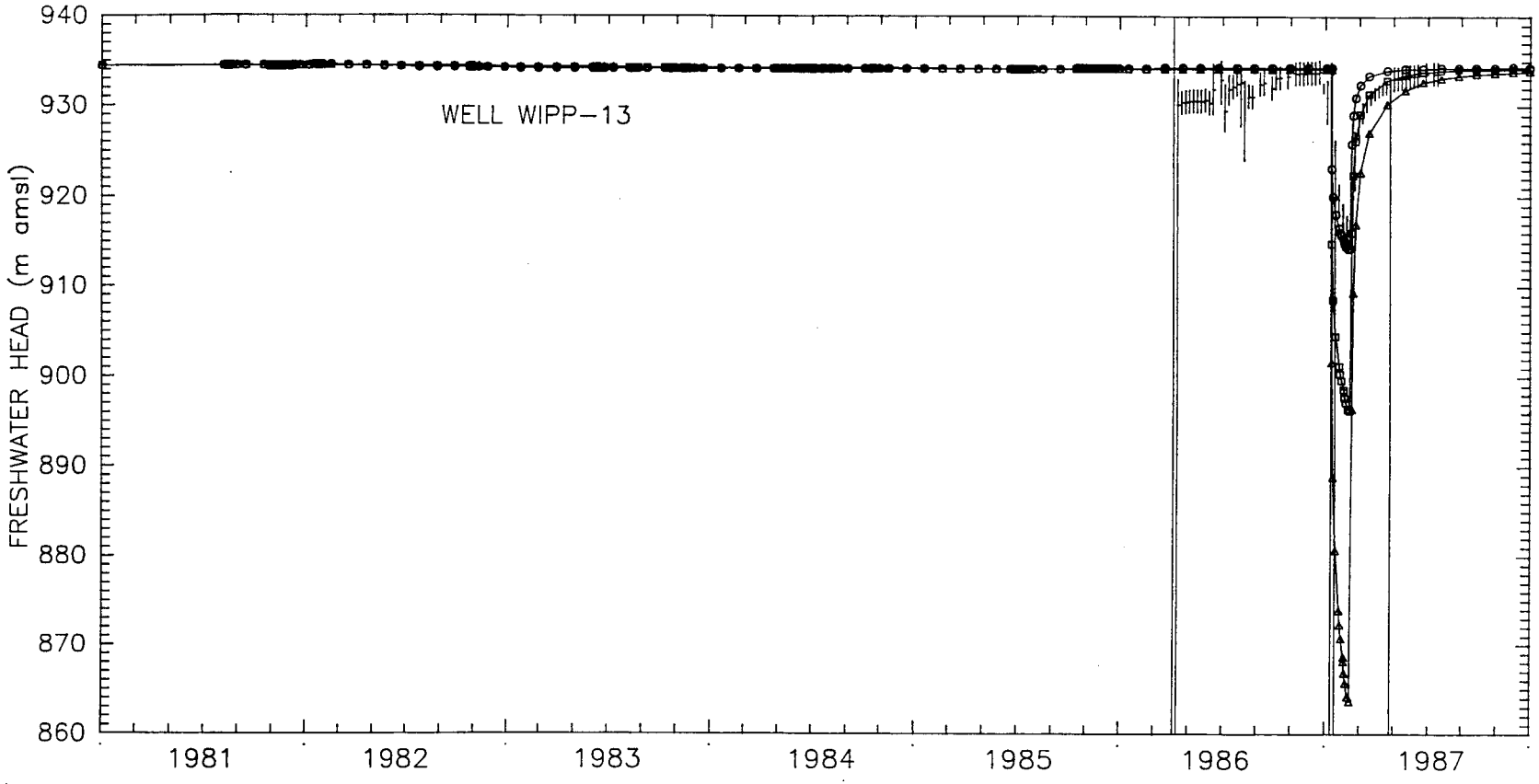

LEGEND:

- Calculated Freshwater Heads Using T=0.5 x TSS
- Calculated Freshwater Heads Using T=1 x TSS
- Calculated Freshwater Heads Using T=2 x TSS
- Observed Freshwater Heads (Water Level Data)
- Observed Freshwater Heads (Transducer Data)

TSS = Transmissivities of the Calibrated Steady-State Model

Drawn by	Date
Checked by	Date
Revisions	Date
H09700R554	

INTERA Technologies

Sensitivity of Calculated Transient Freshwater Heads at WIPP-13 to Transmissivity

Figure 5.4j

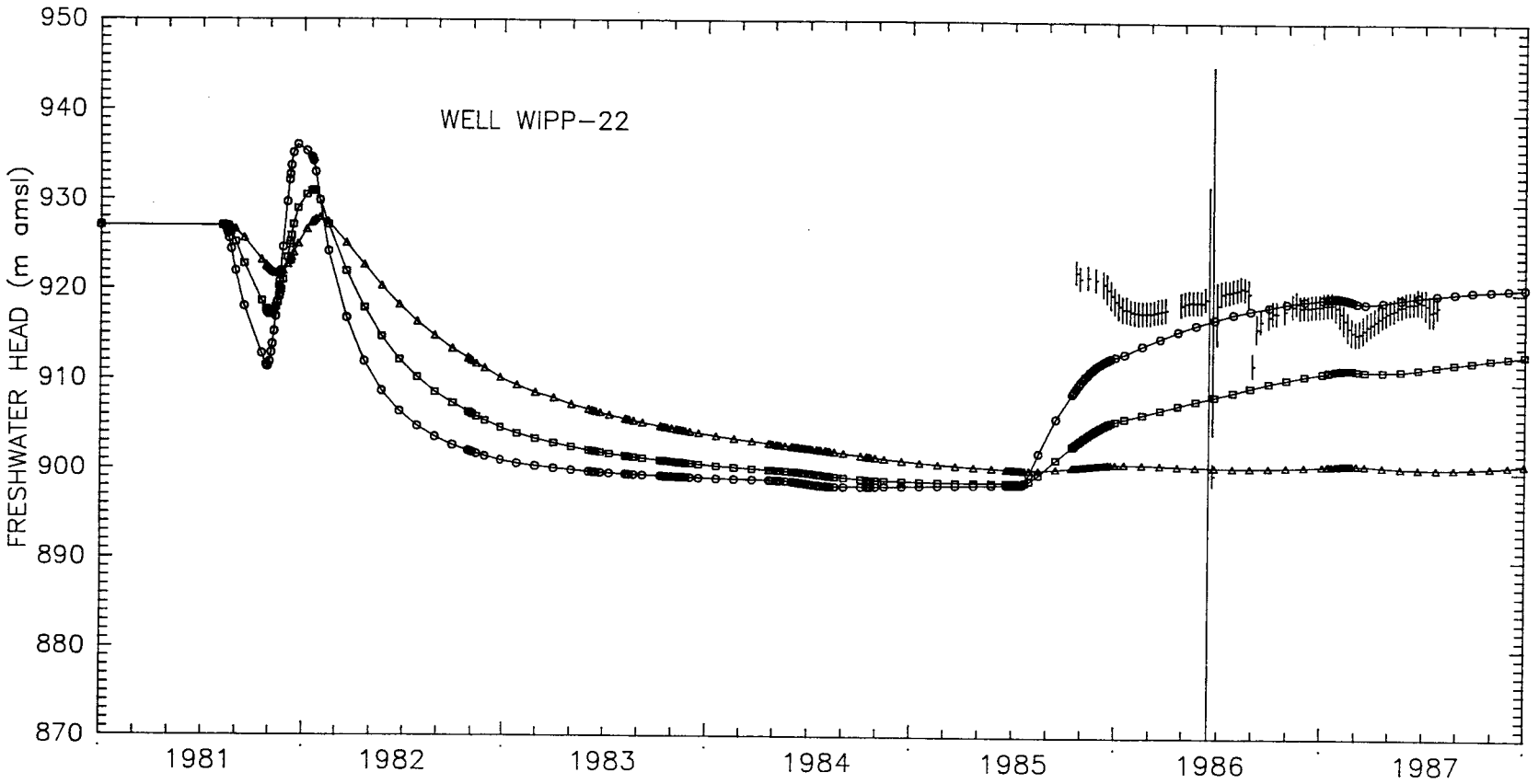

LEGEND:

- Calculated Freshwater Heads Using T=0.5 x TSS
- Calculated Freshwater Heads Using T=1 x TSS
- Calculated Freshwater Heads Using T=2 x TSS
- Observed Freshwater Heads (Water Level Data)
- Observed Freshwater Heads (Transducer Data)

TSS = Transmissivities of the Calibrated Steady-State Model

Drawn by	Date
Checked by	Date
Revisions	Date
H09700554	

Sensitivity of Calculated Transient Freshwater Heads at WIPP-22 to Transmissivity

INTERA Technologies

Figure 5.4k

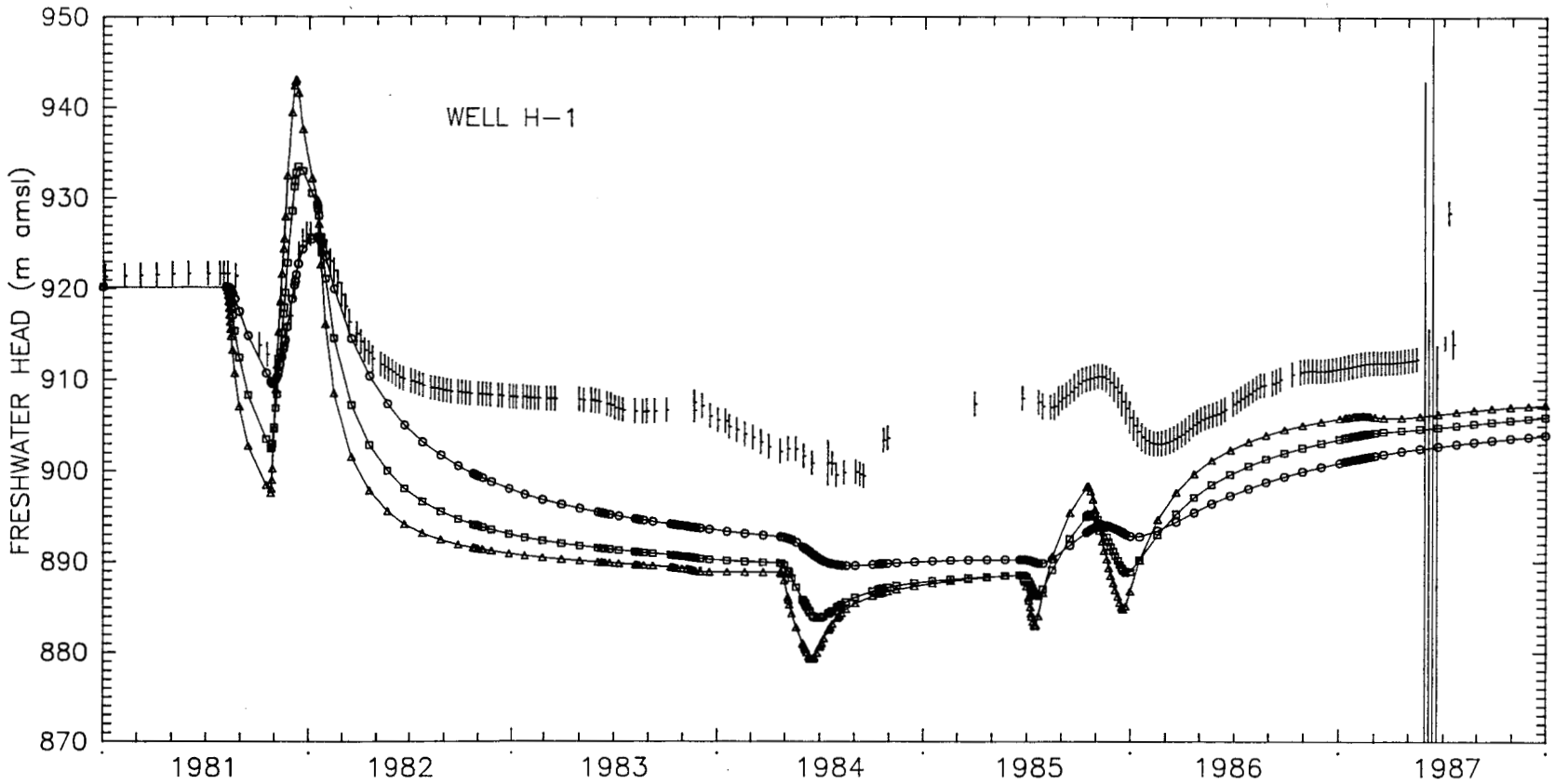

LEGEND:

- Calculated Freshwater Heads Using S=1E-5
- Calculated Freshwater Heads Using S=2E-5
- Calculated Freshwater Heads Using S=5E-5
- Observed Freshwater Heads (Water Level Data)
- Observed Freshwater Heads (Transducer Data)

Drawn by	Date
Checked by	Date
Revisions	Date
4097008554	

INTERA Technologies

Sensitivity of Calculated Transient Freshwater Heads at H-1 to Storativity

Figure 5.5a

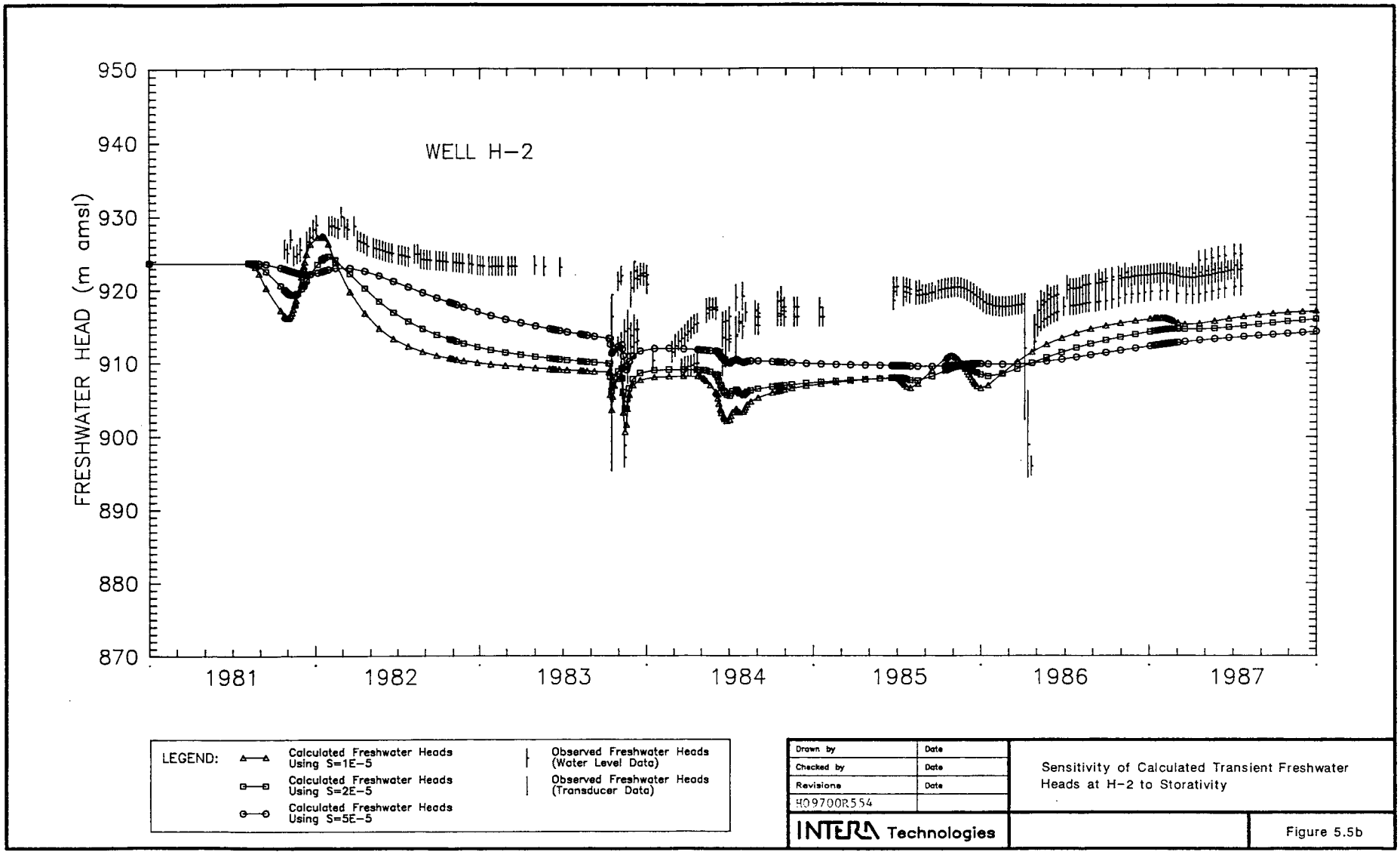

Drawn by	Date
Checked by	Date
Revisions	Date
409700R554	

INTERA Technologies

Sensitivity of Calculated Transient Freshwater Heads at H-2 to Storativity

Figure 5.5b

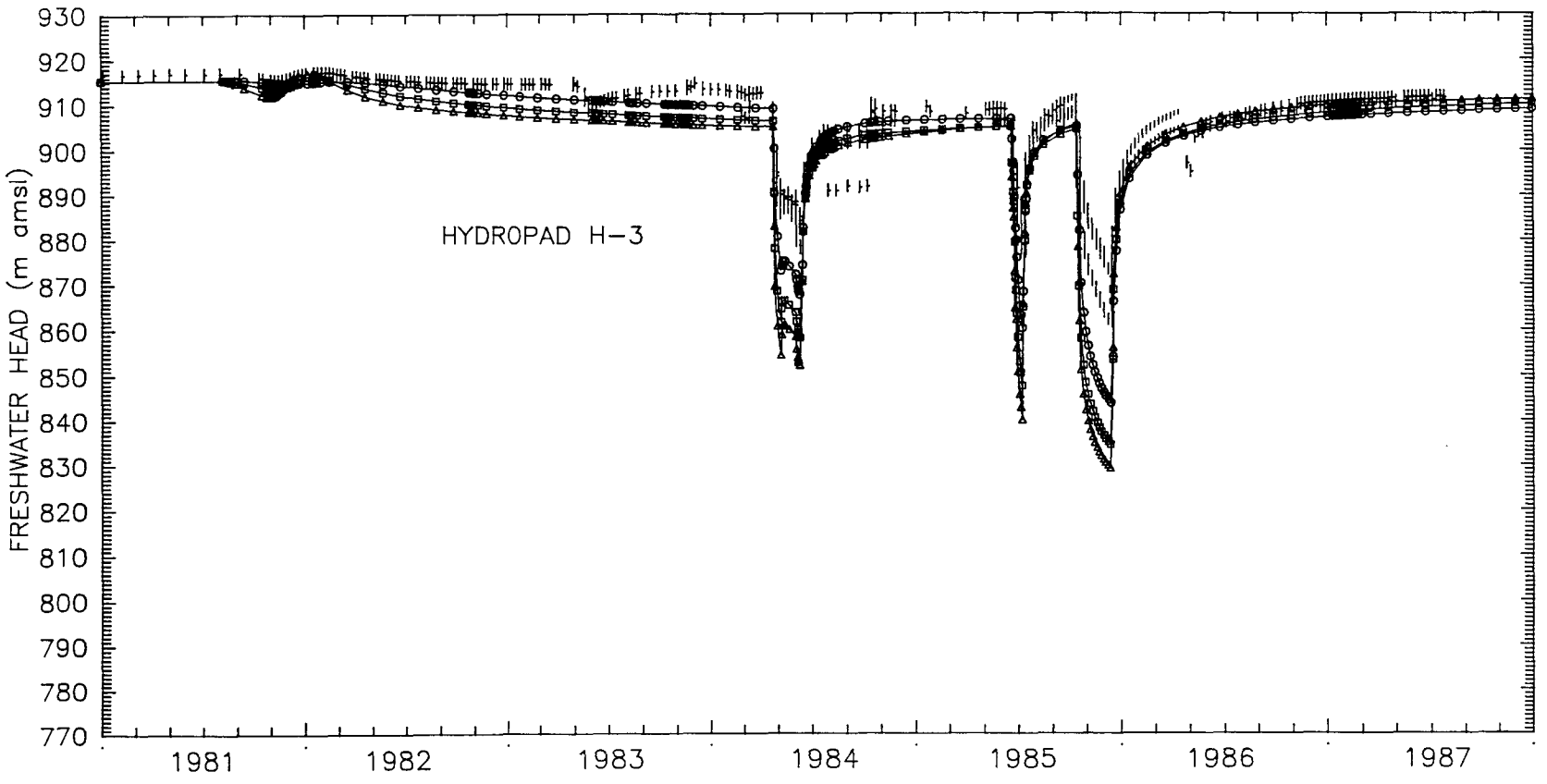

LEGEND:

- Calculated Freshwater Heads Using S=1E-5
- Calculated Freshwater Heads Using S=2E-5
- Calculated Freshwater Heads Using S=5E-5
- Observed Freshwater Heads (Water Level Data)
- Observed Freshwater Heads (Transducer Data)

Drawn by	Date
Checked by	Date
Revisions	Date
H097008554	

INTERA Technologies

Sensitivity of Calculated Transient Freshwater Heads at H-3 to Storativity

Figure 5.5c

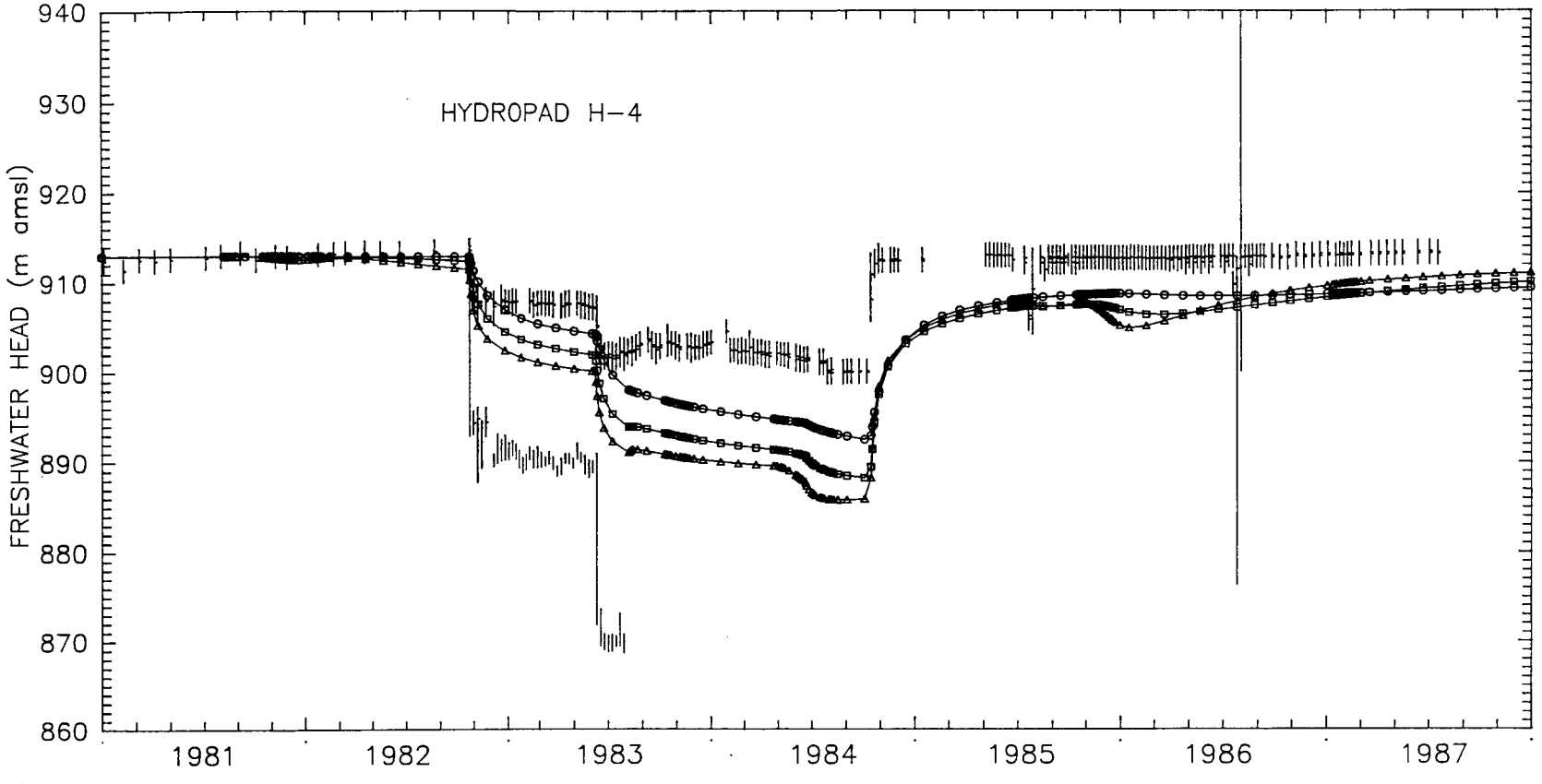

LEGEND:

- Calculated Freshwater Heads Using S=1E-5
- Calculated Freshwater Heads Using S=2E-5
- Calculated Freshwater Heads Using S=5E-5
- Observed Freshwater Heads (Water Level Data)
- Observed Freshwater Heads (Transducer Data)

Drawn by	Date
Checked by	Date
Revisions	Date
H09700R554	

INTERA Technologies

Sensitivity of Calculated Transient Freshwater Heads at H-4 to Storativity

Figure 5.5d

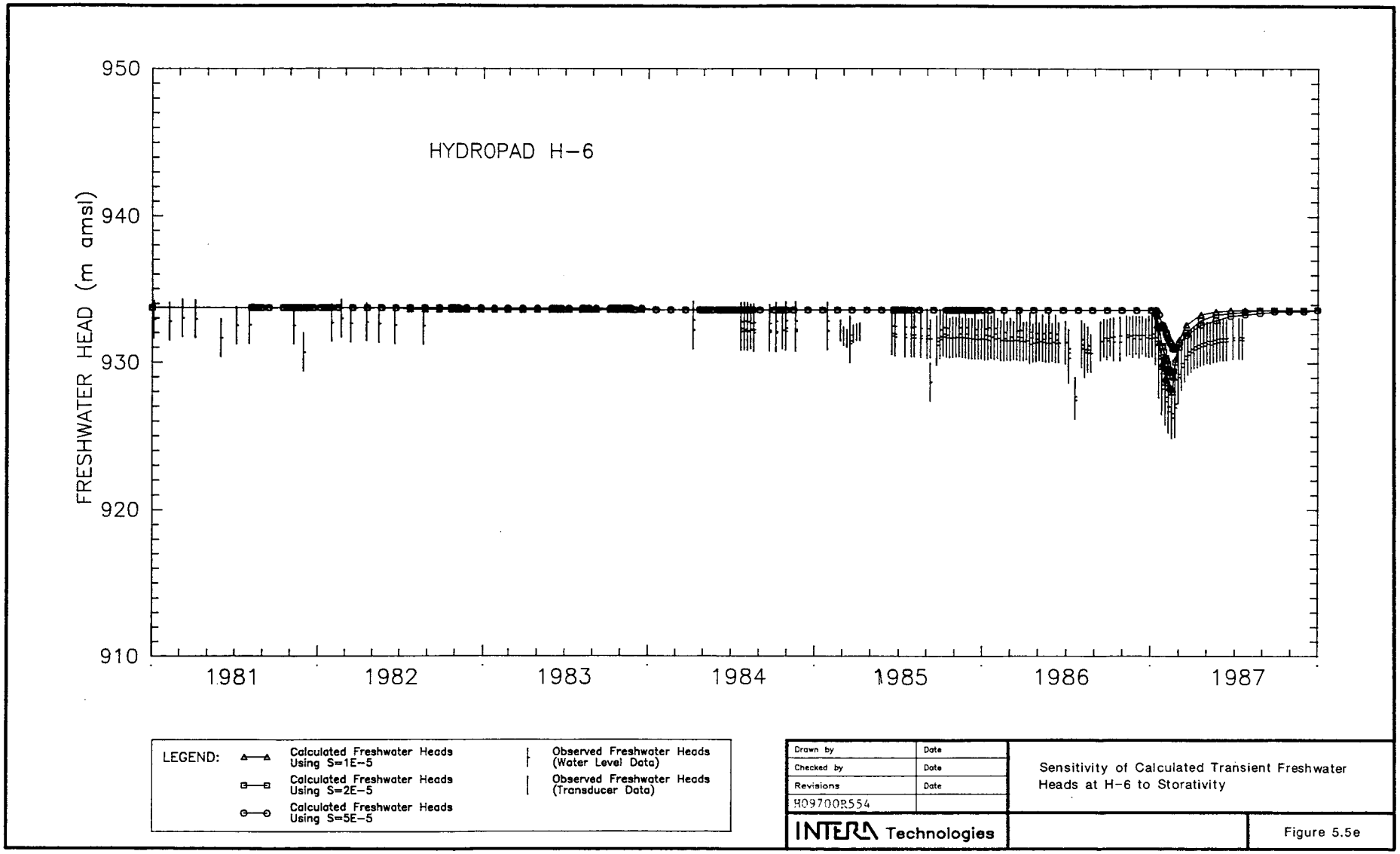
HYDROPAD H-6
FRESHWATER HEAD (m amsl)
950
940
930
920
910
1981
1982
1983
1984
1985
1986
1987
LEGEND:
Calculated Freshwater Heads Using S=1E-5
Calculated Freshwater Heads Using S=2E-5
Calculated Freshwater Heads Using S=5E-5
Observed Freshwater Heads (Water Level Data)
Observed Freshwater Heads (Transducer Data)
Drawn by
Date
Checked by
Date
Revisions
Date
M09700R554
INTERA Technologies
Sensitivity of Calculated Transient Freshwater Heads at H-6 to Storativity
Figure 5.5e

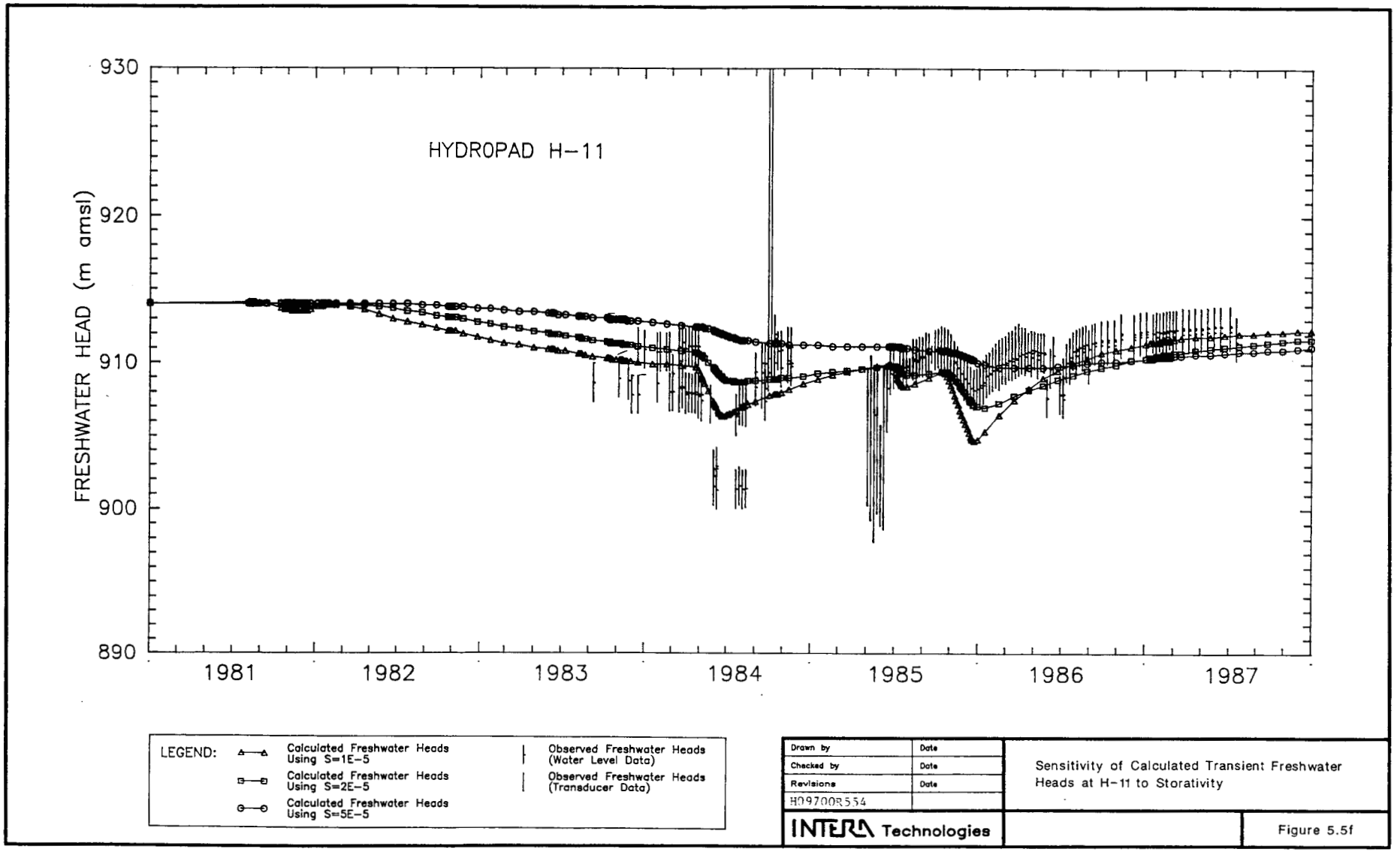
HYDROPAD H-11
FRESHWATER HEAD (m amsl)
930
920
910
900
890
1981
1982
1983
1984
1985
1986
1987
LEGEND:
Calculated Freshwater Heads Using S=1E-5
Calculated Freshwater Heads Using S=2E-5
Calculated Freshwater Heads Using S=5E-5
Observed Freshwater Heads (Water Level Data)
Observed Freshwater Heads (Transducer Data)
Drawn by
Date
Checked by
Date
Revisions
Date
H09700R554
INTERA Technologies
Sensitivity of Calculated Transient Freshwater Heads at H-11 to Storativity
Figure 5.5f

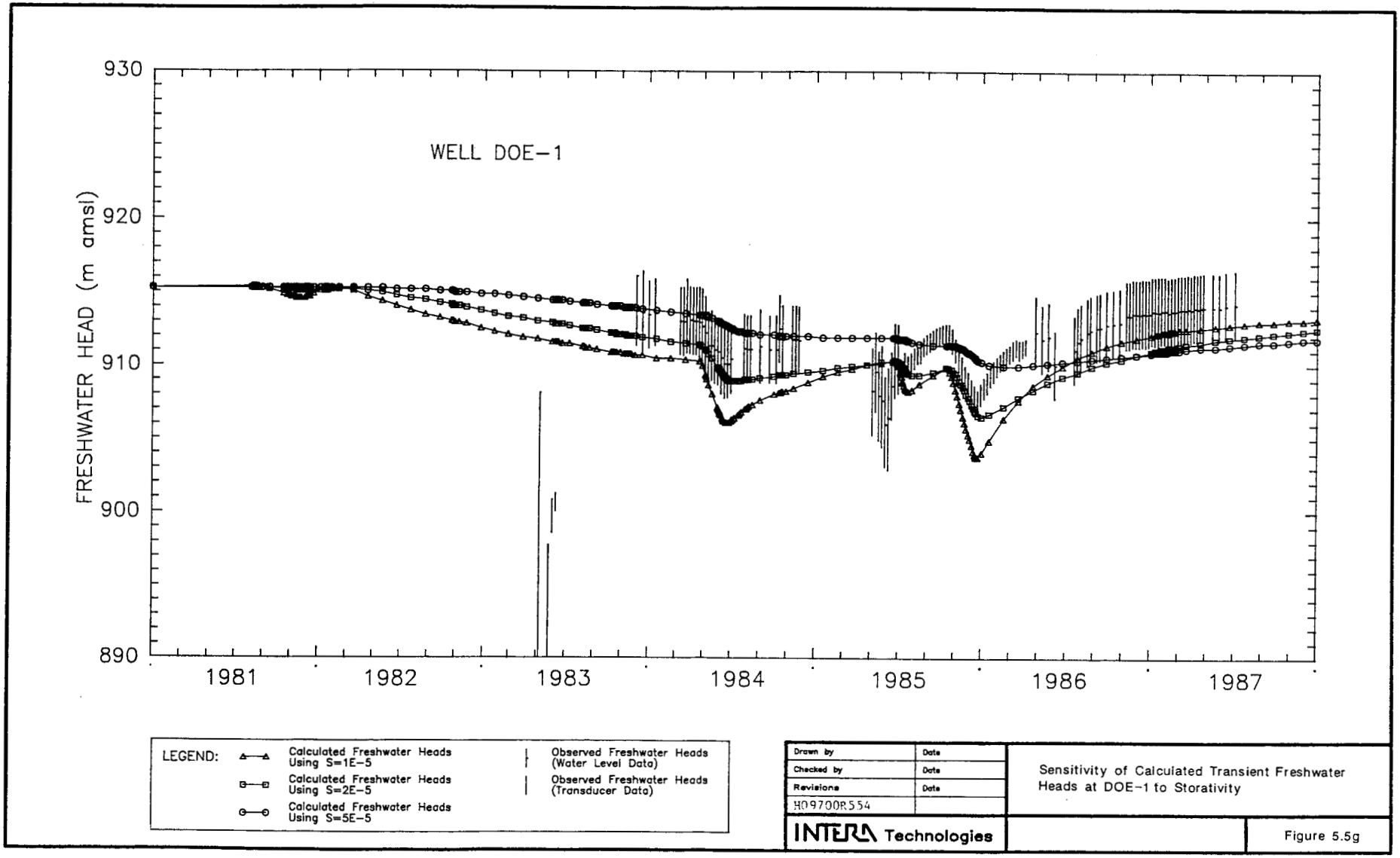

Drawn by	Date
Checked by	Date
Revisions	Date
H09700R554	

INTERA Technologies

Sensitivity of Calculated Transient Freshwater Heads at DOE-1 to Storativity

Figure 5.5g

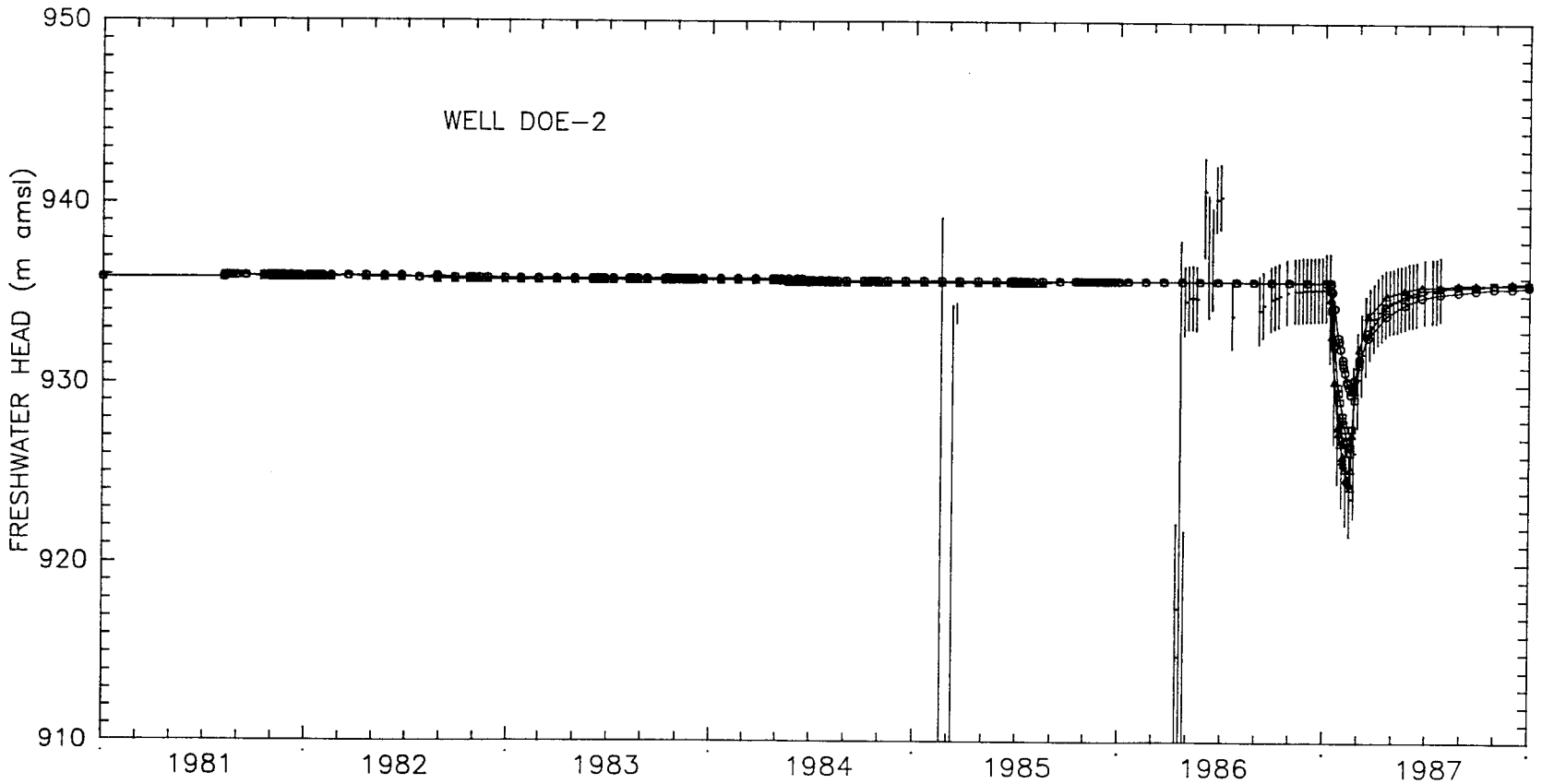

Drawn by	Date
Checked by	Date
Revisions	Date
H09700R554	

INTERA Technologies

Sensitivity of Calculated Transient Freshwater Heads at DOE-2 to Storativity

Figure 5.5h

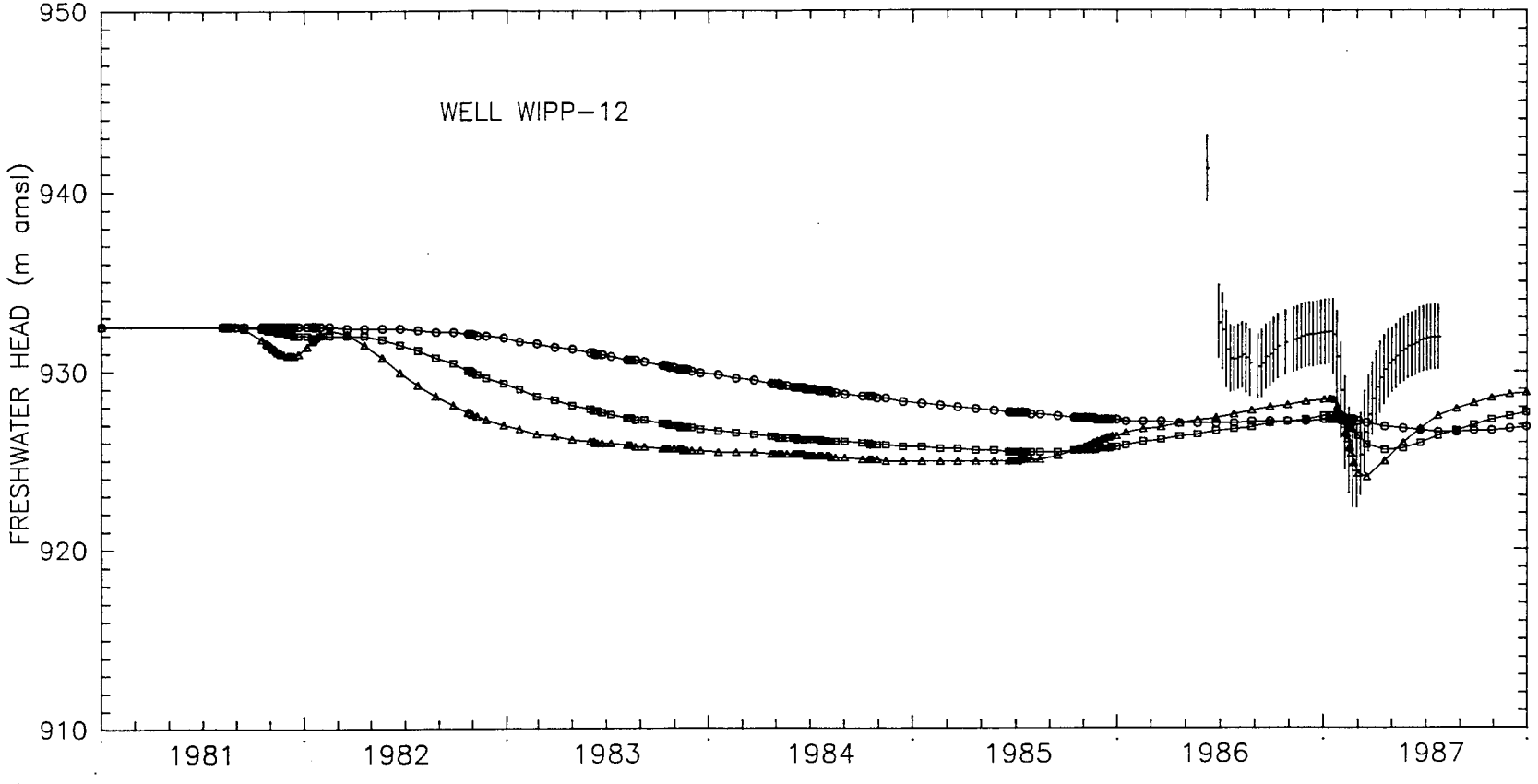

LEGEND:

- Calculated Freshwater Heads Using S=1E-5
- Calculated Freshwater Heads Using S=2E-5
- Calculated Freshwater Heads Using S=5E-5
- Observed Freshwater Heads (Water Level Data)
- Observed Freshwater Heads (Transducer Data)

Drawn by	Date
Checked by	Date
Revisions	Date
H09700R554	

INTERA Technologies

Sensitivity of Calculated Transient Freshwater Heads at WIPP-12 to Storativity

Figure 5.5i

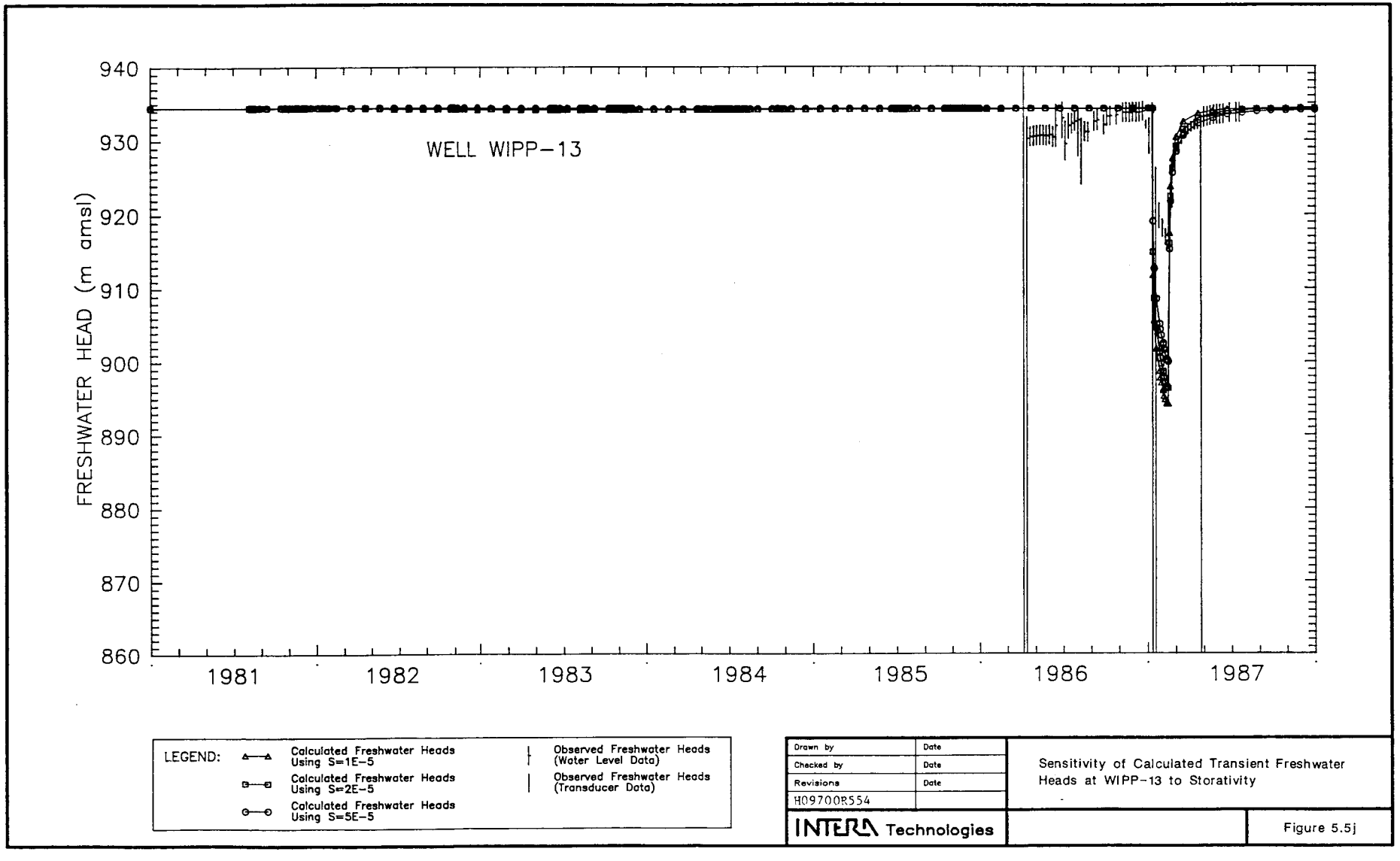

Drawn by	Date
Checked by	Date
Revisions	Date
H09700R554	

INTERA Technologies

Sensitivity of Calculated Transient Freshwater Heads at WIPP-13 to Storativity

Figure 5.5j

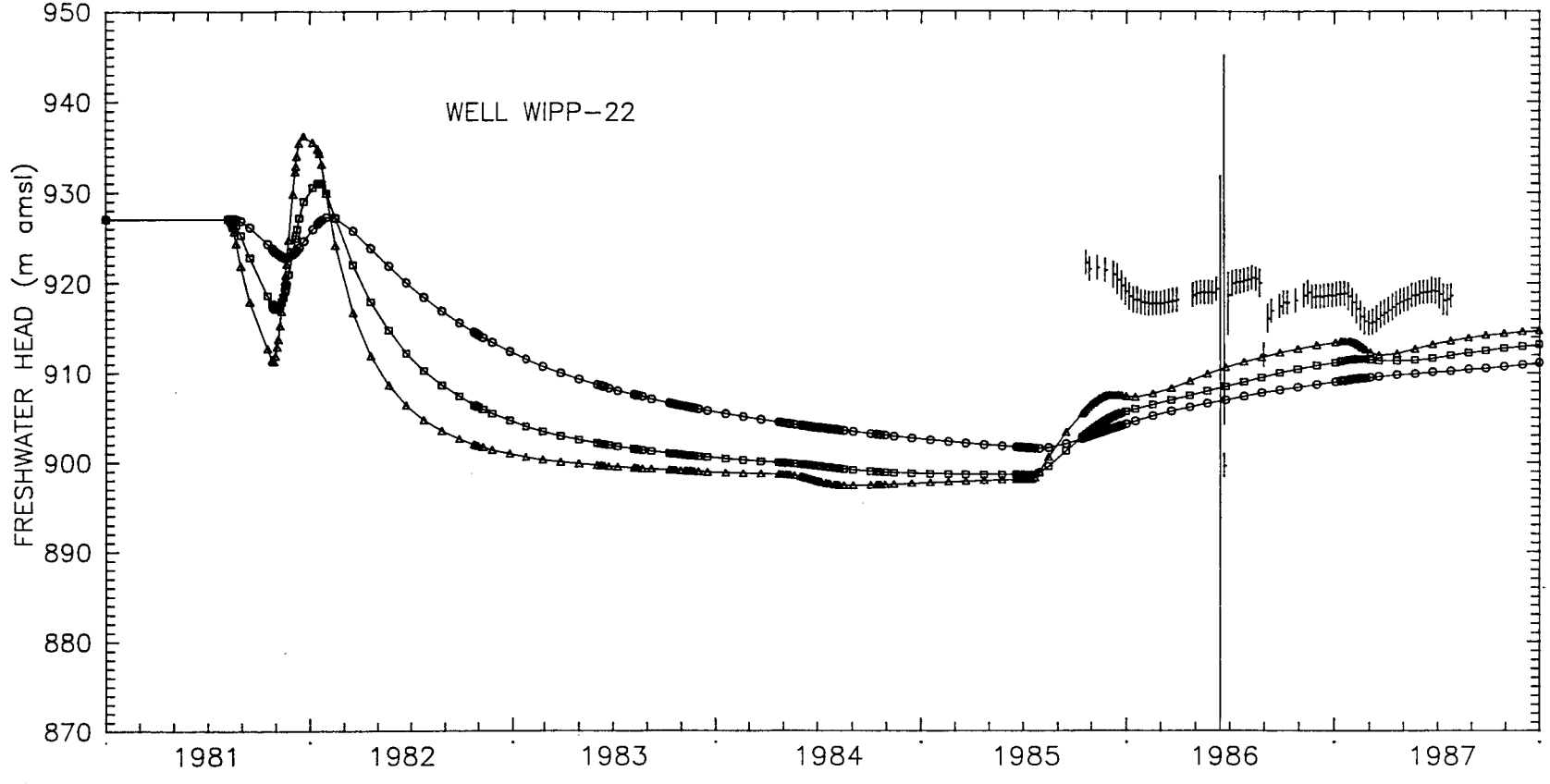

LEGEND:

- Calculated Freshwater Heads Using S=1E-5
- Calculated Freshwater Heads Using S=2E-5
- Calculated Freshwater Heads Using S=5E-5
- Observed Freshwater Heads (Water Level Data)
- Observed Freshwater Heads (Transducer Data)

Drawn by	Date
Checked by	Date
Revisions	Date
H09700R554	

INTERA Technologies

Sensitivity of Calculated Transient Freshwater Heads at WIPP-22 to Storativity

Figure 5.5k

UTM Coordinates of the Model-Area Corners:

Southwest corner:	35 72 000 mN	6 00 000 mE
Southeast corner:	35 72 000 mN	6 24 000 mE
Northeast corner:	35 97 000 mN	6 24 000 mE
Northwest corner:	35 97 000 mN	6 00 000 mE

Dimensions of the Model Area:

East - West:	24.0 km
North - South:	25.0 km
Area:	600.0 km^2

Grid Block Dimensions (m):

From West to East:	2700, 2600, 2200, 1100, 1000, 700, 600, 700, 600, 350, 200, 200, 200, 200, 150, 150, 150, 250, 450, 500, 600, 800, 1000, 2000, 2300, 2300.
From South to North:	2000, 1000, 1000, 1000, 800, 500, 300, 300, 400, 520, 320, 320, 320, 240, 260, 260, 260, 190, 140, 140, 140, 160, 140, 140, 190, 300, 360, 220, 220, 220, 340, 220, 140, 120, 220, 400, 700, 1000, 1400, 1600, 1800, 1600, 1600, 1500.

Drawn by	Date	Coordinates and Dimensions of the Model Area and the Grid Blocks
Checked by	Date	
Revisions	Date	
INTERA Technologies		Table 3.1

Fluid Properties:			References
Temperature	=	25 °C	INTERA (1986)
Compressibility	=	4.53×10^{-10} m^2/N (25°C)	Langguth and Voigt (1980)
Thermal Expansion Factor	=	2.07×10^{-4} °C-1	Kuchling (1982)
Heat Capacity	=	$4.18 \times 10^{+3}$ J/kg °C	Kuchling (1982)
Viscosity	=	1.0×10^{-3} Pa s	
Density Fresh	=	1000 kg/m^3	
Brine	=	2000 kg/m^3	
Rock Properties:			
Compressibility	=	1.1×10^{-9} m^2/N	Freeze and Cherry (1979)
Heat Capacity	=	$8.0 \times 10^{+2}$ J/kg°C	Kuchling (1982)
Density	=	2500 kg/m^3	Kuchling (1982)
Transport Properties:			
Longitudinal Dispersivity	=	50.0 m	Haug et al. (1987)
Transverse Dispersivity	=	2.5 m	Haug et al. (1987)
Molecular Diffusivity in Geologic Medium	=	1.6×10^{-10} m^2/s	Bear (1972), Lerman (1979)

Drawn by	Date	Physical Model Constants	
Checked by	Date		
Revisions	Date		
INTERA Technologies			Table 3.2

LOCATION	TRANSMISSIVITY		STORATIVITY	
	(log m^2/s)	(m^2/s)	(log S)	(S)
H-1	-6.12	7.56E-07		
H-2	-6.25	5.61E-07	-4.92	1.20E-05
H-3	-5.61	2.47E-06		
H-4	-5.99	1.02E-06	-5.34	4.62E-06
H-5	-6.82	1.52E-07	-4.69	2.05E-05
H-6	-4.10	7.95E-05	-4.75	1.80E-05
H-7	-2.96	1.11E-03	-3.09	8.20E-04
H-8	-5.05	8.86E-06		
H-9	-3.76	1.73E-04		
H-10	-7.12	7.56E-08		
H-11	-4.56	2.76E-05	-3.03	9.39E-04
H-12	-6.74	1.84E-07		
H-14	-6.48	3.29E-07		
H-15	-6.88	1.32E-07		
H-16	-6.12	7.56E-07		
H-17	-6.67	2.16E-07		
DOE-1	-4.93	1.19E-05		
DOE-2	-4.02	9.61E-05		
P-14	-3.64	2.30E-04		
P-15	-7.03	9.26E-08		
P-17	-5.86	1.38E-06		
P-18	-8.73	1.87E-09		
WIPP-12	-7.49	3.24E-08		
WIPP-13	-4.13	7.45E-05		
WIPP-18	-6.49	3.24E-07		
WIPP-19	-6.19	6.48E-07		
WIPP-21	-6.57	2.70E-07		
WIPP-22	-6.40	4.00E-07		
WIPP-25	-3.54	2.92E-04		
WIPP-26	-2.87	1.35E-03		
WIPP-27	-3.15	7.02E-04		
WIPP-28	-4.71	1.94E-05		
WIPP-29	-3.00	1.00E-03		
WIPP-30	-6.49	3.24E-07	-4.00	1.00E-04
ERDA-9	-6.29	5.08E-07		
CB-1	-6.52	3.02E-07		
ENGLE	-4.33	4.64E-05		
USGS-1	-3.26	5.54E-04	-4.70	2.00E-05

Drawn by	Date
Checked by	Date
Revisions	Date

Culebra Transmissivity and Storativity at the WIPP-Area Boreholes

INTERA Technologies

Table 3.3

Selected Linear East-West Trend:

$z = 138.8642 - 0.2354x$

with z: log Transmissivity (m^2/s)
x: UTM coordinate (km East)

Theoretical Semi-variogram:

Type : spherical
: $\gamma(h=0) = 0$
: $\gamma(0<h<a) = \omega(1.5h/a - 0.5(h/a)^3) + c$
: $\gamma(h>a) = \omega + c$

a	: 3.012 km	Range	: 3.0 km
ω	: 0.9355	Sill	: 0.94 (ω + c)
c	: 0.0	Nugget	: 0.0 (c)

Consistency Check:

Kriged Average Error	: 0.0000
Kriged Mean Square Error	: 0.5161
Reduced Mean Square Error	: 1.0001

Drawn by	Date
Checked by	Date
Revisions	Date

Results of the Semi-Variogram Analysis on the Culebra Transmissivities

INTERA Technologies

Table 3.4

Location	Undisturbed Equivalant Freshwater Head (m amsl)	Uncertainty of Observed Head (m)
H-1	921.6	±2.0
H-2b	923.5	±2.5
H-3b1	917.1	±3.0
H-4b	913.3	±2.0
H-5b	933.5	±2.0
H-6b	932.3	±2.0
H-7b1	912.6	±1.0
H-8b	911.8	±1.5
H-9b	907.0	±2.0
H-10b	920.8	±2.5
H-11b2	912.5	±2.0
H-12	913.5	±1.5
H-14	915.0	±1.5
H-15	918.0	±5.0
H-17	913.2	N/A*
P-14	927.0	±2.0
P-15	916.4	±2.5
P-17	912.6	±2.5
WIPP-12	932.2	±3.0
WIPP-13	934.0	±2.5
WIPP-18	930.0	±2.0
WIPP-25	931.0	±2.0
WIPP-26	917.5	±1.5
WIPP-27	937.5	±1.5
WIPP-28	938.1	±1.5
WIPP-29	905.4	±1.0
WIPP-30	934.7	±2.0
CB-1	911.2	±2.0
DOE-1	915.0	±2.5
DOE-2	935.4	±2.5
USGS-1	909.0	±1.5

*See Appendix E.

Drawn by	Date	Culebra Undisturbed Equivalent Freshwater Heads and the Associated Uncertainties
Checked by	Date	
Revisions	Date	
INTERA Technologies		Table 3.5

Location	Formation-Fluid Density (g/cm^3)
H-1	1.022
H-2	1.009
H-3	1.036
H-4	1.016
H-5	1.102
H-6	1.039
H-7b	1.001
H-8b	1.000
H-9b	1.001
H-10b	1.047
H-11	1.078
H-12	1.093
H-14	1.008
H-15	1.153
H-17	1.103
P-14	1.017
P-15	1.015
P-17	1.061
WIPP-13	1.043
WIPP-25	1.008
WIPP-26	1.012
WIPP-28	1.032
WIPP-30	1.020
Engle	1.001
DOE-1	1.088
DOE-2	1.041

Drawn by	Date	Culebra Formation-Fluid Densities at the WIPP-Area Boreholes
Checked by	Date	
Revisions	Date	
INTERA Technologies		Table 3.6

Model Indices I	J	K	Grid Block Center Elev m	Freshwater Head m	Fluid Density kg/m3
Western Boundary					
1	1	1	897.5	907.3	1000.0
1	2	1	899.8	907.5	1000.0
1	3	1	901.2	907.8	1000.0
1	4	1	902.1	908.2	1000.5
1	5	1	902.6	908.5	1001.5
1	6	1	901.8	909.0	1002.2
1	7	1	901.9	909.3	1002.7
1	8	1	901.9	909.6	1003.0
1	9	1	901.8	910.0	1003.3
1	10	1	901.6	910.5	1003.5
1	11	1	901.2	911.1	1003.7
1	12	1	900.7	911.5	1003.5
1	13	1	900.0	912.0	1003.4
1	14	1	899.3	912.4	1003.3
1	15	1	898.6	912.8	1003.1
1	16	1	897.7	913.9	1002.9
1	17	1	896.2	914.4	1002.7
1	18	1	895.2	914.9	1002.4
1	19	1	894.5	915.2	1002.3
1	20	1	893.9	915.5	1002.1
1	21	1	893.2	915.8	1001.9
1	22	1	892.5	916.1	1001.7
1	23	1	891.8	916.4	1001.5
1	24	1	891.2	916.7	1001.3
1	25	1	890.4	917.0	1001.2
1	26	1	889.2	917.5	1000.9
1	27	1	887.7	918.2	1000.6
1	28	1	886.4	918.7	1000.4
1	29	1	885.0	919.2	1000.3
1	30	1	884.1	919.6	1000.2
1	31	1	883.0	920.1	1000.1
1	32	1	881.9	920.7	1000.0
1	33	1	881.3	921.1	1000.0
1	34	1	880.9	921.4	1000.0
1	35	1	880.4	921.7	1000.0
1	36	1	879.5	922.3	1000.0
1	37	1	878.3	923.3	1000.0
1	38	1	877.1	924.6	1000.0
1	39	1	876.2	925.9	1000.0
1	40	1	876.8	928.0	1000.0
1	41	1	878.3	930.0	1000.0
1	42	1	880.9	931.5	1000.0
1	43	1	883.8	932.6	1000.0

Drawn by	Date	Boundary Conditions for the Initial Simulation	
Checked by	Date		
Revisions	Date		
INTERA Technologies			Table 4.1

Model Indices I	J	K	Grid Block Center Elev m	Freshwater Head m	Fluid Density kg/m3
Northern Boundary					
1	44	1	886.4	936.5	1000.0
2	44	1	884.7	937.7	1000.9
3	44	1	879.9	938.3	1009.7
4	44	1	881.1	938.4	1016.7
5	44	1	881.9	938.4	1021.2
6	44	1	882.3	938.4	1027.7
7	44	1	882.0	938.4	1031.8
8	44	1	880.6	938.3	1036.2
9	44	1	877.8	938.3	1040.8
10	44	1	875.1	938.2	1044.3
11	44	1	873.2	938.1	1046.5
12	44	1	871.7	938.1	1048.1
13	44	1	870.1	938.1	1049.7
14	44	1	868.5	938.0	1051.3
15	44	1	867.1	938.0	1052.8
16	44	1	865.8	938.0	1054.1
17	44	1	864.5	937.9	1055.4
18	44	1	862.8	937.9	1053.4
19	44	1	859.7	937.8	1056.3
20	44	1	855.3	937.7	1063.1
21	44	1	850.1	937.5	1068.5
22	44	1	843.1	937.4	1076.4
23	44	1	833.4	937.1	1086.3
24	44	1	815.6	936.7	1105.4
25	44	1	785.9	936.1	1134.7
26	44	1	755.3	935.7	1163.0
Southern Boundary					
2	1	1	893.2	909.7	1000.0
3	1	1	886.9	910.8	1000.0
4	1	1	880.5	910.5	1000.9
5	1	1	874.7	910.4	1004.7
6	1	1	869.1	910.3	1008.7
7	1	1	864.2	910.3	1012.9
8	1	1	858.9	910.3	1017.4
9	1	1	855.3	910.2	1022.4
10	1	1	850.6	910.2	1026.8
11	1	1	847.8	910.2	1029.3
12	1	1	845.7	910.2	1031.1
13	1	1	843.5	910.2	1035.0
14	1	1	841.3	910.2	1036.8
15	1	1	839.3	910.2	1038.3
16	1	1	837.6	910.2	1039.7
17	1	1	835.8	910.2	1041.1
18	1	1	833.4	910.2	1043.0
19	1	1	829.1	910.3	1045.7
20	1	1	823.1	910.7	1047.7
21	1	1	815.8	911.0	1051.7
22	1	1	806.2	911.5	1055.9
23	1	1	793.4	912.5	1060.0
24	1	1	771.9	914.2	1062.9
25	1	1	740.7	917.1	1060.6
26	1	1	709.3	920.2	1055.1

Drawn by	Date
Checked by	Date
Revisions	Date

Boundary Conditions for the Initial Simulation

INTERA Technologies

Table 4.1 (cont.)

Location	Difference Between Calculated and Observed Freshwater Head (m)	Uncertainty of Observed Freshwater Head (m)
H-1	-3.71	±2.0
H-2	-5.21	±2.5
H-3	-.04	±3.0
H-4	.88	±2.0
H-5	-10.02	±2.0
H-6	-11.61	±2.0
H-7	-2.13	±1.0
H-10	-.87	±2.5
H-11	4.64	±2.0
H-12	1.51	±1.5
H-14	1.54	±1.5
H-15	1.75	±5.0
H-17	3.55	N/A*
P-14	-8.70	±2.0
P-15	-2.69	±2.5
P-17	1.63	±2.5
WIPP-12	-10.94	±3.0
WIPP-13	-12.66	±2.5
WIPP-18	-9.71	±2.0
WIPP-25	-11.78	±2.0
WIPP-26	-2.73	±1.5
WIPP-27	-6.07	±1.5
WIPP-28	-3.24	±1.5
WIPP-30	-8.82	±2.0
CB-1	2.90	±2.0
DOE-1	3.19	±2.5
DOE-2	-12.70	±2.5

*See Appendix E.

Drawn by	Date	Differences Between Calculated and Observed Freshwater Heads for the Initial Simulation
Checked by	Date	
Revisions	Date	
INTERA Technologies		Table 4.2

Model Indices I	J	K	Grid Block Center Elev m	Freshwater Head m	Fluid Density kg/m3
Western Boundary					
1	1	1	897.5	910.0	1000.0
1	2	1	899.8	910.6	1000.0
1	3	1	901.2	911.0	1000.0
1	4	1	902.1	911.4	1000.5
1	5	1	902.6	911.8	1001.5
1	6	1	901.8	912.0	1002.2
1	7	1	901.9	912.4	1002.7
1	8	1	901.9	912.8	1003.0
1	9	1	901.8	913.2	1003.3
1	10	1	901.6	913.6	1003.5
1	11	1	901.2	914.0	1003.7
1	12	1	900.7	914.4	1003.5
1	13	1	900.0	914.8	1003.4
1	14	1	899.3	915.2	1003.3
1	15	1	898.6	915.6	1003.1
1	16	1	897.7	916.0	1002.9
1	17	1	896.2	916.8	1002.7
1	18	1	895.2	917.6	1002.4
1	19	1	894.5	918.3	1002.3
1	20	1	893.9	919.1	1002.1
1	21	1	893.2	919.8	1001.9
1	22	1	892.5	920.6	1001.7
1	23	1	891.8	921.3	1001.5
1	24	1	891.2	922.1	1001.3
1	25	1	890.4	922.9	1001.2
1	26	1	889.2	923.6	1000.9
1	27	1	887.7	924.4	1000.6
1	28	1	886.4	925.1	1000.4
1	29	1	885.0	925.9	1000.3
1	30	1	884.1	926.6	1000.2
1	31	1	883.0	927.5	1000.1
1	32	1	881.9	928.2	1000.0
1	33	1	881.3	929.0	1000.0
1	34	1	880.9	929.7	1000.0
1	35	1	880.4	930.5	1000.0
1	36	1	879.5	931.2	1000.0
1	37	1	878.3	932.1	1000.0
1	38	1	877.1	934.0	1000.0
1	39	1	876.2	934.5	1000.0
1	40	1	876.8	936.0	1000.0
1	41	1	878.3	938.0	1000.0
1	42	1	880.9	939.0	1000.0
1	43	1	883.8	940.0	1000.0

Drawn by	Date
Checked by	Date
Revisions	Date

Boundary Conditions for the Steady-State Calibrated Model

INTERA Technologies

Table 4.3

Model Indices I	J	K	Grid Block Center Elev m	Freshwater Head m	Fluid Density kg/m3
Northern Boundary					
1	44	1	886.4	942.4	1000.0
2	44	1	884.7	941.7	1000.9
3	44	1	879.9	941.0	1009.7
4	44	1	881.1	941.1	1016.7
5	44	1	881.9	941.2	1021.2
6	44	1	882.3	941.4	1027.7
7	44	1	882.0	941.5	1031.8
8	44	1	880.6	941.7	1036.2
9	44	1	877.8	941.9	1040.8
10	44	1	875.1	942.0	1044.3
11	44	1	873.2	942.1	1046.5
12	44	1	871.7	942.2	1048.1
13	44	1	870.1	942.2	1049.7
14	44	1	868.5	942.3	1051.3
15	44	1	867.1	942.3	1052.8
16	44	1	865.8	942.4	1054.1
17	44	1	864.5	942.4	1055.4
18	44	1	862.8	942.5	1053.4
19	44	1	859.7	942.6	1056.3
20	44	1	855.3	942.7	1063.1
21	44	1	850.1	942.8	1068.5
22	44	1	843.1	943.0	1076.4
23	44	1	833.4	943.3	1086.3
24	44	1	815.6	943.7	1105.4
25	44	1	785.9	944.3	1134.7
26	44	1	755.3	946.0	1163.0
Southern Boundary					
2	1	1	893.2	910.0	1000.0
3	1	1	886.9	910.0	1000.0
4	1	1	880.5	910.0	1000.9
5	1	1	874.7	910.0	1004.7
6	1	1	869.1	910.0	1008.7
7	1	1	864.2	910.0	1012.9
8	1	1	858.9	910.0	1017.4
9	1	1	855.3	910.0	1022.4
10	1	1	850.6	910.0	1026.8
11	1	1	847.8	910.0	1029.3
12	1	1	845.7	910.0	1031.1
13	1	1	843.5	910.0	1035.0
14	1	1	841.3	910.0	1036.8
15	1	1	839.3	910.0	1038.3
16	1	1	837.6	910.0	1039.7
17	1	1	835.8	910.3	1041.1
18	1	1	833.4	910.5	1043.0
19	1	1	829.1	911.0	1045.7
20	1	1	823.1	911.5	1047.7
21	1	1	815.8	912.0	1051.7
22	1	1	806.2	912.5	1055.9
23	1	1	793.4	913.0	1060.0
24	1	1	771.9	914.0	1062.9
25	1	1	740.7	918.0	1060.6
26	1	1	709.3	920.1	1055.1

Drawn by	Date
Checked by	Date
Revisions	Date

Boundary Conditions for the Steady-State Calibrated Model

INTERA Technologies

Table 4.3 (cont.)

Location	Difference Between Calculated and Observed Freshwater Head (m)	Uncertainty of Observed Freshwater Head (m)
H-1	-1.37	±2.0
H-2	.24	±2.5
H-3	-1.68	±3.0
H-4	-.33	±2.0
H-5	1.69	±2.0
H-6	1.47	±2.0
H-7	-2.13	±1.0
H-10	-1.04	±2.5
H-11	1.54	±2.0
H-12	.64	±1.5
H-14	.81	±1.5
H-15	2.09	±5.0
H-17	.89	N/A*
P-14	.98	±2.0
P-15	.50	±2.5
P-17	-1.17	±2.5
WIPP-12	.33	±3.0
WIPP-13	.47	±2.5
WIPP-18	-1.40	±2.0
WIPP-25	-1.67	±2.0
WIPP-26	.24	±1.5
WIPP-27	.55	±1.5
WIPP-28	.32	±1.5
WIPP-30	.43	±2.0
CB-1	.49	±2.0
DOE-1	.32	±2.5
DOE-2	.46	±2.5

*See Appendix E.

Drawn by	Date
Checked by	Date
Revisions	Date

Differences Between Calculated and Observed Freshwater Heads for the Steady-State Calibrated Model

INTERA Technologies

Table 4.4

Location	Differences Between Calculated and Observed Freshwater Head (m)	Uncertainty of Observed Freshwater Head (m)
H-1	1.11	±2.0
H-2	1.88	±2.5
H-3	1.83	±3.0
H-4	2.67	±2.0
H-5	1.89	±2.0
H-6	1.48	±2.0
H-7	-2.13	±1.0
H-10	-.98	±2.5
H-11	5.16	±2.0
H-12	.91	±1.5
H-14	3.93	±1.5
H-15	5.01	±5.0
H-17	3.07	N/A*
P-14	1.01	±2.0
P-15	1.34	±2.5
P-17	.79	±2.5
WIPP-12	.74	±3.0
WIPP-13	.50	±2.5
WIPP-18	-.36	±2.0
WIPP-25	-1.67	±2.0
WIPP-26	.24	±1.5
WIPP-27	.55	±1.5
WIPP-28	.32	±1.5
WIPP-30	.44	±2.0
CB-1	3.31	±2.0
DOE-1	4.00	±2.5
DOE-2	.48	±2.5

*See Appendix E.

Drawn by	Date	Differences Between Calculated and Observed Freshwater Heads for Sensitivity Case 2 (Intermediate-Transmissivity-Value Pilot Points Near H-11)
Checked by	Date	
Revisions	Date	
INTERA Technologies		Table 4.6

Location	Differences Between Calculated and Observed Freshwater Head (m)	Uncertainty of Observed Freshwater Head (m)
H-1	3.63	±2.0
H-2	3.63	±2.5
H-3	5.26	±3.0
H-4	4.06	±2.0
H-5	2.09	±2.0
H-6	1.48	±2.0
H-7	-2.12	±1.0
H-10	-.91	±2.5
H-11	8.65	±2.0
H-12	1.04	±1.5
H-14	7.70	±1.5
H-15	7.79	±5.0
H-17	5.52	N/A*
P-14	.91	±2.0
P-15	1.04	±2.5
P-17	2.87	±2.5
WIPP-12	1.13	±3.0
WIPP-13	.51	±2.5
WIPP-18	.65	±2.0
WIPP-25	-1.68	±2.0
WIPP-26	.24	±1.5
WIPP-27	.55	±1.5
WIPP-28	.32	±1.5
WIPP-30	.44	±2.0
CB-1	5.41	±2.0
DOE-1	7.41	±2.5
DOE-2	.49	±2.5

*See Appendix E.

Drawn by	Date	Differences Between Calculated and Observed Freshwater Heads for Sensitivity Case 1 (Without High-Transmissivity-Value Pilot Points Near H-11)
Checked by	Date	
Revisions	Date	
INTERA Technologies		Table 4.5

Location	Difference Between Calculated and Observed Freshwater Head (m)	Uncertainty of Observed Freshwater Head (m)
H-1	-.08	±2.0
H-2	1.22	±2.5
H-3	.00	±3.0
H-4	1.43	±2.0
H-5	2.00	±2.0
H-6	1.72	±2.0
H-7	-.24	±1.0
H-10	-.68	±2.5
H-11	3.39	±2.0
H-12	2.50	±1.5
H-14	2.38	±1.5
H-15	3.58	±5.0
H-17	2.78	N/A*
P-14	1.54	±2.0
P-15	1.89	±2.5
P-17	.73	±2.5
WIPP-12	.74	±3.0
WIPP-13	.71	±2.5
WIPP-18	-.71	±2.0
WIPP-25	-1.23	±2.0
WIPP-26	1.49	±1.5
WIPP-27	.61	±1.5
WIPP-28	.39	±1.5
WIPP-30	.61	±2.0
CB-1	2.34	±2.0
DOE-1	2.14	±2.5
DOE-2	.69	±2.5

*See Appendix E.

Drawn by	Date	Differences Between Calculated and Observed Freshwater Heads for Sensitivity Case 3 (Increased Heads Along the Southwestern Boundaries)	
Checked by	Date		
Revisions	Date		
INTERA Technologies			Table 4.7

APPENDIX A BOREHOLE COORDINATES

A spreadsheet of the borehole coordinates (Table A.1) was generated to reduce the possibility of error in calculating UTM coordinates for the WIPP-area boreholes. A spreadsheet program was utilized to calculate the relative-distance vector from a borehole to the nearest reference borehole within the same township and range. A reference borehole is a borehole which has UTM coordinates determined by the satellite survey performed in 1984 (Hydro Geo Chem, 1985). These boreholes are identified in the reference column of the spreadsheet with SAT SUR 84. With the exception of the reference boreholes, the reference column refers the reader to the data source for the distances used to locate a well in a section of a township and range.

Once the relative-distance vector between a borehole and its reference borehole is calculated, the spreadsheet algorithm rotates the distance components 0.633 degrees clockwise to the UTM-coordinate system. This occurs because the township and range coordinate system is not parallel to the UTM-coordinate system. Thus, a rotation of the relative distance vector components must be performed before the relative distance may be added to the reference boreholes UTM coordinates. The 0.633 value was calculated from differences of relative angles between boreholes using UTM satellite survey values and township and range values. The UTM coordinates for a borehole are then simply the addition of the UTM relative-distance vector to the UTM coordinates of its reference borehole.

REFERENCES

Beauheim, R.L., 1987. Interpretations of Single-Well Hydraulic Tests Conducted at and Near the Waste Isolation Pilot Plant (WIPP) Site, 1983-1987. Sandia National Laboratories, SAND87-0039.

Cooper, J.B. and V.M. Glanzman, 1971. Geohydrology of Project Gnome Site, Eddy County, New Mexico. U.S. Geological Survey, Professional Paper 712-A, 28 p.

Hydro Geo Chem, Inc., 1985. WIPP Hydrology Program, Waste Isolation Pilot Plant, SENM, Hydrologic Data Report #1. Sandia National Laboratories, Contractor Report SAND85-7206, 710 p.

Jarolimek, L., M.J. Timmer, and D.W. Powers, 1983. Correlation of Drillhole and Shaft Logs, Waste Isolation Pilot Plant (WIPP) Project, Southeastern New Mexico. U.S. Department of Energy, TME 3179.

Kelley, V.A., and J.F. Pickens, 1986. Interpretation of the Convergent-Flow Tracer Tests Conducted in the Culebra Dolomite at the H-3 and H-4 Hydropads at the Waste Isolation Pilot Plant (WIPP) Site. Sandia National Laboratories, Contractor Report SAND86-7161.

Mercer, J.W., 1983. Geohydrology of the Proposed Waste Isolation Pilot Plant Site, Los Medanos Area, Southeastern New Mexico. U.S. Geological Survey, Water-Resources Investigations 83-4016, 113 p.

Reddy, D., 1986. Personal Communication, Carlsbad, New Mexico.

Reddy, D., 1987. Personal Communication, Carlsbad, New Mexico.

WIPP-SITE OBSERVATION-WELL UTM COORDINATE CALCULATIONS

OBSERVATION WELL	LOCATION SEC	T	R	DISTANCE IN FEET FROM SECTION LINES FNL	FEL	UTM COORDINATES NORTH	EAST	REFERENCE WELL	REFERENCES
H-1	29	T22S	R31E	623.31	1082.75	3581672.40	613426.50		SAT SUR 84
H-2A	29	T22S	R31E	726.17	3581.57	3581649.47	612664.55	H-1	MERCER 83
H-2B	29	T22S	R31E	695.57	3619.43	3581658.92	612653.11	H-1	MERCER 83
H-2C	29	T22S	R31E	637.15	3571.38	3581676.57	612667.96	H-1	MERCER 83
H-3B1	29	T22S	R31E	3194.70	138.10	3580885.50	613705.75	H-1	MERCER 83
H-3B2	29	T22S	R31E	3157.98	231.32	3580897.00	613677.46	H-1	SAND86-7161
H-3B3	29	T22S	R31E	3258.07	217.77	3580866.45	613681.26	H-1	SAND86-7161
H-4A	5	T23S	R31E	545.89	4560.00	3578465.35	612404.00	H-4B	MERCER 83
H-4B	5	T23S	R31E	498.47	4647.46	3578480.10	612377.50		SAT SUR 84
H-4C	5	T23S	R31E	446.36	4562.11	3578495.69	612403.69	H-4B	MERCER 83
H-5A	15	T23S	R31E	1093.12	184.33	3584782.92	616882.79		SAT SUR 84
H-5B	15	T23S	R31E	1006.80	234.21	3584809.40	616867.88	H-5A	MERCER 83
H-5C	15	T23S	R31E	1006.47	134.20	3584809.16	616898.36	H-5A	MERCER 83
H-6A	18	T22S	R31E	283.80	5005.07	3584962.35	610584.55	H-6C	MERCER 83
H-6B	18	T22S	R31E	195.61	4957.85	3584989.07	610599.24	H-6C	MERCER 83
H-6C	18	T22S	R31E	280.61	4905.19	3584962.99	610615.00		SAT SUR 84
H-7A	14	T23S	R31E	2495.04	2787.65	3574668.93	608104.17		SAT SUR 84
H-7B1	14	T23S	R30E	2565.80	2716.55	3574647.12	608125.60	H-7A	MERCER 83
H-7C	14	T23S	R30E	2591.93	2812.49	3574639.48	608096.27	H-7A	MERCER 83
H-8A	23	T24S	R30E	1962.61	1486.59	3563566.60	608641.85	H-8B	MERCER 83
H-8B	23	T24S	R30E	1994.76	1405.39	3563556.53	608666.49		SAT SUR 84
H-8C	23	T24S	R30E	2059.39	1470.14	3563537.05	608646.54	H-8B	MERCER 83
H-9A	4	T24S	R31E	2392.14	5141.08	3568265.50	613946.29	H-9B	MERCER 83
H-9B	4	T24S	R31E	2391.04	4996.37	3568265.35	613990.40		SAT SUR 84
H-9C	4	T24S	R31E	2479.06	5091.98	3568238.84	613960.96	H-9B	MERCER 83
H-10A	20	T23S	R32E	4846.96	2068.91	3572460.79	622953.64	H-10B	MERCER 83
H-10B	20	T23S	R32E	4795.46	1984.84	3572476.20	622979.44		SAT SUR 84
H-10C	20	T23S	R32E	4895.46	1981.84	3572445.71	622980.02	H-10B	MERCER 83
H-11B1	33	T22S	R31E	3769.33	173.91	3579137.19	615338.97	H-11B3	REDDY 7/86
H-11B2	33	T22S	R31E	3843.84	168.62	3579114.47	615340.33	H-11B3	REDDY 7/86
H-11B3	33	T22S	R31E	3778.49	105.22	3579134.17	615359.87		SAT SUR 84
H-12						3575441.64	617017.80		SAT SUR 84
H-14	29	T22S	R31E	4907.80	4717.60	3580378.80	612304.22	H-1	REDDY 10/86
H-15	28	T22S	R31E	88.67	174.30	3581814.50	615314.45	H-1	REDDY 10/86
H-16	20	T22S	R31E	4167.19	1241.19	3582202.08	613384.06	H-1	REDDY 8/87
H-17	3	T23S	R31E	3814.00	4287.00	3577432.79	615694.72	H-4B	REDDY 8/87
H-18	20	T22S	R31E	964.00	4834.00	3583190.47	612299.82	H-1	REDDY 9/87
P-1	29	T22S	R31E	4952.00	4728.00	3580365.36	612300.90	H-1	MERCER 83
P-2	28	T22S	R31E	121.00	171.00	3581804.64	615315.35	H-1	MERCER 83
P-3	20	T22S	R31E	5176.00	3126.00	3581900.96	612806.20	H-1	MERCER 83
P-4	28	T22S	R31E	5131.00	1485.00	3580282.09	614897.98	H-1	MERCER 83
P-5	17	T22S	R31E	5094.00	160.00	3583525.22	613728.26	H-1	MERCER 83
P-6	30	T22S	R31E	2509.00	5085.00	3581128.94	610591.06	H-1	MERCER 83
P-7	5	T23S	R31E	514.00	4887.00	3578476.17	612304.44	H-4B	MERCER 83
P-8	4	T23S	R31E	640.00	5188.00	3578421.00	613821.54	H-4B	MERCER 83
P-9	33	T22S	R31E	3787.00	126.00	3579186.28	615329.43	P-18	MERCER 83
P-10	26	T22S	R31E	2341.00	4957.00	3581216.96	617098.20	P-18	MERCER 83
P-11	23	T22S	R31E	156.00	5097.00	3583458.04	616980.12	H-5A	MERCER 83
P-12	24	T22S	R30E	165.00	198.00	3583421.53	610462.71	P-14	MERCER 83
P-13	18	T22S	R31E	110.00	5133.00	3585015.76	610546.14	H-6C	MERCER 83
P-14	24	T22S	R30E	4971.00	4667.00	3581971.79	609084.43		SAT SUR 84
P-15	31	T22S	R31E	4869.00	5090.00	3578739.00	610624.60		SAT SUR 84
P-16	5	T23S	R31E	4341.00	3633.00	3577305.54	612673.75	H-4B	MERCER 83
P-17	4	T23S	R31E	3924.00	4882.00	3577419.05	613903.74	H-4B	MERCER 83

Drawn by	Date	WIPP-Area Borehole UTM Coordinates
Checked by	Date	
Revisions	Date	
HO9700R554		
INTERA Technologies		Table A.1

WIPP-SITE OBSERVATION-WELL UTM COORDINATE CALCULATIONS

OBSERVATION WELL	LOCATION SEC	T	R	DISTANCE IN FEET FROM SECTION LINES FNL	FEL	UTM COORDINATES NORTH	EAST	REFERENCE WELL	REFERENCES
P-18	26	T22S	R31E	5141.00	733.00	3580349.33	618376.18		SAT SUR 84
P-19	23	T22S	R31E	3628.00	2945.00	3582427.19	617724.88	P-18	MERCER 83
P-20	14	T22S	R31E	4479.00	79.00	3583732.81	618512.75	H-5A	MERCER 83
P-21	15	T22S	R31E	859.00	130.00	3584854.09	616900.14	H-5A	MERCER 83
WIPP-11	9	T22S	R31E	711.07	4885.92	3586564.41	613832.91	AEC-8	MERCER 83
WIPP-12	17	T22S	R31E	5132.10	83.91	3583513.35	613751.32	H-1	MERCER 83
WIPP-13	17	T22S	R31E	2714.32	3549.41	3584261.93	612703.23	H-1	MERCER 83
WIPP-16	5	T21S	R30E	2925.00	5140.00	3597063.02	602457.22	WIPP-27	MERCER 83
WIPP-18	20	T22S	R31E	983.58	11.45	3583168.25	613769.59	H-1	MERCER 83
WIPP-19	20	T22S	R31E	2292.66	12.68	3582769.27	613764.81	H-1	MERCER 83
WIPP-21	20	T22S	R31E	3728.92	11.74	3582331.51	613760.25	H-1	MERCER 83
WIPP-22	20	T22S	R31E	2735.55	11.94	3582634.28	613763.54	H-1	MERCER 83
WIPP-25	15	T22S	R30E	3427.28	2838.10	3584025.22	606386.67		SAT SUR 84
WIPP-26	29	T22S	R30E	2232.27	12.20	3581041.22	603994.77		SAT SUR 84
WIPP-27	21	T21S	R30E	89.79	3794.97	3593077.03	604432.62		SAT SUR 84
WIPP-28	18	T21S	R31E	98.72	2400.99	3594734.96	611376.93	WIPP-30	SAT SUR 84
WIPP-29	34	T22S	R29E	4873.38	1827.54	3578773.00	596940.83		SAT SUR 84
WIPP-30	33	T21S	R31E	667.50	5102.59	3589707.33	613716.77		SAT SUR 84
WIPP-33	13	T22S	R30E	3518.00	2853.00	3584017.80	609659.99	P-14	MERCER 83
WIPP-34	9	T22S	R31E	5078.00	3280.00	3585228.02	614307.66	AEC-8	MERCER 83
AEC-7	31	T21S	R32E	2040.00	2040.00	3589376.43	621131.67		SAT SUR 84
AEC-8	11	T22S	R31E	935.00	3301.00	3586455.24	617533.75		SAT SUR 84
ERDA-6	35	T21S	R31E	3128.00	910.00	3588907.71	618204.85	WIPP-30	MERCER 83
ERDA-9	20	T22S	R31E	5012.77	176.74	3581940.77	613705.64	H-1	MERCER 83
ERDA-10	34	T23S	R30E	200.00	2327.00	3570556.86	606589.67	H-7A	MERCER 83
CB-1	5	T23S	R31E	1989.50	2017.06	3578016.79	613174.18	H-4B	REDDY 2/87
ENGLE	4	T24S	R31E	5020.00	1980.00	3567453.92	614900.89	H-9B	SAND87-0039
USGS-1	34	T23S	R30E	3630.00	2970.00	3569513.62	606382.14	H-7A	COOPER GLANZ
FF-127	2	T23S	R30E	4867.50	412.50	3577156.37	608855.66	H-7A	COOPER GLANZ
DOE-1	28	T22S	R31E	5098.00	610.00	3580298.26	615196.33		SAT SUR 84
DOE-2	8	T22S	R31E	4575.93	128.19	3585119.40	613720.11		SAT SUR 84
WHS	20	T22S	R31E	4612.00	551.00	3582064.18	613592.92	H-1	DOE RPT# TME3179
CSS	20	T22S	R31E	4212.00	576.00	3582186.18	613586.65	H-1	DOE RPT# TME3179
EXS	20	T22S	R31E	4612.00	151.00	3582062.83	613714.83	H-1	DOE RPT# TME3179

Drawn by	Date
Checked by	Date
Revisions	Date
H09700R554	

WIPP-Area Borehole UTM Coordinates

INTERA Technologies

Table A.1 (cont.)

APPENDIX B CULEBRA ELEVATIONS

The Culebra elevations in meters above mean sea level (m amsl) in the WIPP-area boreholes are presented in Table B.1. The elevations are calculated from the referenced ground-surface elevations and the stratigraphic information taken from data sources for these particular boreholes. Several references are used for the ground-surface elevation values including published references, personal communication with R.L. Beauheim at Sandia National Laboratories, and recent surveys performed by D. Reddy of Carlsbad, New Mexico. Where possible, the Beauheim-recommended elevation was chosen as the most representative. In instances where boreholes did not have a Beauheim-recommended value, other references were used to determine a ground-surface elevation.

The depths to the Culebra top, center, and bottom are listed in Table B.1 and are taken from INTERA (1987). These values are presented in feet below ground surface. The elevations of the top, center, and bottom of the Culebra in meters above mean sea level are also listed in Table B.1. These values are calculated from the surface elevations and depth values.

REFERENCES:

Beauheim, R.L., 1987. Interpretations of Single-Well Hydraulic Tests Conducted at and Near the Waste Isolation Pilot Plant (WIPP) Site, 1983-1987. Sandia National Laboratories, SAND87-0039.

Davies, P.B., 1988. Variable-Density Ground-Water Flow and Paleohydrology in the Region Surrounding the Waste Isolation Pilot Plant (WIPP), Southeastern New Mexico. U.S. Geological Survey, Water Resources Investigations.

INTERA Technologies, Inc., 1986. WIPP Hydrology Program, Waste Isolation Pilot Plant, SENM, Hydrologic Data Report #3. Sandia National Laboratories, Contractor Report SAND86-7109.

INTERA Technologies, 1987. Field Operations Plan for Monitoring of Ground-Water Observation Wells at the Waste Isolation Pilot Plant (WIPP) Site. Prepared for Sandia National Laboratories.

Mercer, J.W., 1983. Geohydrology of the Proposed Waste Isolation Pilot Plant Site, Los Medanos Area, Southeastern New Mexico. U.S. Geological Survey, Water-Resources Investigations 83-4016, 113 p.

Reddy, D., 1986. Personal Communication, Carlsbad, New Mexico.

Reddy, D., 1987. Personal Communication, Carlsbad, New Mexico.

ELEVATION DATA BASE - UPDATED 12-29-87

WELL	GROUND-SURFACE ELEV FT AMSL	GROUND-SURFACE ELEV SOURCE	CULEBRA DEPTH FT BGS T	C	B	CULEBRA ELEVATION M AMSL T	C	B	CUL THICK M
H-1	3397.9	MERCER 83	676	688	699	829.6	826.1	822.6	7.0
H-2A	3377.8	RLB	623	634	645	839.7	836.3	833.0	6.7
H-2B1	3377.6	RLB	624	633	642	839.3	836.6	833.8	5.5
H-2B2	3377.6	REDDY	623	634	645	839.6	836.2	832.9	6.7
H-2C	3377.7	RLB	624	633	642	839.3	836.6	833.8	5.5
H-3B1	3389.4	RLB	670	682	694	828.9	825.2	821.6	7.3
H-3B2	3388.3	S 86-7109	676	688	700	826.7	823.1	819.4	7.3
H-3B3	3387.1	S 86-7109	673	685	696	827.3	823.8	820.3	7.0
H-4A	3332.8	RLB	496	508	520	864.7	861.0	857.3	7.3
H-4B	3332.7	RLB	490	503	516	866.4	862.5	858.5	7.9
H-4C	3332.5	RLB	490	503	516	866.4	862.4	858.5	7.9
H-5A	3505.6	RLB	897	909	920	795.1	791.6	788.1	7.0
H-5B	3505.4	RLB	897	909	920	795.0	791.5	788.0	7.0
H-5C	3505.8	RLB	899	912	924	794.5	790.7	786.9	7.6
H-6A	3347.3	MERCER 83	604	616	627	836.1	832.6	829.1	7.0
H-6B	3347.6	MERCER 83	604	616	627	836.2	832.7	829.2	7.0
H-6C	3347.9	MERCER 83	604	616	627	836.3	832.8	829.3	7.0
H-7B1	3163.6	RLB	237	256	274	892.0	886.4	880.8	11.3
H-7B2	3164.0	CALCULATED	237	256	274	892.1	886.5	880.9	11.3
H-7C	3163.4	RLB	237	256	274	892.0	886.3	880.7	11.3
H-8B	3433.8	S 87-0039	588	601	614	867.4	863.4	859.5	7.9
H-8C	3433.0	MERCER 83	588	601	614	867.2	863.2	859.2	7.9
H-9A	3405.4	RLB	647	662	677	840.8	836.2	831.6	9.1
H-9B	3405.6	MERCER 83	647	662	677	840.8	836.2	831.7	9.1
H-9C	3405.9	MERCER 83	647	662	677	840.9	836.3	831.8	9.1
H-10B	3687.0	MERCER 83	1360	1376	1391	709.3	704.5	699.8	9.4
H-10C	3686.9	MERCER 83	1360	1376	1391	709.2	704.5	699.8	9.4
H-11B1	3412.1	REDDY	730	743	756	817.5	813.5	809.6	7.9
H-11B2	3412.1	REDDY	733	745	757	816.6	812.9	809.3	7.3
H-11B3	3412.1	REDDY	734	747	759	816.3	812.5	808.7	7.6
H-12	3426.0	REDDY	823	837	850	793.4	789.3	785.2	8.2
H-14	3345.6	RLB	545	559	572	853.6	849.5	845.4	8.2
H-15	3480.2	RLB	861	872	883	798.3	795.0	791.6	6.7
H-16	3409.6	REDDY	700	712	724	826.0	822.2	818.4	7.6
H-17	3384.0	REDDY	706	719	731	816.3	812.4	808.5	7.8

Drawn by	Date
Checked by	Date
Revisions	Date
H09700R554	

Ground-Surface and Culebra Dolomite Elevations for WIPP-Area Boreholes

INTERA Technologies

Table B.1

ELEVATION DATA BASE - UPDATED 12-29-87

WELL	GROUND-SURFACE ELEV FT AMSL	GROUND-SURFACE ELEV SOURCE	CULEBRA DEPTH FT BGS			CULEBRA ELEVATION M AMSL			CUL THICK M
			T	C	B	T	C	B	
DOE-1	3465.1	REDDY	820	832	843	806.2	802.7	799.2	7.0
DOE-2	3418.4	RLB	824	835	846	790.8	787.4	784.1	6.7
P-1	3345.1	MERCER 83	538	552	565	855.6	851.5	847.4	8.2
P-2	3479.4	MERCER 83	857	870	883	799.3	795.3	791.4	7.9
P-3	3382.7	MERCER 83	642	654	665	835.4	831.9	828.4	7.0
P-4	3443.8	MERCER 83	775	789	802	813.5	809.3	805.2	8.2
P-5	3470.9	MERCER 83	804	816	827	812.9	809.4	805.9	7.0
P-6	3354.1	MERCER 83	537	549	560	858.7	855.1	851.6	7.0
P-7	3332.0	MERCER 83	496	509	522	864.4	860.5	856.5	7.9
P-8	3338.6	MERCER 83	563	576	588	846.0	842.2	838.4	7.6
P-9	3411.5	MERCER 83	734	746	757	816.1	812.6	809.1	7.0
P-10	3509.3	MERCER 83	931	944	957	785.9	781.9	777.9	7.9
P-11	3503.9	MERCER 83	912	925	938	790.0	786.0	782.1	7.9
P-12	3373.6	MERCER 83	633	645	656	835.3	831.8	828.3	7.0
P-13	3345.2	MERCER 83	604	616	627	835.5	832.0	828.5	7.0
P-14	3359.8	REDDY	573	584	595	849.4	846.1	842.7	6.7
P-15	3309.8	RLB	413	424	435	882.9	879.6	876.2	6.7
P-16	3317.9	MERCER 83	500	512	523	858.9	855.4	851.9	7.0
P-17	3335.8	REDDY	558	571	583	846.7	842.9	839.1	7.6
P-18	3477.3	REDDY	912	926	940	781.9	777.6	773.4	8.5
P-19	3545.1	MERCER 83	967	982	997	785.8	781.2	776.7	9.1
P-20	3552.7	MERCER 83	953	966	979	792.4	788.4	784.5	7.9
P-21	3509.0	MERCER 83	899	912	924	795.5	791.7	787.9	7.6
WIPP-11	3426.1	MERCER 83	844	856	867	787.0	783.5	780.0	7.0
WIPP-12	3471.3	REDDY	810	823	835	811.2	807.4	803.5	7.6
WIPP-13	3405.4	RLB	701	713	724	824.3	820.8	817.3	7.0

Drawn by	Date
Checked by	Date
Revisions	Date
H09700R554	

Ground-Surface and Culebra Dolomite Elevations for WIPP-Area Boreholes

INTERA Technologies

Table B.1 (cont.)

ELEVATION DATA BASE - UPDATED 12-29-87

WELL	GROUND-SURFACE ELEV FT AMSL	GROUND-SURFACE ELEV SOURCE	CULEBRA DEPTH FT BGS T	C	B	CULEBRA ELEVATION M AMSL T	C	B	CUL THICK M
WIPP-18	3456.4	RLB	787	798	808	813.6	810.4	807.2	6.4
WIPP-19	3433.1	S 87-0039	756	768	779	816.0	812.5	809.0	7.0
WIPP-21	3417.1	REDDY	729	741	753	819.3	815.7	812.0	7.3
WIPP-22	3425.8	S 87-0039	742	753	764	818.0	814.7	811.3	6.7
WIPP-25	3212.5	RLB	447	460	472	842.9	839.1	835.3	7.6
WIPP-26	3151.7	RLB	186	198	209	904.0	900.4	896.9	7.0
WIPP-27	3177.2	RLB	292	305	318	879.4	875.4	871.5	7.9
WIPP-28	3346.6	RLB	420	433	446	892.0	888.1	884.1	7.9
WIPP-29	2977.0	RLB	12	27	42	903.7	899.1	894.6	9.1
WIPP-30	3427.5	RLB	631	642	653	852.4	849.0	845.7	6.7
ERDA-6	3540.2	MERCER 83	710	723	735	862.6	858.8	855.0	7.6
ERDA-9	3408.8	RLB	704	716	727	824.4	820.9	817.4	7.0
ERDA-10	3371.2	MERCER 83	476	490	504	882.5	878.2	873.9	8.5
CB-1	3327.3	RLB	503	516	529	860.8	856.9	852.9	7.9
ENGLE T	3419.0	S 87-0039	659	670	681	841.2	837.9	834.5	6.7
AEC-7	3654.0	MERCER 83	870	883	896	848.6	844.6	840.6	7.9
AEC-8	3531.5	MERCER 83	833	846	859	822.5	818.5	814.6	7.9
FFG242 +							726.2		
								AVG = THICKNESS	7.7 m

REFERENCES

+ - FFG242 DEPTH TO BASE OF CULEBRA VALUE FROM DAVIES (1988)
A THICKNESS OF EIGHT M IS ASSUMED FOR MIDPOINT-VALUE CALCULATION

Drawn by	Date
Checked by	Date
Revisions	Date
H09700R554	

Ground-Surface and Culebra Dolomite Elevations for WIPP-Area Boreholes

INTERA Technologies

Table B.1 (cont.)

APPENDIX C CULEBRA TRANSMISSIVITIES

The Culebra transmissivity data base is presented in Table C.1. For each borehole, Table C.1 contains:

1) the references for the cited transmissivity values;
2) the type of tests performed;
3) the reported transmissivity value in ft^2/day;
4) the equivalent transmissivity in m^2/s and its $\log_{10}$ value;
5) the selected transmissivity values used in determining the representative value (see below for explanation);
6) the average log transmissivity of the selected values;
7) the representative borehole and hydropad transmissivity values (and their logs) which are used in the modeling.
8) comments;
9) possible pilot-point transmissivity values (denoted by a plus sign).

The transmissivity values are tabulated based upon the type of hydraulic test performed. Pumping and slug tests produce the transmissivity values needed in a kriging analyses (i.e., local-scale values). This is because the transmissivity is ultimately assigned to a grid block that is on the scale of tens of meters. Thus, transmissivity values determined from regional-scale interference tests, which stress hundreds of meters, or from DST's, which stress only a very small portion of the formation, are not considered to represent the local scale. The values determined from these large- and small-scale tests were therefore not selected in the calculation of the final representative transmissivity. Small-scale interference tests within a hydropad are considered representative. For example, each of the three wells at the H-6 hydropad has had several pumping tests performed. The interference values determined within the hydropad are considered to represent local-scale conditions and were therefore included as selected values.

The second selection criterion is the quality of the value from the local-scale test. On several occasions, tests at a borehole have produced several values that are consistent and one value that is not. This latter value could result from a poor test or a poor analytical fit to the test data. One example of this occurring is at borehole H-3b1, where a value of 27 ft^2/day was determined for a slug test. An earlier bailer test gave a value of 12 ft^2/day. These values were subsequently averaged and presented as 19 ft^2/day in Mercer (1983). The other values at this well and at the other wells in the hydropad are between 1 and 3 ft^2/day. Therefore, the higher number was not considered consistent and was not selected for use in calculation of the mean and standard deviation of the log transmissivity values for the hydropad.

The above criteria were used as guidelines, and were not adhered to strictly in all cases. DST values were selected on several occasions in order to have more than a single value at a borehole (e.g., H-14, H-15). The selected DST values were, however, consistent with the other values at the boreholes.

Once values were selected, the mean of the log of the selected transmissivity values was calculated. These calculations do not use reported regional-interference test values.

The Culebra transmissivity data base (Table C.1) was also used to determine the uncertainty associated with the selected transmissivity values. This was done to (1) quantify the uncertainty of the transmissivity at a given borehole, and (2) incorporate the results into the K603 kriging exercise. Therefore, the standard deviation and variance of the selected transmissivity values for a given borehole or hydropad were calculated. In this calculation all data with the exception of the regional-scale interference values were used. The resulting values are indicators for the reproducibility of hydraulic testing results at the different hydropads or boreholes. It is assumed that the hydraulic tests have tested a

sufficiently representative rock volume. The standard deviation, therefore, may be interpreted as the uncertainty associated with the transmissivity values. In addition, a normal error distribution is assumed. Thus, the selected transmissivity value plus or minus two standard deviations corresponds to a 95% confidence interval of the transmissivity at a particular borehole or hydropad.

In order to be a reliable indicator, a statistical value such as the standard deviation has to be based on a sufficiently large number of measurements (e.g., 30). Most standard deviations in Table C.2 are based on a much smaller number. Some of these standard deviations are very small (e.g., at P-15) and appear to erroneously indicate a very low uncertainty associated with the transmissivity data. Therefore, it was assumed that the minimum uncertainty associated with pumping-test results is half an order of magnitude, which corresponds to an uncertainty on the log scale of 0.25 (log m^2/s). For the other tests such as DSTs or slug tests, a minimum uncertainty of one order of magnitude (corresponding to a standard deviation of 0.5) was assumed.

The resulting standard deviations and variances as they were used for the K603 kriging of the transmissivity field are listed in the last two columns in Table C.2.

REFERENCES

The references for the data sources are listed at the end of Table C.1.

CULEBRA TRANSMISSIVITY DATABASE - UPDATED 12-29-87

ABBREVIATIONS ;
I = INTERFERENCE
R = RECOVERY
D = DRAWDOWN
OB = OBSERVATION
(WELL) = PUMPING WELL
UE = UNPUBLISHED ESTIMATE
+ = POSSIBLE VALUE FOR PILOT POINT POSITIONED BETWEEN PUMPING AND OBSERVATION WELL

WELL	REFERENCES	YEAR OF REFERENCE	TYPE OF TEST	REPORTED CULEBRA TRANSMISSIVITIES ft2/day	m2/s	log m2/s	SELECTED VALUES (YES or NO)	AVERAGE OF SELECTED VALUES (PER HYDROPAD OR WELL LOCATION)	TRANSMISSIVITY VALUES USED FOR KRIGING log m2/s	m2/s	COMMENTS
H-1	BEAUHEIM	'87b	SLUG	0.7	7.56E-07	-6.1215	YES	NA	-6.1215	7.56E-07	VALUE ASSIGNED TO H-1 BOREHOLE
	BEAUHEIM	'87a	I - OB(H3B2)	0.46	4.97E-07 +	-6.3038	NO				
	MERCER	'83	SLUG	0.07	7.56E-08	-7.1215	NO				
	SEWARD	'82	DST	0.08	8.64E-08	-7.0635	NO				
	BEAUHEIM	'87c	I - OB(W-13)	20.	2.16E-05 +	-4.6655	NO				
H-2a											
H-2b1	MERCER	'83	SLUG	0.4	4.32E-07	-6.3645	YES				
	GONZALEZ	'83	PUMPING	0.7	7.56E-07	-6.1215	YES				
	SEWARD	'82	DST	0.5	5.40E-07	-6.2676	YES	-6.2512	-6.2512	5.61E-07	VALUE ASSIGNED TO H-2 HYDROPAD
H-2b2	BEAUHEIM	'87a	I - OB(H3B2)	1.2	1.30E-06 +	-5.8874	NO				
	BEAUHEIM	'87c	I - OB(W-13)	16.	1.73E-05 +	-4.7625	NO				
H-2c											
H-3b1	BEAUHEIM	'87a	I - OB(H3B2)	1.8	1.94E-06	-5.7113	YES				
	BEAUHEIM	'87a	I - OB(H3B3)	3.0	3.24E-06	-5.4895	YES				
	MERCER	'83	SLUG	19.0	2.05E-05	-4.6878	NO				
	SEWARD	'82	DST	0.7	7.56E-07	-6.1215	NO				
H-3b2	BEAUHEIM	'87a	I - OB(H3B3)	3.0	3.24E-06	-5.4895	YES				
	BEAUHEIM	'87a	PUMPING '85	1.7	1.84E-06	-5.7361	YES				
H-3b3	BEAUHEIM	'87a	I - OB(H3B2)	1.8	1.94E-06	-5.7113	YES				
	BEAUHEIM	'87a	PUMPING '84	2.9	3.13E-06	-5.5042	YES	-5.6070	-5.6070	2.47E-06	VALUE ASSIGNED TO H-3 HYDROPAD
H-4a	GONZALEZ	'83	I - OB(H4B)D	1.7	1.84E-06	-5.7361	YES				
	GONZALEZ	'83	I - OB(H4B)R	0.9	9.72E-07	-6.0123	YES				
	GONZALEZ	'83	I - OB(H4C)D1	1.1	1.19E-06	-5.9252	YES				
	GONZALEZ	'83	I - OB(H4C)R1	1.3	1.40E-06	-5.8526	YES				
	GONZALEZ	'83	I - OB(H4C)D2	1.3	1.40E-06	-5.8526	YES				
	GONZALEZ	'83	I - OB(H4C)R2	1.6	1.73E-06	-5.7625	YES				
H-4b	GONZALEZ	'83	PUMPING D	0.3	3.24E-07	-6.4895	YES				
	GONZALEZ	'83	PUMPING REC	0.4	4.32E-07	-6.3645	YES				
	MERCER et al	'81	SLUG	0.9	9.72E-07	-6.0123	YES				
	GONZALEZ	'83	I - OB(4C)D1	0.8	8.64E-07	-6.0635	YES				
	GONZALEZ	'83	I - OB(4C)R1	1.3	1.40E-06	-5.8526	YES				
	GONZALEZ	'83	I - OB(4C)D2	1.2	1.30E-06	-5.8874	YES				
	GONZALEZ	'83	I - OB(4C)R2	1.8	1.94E-06	-5.7113	YES				
	SEWARD	'82	DST	0.86	9.29E-07	-6.0321	NO				

Drawn by	Date
Checked by	Date
Revisions	Date
H09700R554	

Culebra Dolomite Transmissivity Data Base

INTERA Technologies

Table C.1

WELL	REFERENCES	YEAR OF REFERENCE	TYPE OF TEST	REPORTED CULEBRA TRANSMISSIVITIES ft2/day	m2/s	log m2/s	SELECTED VALUES (YES or NO)	AVERAGE OF SELECTED VALUES (PER HYDROPAD OR WELL LOCATION)	TRANSMISSIVITY VALUES USED FOR KRIGING log m2/s	m2/s	COMMENTS
H-4c	BEAUHEIM	'87b	SLUG	0.65	7.02E-07	-6.1537	YES				
	GONZALEZ	'83	I - OB(H4B)D	1.5	1.62E-06	-5.7905	YES				
	GONZALEZ	'83	I - OB(H4B)R	0.7	7.56E-07	-6.1215	YES				
	GONZALEZ	'83	PUMPING 1D	0.6	6.48E-07	-6.1884	YES				
	GONZALEZ	'83	PUMPING 1R	1.0	1.08E-06	-5.9666	YES				
	GONZALEZ	'83	PUMPING 2D	0.4	4.32E-07	-6.3645	YES				
	GONZALEZ	'83	PUMPING 2R	1.7	1.84E-06	-5.7361	YES	-5.9922	-5.9922	1.02E-06	VALUE ASSIGNED TO H-4 HYDROPAD
H-5a	GONZALEZ	'83	I - OB(H5C)D	0.15	1.62E-07	-6.7905	YES				
	GONZALEZ	'83	I - OB(H5C)R	0.19	2.05E-07	-6.6878	YES				
	GONZALEZ	'83	I - OB(H5B)D	0.11	1.19E-07	-6.9252	YES				
	GONZALEZ	'83	I - OB(H5B)R	0.20	2.16E-07	-6.6655	YES				
H-5b	GONZALEZ	'83	PUMPING R	0.22	2.38E-07	-6.6242	YES				
	GONZALEZ	'83	I - OB(H5C)D	0.12	1.30E-07	-6.8874	YES				
	GONZALEZ	'83	I - OB(H5C)R	0.24	2.59E-07	-6.5864	YES				
	DENN. & MERCER	'82	SLUG	0.20	2.16E-07	-6.6655	YES				
	SEWARD	'82	DST	0.86	9.29E-07	-6.0321	NO				
H-5c	GONZALEZ	'83	PUMPING D	0.04	4.32E-08	-7.3645	YES				
	GONZALEZ	'83	PUMPING R	0.11	1.19E-07	-6.9252	YES				
	GONZALEZ	'83	I - OB(H5B)D	0.16	1.73E-07	-6.7625	YES				
	GONZALEZ	'83	I - OB(H5B)R	0.11	1.19E-07	-6.9252	YES	-6.8175	-6.8175	1.52E-07	VALUE ASSIGNED TO H-5 HYDROPAD
H-6a	BEAUHEIM	'87c	I - OB(W-13)	71.	7.67E-05 +	-4.1153	NO				
	GONZALEZ	'83	I - OB(H6B)D	67.	7.24E-05	-4.1405	YES				
	GONZALEZ	'83	I - OB(H6B)R	77.	8.32E-05	-4.0801	YES				
	GONZALEZ	'83	I - OB(H6C)D1	87.	9.40E-05	-4.0271	YES				
	GONZALEZ	'83	I - OB(H6C)R1	66.	7.13E-05	-4.1470	YES				
	GONZALEZ	83	I - OB(H6C)D2	70.	7.56E-05	-4.1215	YES				
	GONZALEZ	'83	I - OB(H6C)R2	69.	7.45E-05	-4.1277	YES				
H-6b	BEAUHEIM	'87c	I - OB(W-13)	69.	7.45E-05 +	-4.1277	NO				
	BEAUHEIM	'86	I - OB(DOE2)	61.	6.59E-05 +	-4.1812	NO				
	GONZALEZ	'83	PUMPING D	79.	8.53E-05	-4.0689	YES				
	GONZALEZ	'83	PUMPING R	88.	9.50E-05	-4.0221	YES				
	GONZALEZ	'83	I - OB(H6C)D1	86.	9.29E-05	-4.0321	YES				
	GONZALEZ	'83	I - OB(H6C)R1	63.	6.80E-05	-4.1672	YES				
	GONZALEZ	'83	I - OB(H6C)D2	69.	7.45E-05	-4.1277	YES				
	GONZALEZ	'83	I - OB(H6C)R2	67.	7.24E-05	-4.1405	YES				
	DENNEHY	'82	PUMPING D '79	73.	7.88E-05	-4.1033	YES				
	DENNEHY	'82	PUMPING R '79	83.	8.96E-05	-4.0475	YES				
	SEWARD	'82	DST	75.	8.10E-05	-4.0915	NO				
H-6c	GONZALEZ	'83	PUMPING 1R	71.	7.67E-05	-4.1153	YES				
	GONZALEZ	'83	I - OB(H6B)D	70.	7.56E-05	-4.1215	YES				
	GONZALEZ	'83	I - OB(H6B)R	77.	8.32E-05	-4.0801	YES				
	GONZALEZ	'83	PUMPING 2D	72.	7.78E-05	-4.1092	YES				
	GONZALEZ	'83	PUMPING 2R	72.	7.78E-05	-4.1092	YES	-4.0994	-4.0994	7.95E-05	VALUE ASSIGNED TO H-6 HYDROPAD
H-7a											

Drawn by	Date
Checked by	Date
Revisions	Date
HD9700R554	

INTERA Technologies

Culebra Dolomite Transmissivity Data Base

Table C.1 (cont.)

WELL	REFERENCES	YEAR OF REFERENCE	TYPE OF TEST	REPORTED CULEBRA TRANSMISSIVITIES ft2/day	m2/s	log m2/s	SELECTED VALUES (YES or NO)	AVERAGE OF SELECTED VALUES (PER HYDROPAD OR WELL LOCATION)	TRANSMISSIVITY VALUES USED FOR KRIGING log m2/s	m2/s	COMMENTS
H-7b1	MERCER	'83	PUMPING	>1000	1.00E-03	-3.0000	YES				
H-7b2	INTERA	UE	PUMPING '86	1134.	1.22E-03	-2.9120	YES	-2.9560	-2.9560	1.11E-03	VALUE ASSIGNED TO H-7 HYDROPAD
H-7c											
H-8a											
H-8b	BEAUHEIM	'87b	PUMPING	8.2	8.86E-06	-5.0528	YES				
	MERCER	'83	PUMPING	16.0	1.73E-05	-4.7625	NO	-5.0528	-5.0528	8.86E-06	VALUE ASSIGNED TO H-8 HYDROPAD
H-8c											
H-9a											
H-9b	MERCER	'83	PUMPING	231.	2.49E-04	-3.6030	YES				
	INTERA	UE	PUMPING '83	111.	1.20E-04	-3.9213	YES	-3.7621	-3.7621	1.73E-04	VALUE ASSIGNED TO H-9 HYDROPAD
H-9c											
H-10a											
H-10b	MERCER	'83	SLUG	0.07	7.56E-08	-7.1215	YES	NA	-7.1215	7.56E-08	VALUE ASSIGNED TO H-10 HYDROPAD
H-10c											
H-11b1	SAULNIER	'87	PUMPING '84	11.3	1.22E-05	-4.9135	NO				
	SAULNIER	'87	I - OB(H11B3)'84	25.5	2.75E-05	-4.5600	YES				
	SAULNIER	'87	I - OB(H11B3)'85	24.8	2.68E-05	-4.5721	YES				
	SAULNIER	'87	I - OB(H11B2)	25.4	2.74E-05	-4.5617	YES				
	BEAUHEIM	'87a	I - OB(H3B2)	6.8	7.34E-06 +	-5.1341	NO				
H-11b2	SAULNIER	'87	I - OB(H11B3)'84	23.8	2.57E-05	-4.5900	YES				
	SAULNIER	'87	I - OB(H11B3)'85	26.4	2.85E-05	-4.5450	YES				
	SAULNIER	'87	I - OB(H11B1)	23.4	2.53E-05	-4.5974	YES				
H-11b3	SAULNIER	'87	PUMPING '84	26.1	2.82E-05	-4.5499	YES				
	SAULNIER	'87	PUMPING '85	30.7	3.32E-05	-4.4794	YES				
	SAULNIER	'87	I - OB(H11B1)	26.0	2.81E-05	-4.5516	YES				
	SAULNIER	'87	I - OB(H11B2)	23.9	2.58E-05	-4.5882	YES	-4.5595	-4.5595	2.76E-05	VALUE ASSIGNED TO H-11 HYDROPAD
H-12	INTERA	UE	SLUG '87	.17	1.84E-07	-6.7361	YES	NA	-6.7361	1.84E-07	VALUE ASSIGNED TO H-12 BOREHOLE
	INTERA	UE	PUMPING '84	.042	4.54E-08	-7.3433	NO				
H-14	BEAUHEIM	'87b	SLUG	0.30	3.24E-07	-6.4895	YES				
	BEAUHEIM	'87b	DST	0.31	3.35E-07	-6.4752	YES	-6.4823	-6.4823	3.29E-07	VALUE ASSIGNED TO H-14 BOREHOLE
H-15	BEAUHEIM	'87b	SLUG	0.10	1.08E-07	-6.9666	YES				
	BEAUHEIM	'87b	DST	0.15	1.62E-07	-6.7905	YES	-6.8785	-6.8785	1.32E-07	VALUE ASSIGNED TO H-15 BOREHOLE
H-16	BEAUHEIM	UE	SLUG	.70	7.56E-07	-6.1215	YES	NA	-6.1215	7.56E-07	VALUE ASSIGNED TO H-16 BOREHOLE

Drawn by	Date
Checked by	Date
Revisions	Date
HD9700R554	

INTERA Technologies

Culebra Dolomite Transmissivity Data Base

Table C.1 (cont.)

WELL	REFERENCES	YEAR OF REFERENCE	TYPE OF TEST	REPORTED CULEBRA TRANSMISSIVITIES ft2/day	m2/s	log m2/s	SELECTED VALUES (YES or NO)	AVERAGE OF SELECTED VALUES (PER HYDROPAD OR WELL LOCATION)	TRANSMISSIVITY VALUES USED FOR KRIGING log m2/s	m2/s	COMMENTS
H-17	BEAUHEIM	UE	SLUG	.2	2.16E-07	-6.6655	YES	NA	-6.6655	2.16E-07	VALUE ASSIGNED TO H-17 BOREHOLE
DOE-1	BEAUHEIM	'87a	I - OB(H3B2)	5.5	5.94E-06 +	-5.2262	NO				
	BEAUHEIM	'87a	I - OB(H3B3)	12.	1.30E-05 +	-4.8874	NO				
	BEAUHEIM	'87b	PUMPING D	28.	3.02E-05	-4.5194	NO				
	BEAUHEIM	'87b	PUMPING R	11.	1.19E-05	-4.9252	YES	NA	-4.9252	1.19E-05	VALUE ASSIGNED TO DOE-1 BOREHOLE
DOE-2	BEAUHEIM	'86	PUMPING	89.	9.61E-05	-4.0172	YES	NA	-4.0172	9.61E-05	VALUE ASSIGNED TO DOE-2 BOREHOLE
	BEAUHEIM	'87c	I - OB(W-13)	57.	6.16E-05 +	-4.2107	NO				
P-1											
P-2											
P-3											
P-4											
P-5											
P-6											
P-7											
P-8											
P-9											
P-10											
P-11											
P-12											
P-13											
P-14	MERCER	'83	PUMPING	140.	1.51E-04	-3.8204	YES				
	HYDRO GEOCHEM	UE	SLUG	324.	3.50E-04	-3.4560	YES	-3.6382	-3.6382	2.30E-04	VALUE ASSIGNED TO P-14 BOREHOLE
	BEAUHEIM	'87c	I - OB(W-13)	265.	2.86E-04 +	-3.5433	NO				
P-15	BEAUHEIM	87b	SLUG	0.09	9.72E-08	-7.0123	YES				
	MERCER	'83	SLUG	0.07	7.56E-08	-7.1215	YES				
	SEWARD	'82	DST	0.1	1.08E-07	-6.9666	YES	-7.0335	-7.0335	9.26E-08	VALUE ASSIGNED TO P-15 BOREHOLE
P-16											
P-17	BEAUHEIM	'87b	SLUG	1.0	1.08E-06	-5.9666	YES				
	MERCER	'83	SLUG	1.0	1.08E-06	-5.9666	YES				
	HYDRO GEOCHEM	UE	PUMPING	2.1	2.27E-06	-5.6444	YES	-5.8592	-5.8592	1.38E-06	VALUE ASSIGNED TO P-17 BOREHOLE
P-18	MERCER	'83	SLUG	0.001	1.08E-09	-8.9666	YES				
	HYDRO GEOCHEM	UE	SLUG	0.003	3.24E-09	-8.4895	YES	-8.7280	-8.7280	1.87E-09	VALUE ASSIGNED TO P-18 BOREHOLE
P-19											

Drawn by	Date
Checked by	Date
Revisions	Date
HD9700R554	
INTERA Technologies	Culebra Dolomite Transmissivity Data Base
	Table C.1 (cont.)

WELL	REFERENCES	YEAR OF REFERENCE	TYPE OF TEST	REPORTED	CULEBRA TRANSMISSIVITIES		SELECTED VALUES	AVERAGE OF SELECTED VALUES (PER HYDROPAD OR WELL LOCATION)	TRANSMISSIVITY VALUES USED FOR KRIGING		COMMENTS
				ft2/day	m2/s	log m2/s	(YES or NO)		log m2/s	m2/s	
P-20											
P-21											
WIPP-12	INTERA	UE	ACID & DEVEL	0.03	3.24E-08	-7.4895	YES	NA	-7.4895	3.24E-08	VALUE ASSIGNED TO WIPP-12 BOREHOLE
	BEAUHEIM	'87c	I - OB(W-13)	7.9	8.53E-06 +	-5.0689	NO				
WIPP-13	BEAUHEIM	'87c	PUMPING	69.	7.45E-05	-4.1277	YES	NA	-4.1277	7.45E-05	VALUE ASSIGNED TO WIPP-13 BOREHOLE
	BEAUHEIM	'86	I - OB(DOE2)	72.	7.78E-05 +	-4.1092	NO				
WIPP-18	BEAUHEIM	'87b	SLUG	0.30	3.24E-07	-6.4895	YES	NA	-6.4895	3.24E-07	VALUE ASSIGNED TO WIPP-18 BOREHOLE
	BEAUHEIM	'87c	I - OB(W-13)	23.	2.48E-05 +	-4.6048	NO				
WIPP-19	BEAUHEIM	'87b	SLUG	0.60	6.48E-07	-6.1884	YES	NA	-6.1884	6.48E-07	VALUE ASSIGNED TO WIPP-19 BOREHOLE
	BEAUHEIM	'87c	I - OB(W-13)	24.	2.59E-05 +	-4.5864	NO				
WIPP-21	BEAUHEIM	'87b	SLUG	0.25	2.70E-07	-6.5686	YES	NA	-6.5686	2.70E-07	VALUE ASSIGNED TO WIPP-21 BOREHOLE
	BEAUHEIM	'87c	I - OB(W-13)	22.	2.38E-05 +	-4.6242	NO				
WIPP-22	BEAUHEIM	'87b	SLUG	0.37	4.00E-07	-6.3984	YES	NA	-6.3984	4.00E-07	VALUE ASSIGNED TO WIPP-22 BOREHOLE
	BEAUHEIM	'87c	I - OB(W-13)	19.	2.05E-05 +	-4.6878	NO				
WIPP-25	MERCER	'83	PUMPING	270.	2.92E-04	-3.5352	YES	NA	-3.5352	2.92E-04	VALUE ASSIGNED TO WIPP-25 BOREHOLE
	BEAUHEIM	'87c	I - OB(W-13)	650.	7.02E-04 +	-3.1537	NO				
WIPP-26	MERCER	'83	PUMPING	1250.	1.35E-03	-2.8697	YES	NA	-2.8697	1.35E-03	VALUE ASSIGNED TO WIPP-26 BOREHOLE
WIPP-27	MERCER	'83	PUMPING	650	7.02E-04	-3.1537	YES	NA	-3.1537	7.02E-04	VALUE ASSIGNED TO WIPP-27 BOREHOLE
WIPP-28	MERCER	'83	PUMPING	18.	1.94E-05	-4.7113	YES	NA	-4.7113	1.94E-05	VALUE ASSIGNED TO WIPP-28 BOREHOLE
WIPP-29	MERCER	'83	PUMPING	1000.	1.00E-03	-3.0000	YES	NA	-3.0000	1.00E-03	VALUE ASSIGNED TO WIPP-29 BOREHOLE
WIPP-30	MERCER	'83	SLUG	0.3	3.24E-07	-6.4895	YES				
	GONZALEZ	'83	PUMPING	0.02	2.16E-08	-7.6655	NO				
	BEAUHEIM	'87c	I - OB(W-13)	28.	3.02E-05 +	-4.5194	NO	NA	-6.4895	3.24E-07	VALUE ASSIGNED TO WIPP-30 BOREHOLE
ERDA-9	BEAUHEIM	'87b	SLUG	0.47	5.08E-07	-6.2945	YES				
	BEAUHEIM	'87c	I - OB(W-13)	22.	2.38E-05 +	-4.6242	NO	NA	-6.2945	5.08E-07	VALUE ASSIGNED TO ERDA-9 BOREHOLE

Drawn by	Date
Checked by	Date
Revisions	Date
H09700R554	

INTERA Technologies

Culebra Dolomite Transmissivity Data Base

Table C.1 (cont.)

WELL	REFERENCES	YEAR OF REFERENCE	TYPE OF TEST	REPORTED CULEBRA TRANSMISSIVITIES ft2/day	m2/s	log m2/s	SELECTED VALUES (YES or NO)	AVERAGE OF SELECTED VALUES (PER HYDROPAD OR WELL LOCATION)	TRANSMISSIVITY VALUES USED FOR KRIGING log m2/s	m2/s	COMMENTS
CABIN BABY-1	BEAUHEIM	'87b	SLUG	0.28	3.02E-07	-6.5194	YES	NA	-6.5194	3.02E-07	VALUE ASSIGNED TO CABIN BABY BOREHOLE
ENGLE	BEAUHEIM	'87b	PUMPING	43.	4.64E-05	-4.3331	YES	NA	-4.3331	4.64E-05	VALUE ASSIGNED TO ENGLE BOREHOLE
USGS-1	COOPER	'62	PUMPING '60-D	543.	5.86E-04	-3.2318	YES				
	COOPER	'62	PUMPING '60-R	531.	5.73E-04	-3.2415	YES				
	COOPER & GLANZ.	'71	PUMPING '63	468.	5.05E-04	-3.2963	YES	-3.2565	-3.2565	5.54E-04	VALUE ASSIGNED TO USGS-1 BOREHOLE
EX. SHFT.	BEAUHEIM	'87c	I - OB(W-13)	28.	3.02E-05 +	-4.5194	NO				

REFERENCES

BEAUHEIM,R.L., 1986, HYDRAULIC-TEST INTERPRETATIONS FOR WELL DOE-2 AT THE WASTE ISOLATION PILOT PLANT (WIPP) SITE, SAND86-1364.

BEAUHEIM,R.L., 1987a, ANALYSIS OF PUMPING TESTS OF THE CULEBRA DOLOMITE CONDUCTED AT THE H-3 HYDROPAD AT THE WASTE ISOLATION PILOT PLANT (WIPP) SITE, SAND86-2311.

BEAUHEIM,R.L., 1987b, INTERPRETATIONS OF SINGLE-WELL HYDRAULIC TESTS CONDUCTED AT AND NEAR THE WASTE ISOLATION PILOT PLANT (WIPP) SITE, 1983-1987, SAND87-0039.

BEAUHEIM,R.L., 1987c, INTERPRETATION OF THE WIPP-13 MULTIPAD PUMPING TEST OF THE CULEBRA DOLOMITE AT THE WASTE ISOLATION PILOT PLANT (WIPP) SITE, SAND87-2456.

COOPER, JAMES B., 1962, GROUND-WATER INVESTIGATIONS OF THE PROJECT GNOME AREA, EDDY AND LEA COUNTIES, NEW MEXICO; U.S. GEOLOGICAL SURVEY TEI-802, OPEN FILE REPORT. 116p.,12 figs.

COOPER, JAMES B., AND GLANZMAN, V.M.,1971, GEOHYDROLOGY OF PROJECT GNOME SITE, EDDY COUNTY, NEW MEXICO; U.S. GEOLOGICAL SURVEY PROFESSIONAL PAPER 712-A, 28p.

DENNEHY,K.F., 1982, RESULTS OF HYDROLOGIC TESTS AND WATER-CHEMISTRY ANALYSES, WELLS H-6A, H-6B, AND H-6C AT THE PROPOSED WASTE ISOLATION PILOT PLANT SITE, SOUTHEASTERN NEW MEXICO: U.S. GEOLOGICAL SURVEY WATER-RESOURCES INVESTIGATIONS 82-8, 68p.

DENNEHY,K.F.,AND MERCER,J.W., 1982, RESULTS OF HYDROLOGIC TESTS AND WATER-CHEMISTRY ANALYSES, WELLS H-5A, H-5B, AND H-5C AT THE PROPOSED WASTE ISOLATION PILOT PLANT SITE, SOUTHEASTERN NEW MEXICO: U.S. GEOLOGICAL SURVEY WATER-RESOURCES INVESTIGATIONS 82-19, 83p.

GONZALEZ,D.D., 1983, GROUNDWATER FLOW IN THE RUSTLER FORMATION, WASTE ISOLATION PILOT PLANT (WIPP), SOUTHEAST NEW MEXICO (SENM): INTERIM REPORT, SAND82-1012.

MERCER, J.W.,DAVIS P., DENNEHY, K.F., AND GOETZ, C.L. 1981. RESULTS OF HYDROLOGIC TESTS AND WATER-CHEMISTRY ANALYSES, WELLS H-4A, H-4B, AND H-4C AT THE PROPOSED WASTE ISOLATION PILOT PLANT SITE, SOUTHEASTERN NEW MEXICO. USGS WATER RESOURCES INVESTIGATIONS RPT 79-98 (ALBURQUERQUE, NM), 178 pp.

MERCER, J.W., 1983, GEOHYDROLOGY OF THE PROPOSED WASTE ISOLATION PILOT PLANT SITE, LOS MEDANOS AREA, SOUTHEASTERN NEW MEXICO, USGS-WATER RESOURCES INVESTIGATION REPORT 83-4016.

SAULNIER, G.J., 1987, ANALYSIS OF PUMPING TESTS OF THE CULEBRA DOLOMITE CONDUCTED AT THE H-11 HYDROPAD AT THE WASTE ISOLATION PILOT PLANT (WIPP) SITE, SAND87-7124.

SEWARD,P.D., 1982, ABRIDGED BOREHOLE HISTORIES FOR THE WASTE ISOLATION PILOT PLANT (WIPP) STUDIES, SAND82-0080.

Drawn by	Date	Culebra Dolomite Transmissivity Data Base
Checked by	Date	
Revisions	Date	
H09700R554		
INTERA Technologies		Table C.1 (cont.)

TRANSMISSIVITY DATABASE - UNCERTAINTY ANALYSIS - UPDATED 12-29-87

ABBREVIATIONS ; I = INTERFERENCE
R = RECOVERY
D = DRAWDOWN
OB = OBSERVATION
(WELL) = PUMPING WELL
UE = UNPUBLISHED ESTIMATE

WELL	REFERENCES	YEAR OF REFERENCE	TYPE OF TEST	REPORTED CULEBRA TRANSMISSIVITIES ft2/day	m2/s	log m2/s	SELECTED VALUES (YES/NO)	SELECTED VALUES VARIANCE log m2/s	SELECTED VALUES STANDARD DEVIATION log m2/s	VALUES USED FOR KRIGING VARIANCE log m2/s	VALUES USED FOR KRIGING STANDARD DEVIATION log m2/s
H-1	BEAUHEIM	'87b	SLUG	0.7	7.56E-07	-6.1215	YES				
	BEAUHEIM	'87a	I - OB(H3B2)	0.46	4.97E-07		NO				
	MERCER	'83	SLUG	0.07	7.56E-08	-7.1215	YES				
	SEWARD	'82	DST	0.08	8.64E-08	-7.0635	YES				
	BEAUHEIM	'87c	I - OB(W-13)	20	2.16E-05		NO	0.210	0.46	0.210	0.46
H-2b1	MERCER	'83	SLUG	0.4	4.32E-07	-6.3645	YES				
	GONZALEZ	'83	PUMPING	0.7	7.56E-07	-6.1215	YES				
	SEWARD	'82	DST	0.5	5.40E-07	-6.2676	YES				
H-2b2	BEAUHEIM	'87a	I - OB(H3B2)	1.2	1.30E-06		NO				
	BEAUHEIM	'87c	I - OB(W-13)	16	1.73E-05		NO	0.010	0.10	0.063	0.25
H-3b1	BEAUHEIM	'87a	I - OB(H3B2)	1.8	1.94E-06	-5.7113	YES				
	BEAUHEIM	'87a	I - OB(H3B3)	3.0	3.24E-06	-5.4895	YES				
	MERCER	'83	SLUG	19.0	2.05E-05	-4.6878	YES				
	SEWARD	'82	DST	0.7	7.56E-07	-6.1215	YES				
H-3b2	BEAUHEIM	'87a	I - OB(H3B3)	3.0	3.24E-06	-5.4895	YES				
	BEAUHEIM	'87a	PUMPING '85	1.7	1.84E-06	-5.7361	YES				
H-3b3	BEAUHEIM	'87a	I - OB(H3B2)	1.8	1.94E-06	-5.7113	YES				
	BEAUHEIM	'87a	PUMPING '84	2.9	3.13E-06	-5.5042	YES	0.146	0.38	0.146	0.38
H-4a	GONZALEZ	'83	I - OB(H4B)D	1.7	1.84E-06	-5.7361	YES				
	GONZALEZ	'83	I - OB(H4B)R	0.9	9.72E-07	-6.0123	YES				
	GONZALEZ	'83	I - OB(H4C)D1	1.1	1.19E-06	-5.9252	YES				
	GONZALEZ	'83	I - OB(H4C)R1	1.3	1.40E-06	-5.8526	YES				
	GONZALEZ	'83	I - OB(H4C)D2	1.3	1.40E-06	-5.8526	YES				
	GONZALEZ	'83	I - OB(H4C)R2	1.6	1.73E-06	-5.7625	YES				
H-4b	GONZALEZ	'83	PUMPING D	0.3	3.24E-07	-6.4895	YES				
	GONZALEZ	'83	PUMPING REC	0.4	4.32E-07	-6.3645	YES				
	MERCER et al	'81	SLUG	0.9	9.72E-07	-6.0123	YES				
	GONZALEZ	'83	I - OB(4C)D1	0.8	8.64E-07	-6.0635	YES				
	GONZALEZ	'83	I - OB(4C)R1	1.3	1.40E-06	-5.8526	YES				
	GONZALEZ	'83	I - OB(4C)D2	1.2	1.30E-06	-5.8874	YES				
	GONZALEZ	'83	I - OB(4C)R2	1.8	1.94E-06	-5.7113	YES				
	SEWARD	'82	DST	0.86	9.29E-07	-6.0321	YES				

Drawn by	Date
Checked by	Date
Revisions	Date
H09700R554	

INTERA Technologies

Culebra Transmissivity Uncertainties

Table C.2

WELL	REFERENCES	YEAR OF REFERENCE	TYPE OF TEST	REPORTED CULEBRA TRANSMISSIVITIES ft2/day	m2/s	log m2/s	SELECTED VALUES (YES/NO)	SELECTED VALUES VARIANCE log m2/s	SELECTED VALUES STANDARD DEVIATION log m2/s	VALUES USED FOR KRIGING VARIANCE log m2/s	VALUES USED FOR KRIGING STANDARD DEVIATION log m2/s
H-4c	BEAUHEIM	'87b	SLUG	0.65	7.02E-07	-6.1537	YES				
	GONZALEZ	'83	I - OB(H4B)D	1.5	1.62E-06	-5.7905	YES				
	GONZALEZ	'83	I - OB(H4B)R	0.7	7.56E-07	-6.1215	YES				
	GONZALEZ	'83	PUMPING 1D	0.6	6.48E-07	-6.1884	YES				
	GONZALEZ	'83	PUMPING 1R	1.0	1.08E-06	-5.9666	YES				
	GONZALEZ	'83	PUMPING 2D	0.4	4.32E-07	-6.3645	YES				
	GONZALEZ	'83	PUMPING 2R	1.7	1.84E-06	-5.7361	YES	0.047	0.22	0.063	0.25
H-5a	GONZALEZ	'83	I - OB(H5C)D	0.15	1.62E-07	-6.7905	YES				
	GONZALEZ	'83	I - OB(H5C)R	0.19	2.05E-07	-6.6878	YES				
	GONZALEZ	'83	I - OB(H5B)D	0.11	1.19E-07	-6.9252	YES				
	GONZALEZ	'83	I - OB(H5B)R	0.20	2.16E-07	-6.6655	YES				
H-5b	GONZALEZ	'83	PUMPING R	0.22	2.38E-07	-6.6242	YES				
	GONZALEZ	'83	I - OB(H5C)D	0.12	1.30E-07	-6.8874	YES				
	GONZALEZ	'83	I - OB(H5C)R	0.24	2.59E-07	-6.5864	YES				
	DENN. & MERCER	'82	SWUG	0.20	2.16E-07	-6.6655	YES				
	SEWARD	'82	DST	0.86	9.29E-07	-6.0321	YES				
H-5c	GONZALEZ	'83	PUMPING D	0.04	4.32E-08	-7.3645	YES				
	GONZALEZ	'83	PUMPING R	0.11	1.19E-07	-6.9252	YES				
	GONZALEZ	'83	I - OB(H5B)D	0.16	1.73E-07	-6.7625	YES				
	GONZALEZ	'83	I - OB(H5B)R	0.11	1.19E-07	-6.9252	YES	0.082	0.29	0.082	0.29
H-6a	BEAUHEIM	'87c	I - OB(W-13)	71	7.67E-05		NO				
	GONZALEZ	'83	I - OB(H6B)D	67	7.24E-05	-4.1405	YES				
	GONZALEZ	'83	I - OB(H6B)R	77	8.32E-05	-4.0801	YES				
	GONZALEZ	'83	I - OB(H6C)D1	87	9.40E-05	-4.0271	YES				
	GONZALEZ	'83	I - OB(H6C)R1	66	7.13E-05	-4.1470	YES				
	GONZALEZ	83	I - OB(H6C)D2	70	7.56E-05	-4.1215	YES				
	GONZALEZ	'83	I - OB(H6C)R2	69	7.45E-05	-4.1277	YES				
H-6b	BEAUHEIM	'87c	I - OB(W-13)	69	7.45E-05		NO				
	BEAUHEIM	'86	I - OB(DOE2)	61	6.59E-05		NO				
	GONZALEZ	'83	PUMPING	79	8.53E-05	-4.0689	YES				
	GONZALEZ	'83	PUMPING R	88	9.50E-05	-4.0221	YES				
	GONZALEZ	'83	I - OB(H6C)D1	86	9.29E-05	-4.0321	YES				
	GONZALEZ	'83	I - OB(H6C)R1	63	6.80E-05	-4.1672	YES				
	GONZALEZ	'83	I - OB(H6C)D2	69	7.45E-05	-4.1277	YES				
	GONZALEZ	'83	I - OB(H6C)R2	67	7.24E-05	-4.1405	YES				
	DENNEHY	'82	PUMPING D '79	73	7.88E-05	-4.1033	YES				
	DENNEHY	'82	PUMPING R '79	83	8.96E-05	-4.0475	YES				
	SEWARD	'82	DST	75	8.10E-05	-4.0915	YES				
H-6c	GONZALEZ	'83	PUMPING 1R	71	7.67E-05	-4.1153	YES				
	GONZALEZ	'83	I - OB(H6B)D	70	7.56E-05	-4.1215	YES				
	GONZALEZ	'83	I - OB(H6B)R	77	8.32E-05	-4.0801	YES				
	GONZALEZ	'83	PUMPING 2D	72	7.78E-05	-4.1092	YES				
	GONZALEZ	'83	PUMPING 2R	72	7.78E-05	-4.1092	YES	0.002	0.04	0.063	0.25
H-7b1	MERCER	'83	PUMPING	1000	1.00E-03	-3.0000	YES				
H-7b2	INTERA	UE	PUMPING '86	1134	1.22E-03	-2.9120	YES	0.002	0.04	0.063	0.25

Drawn by	Date
Checked by	Date
Revisions	Date
H09700R554	

Culebra Transmissivity Uncertainties

INTERA Technologies

Table C.2 (cont.)

WELL	REFERENCES	YEAR OF REFERENCE	TYPE OF TEST	REPORTED CULEBRA TRANSMISSIVITIES ft2/day	m2/s	log m2/s	SELECTED VALUES (YES/NO)	SELECTED VALUES VARIANCE log m2/s	SELECTED VALUES STANDARD DEVIATION log m2/s	VALUES USED FOR KRIGING VARIANCE log m2/s	VALUES USED FOR KRIGING STANDARD DEVIATION log m2/s
H-8b	BEAUHEIM	'87b	PUMPING	8.2	8.86E-06	-5.0528	YES				
	MERCER	'83	PUMPING	16	1.73E-05	-4.7625	YES	0.021	0.15	0.063	0.25
H-9b	MERCER	'83	PUMPING	231	2.49E-04	-3.6030	YES				
	INTERA	UE	PUMPING '83	111	1.20E-04	-3.9213	YES	0.025	0.16	0.063	0.25
H-10b	MERCER	'83	SLUG	0.07	7.56E-08	-7.1215	YES	NA	NA	0.250	0.50
H-11b1	SAULNIER	'87	PUMPING '84	11.3	1.22E-05	-4.9135	YES				
	SAULNIER	'87	I - OB(H11B3)'84	25.5	2.75E-05	-4.5600	YES				
	SAULNIER	'87	I - OB(H11B3)'85	24.8	2.68E-05	-4.5721	YES				
	SAULNIER	'87	I - OB(H11B2)	25.4	2.74E-05	-4.5617	YES				
	BEAUHEIM	'87a	I - OB(H3B2)	6.8	7.34E-06		NO				
H-11b2	SAULNIER	'87	I - OB(H11B3)'84	23.8	2.57E-05	-4.5900	YES				
	SAULNIER	'87	I - OB(H11B3)'85	26.4	2.85E-05	-4.5450	YES				
	SAULNIER	'87	I - OB(H11B1)	23.4	2.53E-05	-4.5974	YES				
H-11b3	SAULNIER	'87	PUMPING '84	26.1	2.82E-05	-4.5499	YES				
	SAULNIER	'87	PUMPING '85	30.7	3.32E-05	-4.4794	YES				
	SAULNIER	'87	I - OB(H11B1)	26.0	2.81E-05	-4.5516	YES				
	SAULNIER	'87	I - OB(H11B2)	23.9	2.58E-05	-4.5882	YES	0.011	0.11	0.063	0.25
H-12	INTERA	UE	SLUG '87	0.17	1.84E-07	-6.7361	YES				
	INTERA	UE	PUMPING '84	0.042	4.54E-08	-7.3433	YES	0.092	0.30	0.092	0.30
H-14	BEAUHEIM	'87b	SLUG	0.30	3.24E-07	-6.4895	YES				
	BEAUHEIM	'87b	DST	0.31	3.35E-07	-6.4752	YES	0.000	0.01	0.250	0.50
H-15	BEAUHEIM	'87b	SLUG	0.10	1.08E-07	-6.9666	YES				
	BEAUHEIM	'87b	DST	0.15	1.62E-07	-6.7905	YES	0.008	0.09	0.250	0.50
H-16	BEAUHEIM	UE	SLUG	0.70	7.56E-07	-6.1215	YES	NA	NA	0.250	0.50
H-17	BEAUHEIM	UE	SLUG	0.2	2.16E-07	-6.6655	YES	NA	NA	0.250	0.50
DOE-1	BEAUHEIM	'87a	I - OB(H3B2)	5.5	5.94E-06		NO				
	BEAUHEIM	'87a	I - OB(H3B3)	12	1.30E-05		NO				
	BEAUHEIM	'87b	PUMPING D	28	3.02E-05	-4.5194	YES				
	BEAUHEIM	'87b	PUMPING R	11	1.19E-05	-4.9252	YES	0.041	0.20	0.063	0.25
DOE-2	BEAUHEIM	'86	PUMPING	89	9.61E-05	-4.0172	YES				
	BEAUHEIM	'87c	I - OB(W-13)	57	6.16E-05		NO	NA	NA	0.063	0.25

Drawn by	Date
Checked by	Date
Revisions	Date
H09700R554	
INTERA Technologies	

Culebra Transmissivity Uncertainties

Table C.2 (cont.)

WELL	REFERENCES	YEAR OF REFERENCE	TYPE OF TEST	REPORTED CULEBRA TRANSMISSIVITIES ft2/day	m2/s	log m2/s	SELECTED VALUES (YES/NO)	SELECTED VALUES VARIANCE log m2/s	SELECTED VALUES STANDARD DEVIATION log m2/s	VALUES USED FOR KRIGING VARIANCE log m2/s	VALUES USED FOR KRIGING STANDARD DEVIATION log m2/s
P-14	MERCER	'83	PUMPING	140	1.51E-04	-3.8204	YES				
	HYDRO GEOCHEM	UE	SLUG	324	3.50E-04	-3.4560	YES				
	BEAUHEIM	'87c	I - OB(W-13)	265	2.86E-04		NO	0.033	0.18	0.063	0.25
P-15	BEAUHEIM	87b	SLUG	0.09	9.72E-08	-7.0123	YES				
	MERCER	'83	SLUG	0.07	7.56E-08	-7.1215	YES				
	SEWARD	'82	DST	0.1	1.08E-07	-6.9666	YES	0.004	0.06	0.250	0.50
P-17	BEAUHEIM	'87b	SLUG	1.0	1.08E-06	-5.9666	YES				
	MERCER	'83	SLUG	1.0	1.08E-06	-5.9666	YES				
	HYDRO GEOCHEM	UE	PUMPING	2.1	2.27E-06	-5.6444	YES	0.023	0.15	0.250	0.50
P-18	MERCER	'83	SLUG	0.001	1.08E-09	-8.9666	YES				
	HYDRO GEOCHEM	UE	SLUG	0.003	3.24E-09	-8.4895	YES	0.057	0.24	0.250	0.50
WIPP-12	BEAUHEIM	UE	ACID & DEVEL	0.03	3.24E-08	-7.4895	YES				
	BEAUHEIM	'87c	I - OB(W-13)	7.9	8.53E-06		NO	NA	NA	0.250	0.50
WIPP-13	BEAUHEIM	'87c	PUMPING	69	7.45E-05	-4.1277	YES				
	BEAUHEIM	'86	I - OB(DOE2)	72	7.78E-05		NO	NA	NA	0.063	0.25
WIPP-18	BEAUHEIM	'87b	SLUG	0.30	3.24E-07	-6.4895	YES				
	BEAUHEIM	'87c	I - OB(W-13)	23	2.48E-05		NO	NA	NA	0.250	0.50
WIPP-19	BEAUHEIM	'87b	SLUG	0.60	6.48E-07	-6.1884	YES				
	BEAUHEIM	'87c	I - OB(W-13)	24	2.59E-05		NO	NA	NA	0.250	0.50
WIPP-21	BEAUHEIM	'87b	SLUG	0.25	2.70E-07	-6.5686	YES				
	BEAUHEIM	'87c	I - OB(W-13)	22	2.38E-05		NO	NA	NA	0.250	0.50
WIPP-22	BEAUHEIM	'87b	SLUG	0.37	4.00E-07	-6.3984	YES				
	BEAUHEIM	'87c	I - OB(W-13)	19	2.05E-05		NO	NA	NA	0.250	0.50
WIPP-25	MERCER	'83	PUMPING	270	2.92E-04	-3.5352	YES				
	BEAUHEIM	'87c	I - OB(W-13)	650	7.02E-04		NO	NA	NA	0.063	0.25
WIPP-26	MERCER	'83	PUMPING	1250	1.35E-03	-2.8697	YES	NA	NA	0.063	0.25
WIPP-27	MERCER	'83	PUMPING	650	7.02E-04	-3.1537	YES	NA	NA	0.063	0.25
WIPP-28	MERCER	'83	PUMPING	18	1.94E-05	-4.7113	YES	NA	NA	0.063	0.25
WIPP-29	MERCER	'83	PUMPING	1000	1.00E-03	-3.0000	YES	NA	NA	0.063	0.25

Drawn by	Date
Checked by	Date
Revisions	Date
WP09700R554	

Culebra Transmissivity Uncertainties

INTERA Technologies

Table C.2 (cont.)

WELL	REFERENCES	YEAR OF REFERENCE	TYPE OF TEST	REPORTED CULEBRA TRANSMISSIVITIES ft2/day	m2/s	log m2/s	SELECTED VALUES (YES/NO)	SELECTED VALUES VARIANCE log m2/s	SELECTED VALUES STANDARD DEVIATION log m2/s	VALUES USED FOR KRIGING VARIANCE log m2/s	VALUES USED FOR KRIGING STANDARD DEVIATION log m2/s
WIPP-30	MERCER	'83	SLUG	0.3	3.24E-07	-6.4895	YES				
	GONZALEZ	'83	PUMPING	0.02	2.16E-08	-7.6655	YES				
	BEAUHEIM	'87c	I - OB(W-13)	28	3.02E-05		NO	0.346	0.59	0.346	0.59
ERDA-9	BEAUHEIM	'87b	SLUG	0.47	5.08E-07	-6.2945	YES				
	BEAUHEIM	'87c	I - OB(W-13)	22	2.38E-05		NO	NA	NA	0.250	0.50
CABIN BABY-1	BEAUHEIM	'87b	SLUG	0.28	3.02E-07	-6.5194	YES	NA	NA	0.250	0.50
ENGLE	BEAUHEIM	'87b	PUMPING	43	4.64E-05	-4.3331	YES	NA	NA	0.063	0.25
USGS-1	COOPER	'62	PUMPING '60-D	543	5.86E-04	-3.2318	YES				
	COOPER	'62	PUMPING '60-R	531	5.73E-04	-3.2415	YES				
	COOPER & GLANZ.	'71	PUMPING '63	468	5.05E-04	-3.2963	YES	0.001	0.03	0.063	0.25

REFERENCES: see Table C.1

Drawn by	Date
Checked by	Date
Revisions	Date
H09700R554	
INTERA Technologies	

Culebra Transmissivity Uncertainties

Table C.2 (cont.)

WELL	REFERENCES	YEAR OF REFERENCE	TYPE OF TEST	REPORTED CULEBRA TRANSMISSIVITIES ft2/day	m2/s	log m2/s	SELECTED VALUES (YES/NO)	SELECTED VALUES VARIANCE log m2/s	SELECTED VALUES STANDARD DEVIATION log m2/s	VALUES USED FOR KRIGING VARIANCE log m2/s	VALUES USED FOR KRIGING STANDARD DEVIATION log m2/s
WIPP-30	MERCER	'83	SLUG	0.3	3.24E-07	-6.4895	YES				
	GONZALEZ	'83	PUMPING	0.02	2.16E-08	-7.6655	YES				
	BEAUHEIM	'87c	I - OB(W-13)	28	3.02E-05		NO	0.346	0.59	0.346	0.59
ERDA-9	BEAUHEIM	'87b	SLUG	0.47	5.08E-07	-6.2945	YES				
	BEAUHEIM	'87c	I - OB(W-13)	22	2.38E-05		NO	NA	NA	0.250	0.50
CABIN BABY-1	BEAUHEIM	'87b	SLUG	0.28	3.02E-07	-6.5194	YES	NA	NA	0.250	0.50
ENGLE	BEAUHEIM	'87b	PUMPING	43	4.64E-05	-4.3331	YES	NA	NA	0.063	0.25
USGS-1	COOPER	'62	PUMPING '60-D	543	5.86E-04	-3.2318	YES				
	COOPER	'62	PUMPING '60-R	531	5.73E-04	-3.2415	YES				
	COOPER & GLANZ.	'71	PUMPING '63	468	5.05E-04	-3.2963	YES	0.001	0.03	0.063	0.25

REFERENCES: see Table C.1

Drawn by	Date
Checked by	Date
Revisions	Date
H09700R554	
INTERA Technologies	

Culebra Transmissivity Uncertainties

Table C.2 (cont.)

APPENDIX D CULEBRA STORATIVITIES

The Culebra storativity data base is listed in Table D.1. The table format is very similar to that of Table C.1. The values listed for each borehole and/or hydropad were evaluated to determine the most representative value on a scale of tens of meters. The storativity values determined from regional-scale interference tests, slug tests, or DST's were not selected as representative values. The regional-interference values can, however, be assigned to pilot points between the pumping and observation wells in future transient analyses.

REFERENCES

The references corresponding to the data sources are listed at the end of Table D.1.

CULEBRA STORATIVITY DATABASE - UPDATED 11-20-87

ABBREVIATIONS ;
I = INTERFERENCE
R = RECOVERY
D = DRAWDOWN
OB = OBSERVATION
(WELL) = PUMPING WELL
NR = NOT REPORTED
UE = UNPUBLISHED ESTIMATE
+ = POSSIBLE VALUE FOR PILOT POINT POSITIONED BETWEEN PUMPING AND OBSERVATION WELL

WELL	REFERENCES	YEAR OF REFERENCE	TYPE OF TEST	REPORTED CULEBRA S	LOG OF STORATIVITY	SELECTED S VALUE (YES OR NO)	AVERAGE OF SELECTED S VALUES (FOR SINGLE WELL OR HYDROPAD)	CULEBRA STORATIVITY VALUE log	-	COMMENTS
H-1	BEAUHEIM	'87b	SLUG	NR						
	MERCER	'83	SLUG	1.0E-04	-4.0000	NO				
	SEWARD	'82	DST	NR						
	BEAUHEIM	'87a	I - OB(H3B2)	2.7E-05 +	-4.5686	NO				
	BEAUHEIM	'87c	I - OB(W-13)	1.3E-04 +	-3.8861	NO				
H-2a										
H-2b1	MERCER	'83	SLUG	1.0E-09	-9.0000	NO				
	GONZALEZ	'83	PUMPING	1.2E-05	-4.9208	YES	NA	-4.9208	1.20E-05	VALUE ASSIGNED TO H-2 HYDROPAD
	SEWARD	'82	DST	1.0E-09	-9.0000	NO				
H-2b2	BEAUHEIM	'87c	I - OB(W-13)	7.3E-05 +	-4.1367	NO				
	BEAUHEIM	'87a	I - OB(H3B2)	3.0E-05 +	-4.5229	NO				
H-2c										
H-3b1	BEAUHEIM	'87a	I - OB(H3B2)	NR						
	BEAUHEIM	'87a	I - OB(H3B3)	NR						
	MERCER	'83	SLUG	NR						
	SEWARD	'82	DST	NR						
H-3b2	BEAUHEIM	'87a	I - OB(H3B3)	NR						
	BEAUHEIM	'87a	PUMPING '85	NR						
H-3b3	BEAUHEIM	'87a	I - OB(H3B2)	NR						
	BEAUHEIM	'87a	PUMPING '84	NR						
H-4a	GONZALEZ	'83	I - OB(H4B)D	3.13E-06	-5.5045	YES				
	GONZALEZ	'83	I - OB(H4B)R	NR						
	GONZALEZ	'83	I - OB(H4C)D1	8.04E-06	-5.0947	YES				
	GONZALEZ	'83	I - OB(H4C)R1	NR						
	GONZALEZ	'83	I - OB(H4C)D2	5.62E-06	-5.2503	YES				
	GONZALEZ	'83	I - OB(H4C)R2	NR						
H-4b	GONZALEZ	'83	PUMPING D	NR						
	GONZALEZ	'83	PUMPING REC	NR						
	MERCER et al	'81	SLUG	1E-09	-9.0000	NO				
	GONZALEZ	'83	I - OB(4C)D1	1E-06	-6.0000	YES				
	GONZALEZ	'83	I - OB(4C)R1	8.64E-06	-5.0635	YES				
	GONZALEZ	'83	I - OB(4C)D2	NR						
	GONZALEZ	'83	I - OB(4C)R2	6.48E-06	-5.1884	YES				
	SEWARD	'82	DST	1E-06	-6.0000	NO				

Drawn by	Date
Checked by	Date
Revisions	Date
409700R554	

Culebra Dolomite Storativity Data Base

INTERA Technologies

Table D.1

WELL	REFERENCES	YEAR OF REFERENCE	TYPE OF TEST	REPORTED CULEBRA S	LOG OF STORATIVITY	SELECTED S VALUE (YES OR NO)	AVERAGE OF SELECTED S VALUES (FOR SINGLE WELL OR HYDROPAD)	CULEBRA STORATIVITY VALUE log	CULEBRA STORATIVITY VALUE -	COMMENTS
H-4c	BEAUHEIM	'87b	SLUG	NR						
	GONZALEZ	'83	I - OB(H4B)D	5.67E-06	-5.2464	YES				
	GONZALEZ	'83	I - OB(H4B)R	NR						
	GONZALEZ	'83	PUMPING 1D	NR						
	GONZALEZ	'83	PUMPING 1R	NR						
	GONZALEZ	'83	PUMPING 2D	NR						
	GONZALEZ	'83	PUMPING 2R	NR			-5.3354	-5.3354	4.62E-06	VALUE ASSIGNED TO H-4 HYDROPAD
H-5a	GONZALEZ	'83	I - OB(H5C)D	2.50E-05	-4.6021	YES				
	GONZALEZ	'83	I - OB(H5C)R	NR						
	GONZALEZ	'83	I - OB(H5B)D	9.34E-06	-5.0297	YES				
	GONZALEZ	'83	I - OB(H5B)R	NR						
H-5b	GONZALEZ	'83	PUMPING R	NR						
	GONZALEZ	'83	I - OB(H5C)D	2.60E-05	-4.5850	YES				
	GONZALEZ	'83	I - OB(H5C)R	NR						
	DENN. & MERCER	'82	SLUG	1E-05	-5.0000	NO				
	SEWARD	'82	DST	1E-05	-5.0000	NO				
H-5c	GONZALEZ	'83	PUMPING D	NR						
	GONZALEZ	'83	PUMPING R	NR						
	GONZALEZ	'83	I - OB(H5B)D	2.92E-05	-4.5346	YES				
	GONZALEZ	'83	I - OB(H5B)R	NR			-4.6878	-4.6878	2.05E-05	VALUE ASSIGNED TO H-5 HYDROPAD
H-6a	BEAUHEIM	'87c	I - OB(W-13)	8.2E-06 +	-5.0862	NO				
	GONZALEZ	'83	I - OB(H6B)D	2.20E-05	-4.6576	YES				
	GONZALEZ	'83	I - OB(H6B)R	NR						
	GONZALEZ	'83	I - OB(H6C)D1	2.54E-05	-4.5952	YES				
	GONZALEZ	'83	I - OB(H6C)R1	NR						
	GONZALEZ	83	I - OB(H6C)D2	2.32E-05	-4.6345	YES				
	GONZALEZ	'83	I - OB(H6C)R2	NR						
H-6b	BEAUHEIM	'87c	I - OB(W-13)	7.9E-06 +	-5.1024	NO				
	BEAUHEIM	'86	I - OB(DOE2)	6E-06 •	-5.2218	NO				
	GONZALEZ	'83	PUMPING D	NR						
	GONZALEZ	'83	PUMPING R	NR						
	GONZALEZ	'83	I - OB(H6C)D1	1.42E-05	-4.8477	YES				
	GONZALEZ	'83	I - OB(H6C)R1	NR						
	GONZALEZ	'83	I - OB(H6C)D2	1.45E-05	-4.8386	YES				
	GONZALEZ	'83	I - OB(H6C)R2	NR						
	DENNEHY	'82	PUMPING D '79	NR						
	DENNEHY	'82	PUMPING R '79	NR						
	SEWARD	'82	DST	NR						
H-6c	GONZALEZ	'83	PUMPING 1R	NR						
	GONZALEZ	'83	I - OB(H6B)D	1.26E-05	-4.8996	YES				
	GONZALEZ	'83	I - OB(H6B)R	NR						
	GONZALEZ	'83	PUMPING 2D	NR						
	GONZALEZ	'83	PUMPING 2R	NR			-4.7455	-4.7455	1.80E-05	VALUE ASSIGNED TO H-6 HYDROPAD

Drawn by	Date
Checked by	Date
Revisions	Date
H09700R554	

Culebra Dolomite Storativity Data Base

INTERA Technologies

Table D.1 (cont.)

WELL	REFERENCES	YEAR OF REFERENCE	TYPE OF TEST	REPORTED CULEBRA S	LOG OF STORATIVITY	SELECTED S VALUE (YES OR NO)	AVERAGE OF SELECTED S VALUES (FOR SINGLE WELL OR HYDROPAD)	CULEBRA STORATIVITY VALUE log	CULEBRA STORATIVITY VALUE -	COMMENTS
H-7a										
H-7b1	MERCER	'83	PUMPING	NR						
H-7b2	INTERA	*UE	PUMPING '86	8.2E-04	-3.0862	YES	NA	-3.0862	8.20E-04	VALUE ASSIGNED TO H-7 HYDROPAD
H-7c										
H-8a										
H-8b	BEAUHEIM	'87b	PUMPING	NR						
	MERCER	'83	PUMPING	NR						
H-8c										
H-9a										
H-9b	MERCER	'83	PUMPING	NR						
	INTERA	*UE	PUMPING '83	NR						
H-9c										
H-10a										
H-10b	MERCER	'83	SLUG	1E-04	-4.0000	NO				
H-10c										
H-11b1	SAULNIER	'87	PUMPING '84	NR						
	SAULNIER	'87	I - OB(H11B3)'84	6.3E-04	-3.2007	YES				
	SAULNIER	'87	I - OB(H11B3)'85	4.4E-03	-2.3565	YES				
	SAULNIER	'87	I - OB(H11B2)	6.1E-04	-3.2147	YES				
	BEAUHEIM	'87a	I - OB(H3B2)	7.4E-06 +	-5.1308	NO				
H-11b2	SAULNIER	'87	I - OB(H11B3)'84	7.2E-04	-3.1427	YES				
	SAULNIER	'87	I - OB(H11B3)'85	2.5E-03	-2.6021	YES				
	SAULNIER	'87	I - OB(H11B1)	8.0E-04	-3.0969	YES				
H-11b3	SAULNIER	'87	PUMPING '84	NR						
	SAULNIER	'87	PUMPING '85	NR						
	SAULNIER	'87	I - OB(H11B1)	5.5E-04	-3.2596	YES				
	SAULNIER	'87	I - OB(H11B2)	4.5E-04	-3.3468	YES	-3.0275	-3.0275	9.39E-04	VALUE ASSIGNED TO H-11 HYDROPAD
H-12	INTERA	*UE	SLUG '87	2.0E-06	-5.6990	NO				
	INTERA	*UE	PUMPING '84	NR						
H-14	BEAUHEIM	'87b	SLUG	NR						
	BEAUHEIM	'87b	DST	NR						

Drawn by	Date
Checked by	Date
Revisions	Date
H09700R554	

Culebra Dolomite Storativity Data Base

INTERA Technologies

Table D.1 (cont.)

WELL	REFERENCES	YEAR OF REFERENCE	TYPE OF TEST	REPORTED CULEBRA S	LOG OF STORATIVITY	SELECTED S VALUE (YES OR NO)	AVERAGE OF SELECTED S VALUES (FOR SINGLE WELL OR HYDROPAD)	CULEBRA STORATIVITY VALUE log -	COMMENTS
H-15	BEAUHEIM	'87b	SLUG	NR					
	BEAUHEIM	'87b	DST	NR					
H-16	BEAUHEIM	UE	SLUG	NR					
DOE-1	BEAUHEIM	'87a	I - OB(H3B2)	1.0E-05 +	-5.0000	NO			
	BEAUHEIM	'87a	I - OB(H3B3)	1.2E-05 •	-4.9208	NO			
	BEAUHEIM	'87b	PUMPING D	NR					
	BEAUHEIM	'87b	PUMPING R	NR					
DOE-2	BEAUHEIM	'86	PUMPING	NR					
	BEAUHEIM	'87c	I - OB(W-13)	5.1E-06 +	-5.2924	NO			
P-1									
P-2									
P-3									
P-4									
P-5									
P-6									
P-7									
P-8									
P-9									
P-10									
P-11									
P-12									
P-13									
P-14	BEAUHEIM	'87c	I - OB(W-13)	5.2E-05 +	-4.2840	NO			
	MERCER	'83	PUMPING	NR					
	HYDRO GEOCHEM	UE	SLUG	NR					
P-15	MERCER	'83	SLUG	1E-04	-4.0000	NO			
	SEWARD	'82	DST	1E-04	-4.0000	NO			
	BEAUHEIM	87b	SLUG	NR					
P-16									
P-17	BEAUHEIM	'87b	SLUG	NR					
	MERCER	'83	SLUG	1E-06	-6.0000	NO			
	HYDRO GEOCHEM	UE	PUMPING	NR					
P-18	MERCER	'83	SLUG	NR					
	HYDRO GEOCHEM	UE	SLUG	NR					

Drawn by	Date
Checked by	Date
Revisions	Date
H09700R554	

Culebra Dolomite Storativity Data Base

INTERA Technologies

Table D.1 (cont.)

WELL	REFERENCES	YEAR OF REFERENCE	TYPE OF TEST	REPORTED CULEBRA S	LOG OF STORATIVITY	SELECTED S VALUE (YES OR NO)	AVERAGE OF SELECTED S VALUES (FOR SINGLE WELL OR HYDROPAD)	CULEBRA STORATIVITY VALUE log	CULEBRA STORATIVITY VALUE -	COMMENTS
P-19										
P-20										
P-21										
WIPP-12	BEAUHEIM	UE	ACID & DEVEL	NR						
	BEAUHEIM	'87c	I - OB(W-13)	3.6E-05 +	-4.4437	NO				
WIPP-13	BEAUHEIM	UE	PUMPING							
	BEAUHEIM	'86	I - OB(DOE2)	3E-06 •	-5.5229	NO				
WIPP-18	BEAUHEIM	'87b	SLUG	NR						
	BEAUHEIM	'87b	I - OB(W-13)	4.0E-05 +	-4.3979	NO				
W1PP-19	BEAUHEIM	'87b	SLUG	NR						
	BEAUHEIM	'87b	I - OB(W-13)	4.0E-05 +	-4.3979	NO				
WIPP-21	BEAUHEIM	'87b	SLUG	NR						
	BEAUHEIM	'87c	I - OB(W-13)	5.3E-05 +	-4.2757	NO				
WIPP-22	BEAUHEIM	'87b	SLUG	NR						
	BEAUHEIM	'87c	I - OB(W-13)	4.7E-05 +	-4.3279	NO				
WIPP-25	MERCER	'83	PUMPING	NR						
	BEAUHEIM	'87c	I - OB(W-13)	6.4E-05 +	-4.1938	NO				
WIPP-26	MERCER	'83	PUMPING	NR						
WIPP-27	MERCER	'83	PUMPING	NR						
WIPP-28	MERCER	'83	PUMPING	NR						
WIPP-29	MERCER	'83	PUMPING	NR						
WIPP-30	MERCER	'83	SLUG	1E-04	-4.0000	NO				
	GONZALEZ	'83	PUMPING	1E-04	-4.0000	YES	NA	-4.0000	1.00E-04	VALUE ASSIGNED TO WIPP-30 BOREHOLE
	BEAUHEIM	'87c	I - OB(W-13)	5.6E-06 +	-5.2518	NO				
ERDA-9	BEAUHEIM	'87b	SLUG	NR						
	BEAUHEIM	'87c	I - OB(W-13)	5.4E-05 +	-4.2676	NO				
CABIN BABY-1	BEAUHEIM	'87b	SLUG	NR						
ENGLE	BEAUHEIM	'87b	PUMPING	NR						
USGS-1	COOPER	'62	PUMPING '60-D	NR						
	COOPER	'62	PUMPING '60-R	NR						
	COOPER & GLANZ.	'71	PUMPING '63	2.0E-05	-4.6990	YES	NA	-4.6990	2.00E-05	VALUE ASSIGNED TO USGS-1 BOREHOLE
EX.SHFT	BEAUHEIM	'87c	I - OB(W-13)	5.5E-05 •	-4.2596	NO				

Drawn by	Date
Checked by	Date
Revisions	Date
H09700R554	

Culebra Dolomite Storativity Data Base

INTERA Technologies

Table D.1 (cont.)

REFERENCES

BEAUHEIM,R.L., 1986, HYDRAULIC-TEST INTERPRETATIONS FOR WELL DOE-2 AT THE WASTE ISOLATION PILOT PLANT (WIPP) SITE, SAND86-1364.

BEAUHEIM,R.L., 1987a, ANALYSIS OF PUMPING TESTS OF THE CULEBRA DOLOMITE CONDUCTED AT THE H-3 HYDROPAD AT THE WASTE ISOLATION PILOT PLANT (WIPP) SITE, SAND86-2311.

BEAUHEIM,R.L., 1987b, INTERPRETATIONS OF SINGLE-WELL HYDRAULIC TESTS CONDUCTED AT AND NEAR THE WASTE ISOLATION PILOT PLANT (WIPP) SITE, 1983-1987, SAND87-0039.

BEAUHEIM,R.L., 1987c, INTERPRETATION OF THE WIPP-13 MULTIPAD PUMPING TEST OF THE CULEBRA DOLOMITE AT THE WASTE ISOLATION PILOT PLANT (WIPP) SITE, SAND87-2456.

COOPER, JAMES B., 1962, GROUND-WATER INVESTIGATIONS OF THE PROJECT GNOME AREA, EDDY AND LEA COUNTIES, NEW MEXICO; U.S. GEOLOGICAL SURVEY TEI-802, OPEN FILE REPORT. 116p.,12 figs.

COOPER, JAMES B., AND GLANZMAN, V.M.,1971, GEOHYDROLOGY OF PROJECT GNOME SITE, EDDY COUNTY, NEW MEXICO; U.S. GEOLOGICAL SURVEY PROFESSIONAL PAPER 712-A, 28p.

DENNEHY,K.F., 1982, RESULTS OF HYDROLOGIC TESTS AND WATER-CHEMISTRY ANALYSES, WELLS H-6A, H-6B, AND H-6C AT THE PROPOSED WASTE ISOLATION PILOT PLANT SITE, SOUTHEASTERN NEW MEXICO: U.S. GEOLOGICAL SURVEY WATER-RESOURCES INVESTIGATIONS 82-8.

DENNEHY,K.F.,AND MERCER,J.W., 1982, RESULTS OF HYDROLOGIC TESTS AND WATER-CHEMISTRY ANALYSES, WELLS H-5A, H-5B, AND H-5C AT THE PROPOSED WASTE ISOLATION PILOT PLANT SITE, SOUTHEASTERN NEW MEXICO: U.S. GEOLOGICAL SURVEY WATER-RESOURCES INVESTIGATIONS 82-19, 83p.

GONZALEZ,D.D., 1983, GROUNDWATER FLOW IN THE RUSTLER FORMATION, WASTE ISOLATION PILOT PLANT (WIPP), SOUTHEAST NEW MEXICO (SENM): INTERIM REPORT, SAND82-1012.

MERCER, J.W., DAVIS P., DENNEHY, K.F., AND GOETZ, C.L. 1981. RESULTS OF HYDROLOGIC TESTS AND WATER-CHEMISTRY ANALYSES, WELLS H-4A, H-4B, AND H-4C AT THE PROPOSED WASTE ISOLATION PILOT PLANT SITE, SOUTHEASTERN NEW MEXICO. USGS WATER RESOURCES INVESTIGATIONS RPT 79-98 (ALBURQUERQUE, NM), 178 pp.

MERCER, J.W., 1983, GEOHYDROLOGY OF THE PROPOSED WASTE ISOLATION PILOT PLANT SITE, LOS MEDANOS AREA, SOUTHEASTERN NEW MEXICO, USGS-WATER RESOURCES INVESTIGATION REPORT 83-4016.

SAULNIER, G.J., 1987, ANALYSIS OF PUMPING TESTS OF THE CULEBRA DOLOMITE CONDUCTED AT THE H-11 HYDROPAD AT THE WASTE ISOLATION PILOT PLANT (WIPP) SITE, SAND87-7124

SEWARD,P.D., 1982, ABRIDGED BOREHOLE HISTORIES FOR THE WASTE ISOLATION PILOT PLANT (WIPP) STUDIES, SAND82-0080.

Drawn by	Date	Culebra Dolomite Storativity Data Base
Checked by	Date	
Revisions	Date	
H09700554		
INTERA Technologies		Table D.1 (cont.)

APPENDIX E TRANSIENT FRESHWATER HEADS

Water-level monitoring and well testing using pressure transducers have been performed in boreholes in the Culebra in and around the WIPP site. This modeling study incorporates data from 56 monitoring wells for control and model calibration. Where sufficient data were available from these wells, hydrographs have been constructed which plot freshwater head in meters above mean sea level (m amsl) versus time in years. The term "freshwater head" is utilized in this report and is equivalent to the term "freshwater elevation above mean sea level" because the head values are always related to mean sea level. It refers to the elevation of a column of fresh water with a fluid density of 1 g/cm^3 that would exert a pressure at the elevation of the Culebra equal to the formation pressure.

The hydrographs show the transient freshwater heads resulting from the shaft and well-test activities performed at the site (Appendix G). For most of these hydrographs, an undisturbed freshwater head has been selected which is intended to represent conditions at the site before shaft excavations and hydraulic-characterization studies. This appendix describes the calculations and data used to create these hydrographs, and provides an estimation of the undisturbed hydraulic conditions for use in the calibration of the steady-state model.

Water-level and pressure data for the Culebra have been collected at the WIPP site as depths to water below top of casing or top of tubing measured by steel tape or electronic sounding device, and pressure measured by downhole transducers. These data are reported in Richey (1987), Hydro Geo Chem, Inc. (1985), INTERA Technologies, Inc. and Hydro Geo Chem, Inc. (1985), INTERA Technologies, Inc. (1986), Saulnier et al. (1987), and Stensrud et al. (1987).

Depth-to-water data were converted to equivalent freshwater head as follows:

$$h_f = (d_c - d_w)\frac{\rho}{\rho_f} + Z_c \qquad \text{(E.1)}$$

where h_f = equivalent freshwater head;
d_w = measured depth to water;
d_c = depth to the center of the Culebra dolomite;
Z_c = elevation of the center of the Culebra dolomite above mean sea level;
ρ = average density of the borehole fluid;
ρ_f = freshwater-fluid density (assumed equal to 1.0 g/cm^3).

Transducer pressure data were converted to equivalent freshwater head as follows:

$$h_f = \frac{p}{\rho_f g} + (d_c - d_t)\frac{\rho}{\rho_f} + Z_c \qquad \text{(E.2)}$$

where p = measured transducer pressure;
d_t = depth to transducer;
g = gravitational constant.

All depths are measured relative to a measuring point of known elevation at each well. For the WIPP-site monitoring wells, depths are reported either from the top of casing, the top of tubing, or from the ground surface. Table E.1 summarizes the type of measuring point at each well, the elevation of the measuring point, and the time period the measuring point was used. For some wells listed in Table E.1, more than one measuring point were used at a well at a given time. This results from the use of different measuring points when the U.S. Geological Survey monitoring of some wells through early 1985 overlapped with monitoring by Sandia subcontractors.

The calculation of equivalent freshwater head requires knowledge of the average borehole-fluid density. For each well an estimate of borehole-fluid density as a function of time was determined based upon a summary of the activities at that well (Appendix G), water-quality data available, and borehole pressure-density survey data. The best data for determining the average borehole-fluid densities were obtained from the borehole pressure-density surveys reported in IT (1987), Crawley (1987), and Crawley (in preparation). In these surveys, pressures were measured with downhole transducers at center-of-Culebra depth for a measured depth to water below top of casing, thus allowing a direct calculation of average borehole-fluid density. However, this type of data was not available for any of the wells before late 1986.

Table E.2 summarizes the chronology of borehole-fluid densities for each well used in the model. For each well, the table gives (1) average borehole-fluid density (g/cm^3), (2) a quantitative estimate of uncertainty (g/cm^3), and (3) the time period appropriate. The estimate of the uncertainty of borehole-fluid density is based upon an extensive review of all density measurements and well activities at each monitoring well.

With the values of Culebra elevation, measuring-point elevation, and the average borehole-fluid densities, hydrographs of equivalent freshwater head (m amsl) versus time (years) were created for each well. These hydrographs are plotted in Figures E.1 through E.35. In addition, Figure E.36 is a hydrograph plotting the equivalent freshwater head, based upon pressure measurements, versus time for the transducers installed in the Culebra in the walls of the three shafts at the WIPP site.

From these hydrographs, the undisturbed freshwater heads were estimated. Events which can complicate the determination of undisturbed conditions are well-test activities and shaft activities. Haug et al. (1987) found that since the summer of 1981, the hydraulic state of the Culebra has been significantly influenced by the drilling and excavating of the three

shafts at the WIPP site. Also, numerous well tests have been performed since that date of large enough duration to create sub-regional transients. For these reasons, when possible, the undisturbed freshwater heads were estimated from data collected before December 1981. For some wells, only recent (i.e., 1987) water-level data were available for determining estimates of the undisturbed freshwater heads. Table E.3 summarizes undisturbed freshwater heads for each well along with the approximate date of the measurement on which it is based. In Table E.3, the uncertainty in the borehole-fluid density presented in Table E.2, expressed as g/cm^3, is converted to a head uncertainty based on an average depth of fluid in the borehole above the center of the Culebra. In addition to borehole-fluid-density uncertainty, other trends in the hydrograph data or specific well activities may add uncertainty to these estimates. The final column of Table E.3 combines this uncertainty with the borehole-fluid-density uncertainty to arrive at a total uncertainty, expressed as meters of head, for the undisturbed freshwater-head estimates. This total uncertainty is considered to represent one standard deviation from the mean. When more than one value of undisturbed freshwater head can be estimated from several wells at a hydropad, the value used is from the well with the least uncertainty in the average borehole-fluid-density estimate.

REFERENCES

Crawley, M.E., 1987. Second Data Release Report for the Pressure-Density Survey Program. Prepared by IT Corporation. Draft.

Crawley, M.E., in preparation. Third Data Release Report for the Pressure-Density Survey Program. Prepared by IT Corporation. Draft.

Haug, A., V.A. Kelley, A.M. LaVenue, and J.F. Pickens, 1987. Modeling of Ground-Water Flow in the Culebra Dolomite at the Waste Isolation Pilot Plant (WIPP) Site: Interim Report. Sandia National Laboratories, Contractor Report SAND86-7167.

Hydro Geo Chem, Inc., 1985. WIPP Hydrology Program, Waste Isolation Pilot Plant, SENM, Hydrologic Data Report #1. Sandia National Laboratories, Contractor Report SAND85-7206, 710 p.

INTERA Technologies, Inc. and Hydro Geo Chem, Inc., 1985. WIPP Hydrology Program, Waste Isolation Pilot Plant, SENM, Hydrologic Data Report #2. Sandia National Laboratories, Contractor Report SAND85-7263.

INTERA Technologies, Inc., 1986. WIPP Hydrology Program, Waste Isolation Pilot Plant, SENM, Hydrologic Data Report #3. Sandia National Laboratories, Contractor Report SAND86-7109.

IT Corporation, 1987. Initial Data Release Report for the Pressure-Density Survey Program. Draft.

Richey, S.F., 1987. Water-Level Data from Wells in the Vicinity of the Waste Isolation Pilot Plant, Southeastern New Mexico. U.S. Department of Energy, U.S. Geol. Survey Open-File Report 87-120, 107 p.

Saulnier, G.J., Jr., G.A. Freeze, and W.A. Stensrud, 1987. WIPP Hydrology Program, Waste Isolation Pilot Plant, Southeastern New Mexico, Hydrologic Data Report #4. Sandia National Laboratories, Contractor Report SAND86-7166.

Stensrud, W.A., M.A. Bame, K.D. Lantz, A.M. LaVenue, J.B. Palmer, and G.J. Saulnier, Jr., 1987. WIPP Hydrology Program, Waste Isolation Pilot Plant, Southeastern New Mexico, Hydrologic Data Report #5. Sandia National Laboratories, Contractor Report SAND87-7125.

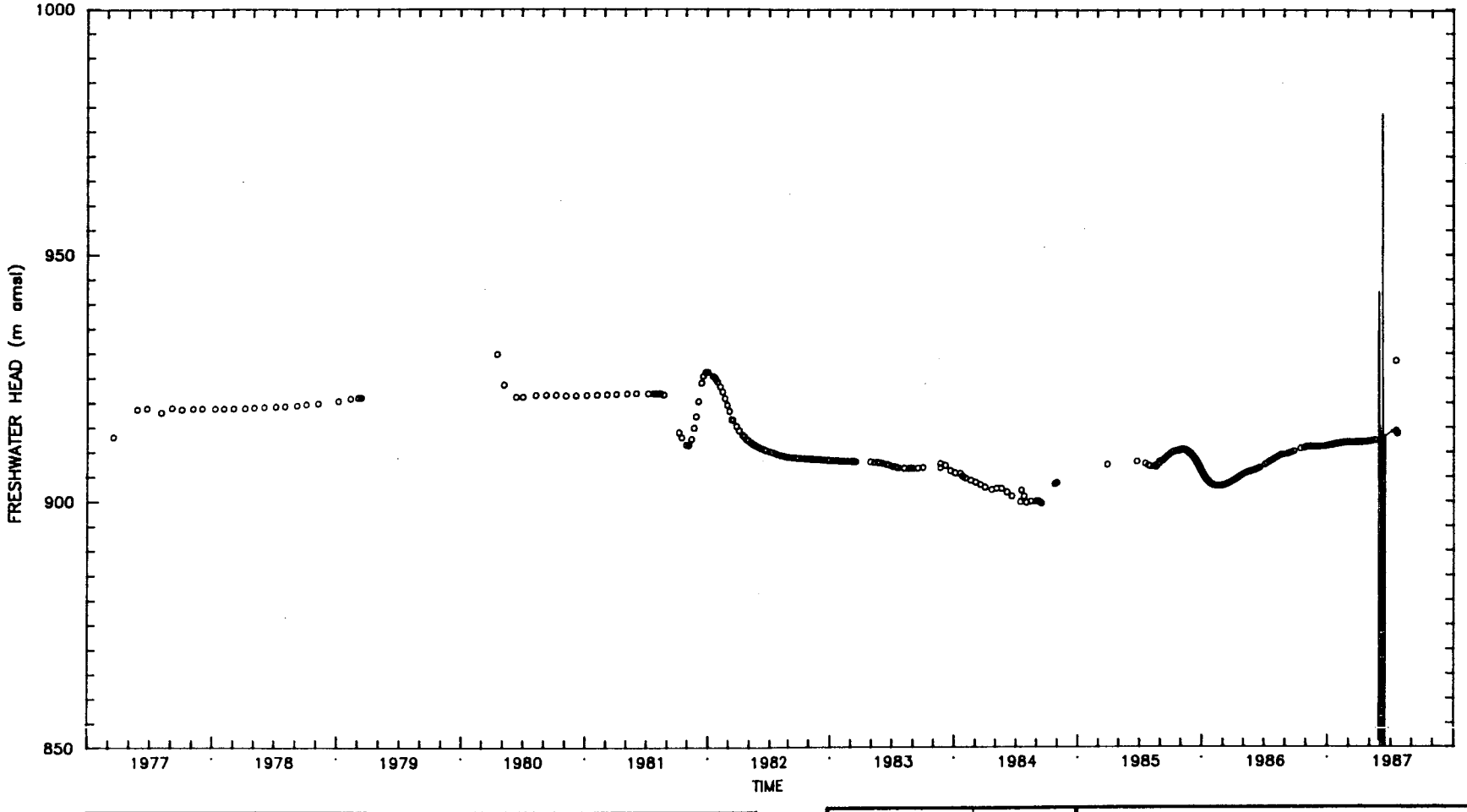

LEGEND: o = H-1/CUL(WL) – = H-1/CUL (T) WL = Water-level data
T = Transducer data

Drawn by	Date
Checked by	Date
Revisions	Date
[illegible]	

INTERA Technologies

Equivalent Freshwater Heads for the Culebra Dolomite at Well H-1

Figure E.1

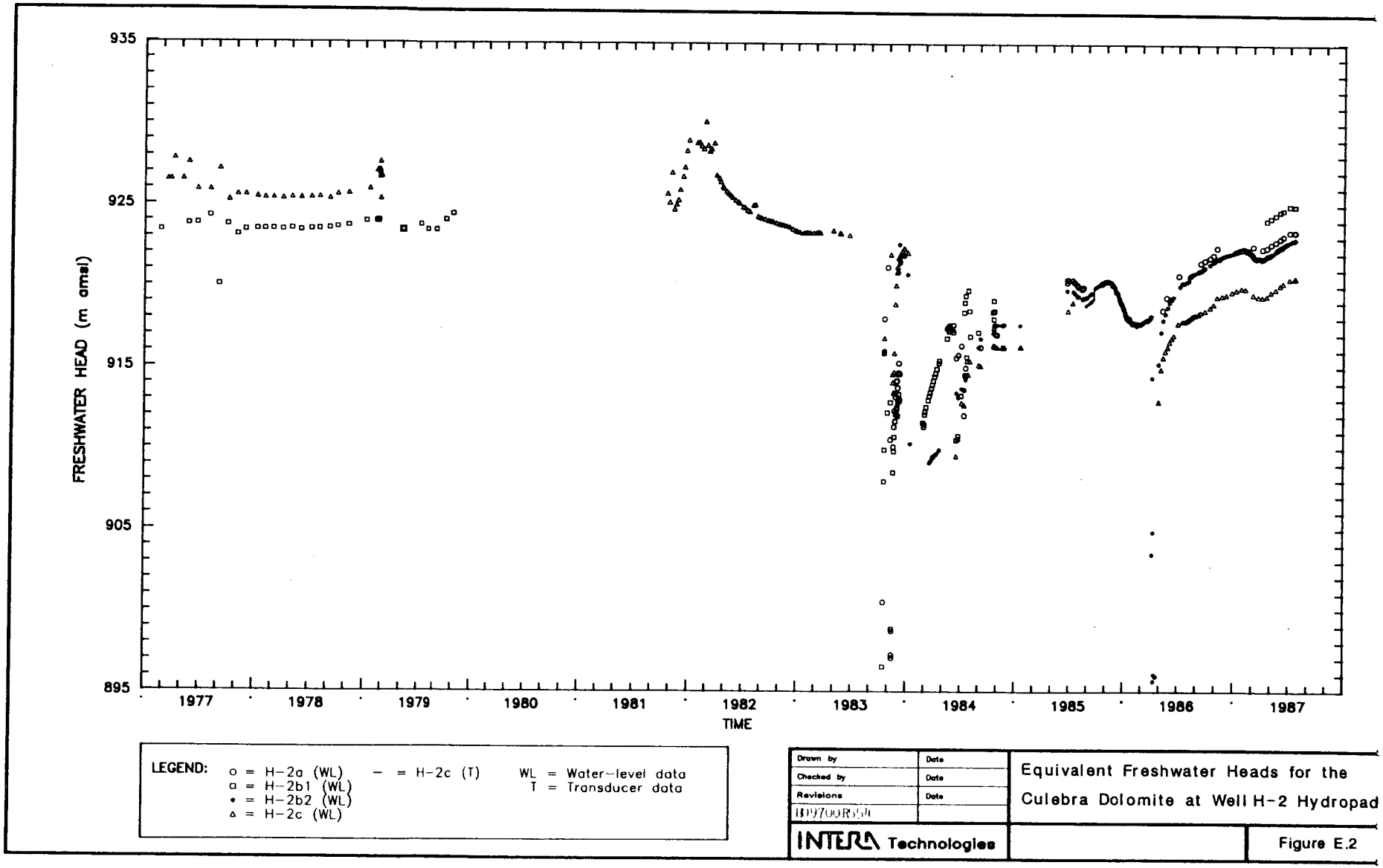
935
925
915
905
895
FRESHWATER HEAD (m amsl)
1977
1978
1979
1980
1981
1982
1983
1984
1985
1986
1987
TIME
LEGEND:
o = H-2a (WL)
□ = H-2b1 (WL)
* = H-2b2 (WL)
Δ = H-2c (WL)
– = H-2c (T)
WL = Water-level data
T = Transducer data
Drawn by
Date
Checked by
Date
Revisions
Date
INTERA Technologies
Equivalent Freshwater Heads for the Culebra Dolomite at Well H-2 Hydropad
Figure E.2

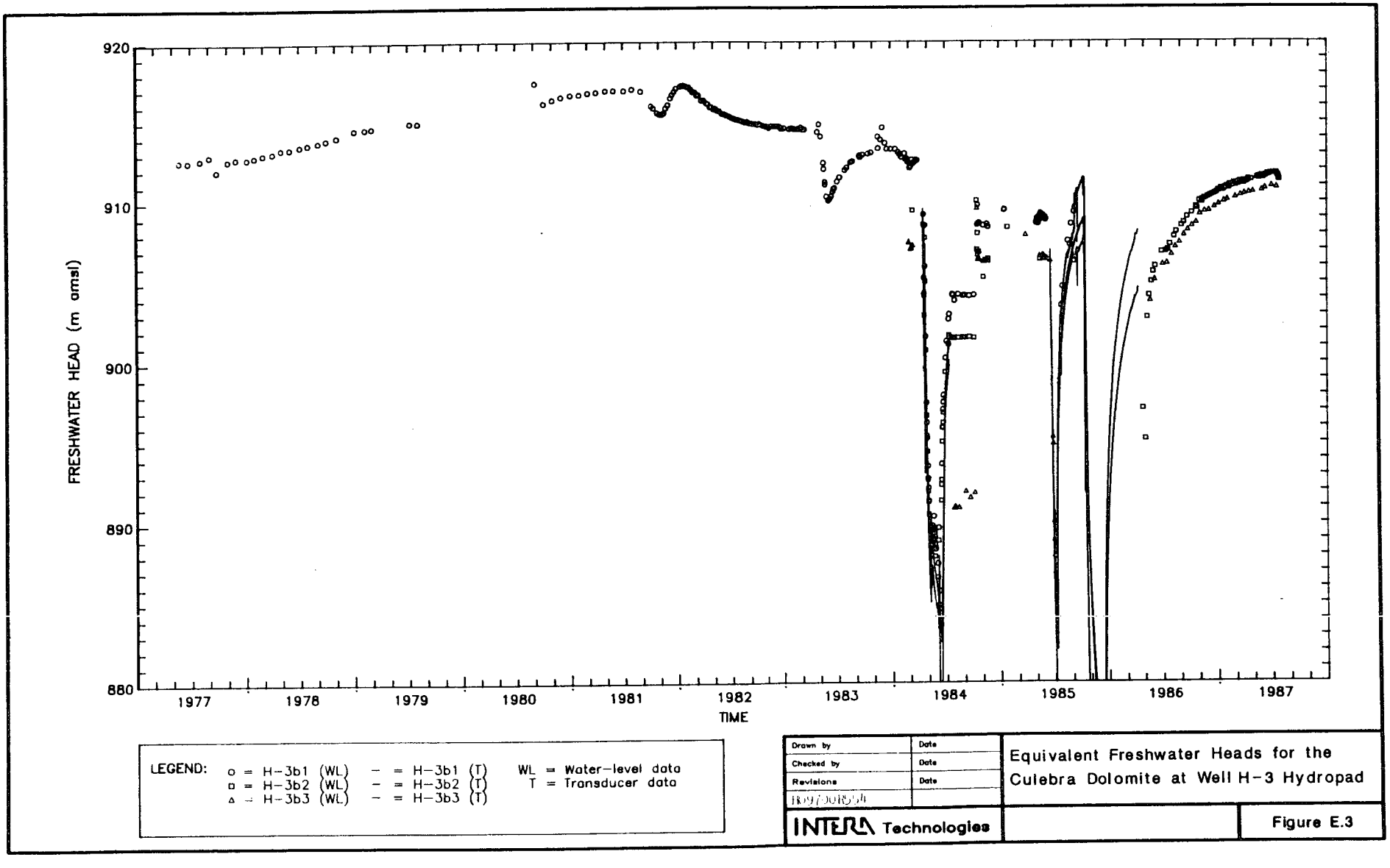
920
910
900
890
880
FRESHWATER HEAD (m amsl)
1977
1978
1979
1980
1981
1982
1983
1984
1985
1986
1987
TIME
LEGEND:
o = H-3b1 (WL)
□ = H-3b2 (WL)
△ = H-3b3 (WL)
– = H-3b1 (T)
– = H-3b2 (T)
– = H-3b3 (T)
WL = Water-level data
T = Transducer data
Drawn by
Date
Checked by
Date
Revisions
Date
INTERA Technologies
Equivalent Freshwater Heads for the Culebra Dolomite at Well H-3 Hydropad
Figure E.3

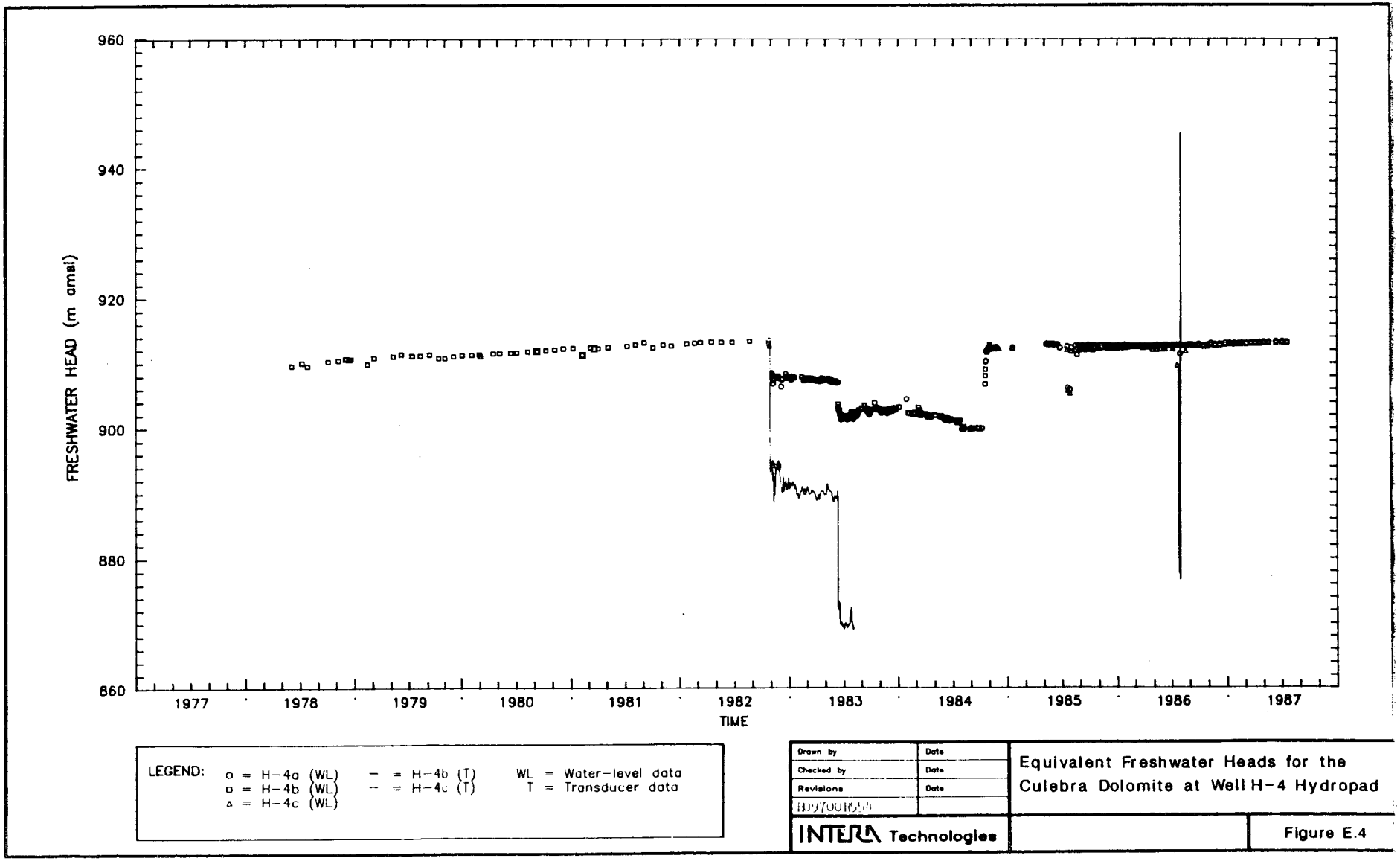
960
940
920
900
880
860
FRESHWATER HEAD (m amsl)
1977
1978
1979
1980
1981
1982
1983
1984
1985
1986
1987
TIME
LEGEND:
o = H-4a (WL)
□ = H-4b (WL)
△ = H-4c (WL)
– = H-4b (T)
– = H-4c (T)
WL = Water-level data
T = Transducer data
Drawn by
Date
Checked by
Date
Revisions
Date
INTERA Technologies
Equivalent Freshwater Heads for the Culebra Dolomite at Well H-4 Hydropad
Figure E.4

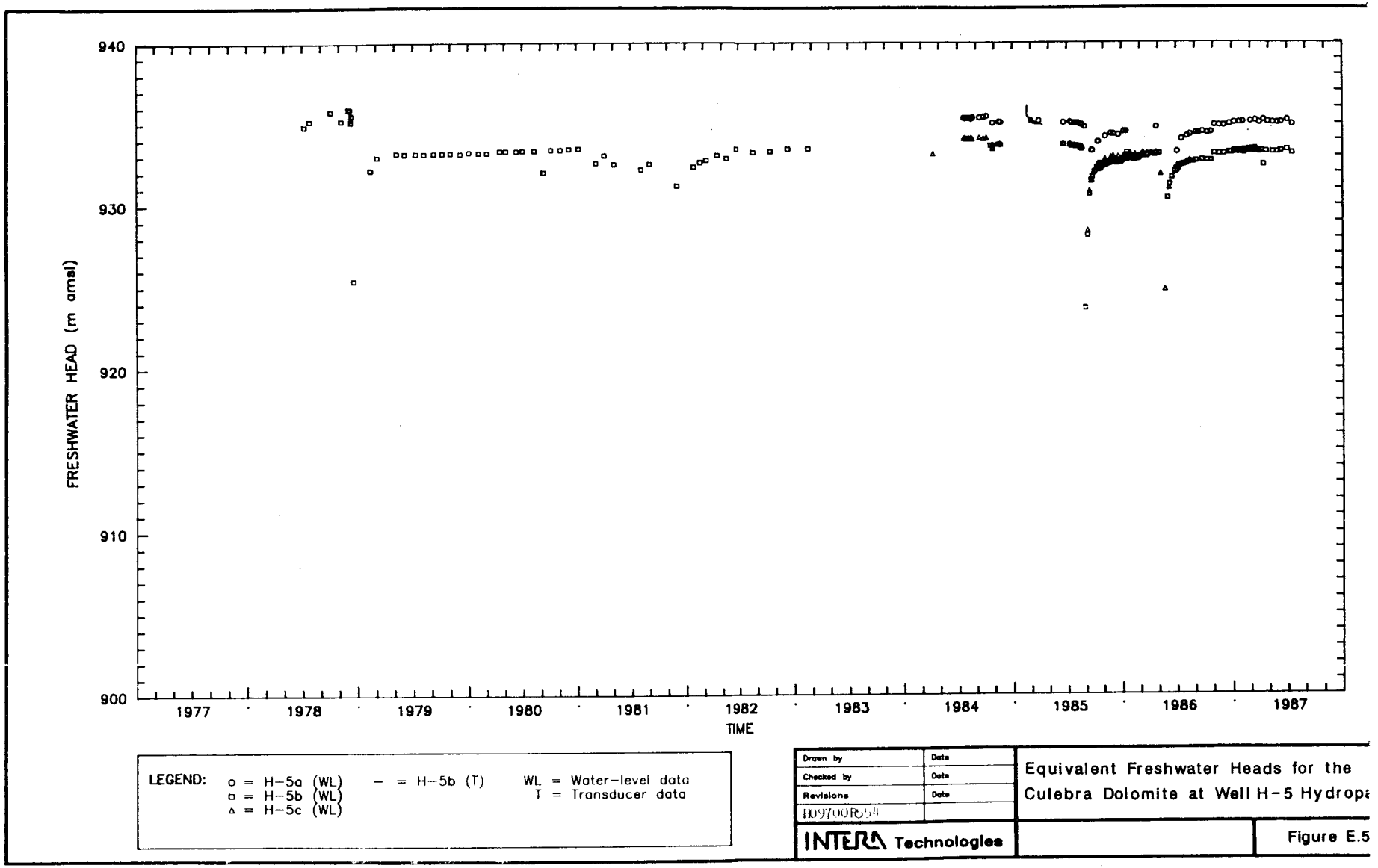
940
930
920
910
900
FRESHWATER HEAD (m amsl)
1977
1978
1979
1980
1981
1982
1983
1984
1985
1986
1987
TIME
LEGEND:
o = H-5a (WL)
□ = H-5b (WL)
△ = H-5c (WL)
– = H-5b (T)
WL = Water-level data
T = Transducer data
Drawn by
Date
Checked by
Date
Revisions
Date
809700R5H
INTERA Technologies
Equivalent Freshwater Heads for the
Culebra Dolomite at Well H-5 Hydropa
Figure E.5

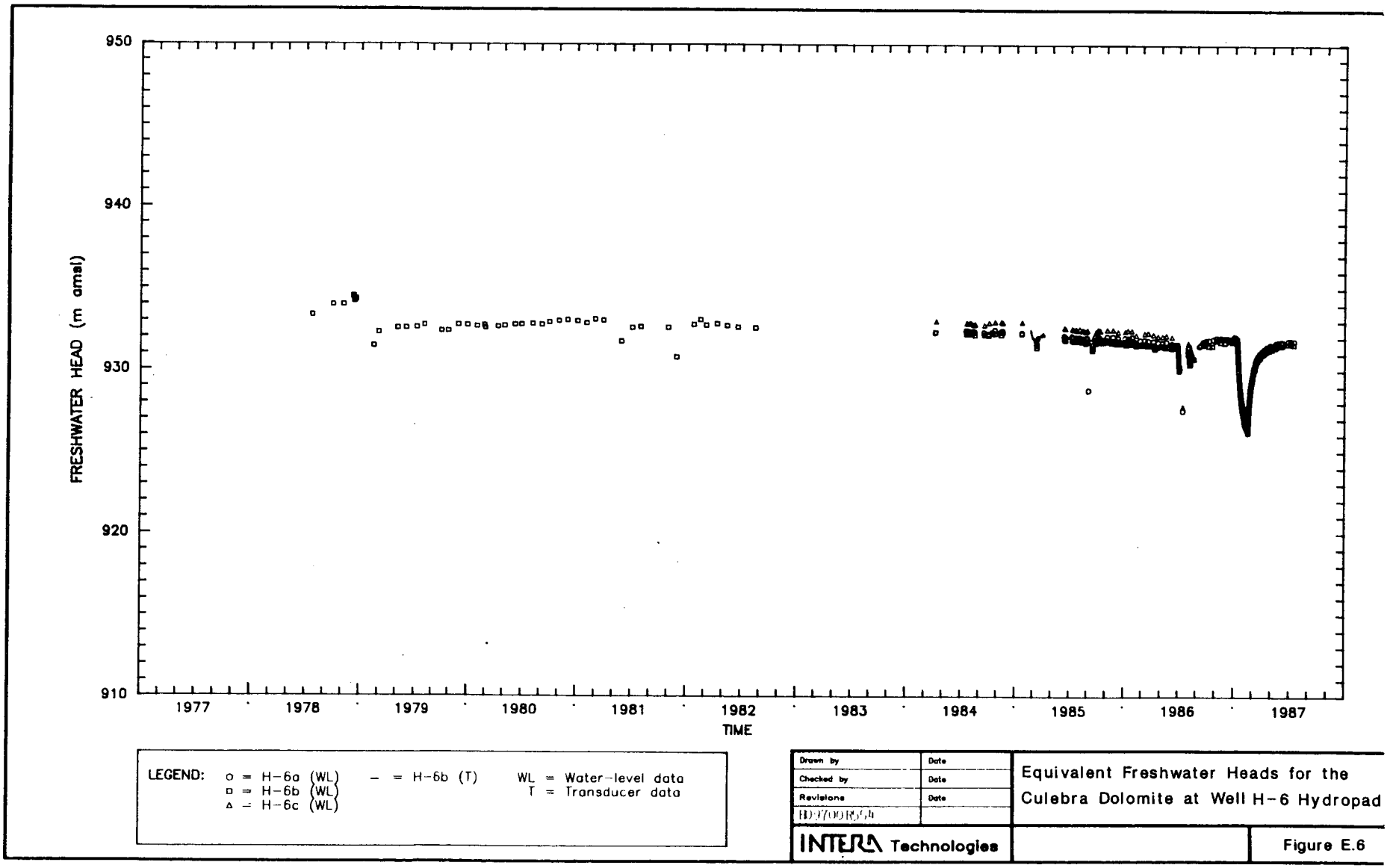
950
940
930
920
910
FRESHWATER HEAD (m amsl)
1977
1978
1979
1980
1981
1982
1983
1984
1985
1986
1987
TIME
LEGEND: o = H-6a (WL) – = H-6b (T) WL = Water-level data
□ = H-6b (WL) T = Transducer data
△ = H-6c (WL)
Drawn by Date
Checked by Date
Revisions Date
INTERA Technologies
Equivalent Freshwater Heads for the Culebra Dolomite at Well H-6 Hydropad
Figure E.6

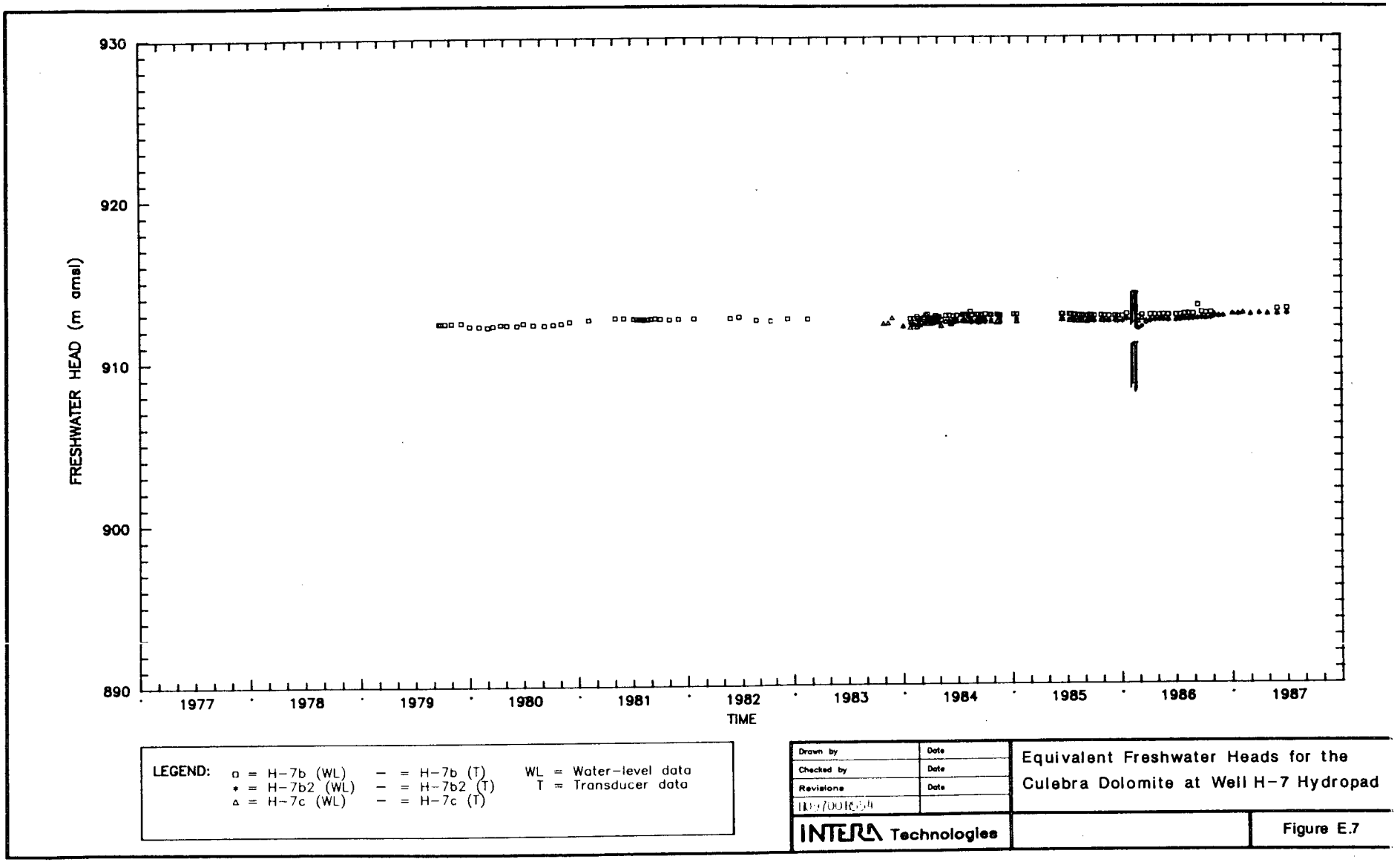
930
920
910
900
890
FRESHWATER HEAD (m amsl)
1977
1978
1979
1980
1981
1982
1983
1984
1985
1986
1987
TIME
LEGEND: □ = H-7b (WL) – = H-7b (T)
* = H-7b2 (WL) – = H-7b2 (T)
△ = H-7c (WL) – = H-7c (T)
WL = Water-level data
T = Transducer data
Drawn by
Date
Checked by
Date
Revisions
Date
INTERA Technologies
Equivalent Freshwater Heads for the Culebra Dolomite at Well H-7 Hydropad
Figure E.7

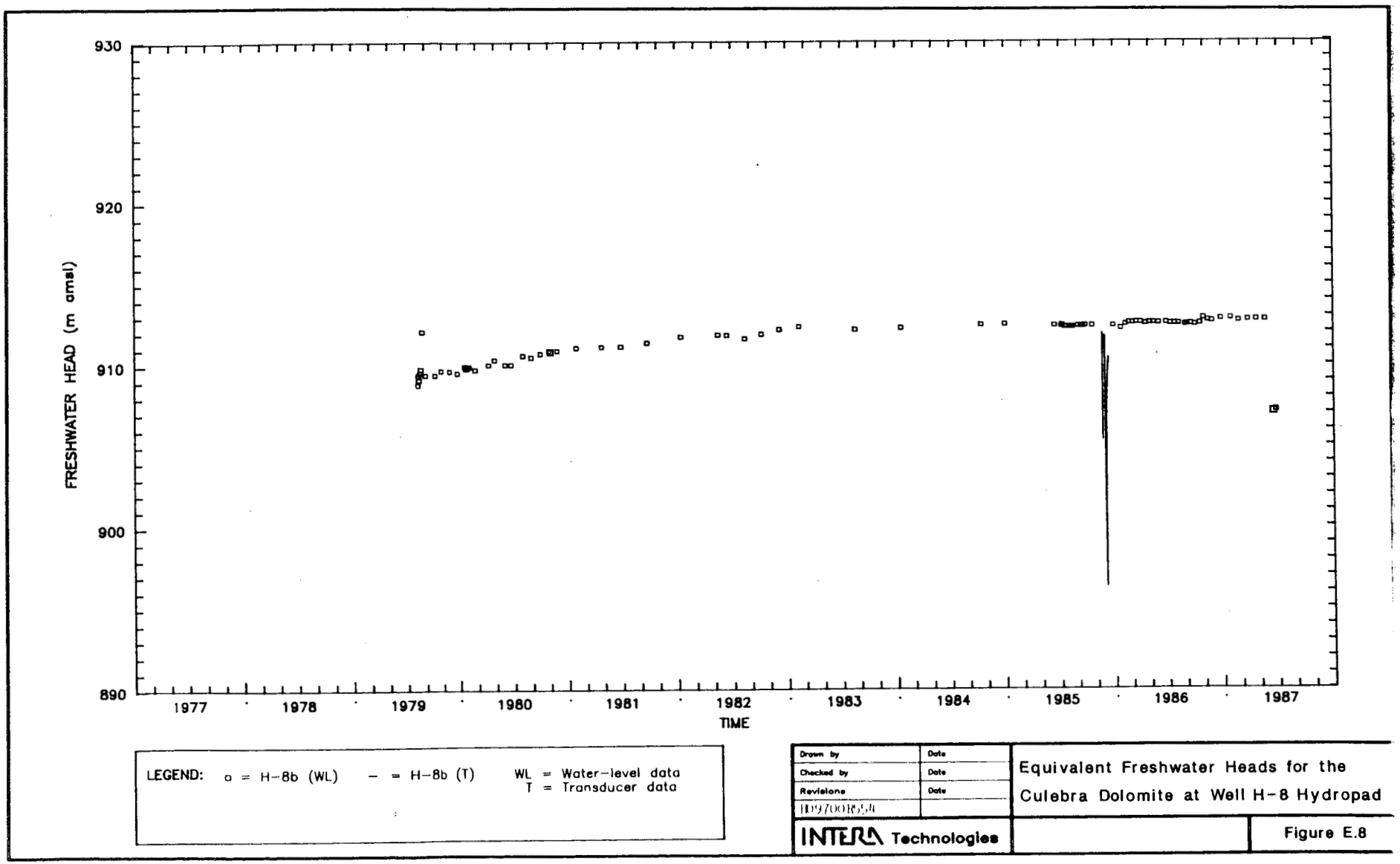
930
920
910
900
890
FRESHWATER HEAD (m amsl)
1977
1978
1979
1980
1981
1982
1983
1984
1985
1986
1987
TIME
LEGEND: o = H-8b (WL) – = H-8b (T)
WL = Water-level data
T = Transducer data
Drawn by
Date
Checked by
Date
Revisions
Date
ID970085A
INTERA Technologies
Equivalent Freshwater Heads for the Culebra Dolomite at Well H-8 Hydropad
Figure E.8

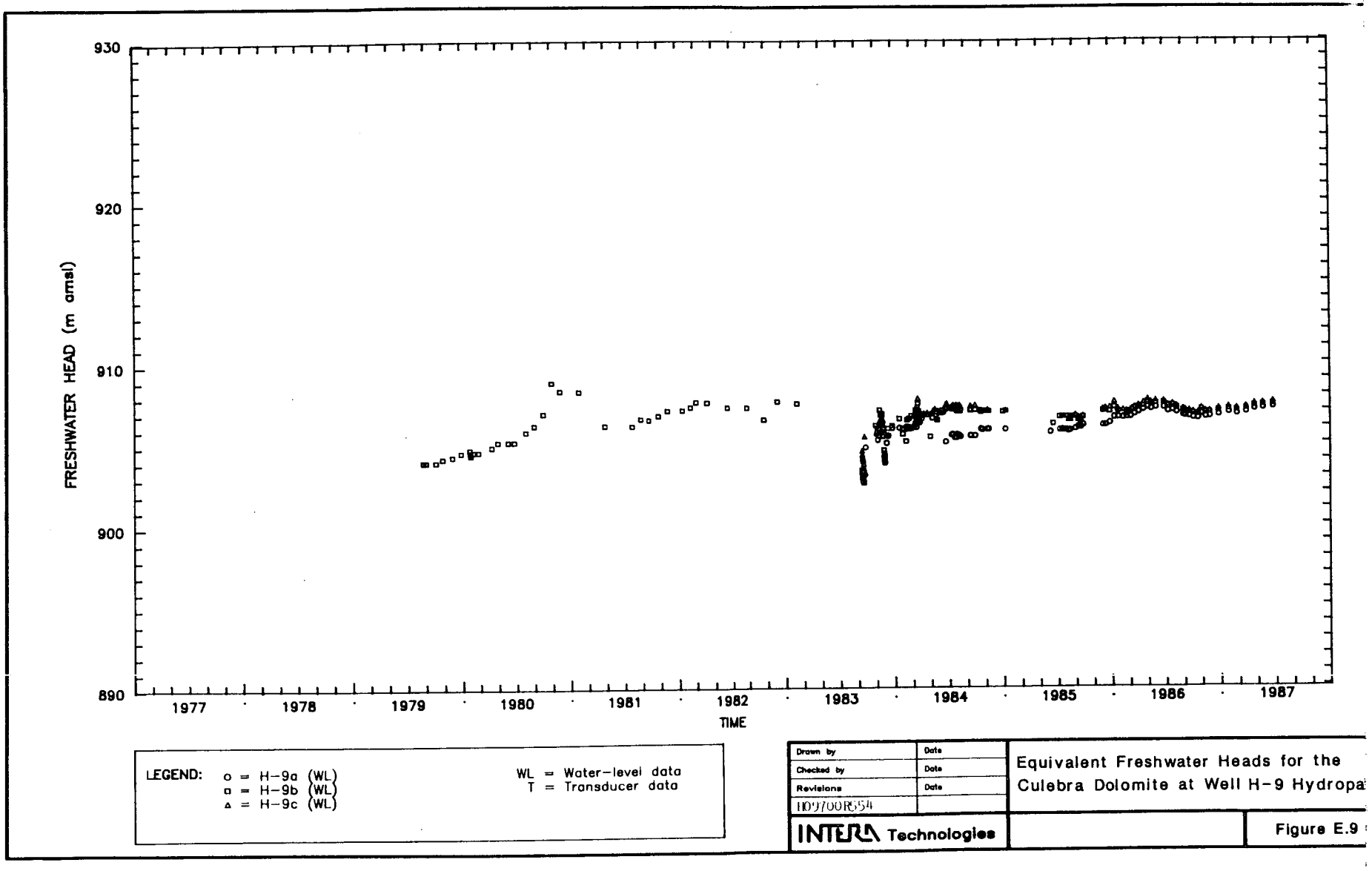
930
920
910
900
890
FRESHWATER HEAD (m amsl)
1977
1978
1979
1980
1981
1982
1983
1984
1985
1986
1987
TIME
LEGEND:
o = H-9a (WL)
□ = H-9b (WL)
△ = H-9c (WL)
WL = Water-level data
T = Transducer data
Drawn by
Date
Checked by
Date
Revisions
Date
109700R54
INTERA Technologies
Equivalent Freshwater Heads for the Culebra Dolomite at Well H-9 Hydropa
Figure E.9

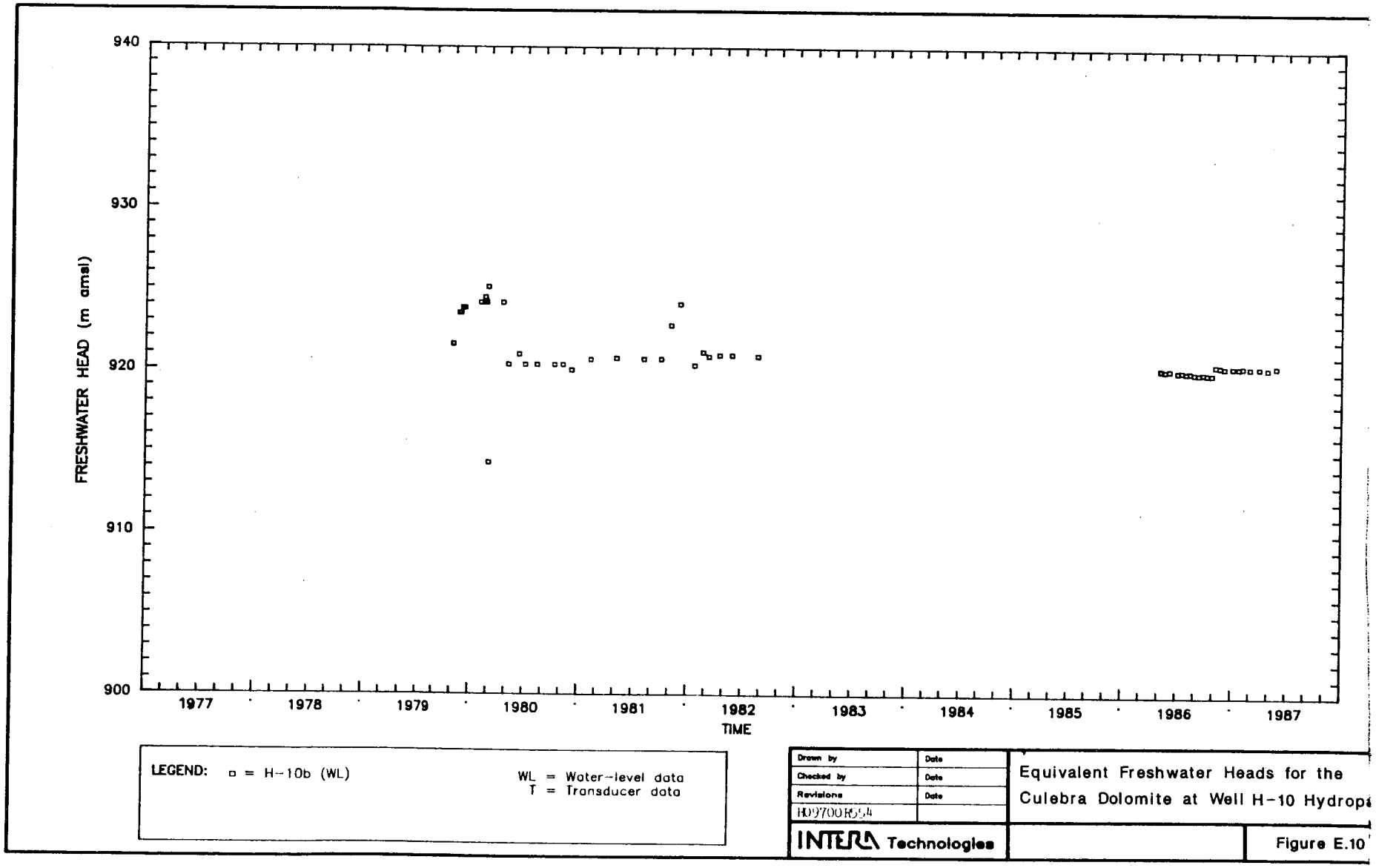
940
930
920
910
900
FRESHWATER HEAD (m amsl)
1977
1978
1979
1980
1981
1982
1983
1984
1985
1986
1987
TIME
LEGEND: ▫ = H-10b (WL)
WL = Water-level data
T = Transducer data
Drawn by
Date
Checked by
Date
Revisions
Date
H09700R5.4
INTERA Technologies
Equivalent Freshwater Heads for the Culebra Dolomite at Well H-10 Hydrop
Figure E.10

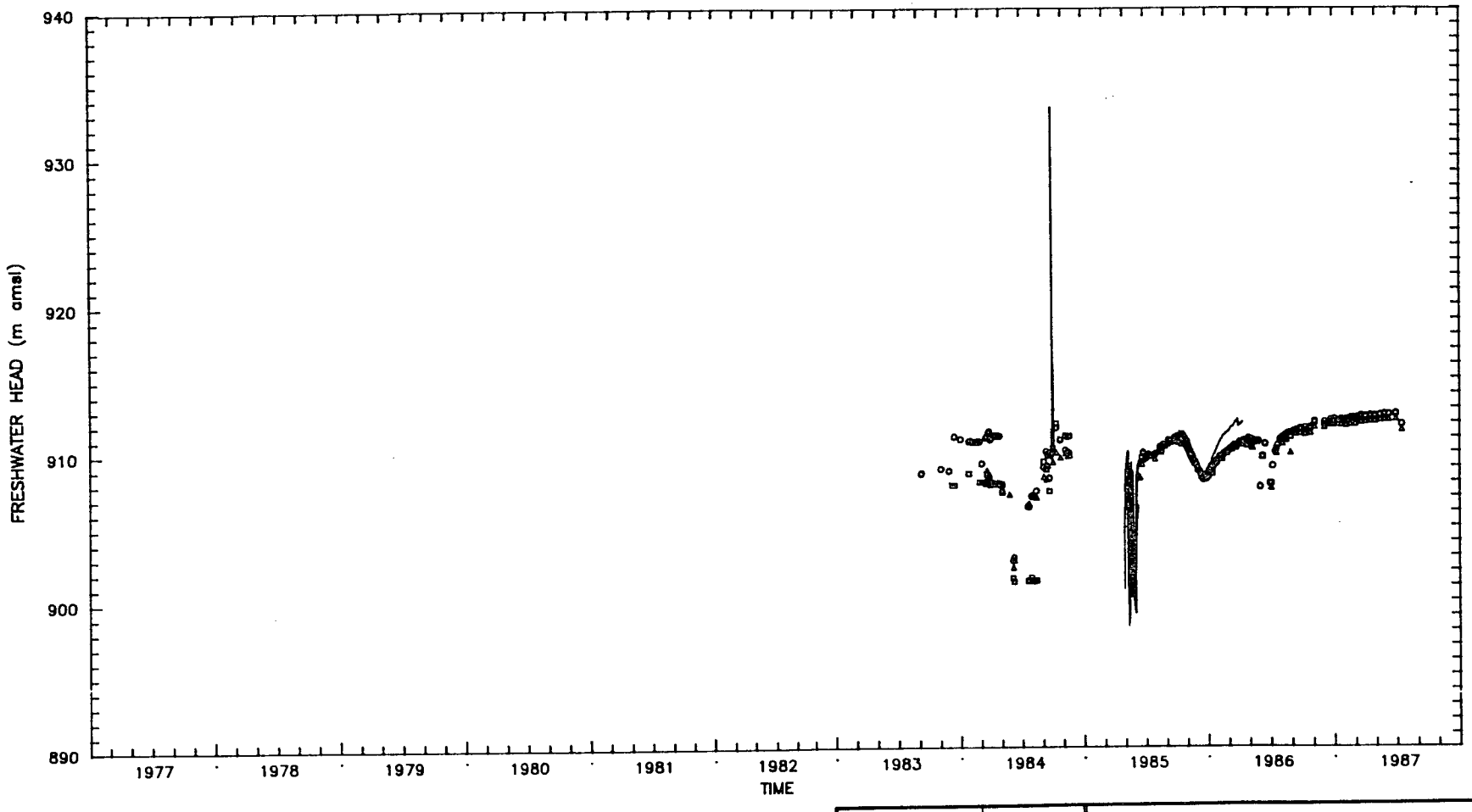

Equivalent Freshwater Heads for the Culebra Dolomite at Well H-11 Hydropad

Figure E.11

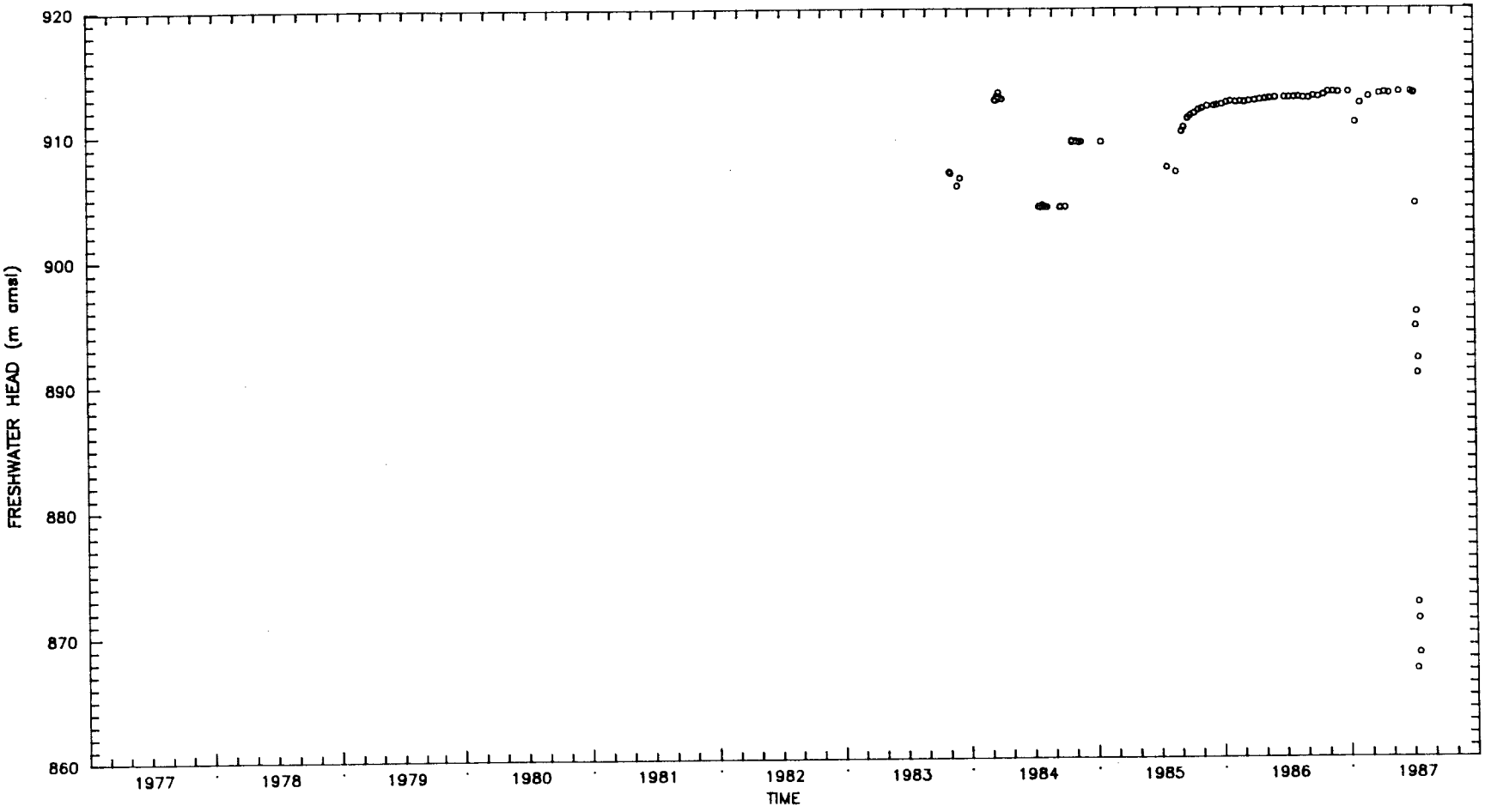

Equivalent Freshwater Heads for the Culebra Dolomite at Well H-12

Figure E.12

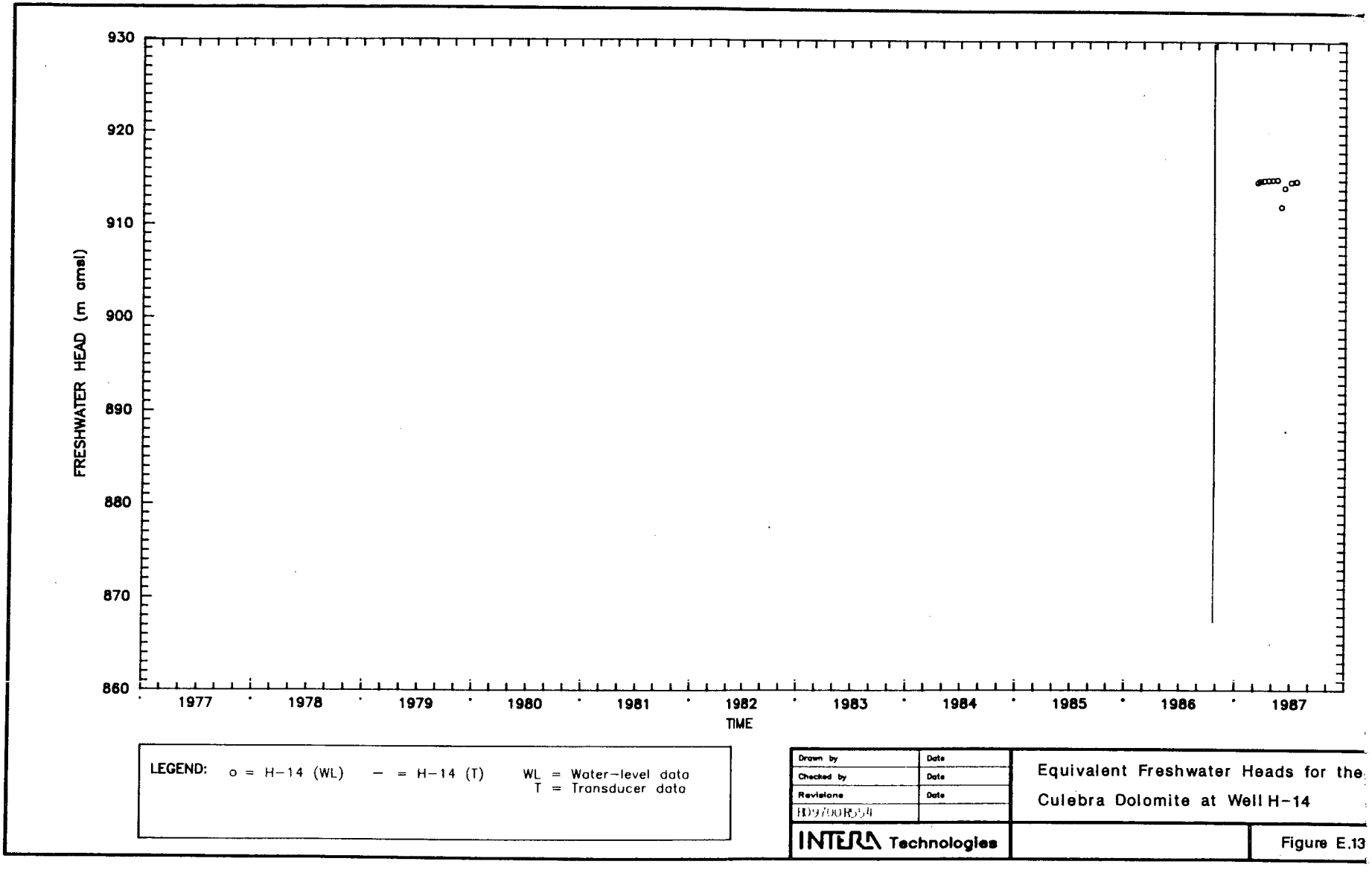
930
920
910
900
890
880
870
860
FRESHWATER HEAD (m amsl)
1977
1978
1979
1980
1981
1982
1983
1984
1985
1986
1987
TIME
LEGEND: o = H-14 (WL) – = H-14 (T) WL = Water-level data T = Transducer data
Drawn by
Date
Checked by
Date
Revisions
Date
HD9700R54
INTERA Technologies
Equivalent Freshwater Heads for the Culebra Dolomite at Well H-14
Figure E.13

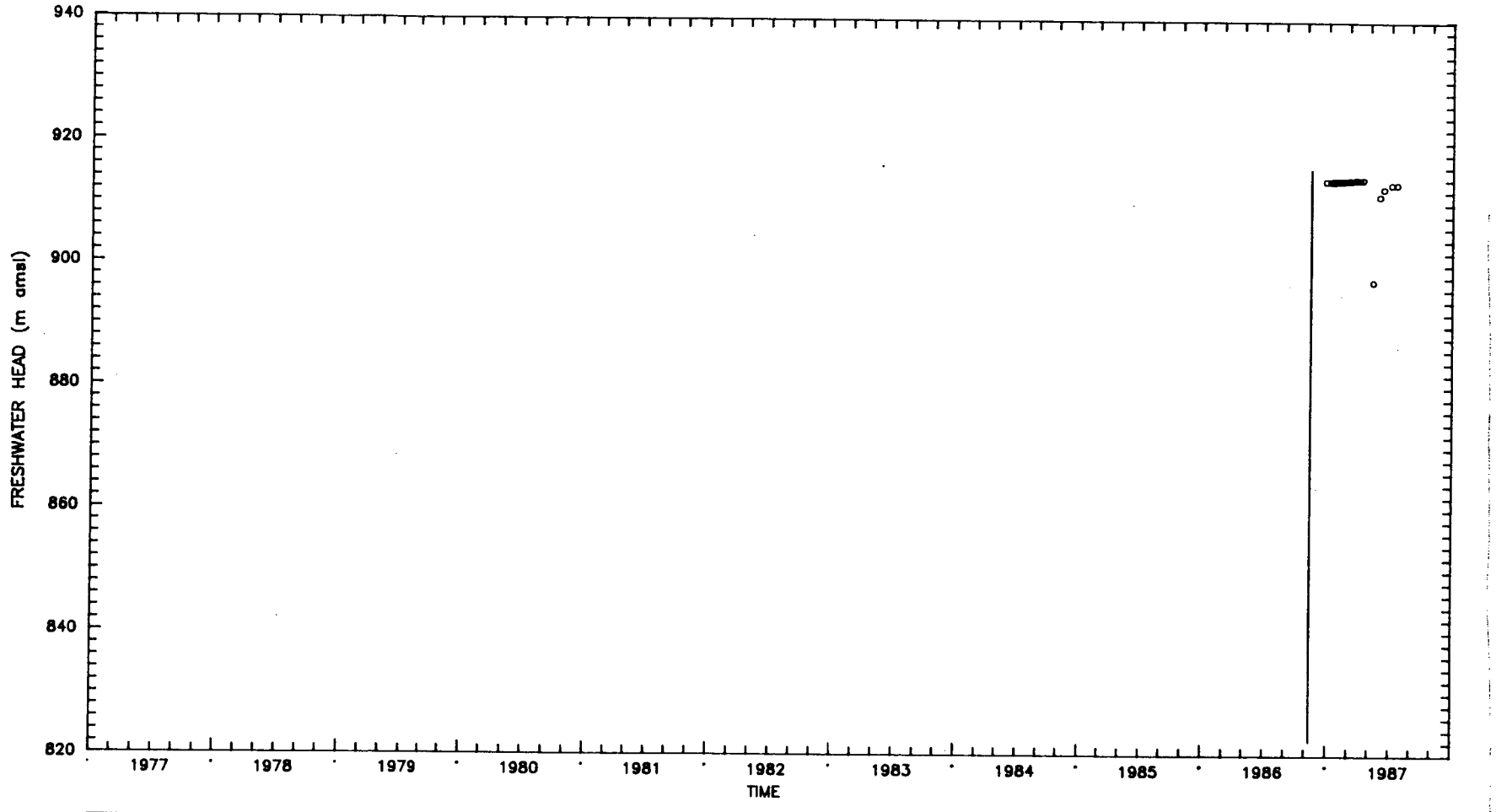
940
920
900
880
860
840
820
FRESHWATER HEAD (m amsl)
1977
1978
1979
1980
1981
1982
1983
1984
1985
1986
1987
TIME
LEGEND: o = H-15 (WL) – = H-15 (T) WL = Water-level data T = Transducer data
Drawn by
Date
Checked by
Date
Revisions
Date
INTERA Technologies
Equivalent Freshwater Heads for the Culebra Dolomite at Well H-15
Figure E.14

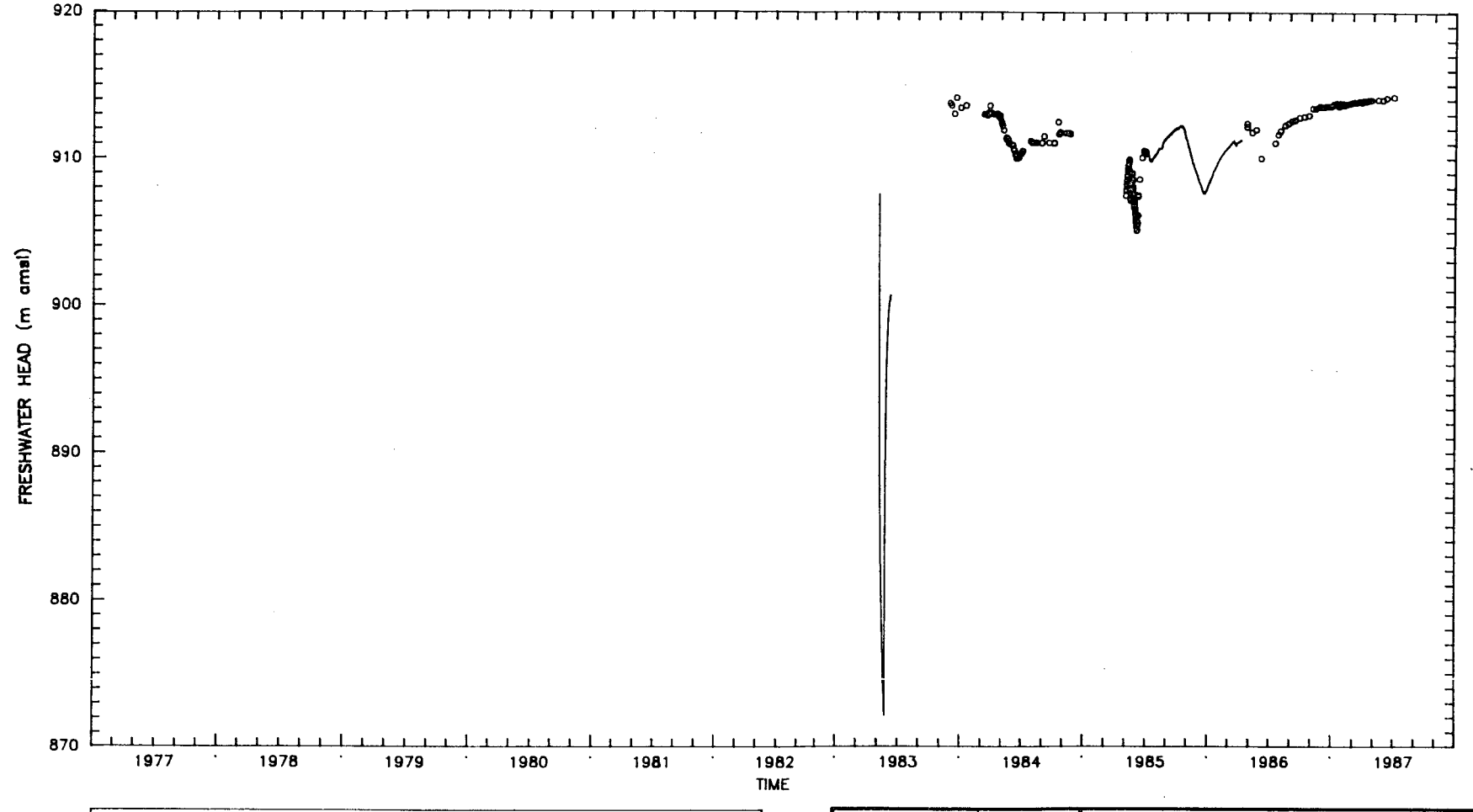

LEGEND: o = DOE-1 (WL) – = DOE-1 (T) WL = Water-level data T = Transducer data

Drawn by	Date
Checked by	Date
Revisions	Date
[illegible]	

INTERA Technologies

Equivalent Freshwater Heads for the Culebra Dolomite at Well DOE-1

Figure E.15

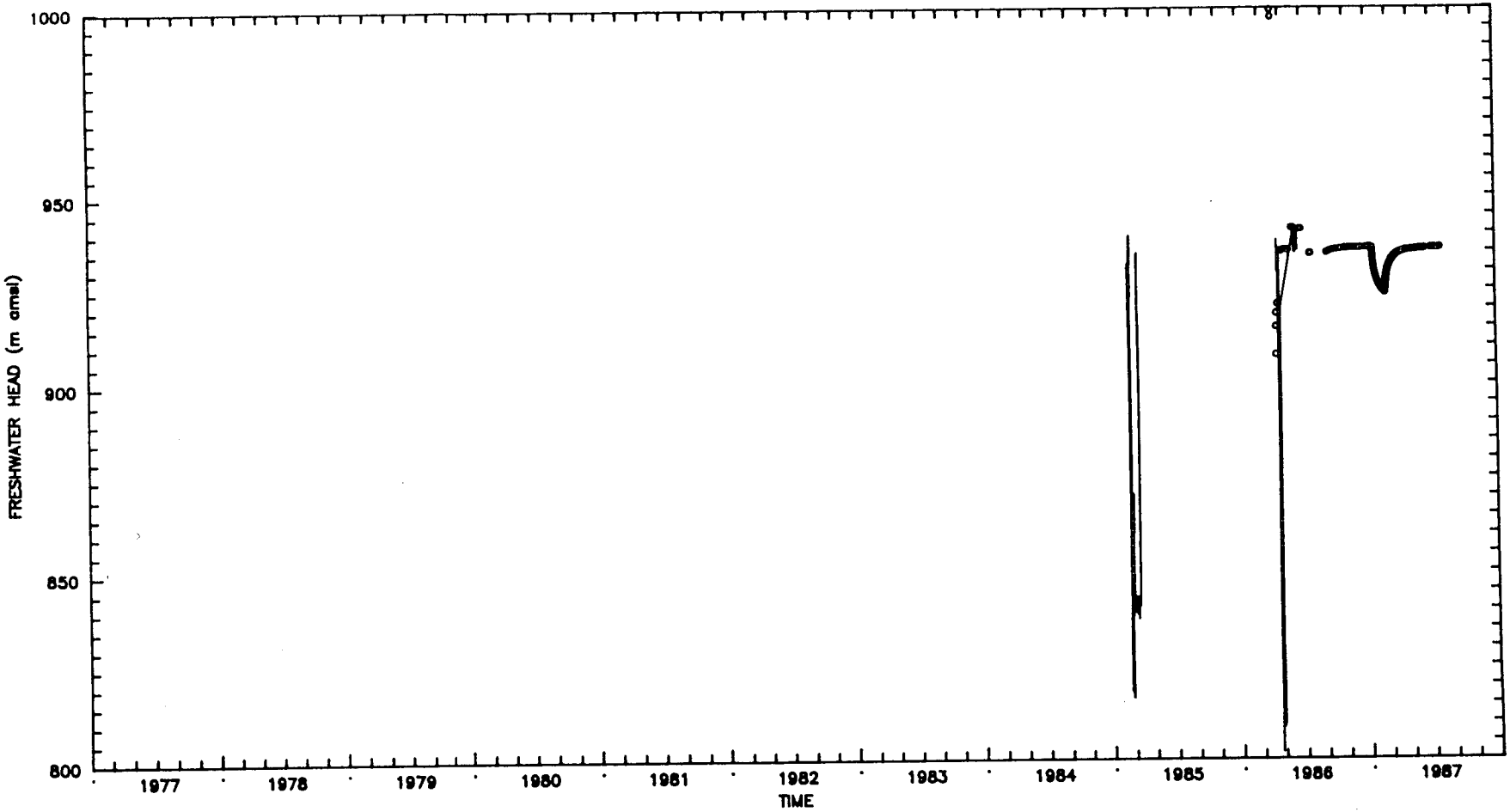

LEGEND: o = DOE-2 (WL) – = DOE-2 (T) WL = Water-level data &T = Transducer data

Drawn by	Date
Checked by	Date
Revisions	Date

INTERA Technologies

Equivalent Freshwater Heads for the Culebra Dolomite at Well DOE-2

Figure E.16

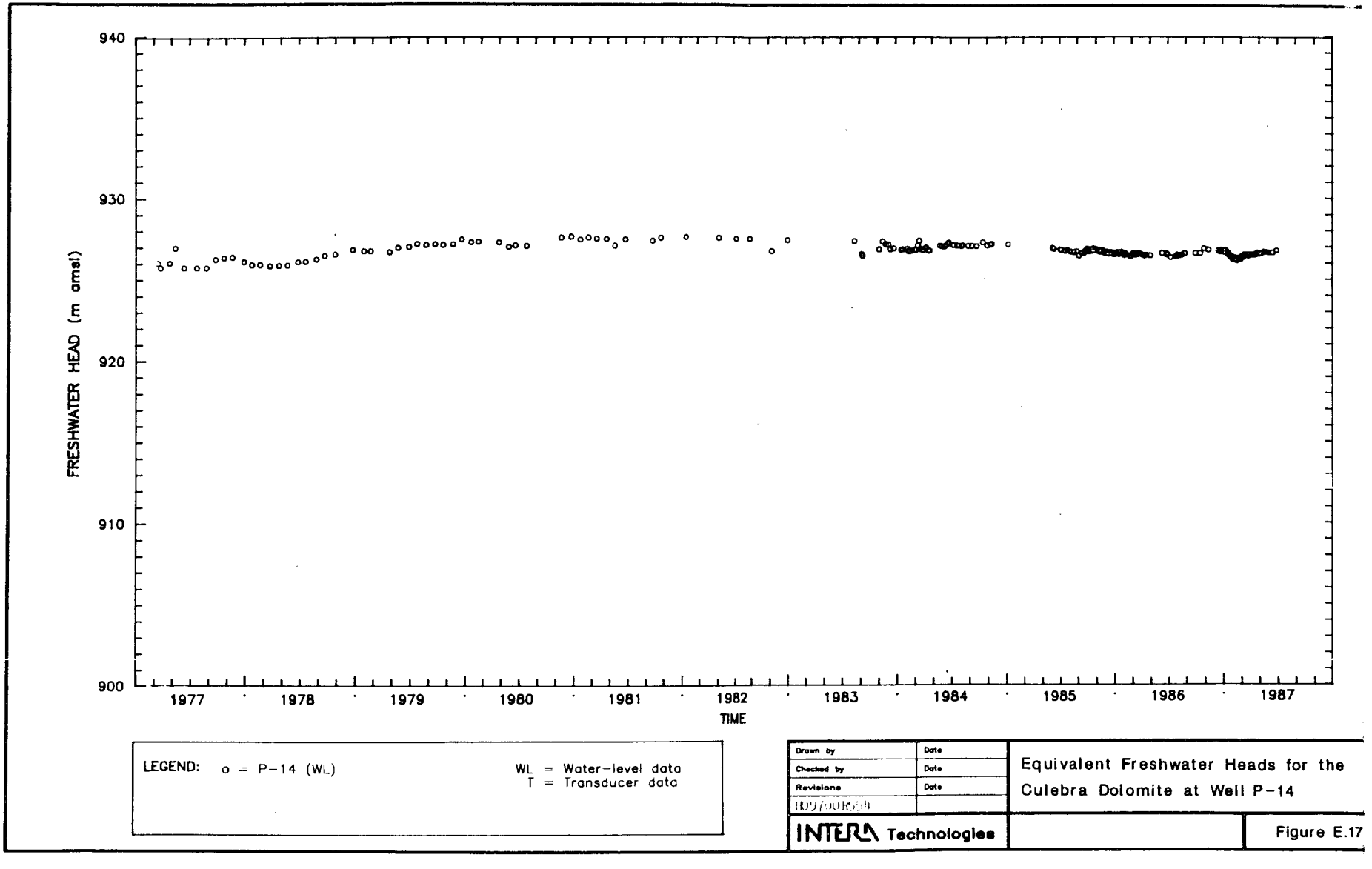
940
930
920
910
900
FRESHWATER HEAD (m amsl)
1977
1978
1979
1980
1981
1982
1983
1984
1985
1986
1987
TIME
LEGEND: o = P-14 (WL)
WL = Water-level data
T = Transducer data
Drawn by
Date
Checked by
Date
Revisions
Date
INTERA Technologies
Equivalent Freshwater Heads for the Culebra Dolomite at Well P-14
Figure E.17

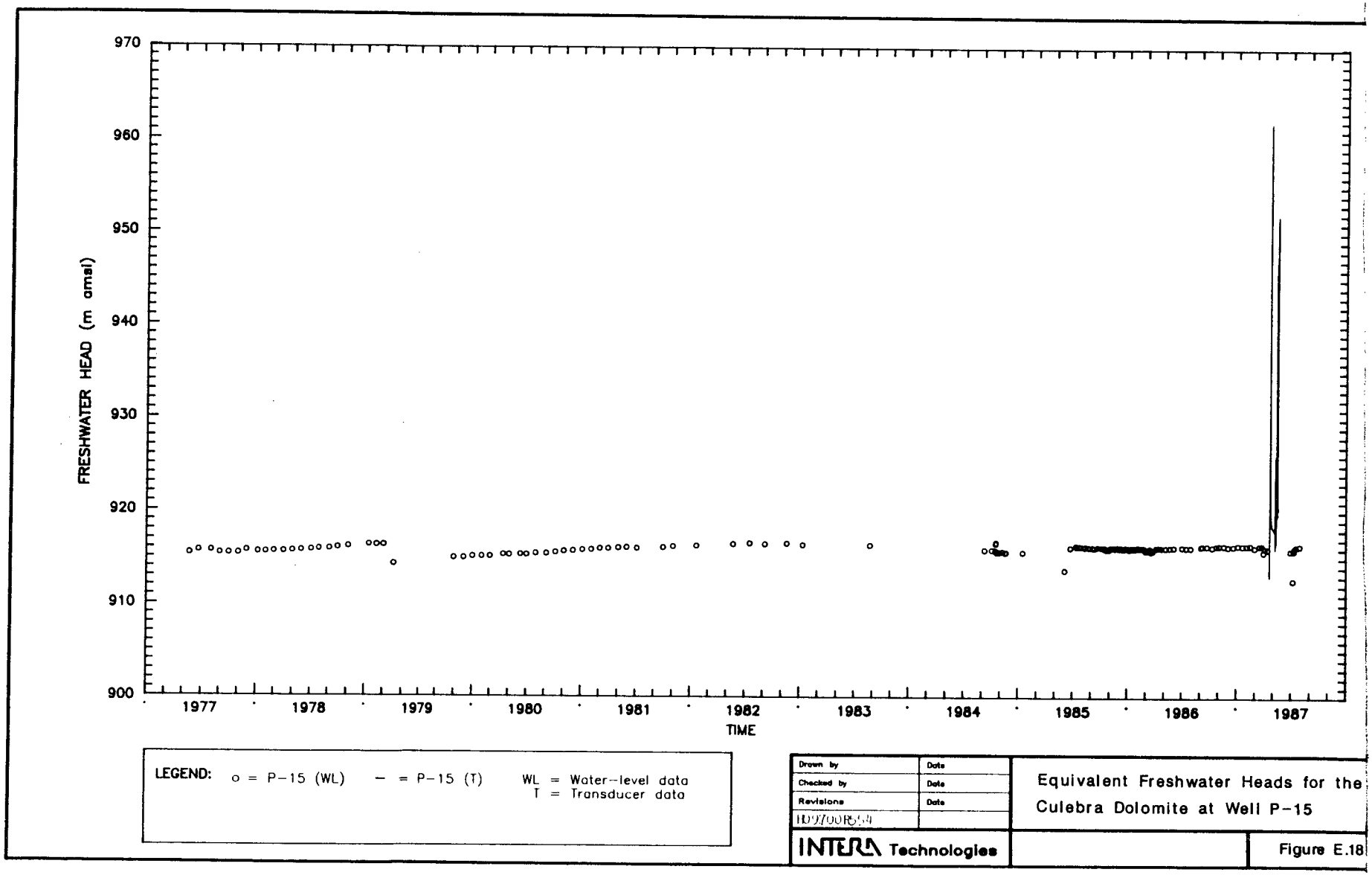
970
960
950
940
930
920
910
900
FRESHWATER HEAD (m amsl)
1977
1978
1979
1980
1981
1982
1983
1984
1985
1986
1987
TIME
LEGEND: o = P-15 (WL) – = P-15 (T) WL = Water-level data T = Transducer data
Drawn by
Checked by
Revisions
Date
Date
Date
Equivalent Freshwater Heads for the Culebra Dolomite at Well P-15
INTERA Technologies
Figure E.18

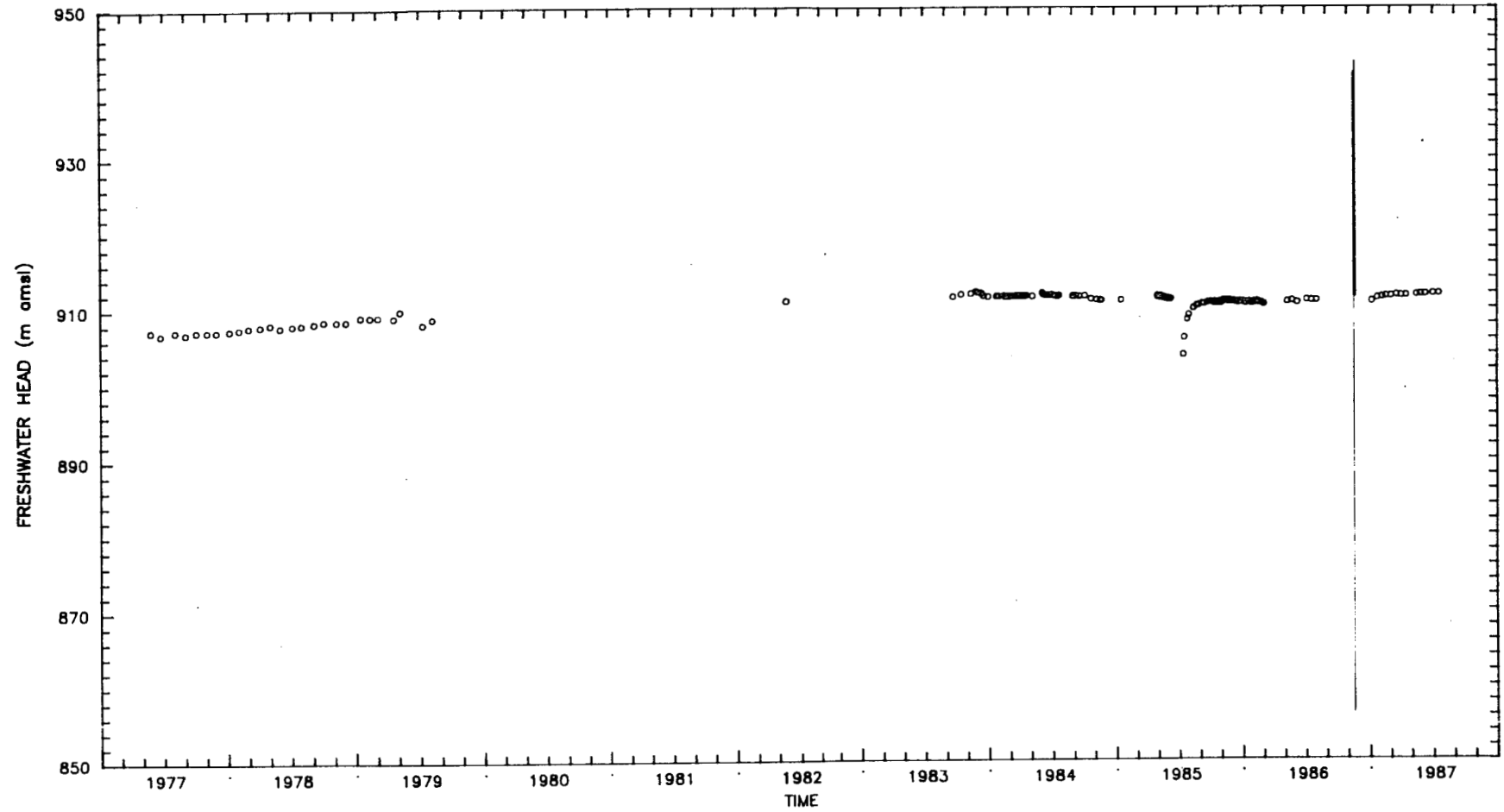

LEGEND: o = P-17 (WL) – = P-17 (T) WL = Water-level data T = Transducer data

Drawn by	Date
Checked by	Date
Revisions	Date
INTERA Technologies	

Equivalent Freshwater Heads for the Culebra Dolomite at Well P-17

Figure E.19

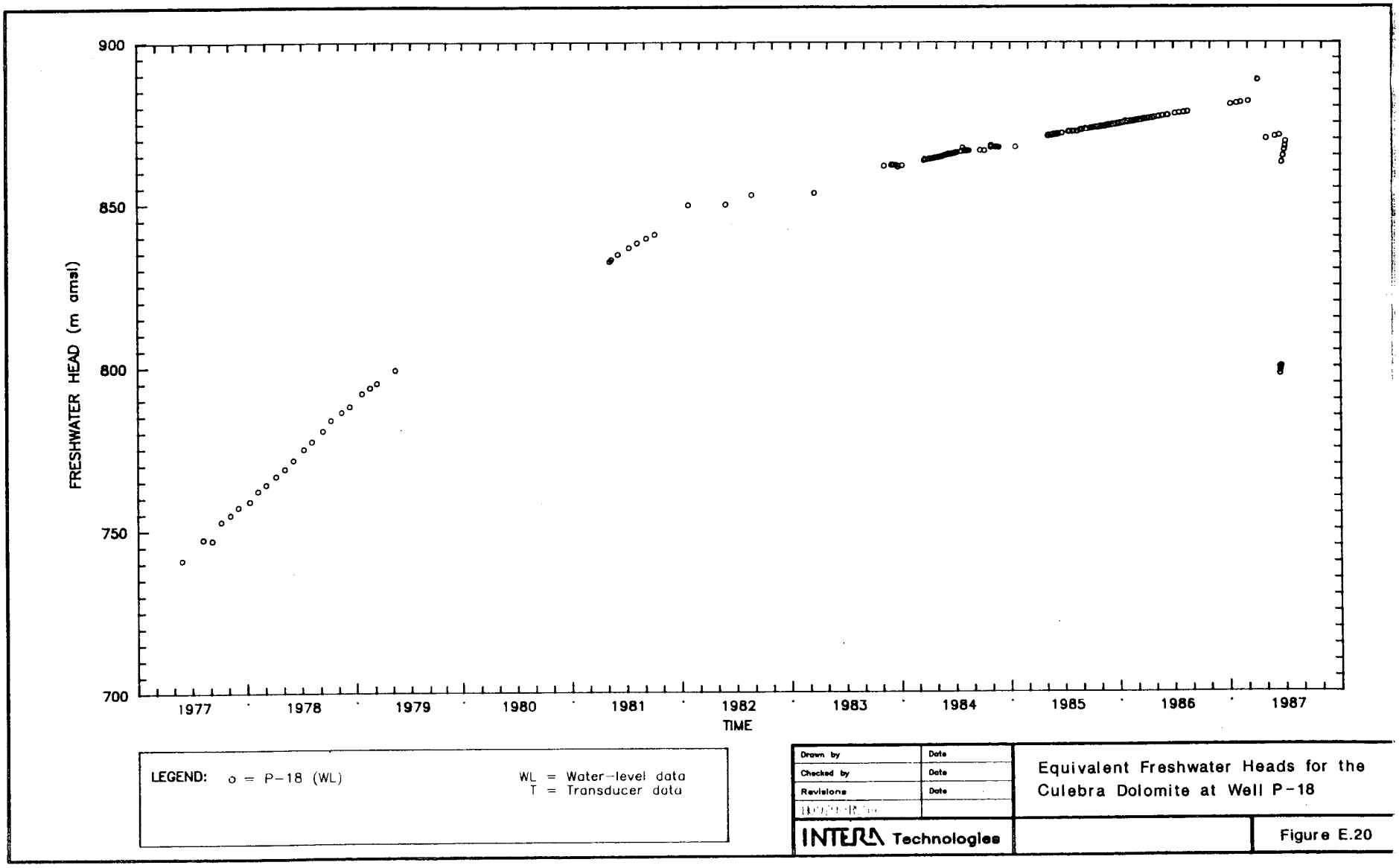
900
850
800
750
700
FRESHWATER HEAD (m amsl)
1977
1978
1979
1980
1981
1982
1983
1984
1985
1986
1987
TIME
LEGEND: o = P-18 (WL)
WL = Water-level data
T = Transducer data
Drawn by
Date
Checked by
Date
Revisions
Date
INTERA Technologies
Equivalent Freshwater Heads for the Culebra Dolomite at Well P-18
Figure E.20

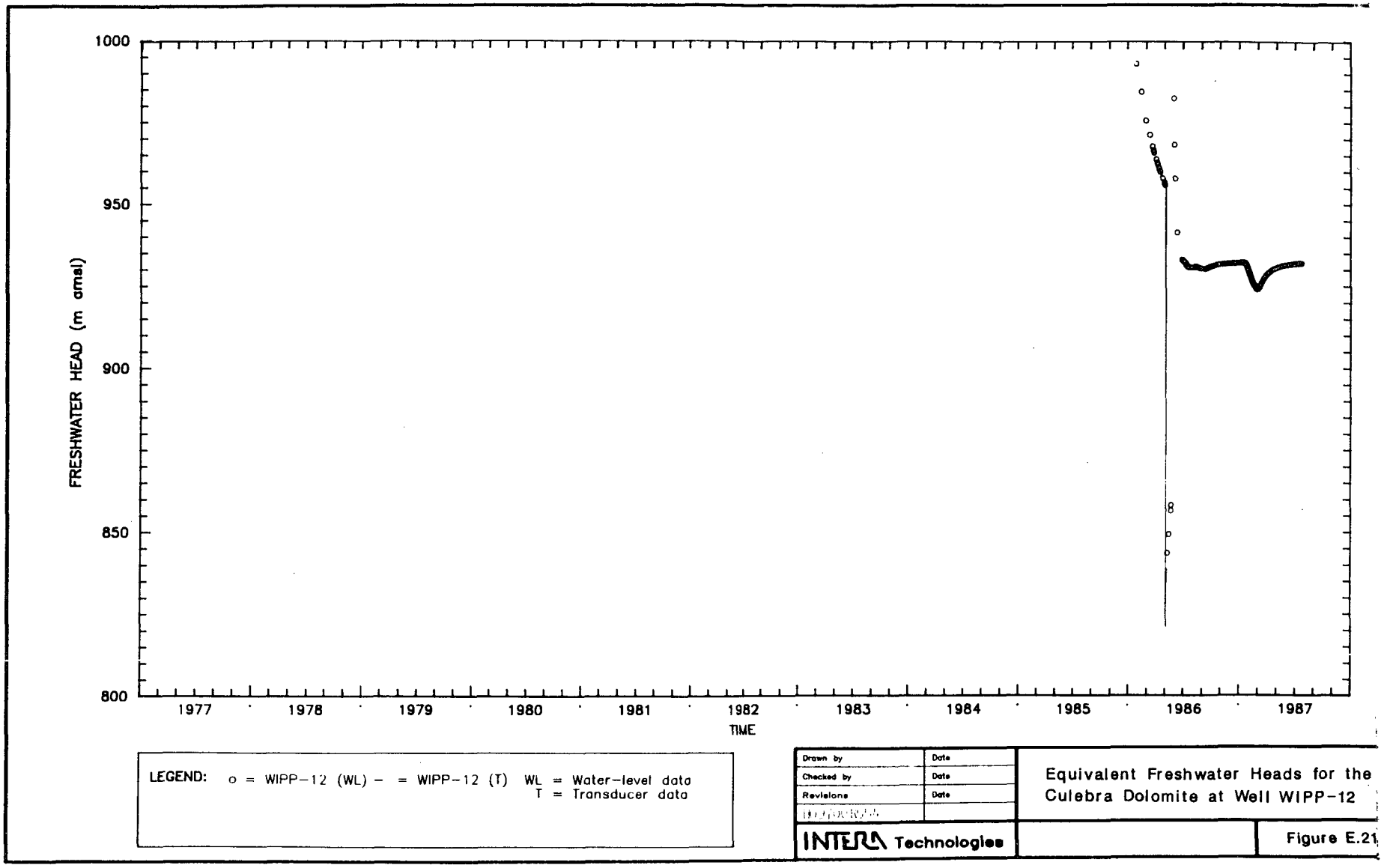
1000
950
900
850
800
FRESHWATER HEAD (m amsl)
1977
1978
1979
1980
1981
1982
1983
1984
1985
1986
1987
TIME
LEGEND: o = WIPP-12 (WL) - = WIPP-12 (T) WL = Water-level data
T = Transducer data
Drawn by
Date
Checked by
Date
Revisions
Date
INTERA Technologies
Equivalent Freshwater Heads for the Culebra Dolomite at Well WIPP-12
Figure E.21

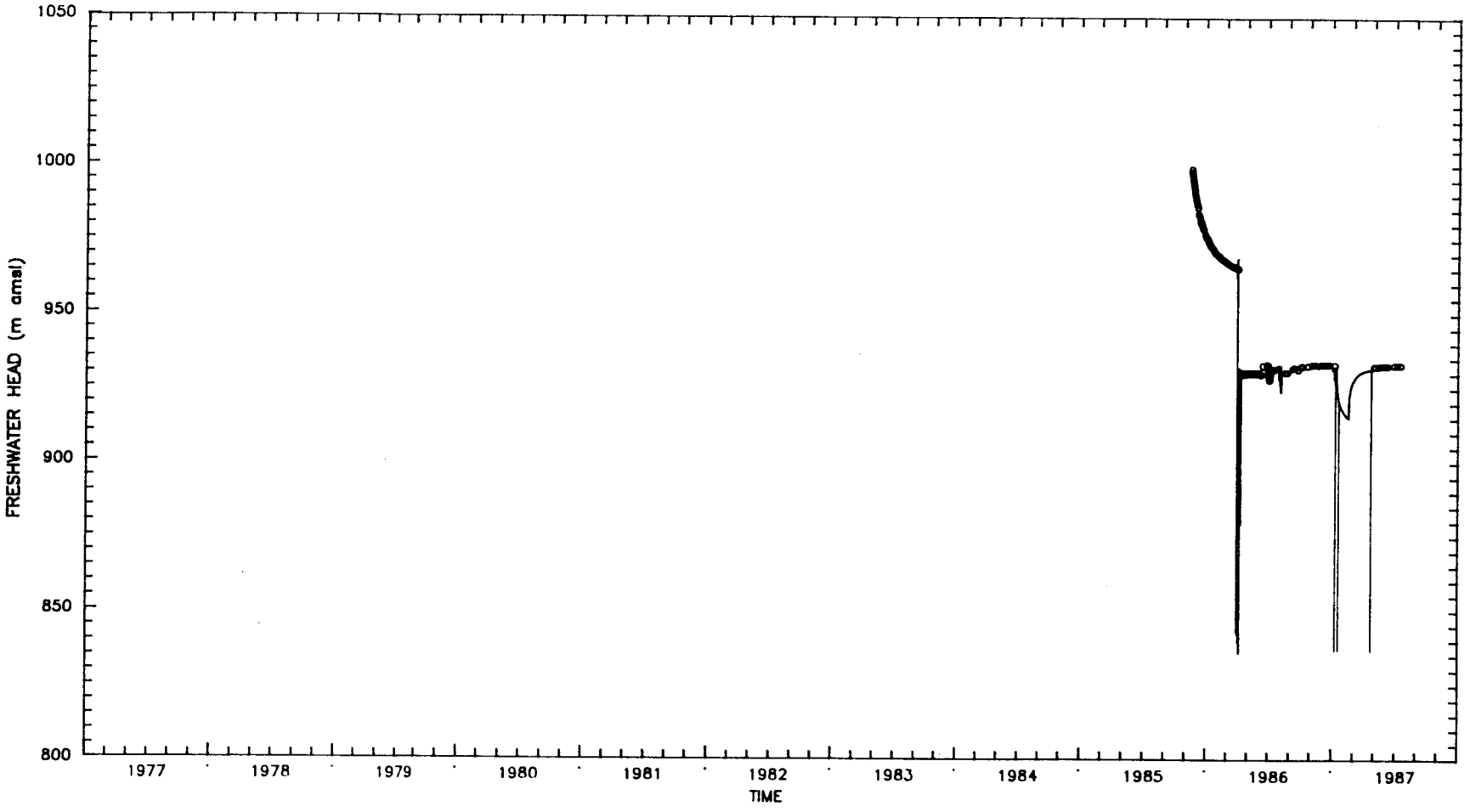

LEGEND: o = WIPP-13 (WL) - = WIPP-13 (T) WL = Water-level data
T = Transducer data

Drawn by	Date
Checked by	Date
Revisions	Date

INTERA Technologies

Equivalent Freshwater Heads for the Culebra Dolomite at Well WIPP-13

Figure E.22

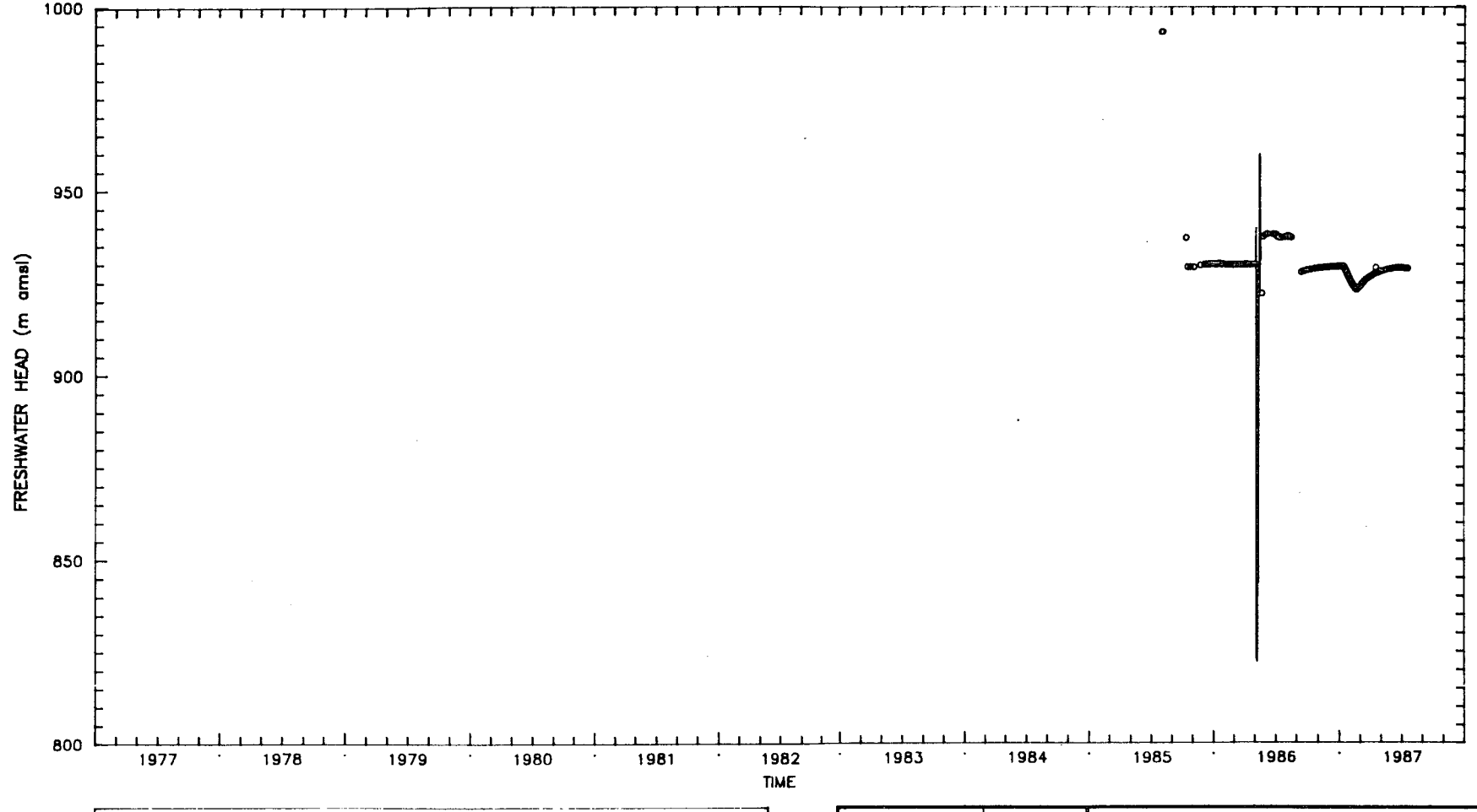

LEGEND: o = WIPP-18 (WL) — = WIPP-18 (T) WL = Water-level data T = Transducer data

Drawn by	Date
Checked by	Date
Revisions	Date

INTERA Technologies

Equivalent Freshwater Heads for the Culebra Dolomite at Well WIPP-18

Figure E.23

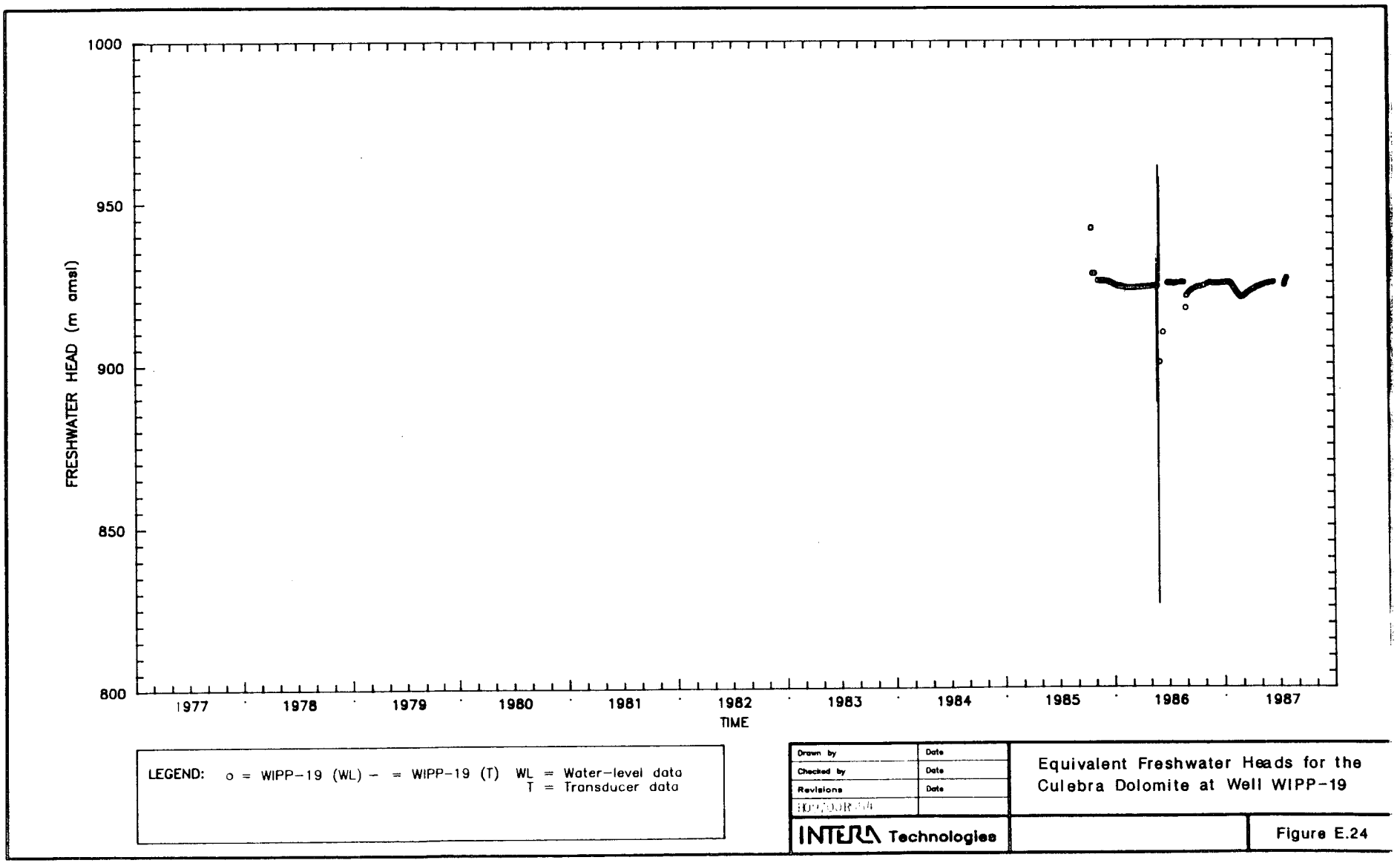
1000
950
900
850
800
FRESHWATER HEAD (m amsl)
1977
1978
1979
1980
1981
1982
1983
1984
1985
1986
1987
TIME
LEGEND: o = WIPP-19 (WL) – = WIPP-19 (T) WL = Water-level data
T = Transducer data
Drawn by
Date
Checked by
Date
Revisions
Date
INTERA Technologies
Equivalent Freshwater Heads for the Culebra Dolomite at Well WIPP-19
Figure E.24

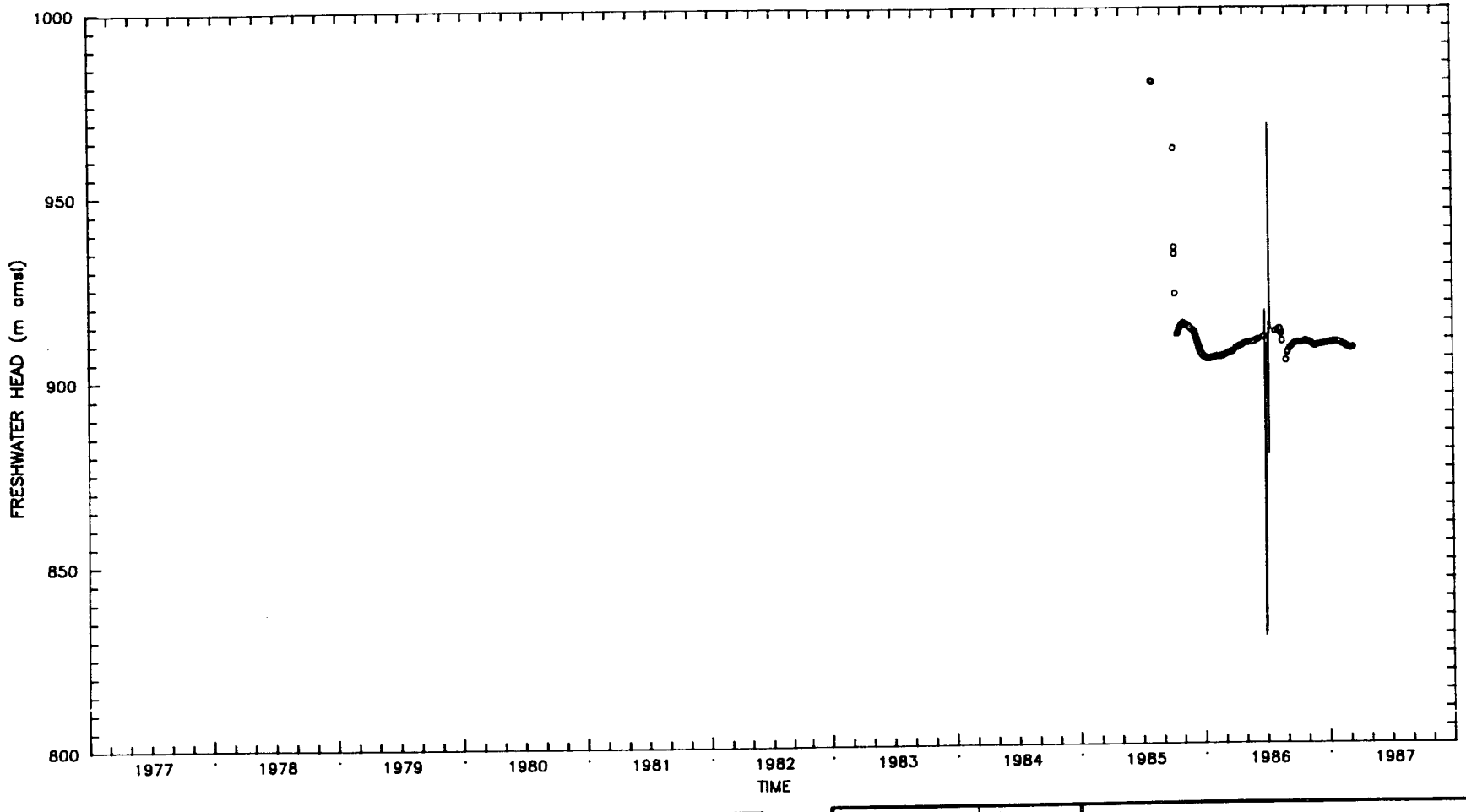

LEGEND: o = WIPP-21 (WL) – = WIPP-21 (T) WL = Water-level data T = Transducer data

Drawn by	Date
Checked by	Date
Revisions	Date
[illegible]	

INTERA Technologies

Equivalent Freshwater Heads for the Culebra Dolomite at Well WIPP-21

Figure E.25

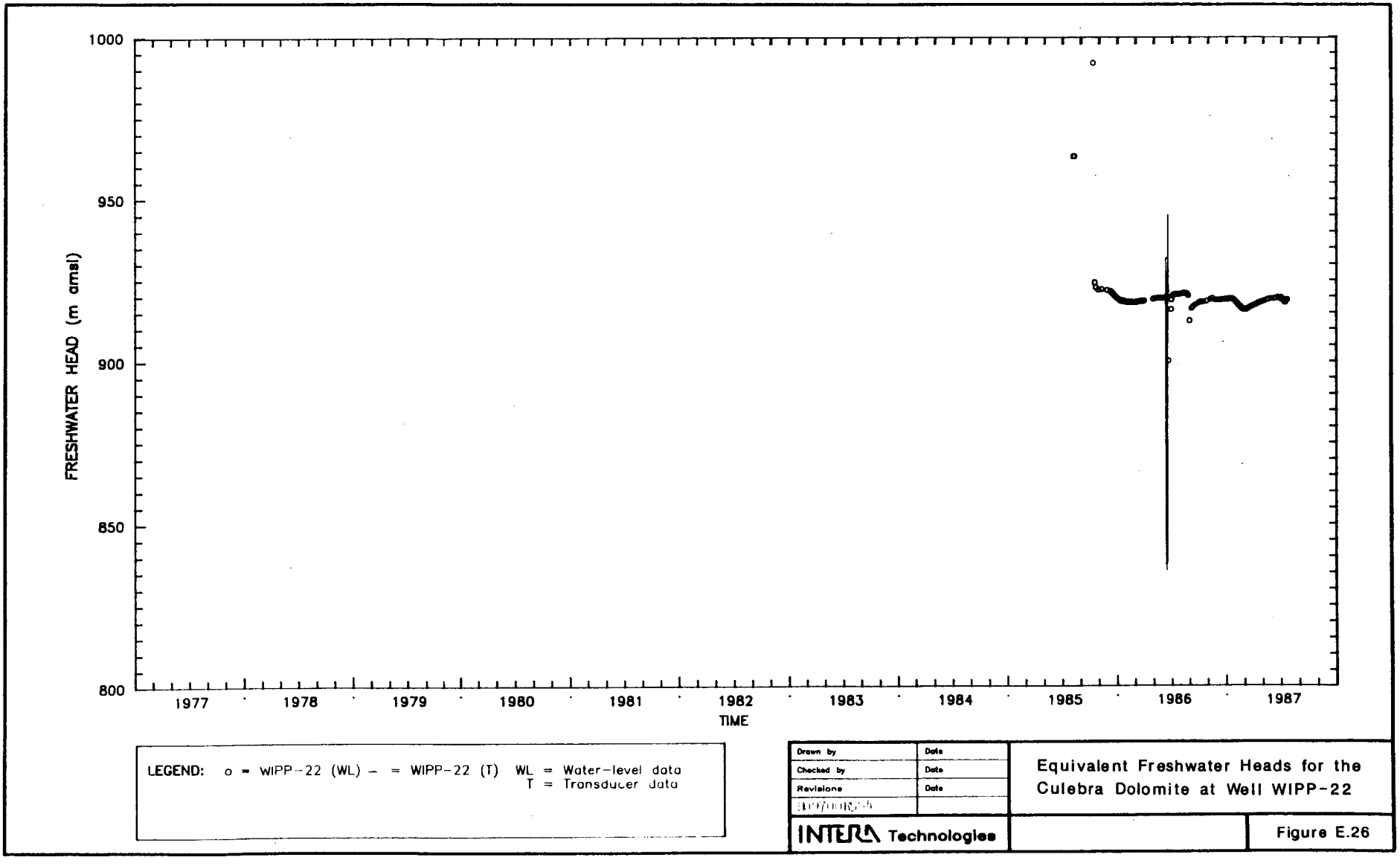
1000
950
900
850
800
FRESHWATER HEAD (m amsl)
1977
1978
1979
1980
1981
1982
1983
1984
1985
1986
1987
TIME
LEGEND: o = WIPP-22 (WL) – = WIPP-22 (T) WL = Water-level data
T = Transducer data
Drawn by
Date
Checked by
Date
Revisions
Date
INTERA Technologies
Equivalent Freshwater Heads for the Culebra Dolomite at Well WIPP-22
Figure E.26

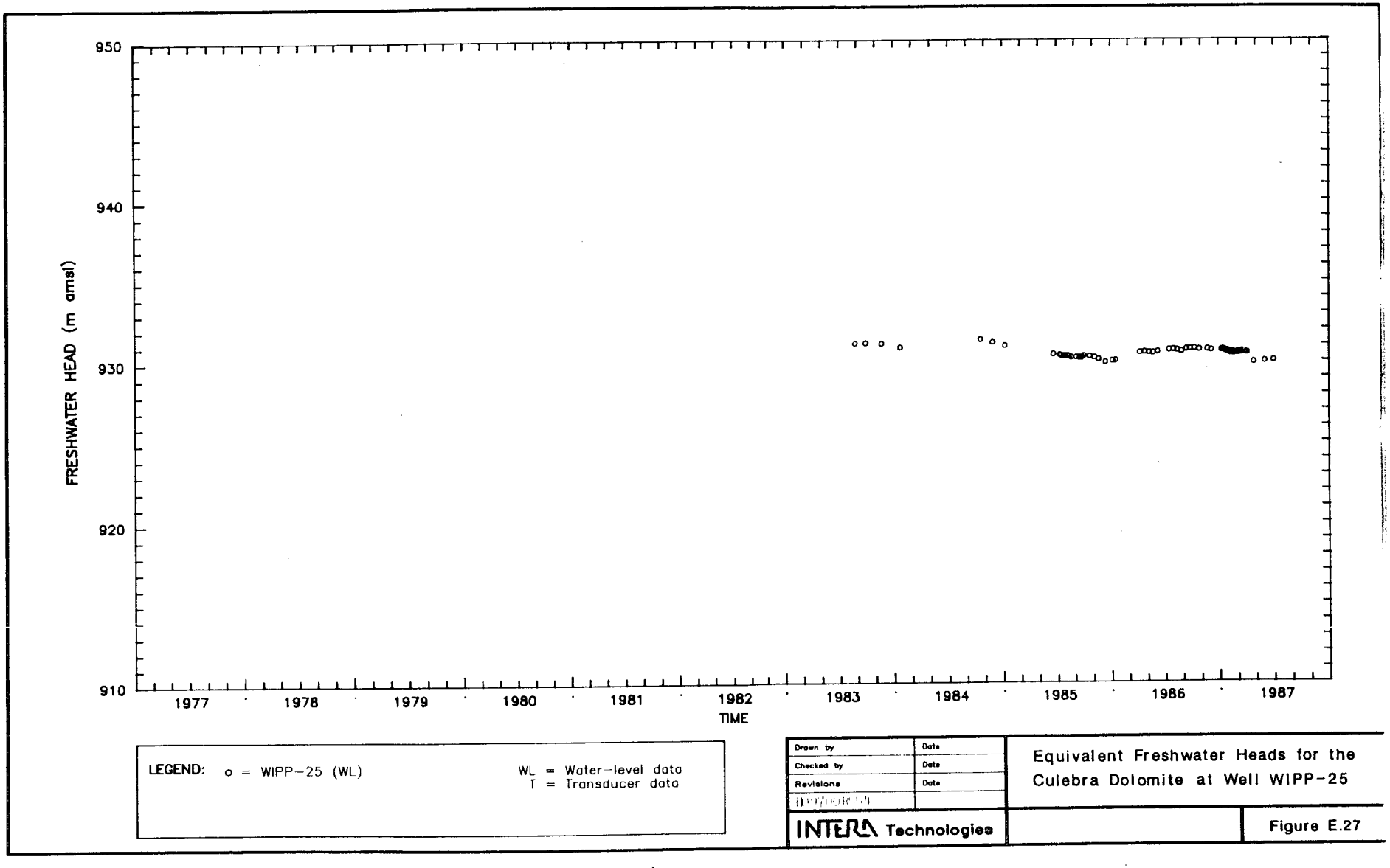
950
940
930
920
910
FRESHWATER HEAD (m amsl)
1977
1978
1979
1980
1981
1982
1983
1984
1985
1986
1987
TIME
LEGEND: o = WIPP-25 (WL)
WL = Water-level data
T = Transducer data
Drawn by
Date
Checked by
Date
Revisions
Date
INTERA Technologies
Equivalent Freshwater Heads for the Culebra Dolomite at Well WIPP-25
Figure E.27

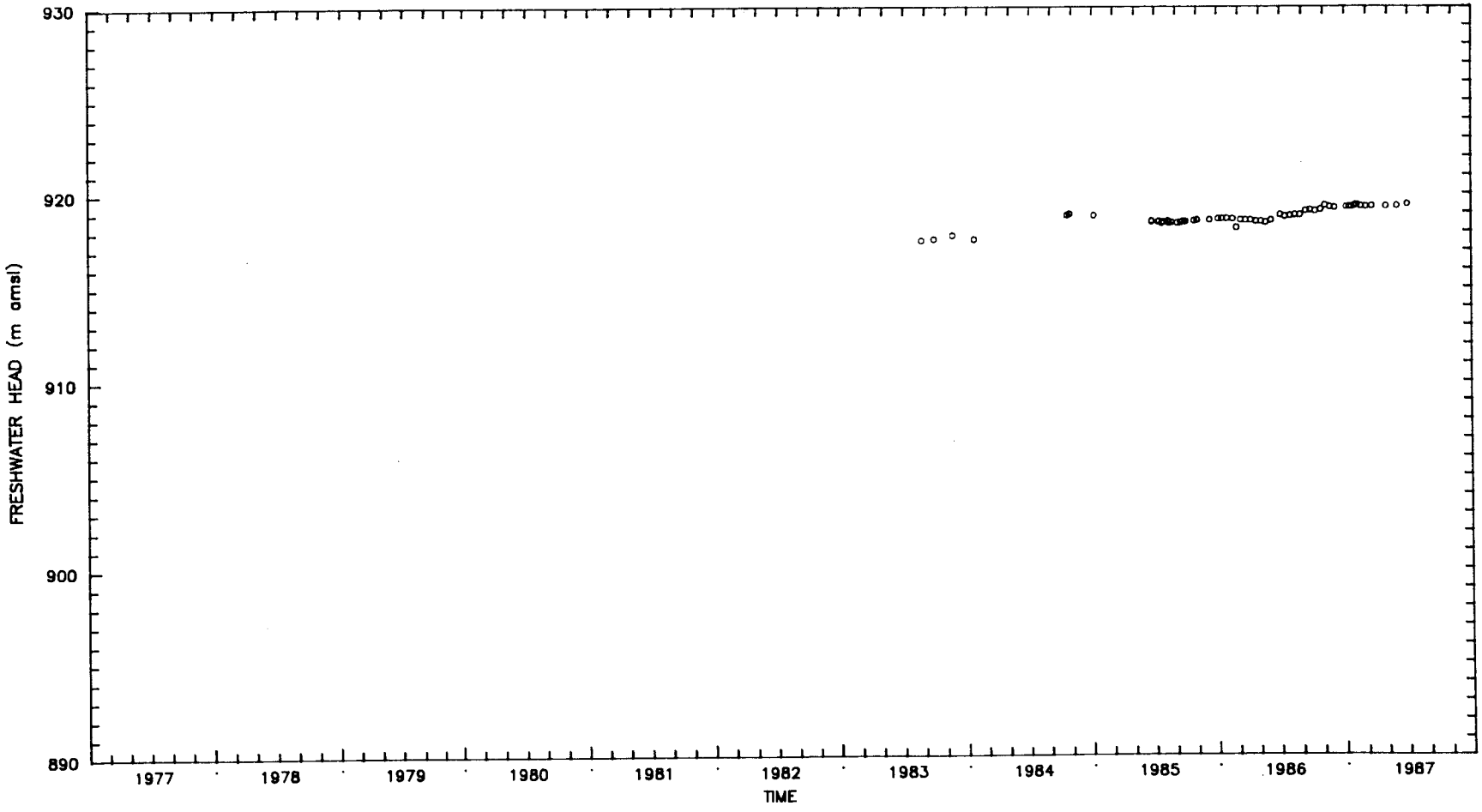

LEGEND: o = WIPP-26 (WL)

WL = Water-level data
T = Transducer data

Drawn by	Date
Checked by	Date
Revisions	Date

INTERA Technologies

Equivalent Freshwater Heads for the Culebra Dolomite at Well WIPP-26

Figure E.28

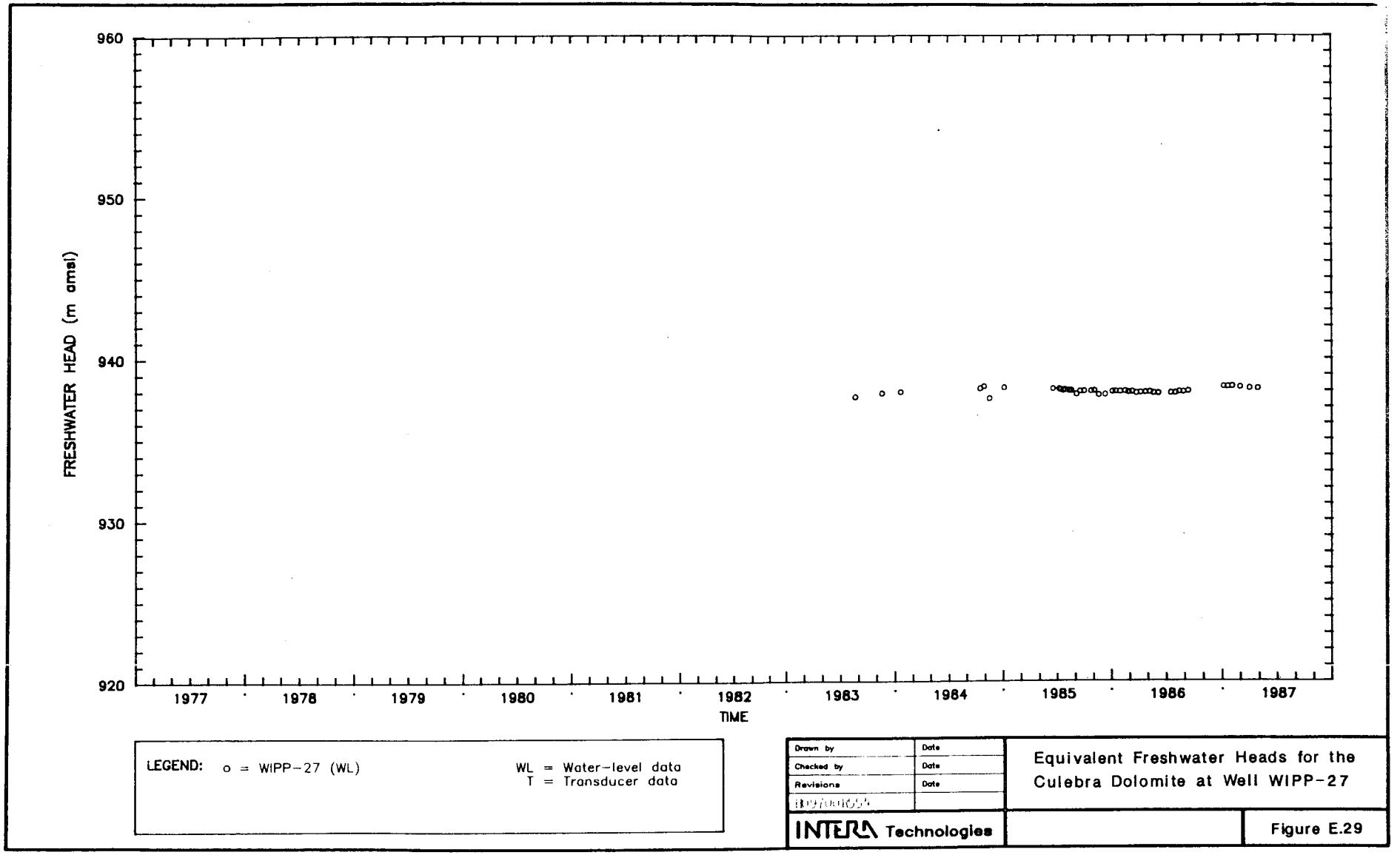
960
950
940
930
920
FRESHWATER HEAD (m amsl)
1977
1978
1979
1980
1981
1982
1983
1984
1985
1986
1987
TIME
LEGEND: o = WIPP-27 (WL)
WL = Water-level data
T = Transducer data
Drawn by
Date
Checked by
Date
Revisions
Date
INTERA Technologies
Equivalent Freshwater Heads for the Culebra Dolomite at Well WIPP-27
Figure E.29

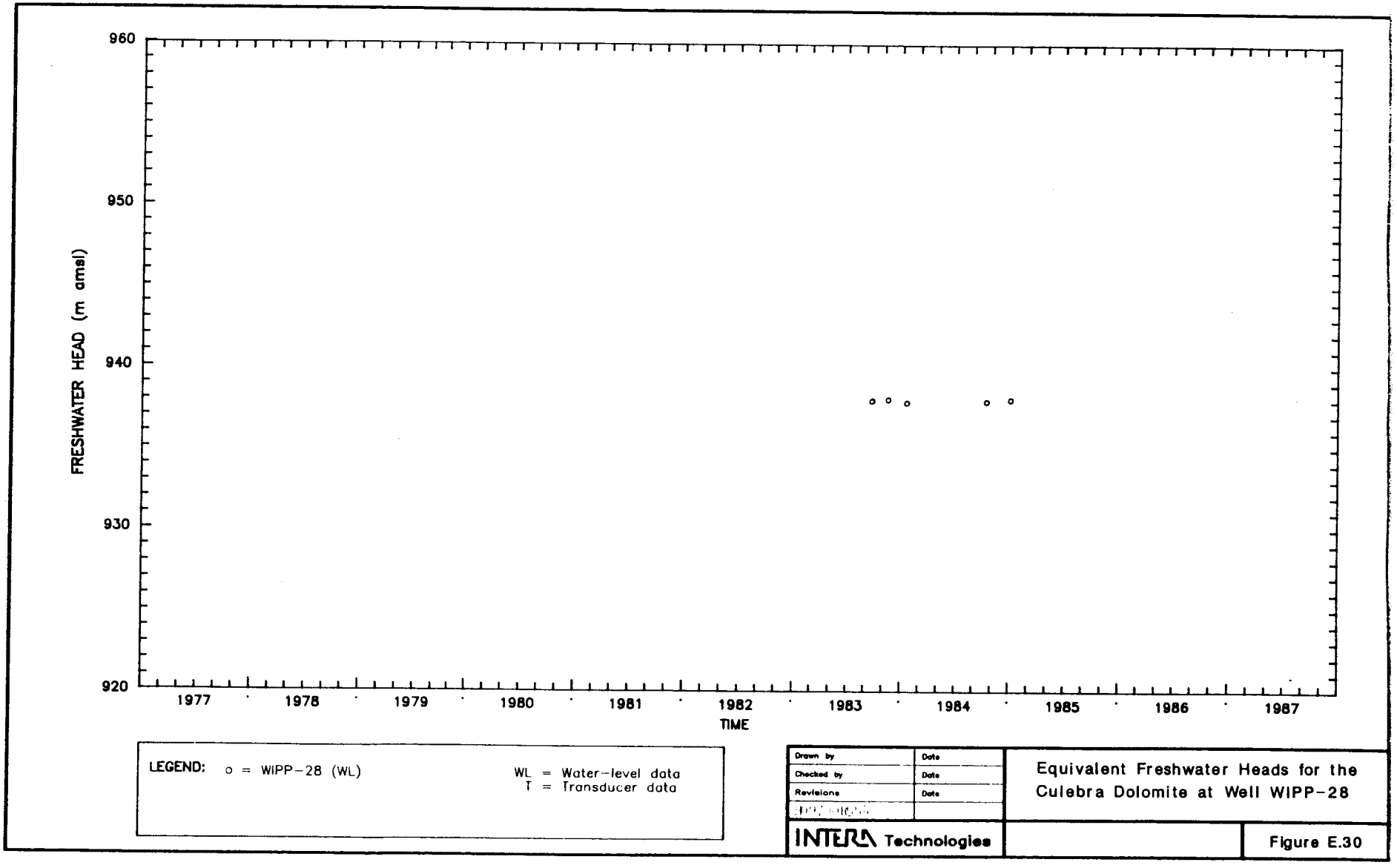
960
950
940
930
920
FRESHWATER HEAD (m amsl)
1977
1978
1979
1980
1981
1982
1983
1984
1985
1986
1987
TIME
LEGEND: o = WIPP-28 (WL)
WL = Water-level data
T = Transducer data
Drawn by
Date
Checked by
Date
Revisions
Date
INTERA Technologies
Equivalent Freshwater Heads for the Culebra Dolomite at Well WIPP-28
Figure E.30

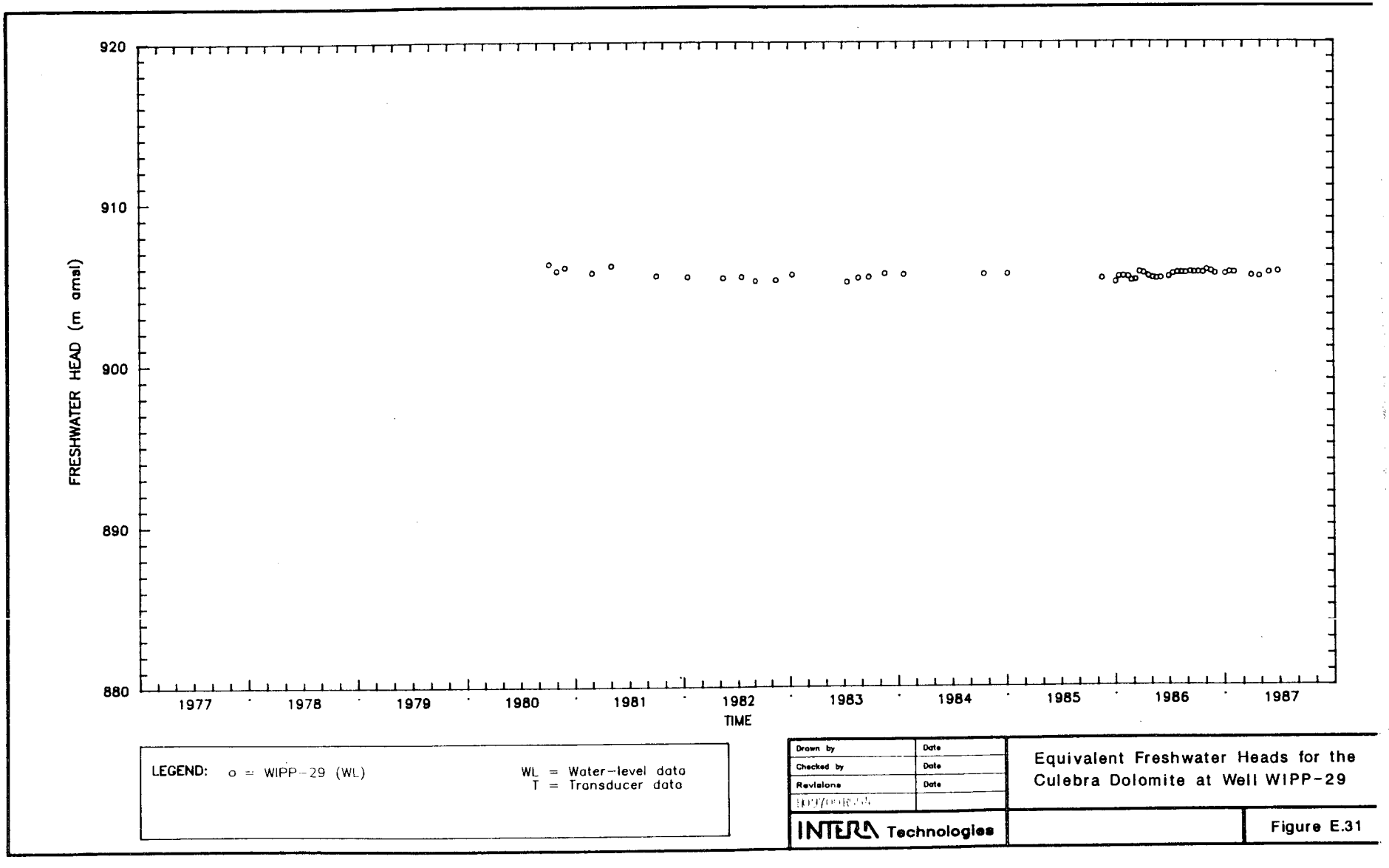
920
910
900
890
880
FRESHWATER HEAD (m amsl)
1977
1978
1979
1980
1981
1982
1983
1984
1985
1986
1987
TIME
LEGEND: o = WIPP-29 (WL)
WL = Water-level data
T = Transducer data
Drawn by
Date
Checked by
Date
Revisions
Date
INTERA Technologies
Equivalent Freshwater Heads for the Culebra Dolomite at Well WIPP-29
Figure E.31

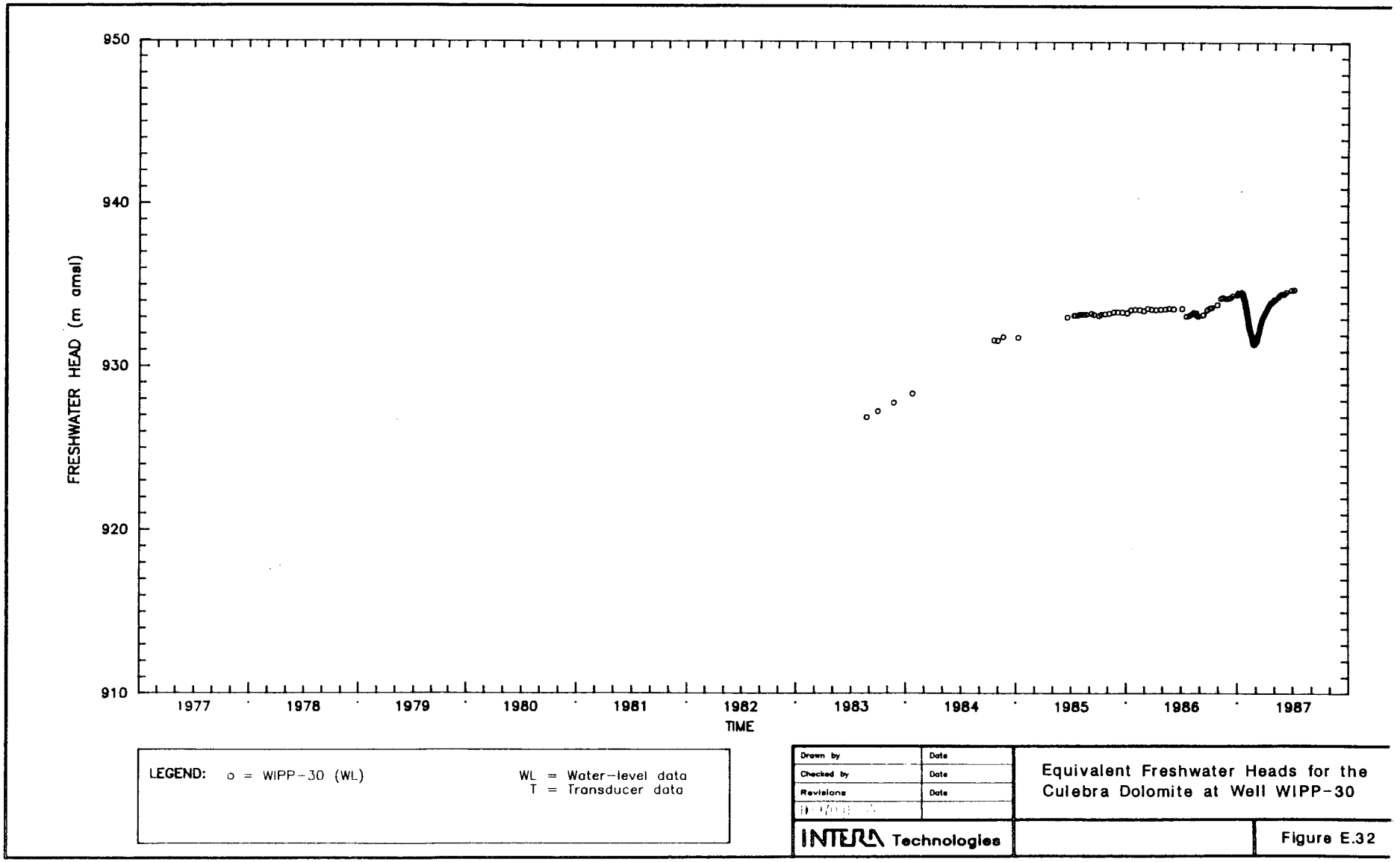
950
940
930
920
910
FRESHWATER HEAD (m amsl)
1977
1978
1979
1980
1981
1982
1983
1984
1985
1986
1987
TIME
LEGEND: o = WIPP-30 (WL)
WL = Water-level data
T = Transducer data
Drawn by
Date
Checked by
Date
Revisions
Date
INTERA Technologies
Equivalent Freshwater Heads for the Culebra Dolomite at Well WIPP-30
Figure E.32

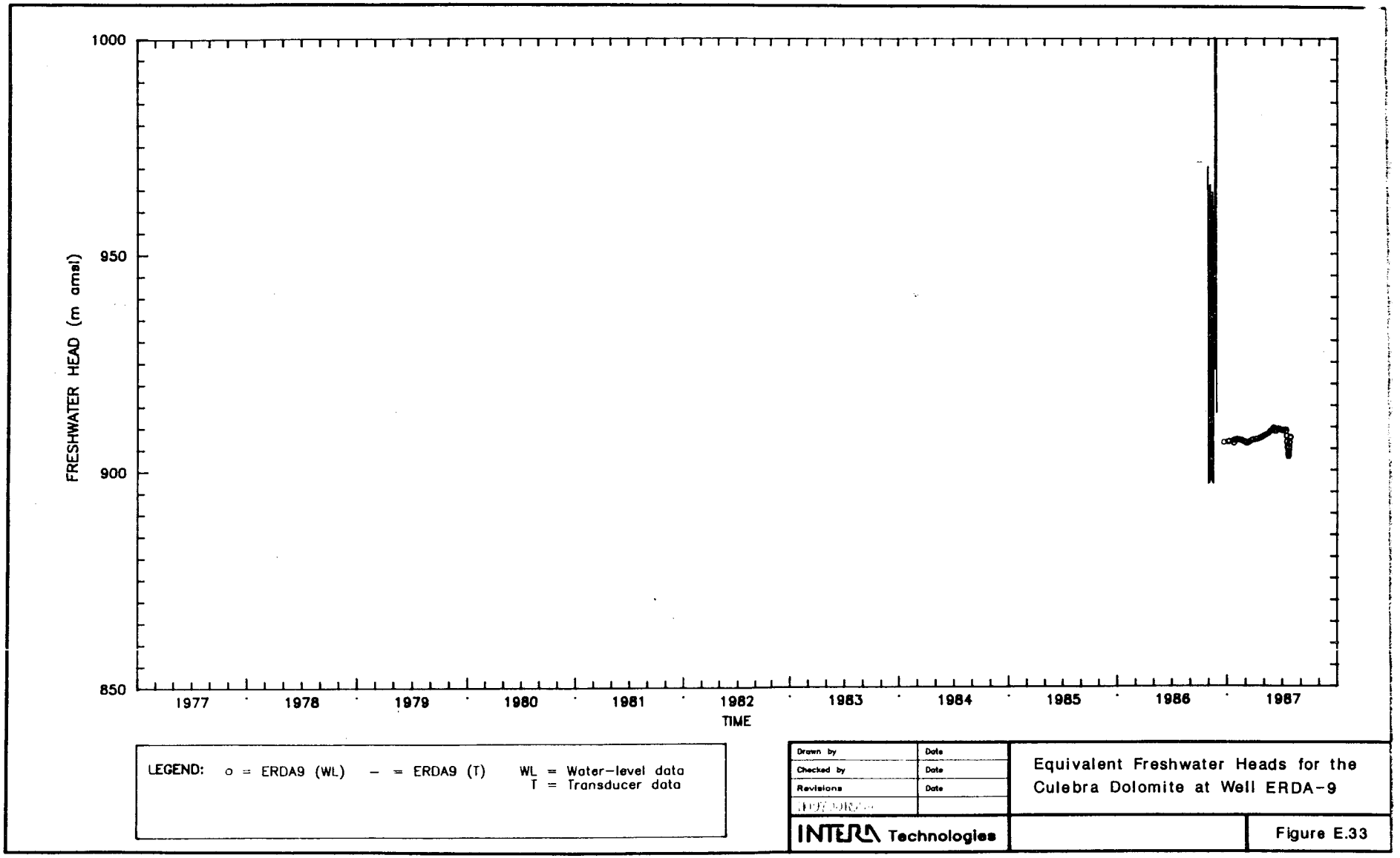
1000
950
900
850
FRESHWATER HEAD (m amsl)
1977
1978
1979
1980
1981
1982
1983
1984
1985
1986
1987
TIME
LEGEND: o = ERDA9 (WL) – = ERDA9 (T) WL = Water-level data T = Transducer data
Drawn by
Date
Checked by
Date
Revisions
Date
INTERA Technologies
Equivalent Freshwater Heads for the Culebra Dolomite at Well ERDA-9
Figure E.33

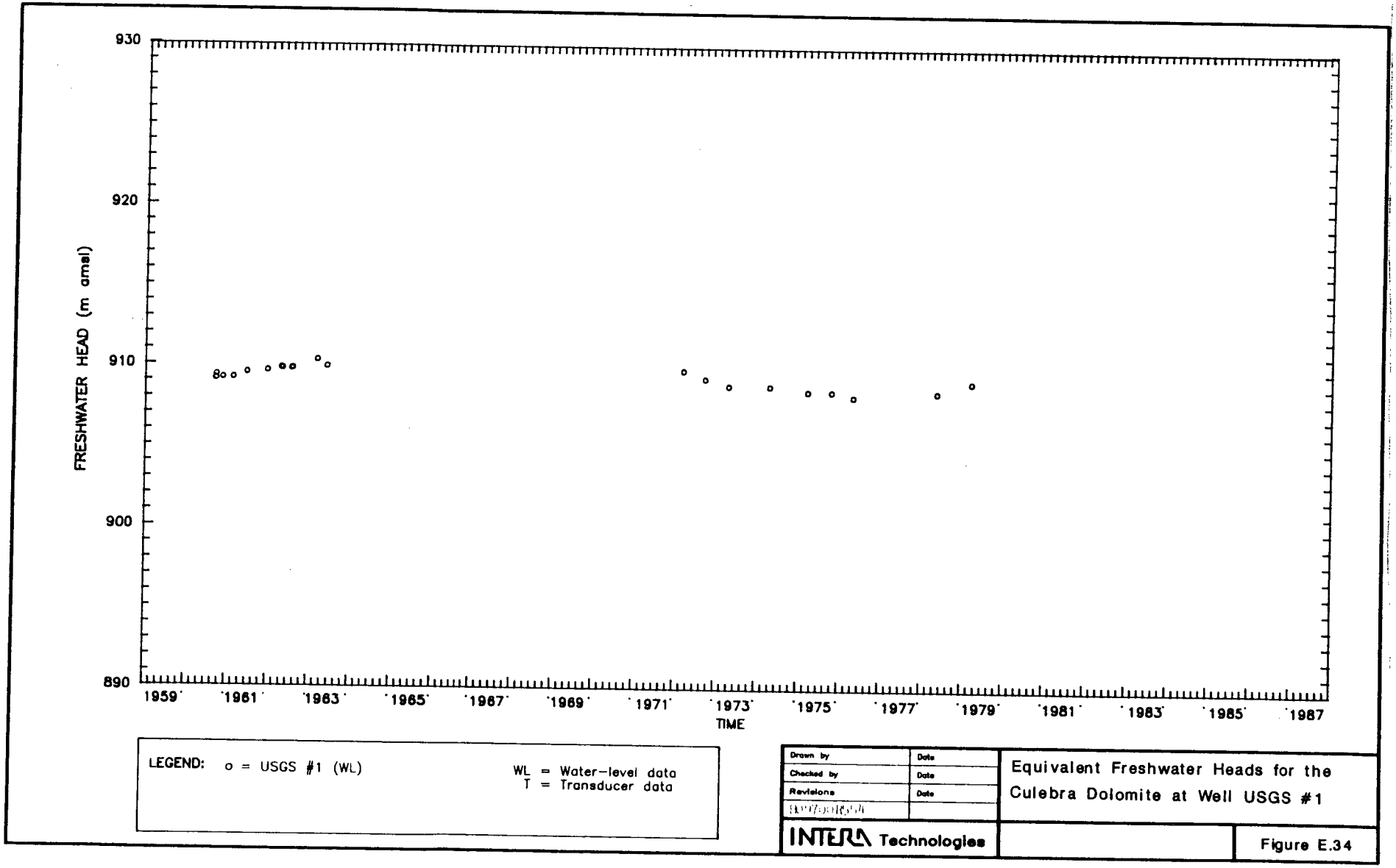
930
920
910
900
890
FRESHWATER HEAD (m amsl)
1959
1961
1963
1965
1967
1969
1971
1973
1975
1977
1979
1981
1983
1985
1987
TIME
LEGEND: o = USGS #1 (WL)
WL = Water-level data
T = Transducer data
Drawn by
Date
Checked by
Date
Revisions
Date
INTERA Technologies
Equivalent Freshwater Heads for the Culebra Dolomite at Well USGS #1
Figure E.34

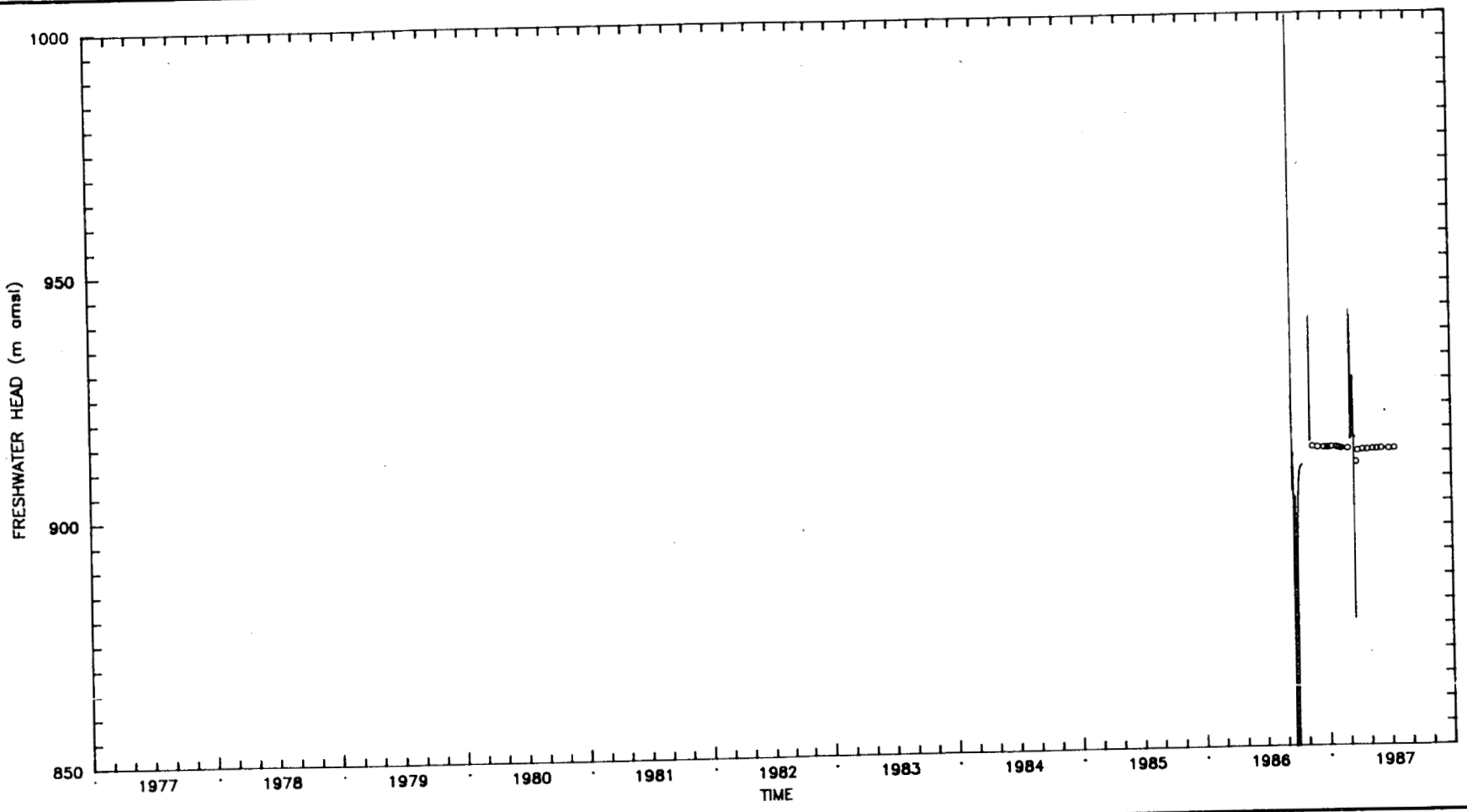

LEGEND: o = CB1 (WL) — = CB1 (T) WL = Water-level data T = Transducer data

Drawn by	Date
Checked by	Date
Revisions	Date

INTERA Technologies

Equivalent Freshwater Heads for the Culebra Dolomite at Well Cabin Baby-1

Figure E.35

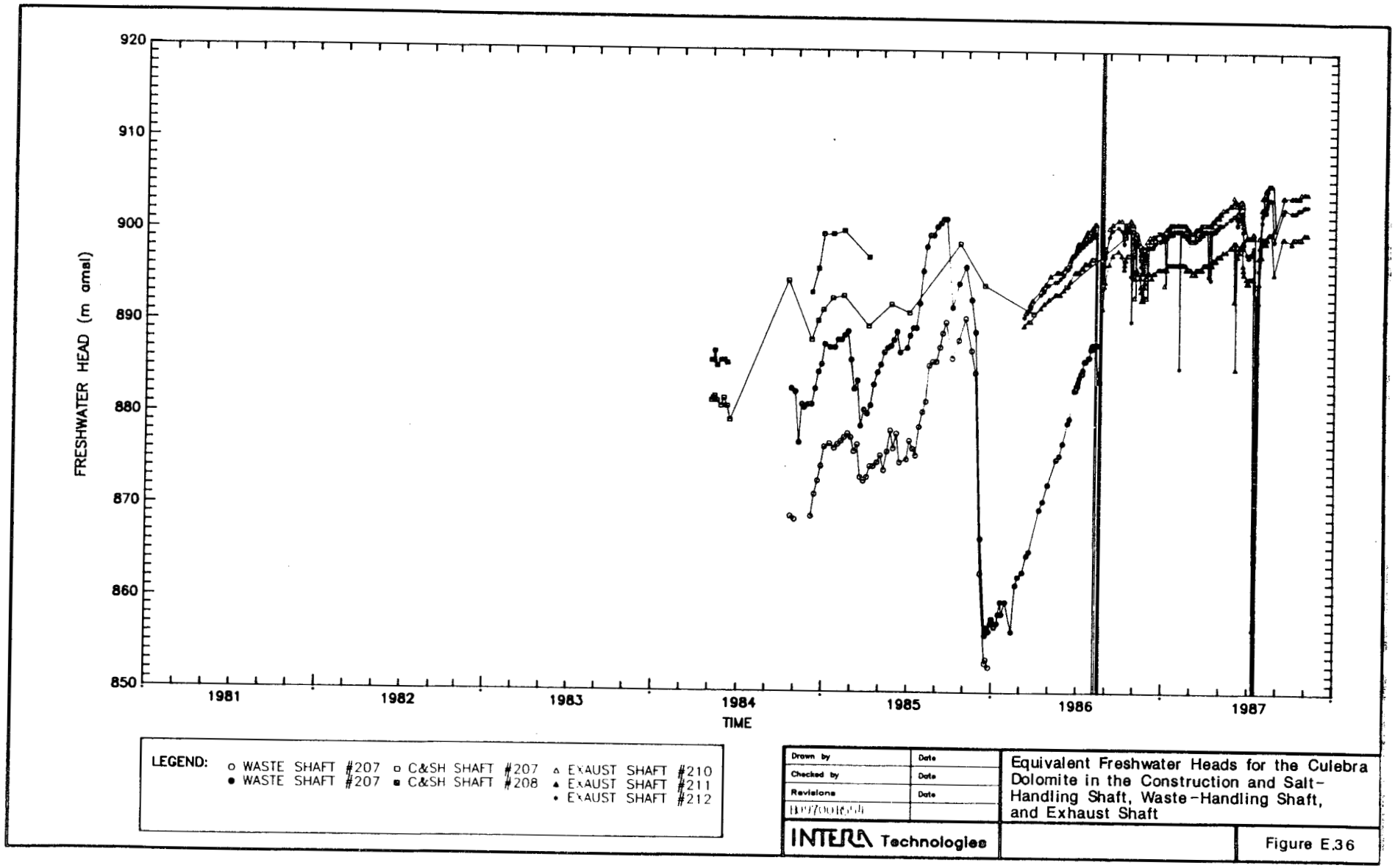
920
910
900
890
880
870
860
850
FRESHWATER HEAD (m amsl)
1981
1982
1983
1984
1985
1986
1987
TIME
LEGEND:
o WASTE SHAFT #207
• WASTE SHAFT #207
□ C&SH SHAFT #207
■ C&SH SHAFT #208
△ EXAUST SHAFT #210
▲ EXAUST SHAFT #211
• EXAUST SHAFT #212
Drawn by
Date
Checked by
Date
Revisions
Date
INTERA Technologies
Equivalent Freshwater Heads for the Culebra Dolomite in the Construction and Salt-Handling Shaft, Waste-Handling Shaft, and Exhaust Shaft
Figure E.36

WELL	REFERENCE ELEVATION (ft amsl)	REFERENCE ELEVATION (m amsl)	MEASURING POINT * (TOC/TOT/GS)	MEASURING-POINT ELEV. (ft amsl)	MEASURING-POINT ELEV. (m amsl)	PERIOD MEASURING POINT APPLICABLE
H-1	3397.9	1035.7	GS	3397.9	1035.7	3/17/77-1/24/84
			TOT	3400.2	1036.4	5/16/83-PRESENT **
H-2A	3377.8	1029.6	TOT	3378.8	1029.9	10/16/83-4/30/84
			TOC	3378.1	1029.6	4/30/84-PRESENT
H-2B1	3377.6	1029.5	GS	3377.6	1029.5	2/21/77-6/24/83
			TOT	3378.9	1029.9	6/24/83-7/10/84
			TOT	3379.8	1030.2	7/10/84-7/8/86
			TOT	3379.3	1030.0	7/8/86-PRESENT
H-2B2	3377.6	1029.5	TOC	3378.4	1029.7	12/5/83-PRESENT
H-2C	3377.7	1029.5	GS	3377.7	1029.5	1/1/77-6/1/83
			TOC	3378.4	1029.7	6/1/83-PRESENT
H-3B1	3389.4	1033.1	GS	3389.4	1033.1	5/25/77-11/21/83
			TOT	3391.3	1033.7	4/30/83-1985
			TOC	3390.6	1033.5	POST-1985
H-3B2	3388.3	1032.8	TOC	3389.0	1033.0	3/12/84-PRESENT
H-3B3	3387.1	1032.4	TOC	3386.4	1032.2	2/27/84-PRESENT
H-4A	3332.8	1015.8	TOT	3333.7	1016.1	10/23/82-PRESENT
H-4B	3332.7	1015.8	GS	3332.7	1015.8	6/2/78-8/20/82
			TOC	3333.4	1016.0	8/20/82-PRESENT
H-4C	3332.5	1015.7	TOC	3333.1	1015.9	10/23/82-PRESENT
H-5A	3505.6	1068.5	TOT	3506.2	1068.7	7/19/84-PRESENT
H-5B	3505.4	1068.4	GS	3505.4	1068.4	7/7/78-10/18/84
			TOC	3506.1	1068.6	10/18/84-PRESENT
H-5C	3505.8	1068.6	TOC	3506.0	1068.6	4/9/84-PRESENT
H-6A	3347.3	1020.2	TOC	3348.1	1020.5	4/9/84-PRESENT
H-6B	3347.6	1020.3	GS	3347.6	1020.3	7/25/78-10/18/84
			TOC	3348.2	1020.5	4/9/84-PRESENT
H-6C	3347.9	1020.4	TOC	3348.5	1020.6	4/9/84-PRESENT
H-7B1	3163.6	964.3	GS	3163.6	964.3	9/19/79-1/7/85
			TOC	3164.3	964.5	1/26/84-PRESENT
H-7B2	3164.0	964.4	TOC	3164.4	964.5	1/2/84-PRESENT
H-7C	3163.4	964.2	TOC	3164.1	964.4	10/28/83-PRESENT
H-8B	3433.8	1046.6	BGS	3433.8	1046.6	8/13/79-1/7/85
			TOC	3434.5	1046.8	1/7/85-PRESENT
H-9A	3405.4	1037.0	TOC	3405.9	1038.1	9/21/83-PRESENT
H-9B	3405.6	1038.0	BGS	3405.6	1038.0	8/29/79-1/7/85
			TOC	3406.3	1038.2	9/21/83-PRESENT
H-9C	3405.9	1038.1	TOC	3407.1	1038.5	6/21/83-PRESENT
H-10B	3687.0	1123.8	BGS	3687.0	1123.8	11/1/79-8/20/82
			TOC	3687.8	1124.0	5/6/86-PRESENT
H-11B1	3412.1	1040.0	TOC	3411.4	1039.8	9/7/83-PRESENT
H-11B2	3412.1	1040.0	TOC	3411.6	1039.9	12/5/83-PRESENT
H-11B3	3412.1	1040.0	TOC	3412.4	1040.1	3/16/84-PRESENT
H-12	3426.0	1044.2	TOC	3427.2	1044.6	11/4/83-PRESENT
H-14	3345.6	1019.7	TOC	3347.2	1020.2	3/11/87-PRESENT

Drawn by	Date
Checked by	Date
Revisions	Date
H09700R554	

Measuring-Point Elevations for the WIPP-Area Boreholes

INTERA Technologies

Table E.1

WELL	REFERENCE ELEVATION (ft amsl)	REFERENCE ELEVATION (m amsl)	MEASURING POINT * (TOC/TOT/GS)	MEASURING-POINT ELEV. (ft amsl)	MEASURING-POINT ELEV. (m amsl)	PERIOD MEASURING POINT APPLICABLE
H-15	3480.2	1060.8	TOC	3481.6	1061.2	12/23/86-PRESENT
DOE-1	3465.1	1056.2	TOC	3465.2	1056.2	12/1/83-PRESENT
DOE-2	3418.4	1041.9	TOC	3419.2	1042.2	4/2/86-PRESENT
P-14	3359.8	1024.1	BGS	3359.8	1024.1	3/27/77-8/24/83
			TOC	3361.1	1024.5	8/24/83-PRESENT
P-15	3309.8	1008.8	BGS	3309.8	1008.8	5/25/77-8/25/83
			TOC	3311.4	1009.3	8/25/83-PRESENT
P-17	3335.8	1016.7	GS	3335.8	1016.7	5/25/77-5/25/82
			TOC	3337.2	1017.2	5/25/82-PRESENT
P-18	3477.3	1059.9	GS	3477.3	1059.9	5/25/77-3/15/83
			TOC	3478.4	1060.2	3/15/83-PRESENT
WIPP-12	3471.3	1058.1	TOC	3472.1	1058.3	10/14/85-PRESENT
WIPP-13	3405.4	1038.0	TOC	3405.8	1038.1	10/27/85-PRESENT
WIPP-18	3456.4	1053.5	TOC	3458.8	1054.2	8/5/85-PRESENT
WIPP-19	3433.1	1046.4	TOC	3435.2	1047.0	8/5/85-PRESENT
WIPP-21	3417.1	1041.5	TOC	3418.9	1042.1	8/5/85-PRESENT
WIPP-22	3425.8	1044.2	TOC	3428.2	1044.9	8/5/85-PRESENT
WIPP-25	3212.5	979.2	GS	3212.5	979.2	8/24/83-1/7/85
			TOC	3214.4	979.7	11/27/84-PRESENT
WIPP-26	3151.7	960.6	GS	3151.7	960.6	8/24/83-1/7/85
			TOC	3153.2	961.1	10/27/84-PRESENT
WIPP-27	3177.2	968.4	GS	3177.2	968.4	8/24/83-1/7/85
			TOT	3179.4	969.1	10/30/84-PRESENT
WIPP-28	3346.6	1020.0	GS	3346.6	1020.0	9/29/83-1/7/85
			TOT	3349.6	1021.0	1/7/85-PRESENT
WIPP-29	2977.0	907.4	GS	2977.0	907.4	10/8/80-1/7/85
			TOC	2978.3	907.8	1/7/85-PRESENT
WIPP-30	3427.5	1044.7	GS	3427.5	1044.7	8/23/83-1/7/85
			TOC	3429.5	1045.3	10/30/84-PRESENT
ERDA-9	3408.8	1039.0	TOC	3410.1	1039.4	1/5/87-PRESENT
CB-1	3327.3	1014.2	TOC	3328.4	1014.5	11/20/86-PRESENT
USGS-1	3425.0	1043.9	GS	3425.0	1043.9	9/22/60-PRESENT

* (TOC) refers to top of casing, (TOT) refers to top of tubing, and (GS) refers to ground surface.
** Present refers to date of latest update of data used in this table (late 1987).

Drawn by	Date
Checked by	Date
Revisions	Date
H09700R554	

Measuring-Point Elevations for the WIPP-Area Boreholes

INTERA Technologies

Table E.1 (cont.)

BOREHOLE-FLUID DENSITIES ; Database Update 09/22/87

WELL	AVERAGE BOREHOLE-FLUID DENSITY (g/cm3)	ESTIMATED FLUID-DENSITY UNCERTAINTY(1) (g/cm3)	TIME PERIOD DENSITY APPLICABLE
H-1	1.020	+/- 0.01	3/17/77-PRESENT (2)
H-2a	1.070	+/- 0.06	07/15/83 - 07/09/84
	1.050		07/09/84 - PRESENT
H-2b1	1.010	+/- 0.01	02/13/77 - 01/09/84
	1.050	+/- 0.04	01/09/84 - PRESENT
H-2b2	1.050	+/- 0.04	12/5/83-PRESENT
H-2c	1.050	- 0.04	1/1/77-PRESENT
H-3b1	1.036	+/- 0.01	5/25/77-PRESENT
H-3b2	1.036	+/- 0.01	3/12/84-PRESENT
H-3b3	1.036	+/- 0.01	2/27/84-PRESENT
H-4a	1.019	+/- 0.02	10/23/82-PRESENT
H-4b	1.019	+/- 0.01	6/2/78-PRESENT
H-4c	1.019	+/- 0.02	10/23/82-PRESENT
H-5a	1.10	+/- 0.02	7/19/84-PRESENT
H-5b	1.10	+/- 0.01	7/7/78-PRESENT
H-5c	1.10	+/- 0.02	4/9/84-PRESENT
H-6a	1.039	+/- 0.02	4/9/84-PRESENT
H-6b	1.039	+/- 0.01	7/25/78-PRESENT
H-6c	1.039	+/- 0.02	4/9/84-PRESENT
H-7b1	1.009	+/- 0.01	9/19/79-PRESENT
H-7b2	1.009	+/- 0.01	1/2/84-PRESENT
H-7c	1.009	+/- 0.01	10/28/83-PRESENT
H-8b	1.000	+ 0.01	8/13/79-PRESENT
H-9a	1.000	+ 0.01	9/21/83-PRESENT
H-9b	1.000	+ 0.01	8/29/79-PRESENT
H-9c	1.000	+ 0.01	6/21/83-PRESENT
H-10b	1.046	+/- 0.01	11/1/79-PRESENT
H-11b1	1.083	+/- 0.01	9/7/83-PRESENT
H-11b2	1.085	+/- 0.01	12/5/83-PRESENT
H-11b3	1.080	+/- 0.01	3/16/84-PRESENT
H-12	1.095	+/- 0.03	12/30/83 - 07/09/84
	1.095	+/- 0.01	07/09/84 - PRESENT
H-14	1.009	+/- 0.01	3/11/87-PRESENT
H-15	1.000	+/- 0.01	11/10/86-4/14/87
	1.143	+/- 0.02	4/14/87-PRESENT
DOE-1	1.090	+/- 0.02	12/1/83-PRESENT
DOE-2	1.060	+/- 0.03	10/12/84-6/30/86
	1.030	+/- 0.01	6/30/86 - PRESENT
P-14	1.013	+/- 0.01	03/07/77 - 12/17/86
	1.007	+/- 0.01	12/17/86 - PRESENT

Drawn by	Date
Checked by	Date
Revisions	Date
H09700R554	

Borehole-Fluid Density and Estimated Density Uncertainty for WIPP-Area Boreholes

INTERA Technologies

Table E.2

WELL	AVERAGE BOREHOLE-FLUID DENSITY (g/cm3)	ESTIMATED FLUID-DENSITY UNCERTAINTY(1) (g/cm3)	TIME PERIOD DENSITY APPLICABLE
P-15	1.015	+ 0.05	05/10/77 - 06/06/85
	1.006		06/06/85 - 03/27/87
	1.006		03/27/87 - PRESENT
P-17	1.063	+/- 0.01	5/25/77-PRESENT
P-18	1.115	+ 0.04	5/25/77-PRESENT
WIPP-12	1.2	- 0.05	10/14/85 - 05/21/86
	0.995	+/- 0.01	05/21/86 - PRESENT
WIPP-13	1.2	- 0.05	10/26/85 - 04/04/86
	1.024	+/- 0.01	04/04/86 - 01/12/87
	1.027	+/- 0.01	01/12/87 - PRESENT
WIPP-18	1.08	+ 0.12	10/11/85 - 05/20/86
	1.1	+/- 0.01	05/20/86 - 08/25/86
	1.098	+/- 0.01	08/25/86 - PRESENT
WIPP-19	1.18	+ 0.02/-0.05	10/09/85 - 05/31/86
	1.096	+/- 0.01	05/31/86 08/22/86
	1.124	+/- 0.01	08/22/86 - PRESENT
WIPP-21	1.000	+/- 0.01	10/06/85 - 06/28/86
	1.012	+/- 0.01	06/28/86 - 08/25/86
	1.020	+/- 0.01	08/25/86 - PRESENT
WIPP-22	1.15	+/- 0.05	10/08/85 - 06/19/86
	1.115	+/- 0.01	06/19/86 - 08/26/86
	1.07	+ 0.04	08/26/86 - PRESENT
WIPP-25	1.008	+/- 0.01	8/24/83-PRESENT
WIPP-26	1.000	+ 0.01	8/24/83-PRESENT
WIPP-27	1.027	+/- 0.01	8/24/83-PRESENT
WIPP-28	1.032	+/- 0.02	9/29/83-PRESENT
WIPP-29	1.170	+/- 0.04	10/8/80-PRESENT
WIPP-30	1.060	+/- 0.01	8/23/83-PRESENT
ERDA-9	1.080	+/- 0.01	1/5/87-PRESENT
CB-1	1.029	+/- 0.01	10/20/86-PRESENT
ENGLE	1.001	+ 0.01	3/4/85-PRESENT
USGS-1	1.000	unknown	9/22/60-PRESENT

(1) Borehole-fluid uncertainty is a judgement based upon a detailed study of the activities at each borehole and the water-quality and pressure-density-survey data available.
(2) Present refers to the final date of latest update of data used in this table (July 1987).

Drawn by	Date	Borehole-Fluid Density and Estimated Density Uncertainty for WIPP-Area Boreholes
Checked by	Date	
Revisions	Date	
H09700R554		
INTERA Technologies		Table E.2 (cont.)

WELL	UNDISTURBED F.W. ELEV (m amsl)	DATE SELECTED	HEAD UNCERTAINTY DUE TO BOREHOLE-FLUID DENSITY(m)(1)	OVERALL HEAD UNCERTAINTY(m) (2)
H-1	921.6	06/81	+/- 1	+/- 2
H-2b1 (3)	923.5	10/77	+/- 2	+/- 2.5
H-3b1	917.1	07/81	+/- 1	+/- 3
H-4b	913.3	08/82	+/- 1	+/- 2
H-5b	933.5	02/80	+/- 1.5	+/- 2
H-6b	932.3	02/79	+/- 1	+/- 2
H-7b	912.6	06/81	+/- 0.5	+/- 1
H-8b	911.8	01/82	+/- 0.5	+/- 1.5
H-9b	907.0	11/81	+/- 1	+/- 2
H-10b	920.8	06/81	+/- 2	+/- 2.5
H-11b3	912.5	06/87	+/- 1	+/- 2
H-12	913.5	03/84	+/- 1	+/- 1.5
H-14	915.0	03/87	+/- 1	+/- 1.5
H-15	918.0	03/87	+/- 1.5	+/- 5
H-17 (4)	913.2	10/87	NA (5)	NA
DOE-1	915.0	07/87	+/- 2	+/- 2.5
DOE-2	935.4	01/87	+/- 1.5	+/- 2.5
P-14	927.0	06/84	+/- 1	+/- 2
P-15	916.4	01/79	+2 /-1	+/- 2.5
P-17	912.6	09/87 EXTRAP	+/- 1	+/- 2.5
WIPP-12	932.2	01/87	+/- 1.5	+/- 3
WIPP-13	934.0	01/87	+/- 1	+/- 2.5
WIPP-18	930.0	01/87 EXTRAP	+/- 1	+/- 2
WIPP-25	931.0	07/83	+/- 1	+/- 2
WIPP-26	917.5	08/83	+ 0.5	+/- 1.5

Drawn by	Date	Undisturbed Freshwater Heads and Uncertainties	
Checked by	Date		
Revisions	Date		
H09700554			
INTERA Technologies			Table E.3

WELL	UNDISTURBED F.W. ELEV (m amsl)	DATE SELECTED	HEAD UNCERTAINTY DUE TO BOREHOLE-FLUID DENSITY(m) (1)	OVERALL HEAD UNCERTAINTY(m) (2)
WIPP-27	937.5	08/83	+ 1	+/- 1.5
WIPP-28	938.1	08/83	+/- 1	+/- 1.5
WIPP-29 (5)	905.4	01/82	+/- 0.5	+/- 1
WIPP-30	934.7	09/87	+/- 1	+/- 2
CB-1	911.2	02/87	+/- 1	+/- 2
USGS-1	909.0	08/60	unknown	+/- 1.5

NA = Not applicable

(1) Uncertainty is based upon the uncertainty in the estimate of the borehole-fluid density only at the time of the static head estimate.

(2) Total head uncertainty takes into account uncertainty introduced by uncertainty in borehole-fluid density and uncertainty introduced by trends in the hydrographs.

(3) When more than one undisturbed head can be estimated for a hydropad, the value used is from the well which has the lowest magnitude of uncertainty in the borehole-fluid density.

(4) H-17 undisturbed head is based upon estimate from drill-stem tests conducted by R. Beauheim (pers. comm. 10/9/87). No transient data from H-17 are included in this modeling effort.

(5) Uncertainty at WIPP-29 could be much larger due to man-made transients in Nash Draw.

Drawn by	Date	Undisturbed Freshwater Heads and Uncertainties	
Checked by	Date		
Revisions	Date		
H09700R554			
INTERA Technologies			Table E.3 (cont.)

APPENDIX F FORMATION-FLUID DENSITIES

To interpret ground-water hydraulic and geochemical data, formation-water density data are required. The densities of water samples from boreholes open to a given formation will be the same as the densities of the formation water only if the samples are not contaminated. Contamination can result from the mixing of formation water with drilling fluids, with fluids used in borehole construction, and with water from other formations. Knowledge of the extent of such contamination, if any, is required to evaluate the composition and density of formation fluids for geochemical purposes and for flow-path validation to support ground-water modeling.

Density and chemical analytical data on Culebra samples have been evaluated for their internal consistency and for indications of how well they may represent the density and chemistry of Culebra formation waters. The evaluation procedures are described in Haug et al. (1987).

Table F.1 lists the density data base. There are some additional entries in this data base that were not present in Haug et al. (1987). The table lists the reference and source of the sample data, the date the sample was taken, and the values of specific gravity or density of the sample. Using the methodology described in Haug et al. (1987), the calculated densities and the density values suggested for modeling purposes are presented. The latter column has been used in this modeling study.

REFERENCES

Haug, A., V.A. Kelley, A.M. LaVenue, and J.F. Pickens, 1987. Modeling of Ground-Water Flow in the Culebra Dolomite at the Waste Isolation Pilot Plant (WIPP) Site: Interim Report. Sandia National Laboratories, Contractor Report SAND86-7167.

Other References: The references for the data sources are listed at the end of Table F.1.

Measured Specific Gravity and Density (g/cm3)

No.	Well Number	Date Sampled	Temp. (°C)	Mercer,1983 (1) sp.grv.	Mercer,1983 (1) density g/cm3	Robinson,1987 (2) sp.grv.	Robinson,1987 (2) density g/cm3	WQSP-Round 1 (3) sp.grv.	WQSP-Round 1 (3) density g/cm3	WQSP-Round 2 (4) sp.grv.	WQSP-Round 2 (4) density g/cm3	HydroGeoChem(5) sp.grv.	HydroGeoChem(5) density g/cm3	Intera Field Data sp.grv.	Intera Field Data density g/cm3	Calculated Density * g/cm3	Source of Data used in Calculation	Density to Use g/cm3
1	H-1	02-Jun-76	23.0	1.016	1.0136											1.0218	USGS	1.022
2	H-2a	21-Apr-86	23.0					1.009	1.0066							1.0085	W-R1-B	1.009
3	H-2b1	22-Feb-77	22.5	1.012	1.0099											1.0058	USGS	1.009
4	H-2b2	16-Nov-83	20.0									1.006	1.0042					
5	H-3b1	17-Mar-77	21.5	1.024	1.0219											1.0396	USGS	1.036
6	H-3b2	16-Dec-85	23.0											1.037	1.0344 (6)			
7	H-3b3	11-Jun-84	(22.5)													1.0381	HGC-B	1.036
8		04-Feb-85	25.0													1.0386	W-R1-B	1.036
9		05-May-86	22.1							1.038	1.0357							
10	H-4b	29-May-81	23.0			1.010	1.0076									1.0151	SNL-B	1.016
11		25-Jul-85	21.5					1.015	1.0129							1.0140	W-R1-B	1.016
12		09-Nov-86	21.1							1.018	1.0160							
13	H-4c	10-Aug-84	(22.5)													1.0145	HGC-B	1.013
14			(22.5)									1.012	1.0097					
15	H-5b	01-Jun-81	24.0			1.10	1.097									1.1077	SNL-B	1.102
16		27-Aug-85	22.5					1.105	1.1015							1.1040	W-R1-B	1.102
17		21-May-86	23.7							1.105	1.1021							
18	H-5c	15-Oct-81	25.0			1.10	1.097									1.1077	SNL-B	1.102
19	H-6b	02-May-81	23.0			1.040	1.0375									1.0410	SNL-B	1.039
20		15-Sep-85	23.5					1.042	1.0394							1.0394	W-R1-B	1.039
21		28-Jul-86	25.6							1.040	1.0368							
22	H-7b	20-Mar-80	(22.5)	1.001	0.9987											1.0015	USGS	1.001
23		26-Mar-86	21.5					1.001	0.9989							1.0005	W-R1-B	1.001
24		21-Feb-86	22.0											1.000	0.9977 (6)			
25	H-8b	11-Feb-80	(22.5)	1.000	0.9977											1.0007	USGS	1.000
26		09-Dec-85	23.0											1.002	0.9995 (6)			
27		22-Jan-86	22.0					1.002	0.9998							1.0001	W-R1-B	1.000
28	H-9b	14-Nov-85	22.0					1.003	1.0007							1.0006	W-R1-B	1.001
29	H-10b	21-Mar-80	(22.5)	1.045	1.0426											1.0465	USGS	1.047
30	H-11b3	13-Oct-84	(22.5)									1.087	1.0845 (9)					
31		23-May-85	22.5					1.091	1.0885							1.0819	W-R1-B	1.078
32		04-Jun-86	24.0							1.081	1.0781							
33	H-12	09-Aug-85	24.0					1.096	1.0930							1.0960	W-R1-B	1.093
34	H-14	11-Dec-86	22.0											1.010	1.0077 (8)			1.008 (11)

Drawn by	Date
Checked by	Date
Revisions	Date
H09700R554	
INTERA Technologies	

Culebra Dolomite Formation-Fluid Density Data Base

Table F.1

No.	Well Number	Date Sampled	Temp. (°C)	Mercer,1983 (1) sp.grv.	Mercer,1983 (1) density g/cm3	Robinson,1987 (2) sp.grv.	Robinson,1987 (2) density g/cm3	WQSP-Round 1 (3) sp.grv.	WQSP-Round 1 (3) density g/cm3	WQSP-Round 2 (4) sp.grv.	WQSP-Round 2 (4) density g/cm3	HydroGeoChem(5) sp.grv.	HydroGeoChem(5) density g/cm3	Intera Field Data sp.grv.	Intera Field Data density g/cm3	Calculated Density * g/cm3	Source of Data used in Calculation	Density to Use g/cm3
35	H-15	11-May-87	24.0											1.160	1.1569 (8)			
36		11-May-87	22.0							1.1560	(12)							1.153 (11)
37	H-17	26-Nov-87	26.5											1.1065				1.103 (11)
38	DOE-1	12-Apr-85	22.5						1.1100							1.0906	W-R1-B	1.088
39		03-Jul-86	23.0							1.091	1.0883							
40	DOE-2	12-Mar-85	21.5						1.0600							1.0431	W-R1-B	1.041
41		04-Jul-86	25.0											1.040	1.0370 (7)			
42		27-Aug-86	22.7							1.043	1.0405							
43	P-14	26-Feb-86	22.5					1.019	1.0167							1.0174	W-R1-B	1.017
44	P-15	10-May-77	21.5	1.080	1.0778											1.0152	USGS	1.015
45	P-17	17-Mar-86	21.5					1.065	1.0626							1.0609	W-R1-B	1.061
46		18-Dec-86	20.9							1.063	1.0609							
47	WIPP-13	18-Feb-87	25.0											1.0460				1.043 (11)
48	WIPP-25	20-Aug-80	23.0			1.010	1.0076									1.0072	SNL-B,F	1.008
49		12-Feb-86	21.5					1.010	1.0079							1.0086	W-R1-B	1.008
50	WIPP-26	24-Aug-80	22.0			1.005	1.0028									1.0094	SNL-B	1.012
51		25-Nov-85	22.0					1.012	1.0098							1.0115	W-R1-B	1.012
52	WIPP-27	22-Aug-80	(22.5)	1.094	1.0915											1.0906	USGS	1.092
53		05-Sep-80	22.0			1.090	1.0876									1.0963	SNL-B	1.092
54	WIPP-28	11-Sep-80	22.5			1.030	1.0277									1.0321	SNL-B	1.032
55	WIPP-29	20-Aug-80	(22.5)	1.178	1.1753											1.1676	USGS	1.213 (10)
56		28-Aug-80	20.0			1.160	1.1580									1.1691	SNL-B	1.213 (10)
57		14-Dec-85	23.0					1.216	1.2131							1.2176	W-R1-B	1.213 (10)
58	WIPP-30	06-Sep-80	21.0			1.02	1.018									1.0204	SNL-B	1.020
59	Engle	04-Mar-85	(22.5)						1.0150							1.0009	W-R1-B	1.001
60	C.B.-1	03-Oct-86	23.0											1.031	1.0285 (7)			

References:

(1) Mercer, J.W., 1983. Geohydrology of the Proposed Waste Isolation Pilot Plant Site, Los Medanos area, Southeastern New Mexico. USGS Water Resources Investigation Report 83-4016, 113 pp.
(2) Robinson, K.L., 1987. Analysis of Solutes in Groundwaters from the Rustler Formation at and Near the WIPP site SAND86-0917; Sandia National Labs
(3) Results are referenced in (2) above
(4) Uhland, D.W., W.S. Randall, and R.C. Carrasco, 1987. Annual Water Quality Data Report. Report DOE-WIPP-87-006, Westinghouse Electric Corporation
(5) Results are referenced in (2) above
(6) Hydrologic Data Report #3 Contractor Report SAND86-7109; INTERA Technologies, Inc., 1986 Salt concentrations are not available for a calculated density therefore a density recommendation is not provided
(7) Hydrologic Data Report #4 Contractor Report SAND86-7166; Saulnier, G.J., Jr., G.A. Freeze, and W.A. Stensrud 1986 Salt concentrations are not available for a calculated density therefore a density recommendation is not provided
(8) Hydrologic Data Report #5 Contractor Report SAND87-7125; Stensrud, W.A., M.A. Bame, K.D. Lantz, A.M. LaVenue, J.B. Palmer, and G.J. Saulnier, Jr. 1987 Salt concentrations are not available for a calculated density, therefore a density recommendation is not provided
(9) Unpublished data from Hydro Geo Chem field notes during grab sampling at Hydropad H-11
(10) Recommended density may reflect ground-water contamination from nearby potash tailings dumps
(11) Value has not undergone Pitzer analytical verification but is believed to be representative of the formation fluid
(12) Personal Communication with W.S. Randall on 10-26-87

SNL-B,F	Sandia National Labs sample - Bendix and field analytical data
SNL-B	Sandia National Labs sample - Bendix analytical data
W-R1-B	WQSP sampling - Round 1; Bendix analytical data
USGS	USGS sample and chemical analyses

* Calculated densities are determined using Pitzer ion-interaction theory for the Cl-salt component of the solution and stoichiometric addition of densities of pure solutions for the SO4-salt components. The technique is discussed in detail in Appendix E of Haug et al., 1987.

Drawn by	Date
Checked by	Date
Revisions	Date
409700R554	

INTERA Technologies

Culebra Dolomite Formation-Fluid Density Data Base

Table F.1 (cont.)

APPENDIX G TRANSIENT TESTS IMPLEMENTED DURING TRANSIENT SIMULATIONS

G.1 Initial Conditions

The purpose of this modeling study is not only to simulate the undisturbed hydrologic conditions but to also simulate the transient behavior of the Culebra dolomite in response to the H-3 and WIPP-13 multipad pumping tests. These tests cannot be simulated adequately by simply assuming undisturbed hydraulic conditions at the beginning of each of the multipad pumping tests. The major disturbing events (i.e., shaft activities and well tests) must be implemented in order to obtain similar initial hydrologic conditions in the Culebra dolomite at the beginning of the H-3 and WIPP-13 multipad pumping tests.

Descriptions of the shaft activities, the well tests that are considered to be significant, and the H-3 and WIPP-13 multipad pumping tests are presented in the following sections.

G.2 Description of Shaft Activities

As already discussed in Section 3.7.4, the hydrogeology of the Culebra dolomite has been influenced by drilling and excavating three shafts (waste-handling shaft, construction and salt-handling shaft, and exhaust shaft) at the center of the WIPP site. These shaft activities have been by far the most important hydrologic disturbances at the WIPP site since 1981, resulting in large changes in the piezometric surface at the central part of the WIPP site (Section 3.7.4).

G.2.1 The Early Shaft History

The first shaft excavated was the construction and salt-handling shaft, formerly called the exploratory shaft. A detailed history of the shaft construction was reported by Fenix and Scisson (1982). This

history was used by Stevens and Beyeler (1985) to model the effect of the shaft drilling and shaft completion on the hydrologic response at the H-1, H-2, and H-3 wells in both the Magenta and the Culebra Dolomite Members of the Rustler Formation. As demonstrated by Stevens and Beyeler (1985), the effect of the exploratory-shaft construction on the pressures in the Culebra dolomite was significant at the well locations H-1, H-2, and H-3.

A synopsis of drilling and construction events relevant to this study is summarized below (modified after Stevens and Beyeler, 1985):

July 4, 1981 : Start of reverse-rotary drilling with 3.68-m diameter. Land-surface elevation is about 1039.4 m amsl.

August 4, 1981 : Drilled into the top of the Culebra dolomite.

August 9, 1981 : Drilled through the bottom of the Culebra dolomite. The drilling-fluid level in the shaft fell below the bottom of the Magenta dolomite (about 847.4 m amsl). Consequently, the fluid pressure in the Culebra dolomite (center at 822 m amsl) fell below 350 kPa.

August 15, 1981 : Drilling-fluid level in the shaft fell below the bottom of the Culebra dolomite; subsequently, ground-water flow from the Culebra dolomite into the shaft was unrestricted and the Culebra dolomite was exposed to atmospheric pressure (about 101 kPa).

October 24, 1981 : Drilling stopped 701 m below land surface; the borehole was filled with brine to about 77 m

below land surface (962 m amsl). The brine density was not reported. Stevens and Beyeler (1985) estimated the ratio of the density of the brine to the density of the formation fluid to be about 1.3. The formation-fluid density at the shaft location is not exactly known, but likely to be between 1.02 g/cm^3 (e.g., at the well H-1) and 1.04 g/cm^3 (e.g., at H-3 or DOE-2). Consequently, it can be assumed that the density of the brine was about 1.3 g/cm^3, which is rather high. Using this density, the pressure at the center of the Culebra dolomite can be calculated to be 1886 kPa. The corresponding equivalent freshwater head equals 1004 m amsl.

October 25, 1981
to
November 15, 1981 : Brine was continually added to the shaft. The drilling fluid level, which was occasionally reported, rose about 35 m over the time period. It is likely that a considerable amount of brine entered the Culebra dolomite during that time period.

November 16, 1981 : The drilling fluid level in the shaft was approximately 997.2 m amsl, resulting in a pressure of about 2334 kPa at the center of the Culebra dolomite (assuming 1.3 g/cm^3 as brine density). This corresponds to an equivalent freshwater head of 1049.7 m amsl.

November 16, 1981
to
December 3, 1981 : The casing was lowered into the shaft. Stevens and Beyeler (1985) assumed that the brine either over-flowed the borehole while the casing was being lowered or the brine level was at ground level. This assumption results in a calculated formation pressure in the Culebra dolomite of 2873 kPa or an equivalent freshwater head of 1104.6 m amsl.

December 4, 1981
to
December 6, 1981 : Beginning December 4, the annular space between the casing and the shaft wall was cemented. Stevens and Beyeler (1985) again made the assumption that the brine in the shaft was either overflowing onto the land surface or was at land surface. Thus it can be assumed that the formation pressure in the Culebra dolomite was about the same as during the casing installation. On December 6, the cement-sealing operation ended.

Thus, the early shaft-history period lasted from July 1981 through December 1981. The effects of the activities at the exploratory shaft during that time period on the hydrologic conditions at the locations of H-1, H-2, and H-3 can be seen in the corresponding diagrams in Appendix E (Figures E.1, E.2, and E.3). All three figures show a sudden decrease of the freshwater head in the third quarter of 1981 which was caused by the first exposure of the Culebra dolomite to atmospheric pressure. The peak elevation, caused by filling the exploratory shaft with brine in December 1981, is also clearly shown

on all three diagrams. The subsequent decrease of the freshwater heads in 1982 reflects the end of the influence by the exploratory shaft and the exposure of the Culebra dolomite to atmospheric pressure at the ventilation shaft (Section G.2.2). Although the above-discussed early shaft activities did not significantly influence the hydrologic conditions in the Culebra dolomite in 1985, they were incorporated into the simulations because their effects represent an excellent test of the behavior of the transient model. The effects of the shafts over the total period of 1981 to 1985, however, did have a pronounced influence on the pressure distribution in the Culebra at the start of the H-3 multipad test in 1985.

G.2.2 The Open-Shaft Period

The drilling of the ventilation shaft (1.83-m diameter), which was widened two years later and renamed the waste-handling shaft (5.8-m diameter), was started in December 1981 and completed in February 1982. Drilling-fluid-level data from this time period are not available. Therefore, it was assumed that, similar to the drilling of the exploratory shaft (Section G.2.1), the drilling-fluid level fell below the Culebra dolomite on January 15, 1982. Subsequently, the ground-water flow from the Culebra dolomite into the shaft was unrestricted, i.e., the Culebra dolomite was again exposed to atmospheric pressure. The ventilation shaft remained open and draining prior to excavation as the waste-handling shaft between November 1983 and August 1984.

The third of the three shafts, the exhaust shaft, was started as a 7-7/8-inch pilot hole in October 1983. It was drilled out to an 11-inch diameter in December 1983. The shaft was then raise-bored to 1.83-m diameter from December 1983 to February 1984. Although the liner plate at the elevation of the Culebra dolomite was grouted during shaft construction in December 1984, considerable seepage

through the lining was observed (more than 1 liter/min). An additional grouting and sealing of the Culebra dolomite was conducted in June and July 1985. The exact date for which the sealing of the Culebra dolomite was effective is not known. Based on the recorded pressures at the waste-handling shaft, it was assumed for modeling purposes that the Culebra dolomite at the exhaust shaft was sealed on July 15, 1985. At the scale of the model, the three shafts can be considered to be a single hydrologic factor in the model. Consequently, it was assumed for the modeling study that the Culebra dolomite was exposed to atmospheric pressure from January 15, 1982 through July 15, 1985. During this time period, the ground-water flow from the Culebra dolomite into at least one of the shafts was assumed to be unrestricted.

The drawdown at the well locations H-1, H-2, and H-3 caused by the open shafts can be seen in the corresponding diagrams in Appendix E (Figures E.1, E.2, and E.3). Subsequent to the spring of 1983, the drawdowns at these wells were disturbed by other activities (e.g., pumping tests). Therefore, the maximum drawdowns caused by the open shaft can only be estimated to be approximately 14 m at H-1, 4 m at H-2, and 2.8 m at H-3.

The recorded data of H-4, H-5, H-6, P-15, and P-17 (Appendix E, Figures E.4, E.5, E.6, E.18, E.19) do not show a clear response to the construction work at the shafts, partly because their water levels were disturbed by other factors. It was assumed that the effects of the open shafts at these well locations were less than 1 m.

No water-level data for the time period before 1984 were available for the locations of DOE-1, H-11, WIPP-18, WIPP-19, WIPP-21, and WIPP-22. Therefore, it is not possible to estimate the effects of the shaft construction on the formation pressures at these locations.

G.2.3 The Shaft Leakage After Shaft Sealing

As mentioned before, the last of the three shafts (i.e., the exhaust shaft) was lined and sealed in July 1985. However, the sealing in all three shafts is not fully effective, allowing formation water from the Culebra to leak through the shaft seals. Pressure transducers monitor the formation pressures behind the shaft liners. Both the observed leakage and the measured formation pressures indicate that the Culebra dolomite has not returned to undisturbed hydrologic conditions and has a formation-pressure drawdown cone around the shaft location. The depth and the size of the continuing drawdown cone will be governed by the long-term pressure at the shaft location and the remaining leakage rates. The hydrologic conditions at the beginning of the H-3 multipad pumping test in October 1985 and the WIPP-13 multipad pumping test in January 1987, therefore, lie somewhere between the conditions caused by exposure to atmospheric pressure for 4 years, and new conditions defined by the remaining shaft leakage.

The existing hydrologic data (Appendix E) indicate that the Culebra freshwater head at the shaft location between July 1985 and October 1985 was somewhere between 885 and 900 m amsl. There are no documented measurements of the total shaft leakage for that time period. Leakage rate measurements taken in the waste-handling shaft in 1986 range between 0.5 and 2 l/min. For the first transient simulations, a total leakage rate (for all three shafts) of 2 l/min was assumed for the sealed but leaking shafts.

G.2.4 Simulation of the Shaft History

In order to simulate the shaft history outlined in the previous sections, a sink/source at the shaft location was included in the model. Technically this was done by placing a pumping/injection well in the grid block that corresponds to the location of the three

shafts. The early shaft history (Section G.2.1) and the open-shaft period (Section G.2.2) were simulated using the pressure-controlled mode of the wellbore submodel (Reeves et al., 1986). Using this model option, the transient pressures at the shaft location during that time period were prescribed. The corresponding leakage or injection rate was automatically adjusted by SWIFT II during the simulation so that the prescribed pressures were maintained at the grid-block center (Figure 5.2).

For the simulation of the sealed but leaking shafts (Section G.2.3), the rate-controlled mode of the wellbore submodel (Reeves et al., 1986) was used. As discussed in Section G.2.3, an assumed leakage rate of 2 l/min was used for this event in the transient simulations presented in Section 5.0.

G.3 Simulation of Well Tests

Since 1981, the hydraulic heads of the Culebra dolomite has not only been disturbed by the shaft activities discussed in the previous section but also by numerous well tests. Important for the hydraulic conditions in the central part of the model area were the tests performed at H-2, H-3, and H-4. Consequently, the tests on these wells or hydropads that were considered to be relevant and for which sufficient data were available were implemented in the model. The following sections discuss the tests which were considered important and the methodology used to simulate these tests.

G.3.1 Well Tests at the H-2 Hydropad

The test history of the H-2 hydropad is rather complicated (Appendix E, Figure E.2), consisting of a number of slug, pumping, and tracer tests. However, for this modeling study, only tests conducted since 1981 were considered. This is because earlier tests are not

likely to have an influence on the hydrologic conditions in the Culebra dolomite in 1985 or 1986.

Based on unpublished information (field-test notebooks prepared by Hydro Geo Chem, Inc. and INTERA Technologies, Inc. for Sandia National Laboratories), the following major tests have been conducted at the H-2 hydropad in the period 1981 to 1985:

- a pumping test at H-2b2 (October 13-16, 1983) with an average pumping rate of 1.47 l/min (calculated for a 72-hour pumping period);

- a second pumping test at H-2b2 (November 8-17, 1983) with an average pumping rate of 1.07 l/min;

- bailing at H-2b1, H-2b2, and H-2c between June 7, 1984 and July 2, 1984. The volumes of ground water removed from the different boreholes during the different tests totaled about 8100 l. This corresponds to an average production rate of 0.23 l/min during that time period;

- a third pumping test at H-2b2 (July 17 - August 2, 1984). During eight pumping periods, about 2600 l were removed from that borehole. This corresponds to an average pumping rate of 0.11 l/min during the time period.

Numerous additional tests or similar activities were performed since 1981, but because they did not last more than 3 or 4 days, they were not considered to be important enough to be implemented into the model. Also, recirculation tracer tests performed at the WIPP site were not considered because these tests do not represent a net removal of ground water from the Culebra.

The well history at the H-2 hydropad was complicated by drilling activities (e.g., H-2b2 in summer 1983), well reconditioning (e.g., all wells at the H-2 hydropad in winter 1983/1984), packer movements and transducer installations (e.g., H-2b1 in July 1984). Sufficient data on these activities were not available to allow incorporation of them into the model. Thus, only the four tests outlined above were implemented into the model using the SWIFT II wellbore submodel (rate-controlled mode). The pumping rates associated with these four tests are illustrated in Figure 5.3.

G.3.2 Convergent-Flow Tracer Tests at the H-3 Hydropad

After completion of the H-3 hydropad early in 1984, the first major test conducted at that hydropad was the convergent-flow tracer test (Hydro Geo Chem, 1985; Kelley and Pickens, 1986). The activities associated with this test included well development, a pumping test designed to evaluate the transmissivity of the Culebra dolomite at the H-3 hydropad, and the pumping period corresponding to the convergent-flow tracer test. The pumping rates associated with these activities are plotted in Figure 5.3. The first two pumping periods (well development) were very short and therefore were not incorporated into the model.

The first pumping period that was incorporated into the model lasted from April 23 through May 7, 1984. An average production rate of 15 l/min was used. On May 7, the pumping rate was lowered in order to prepare for the convergent-flow tracer test which had to be performed under regulated-flow conditions. As Figure 5.3 shows, a pumping rate of about 11.4 l/min was maintained between May 7 and June 3, 1984. From June 3 until the end of the test on June 12, 1984, moderately higher pumping rates were recorded. An average pumping rate of 13.2 l/min was selected for modeling purposes for this latter period.

In summary, the convergent-flow tracer test was implemented as a pumping test using 15 l/min for the time period from April 23 to May 7; 11.4 l/min from May 7 to June 3; and 13.2 l/min from June 3 to June 12, 1984.

G.3.3 Step-Drawdown Test at the H-3 Hydropad

A step-drawdown test was performed at the H-3 hydropad between June 20 and July 10, 1985 (INTERA, 1986). Using the well H-3b2 as a pumping well, the pumping rate was step-wise increased (Figure 5.3) and the responses in the surrounding wells recorded (Appendix E).

As illustrated in Figure 5.3, the following average pumping periods and rates were implemented:

June 20 - June 24, 1985	:	7.75 l/min
June 24 - June 28, 1985	:	15.0 l/min
June 28 - July 5, 1985	:	18.0 l/min
July 5 - July 10, 1985	:	19.25 l/min

These four pumping periods with the corresponding pumping rates were implemented using the rate-controlled mode of the SWIFT II wellbore submodel.

G.3.4 H-3 Multipad Pumping Test

The pumping period of the H-3 multipad pumping test was from October 15, 1985 through December 16, 1985 (INTERA, 1986). Using the H-3b2 well as the pumping well, an average of about 18.5 l/min (Figure 5.3) was removed over a time period of 62 days. The H-3 multipad pumping test was incorporated into the model using the rate-controlled mode of the SWIFT II wellbore submodel.

G.3.5 Convergent-Flow Tracer Test at the H-4 Hydropad

A long-term tracer test was conducted at the H-4 hydropad from October 24, 1982 to October 15, 1984 (Hydro Geo Chem, 1985; Kelley and Pickens, 1986). The withdrawal well was H-4c. The pumping rate during the tracer test (Figure 5.3) can be generally divided into two separate flow periods. The first flow rate started October 24, 1982 with a pumping rate of about 1 l/min which continued until June 10, 1983. At that time, the pumping rate was doubled to 2 l/min and maintained until August 9, 1983. As Figure 5.3 shows, the pumping rate fluctuated around 1.86 l/min during the following months until June 20, 1984. Slightly higher pumping rates, with an estimated average of 2 l/min, were recorded from June 20, 1984 until the end of the tracer test on October 15, 1984. Similar to the other well tests, the H-4 convergent-flow tracer test was implemented into the model using the rate-controlled mode of the SWIFT II wellbore submodel.

G.3.6 WIPP-13 Multipad Pumping Test

The WIPP-13 multipad pumping test consisted of a 36-day constant-rate pumping period followed by a 72-day recovery period. The test began on January 12, 1987, with WIPP-13 being pumped continuously at approximately 116 l/min until February 17, 1987 (Stensrud et al., 1987). The actual pumping rate varied slightly over the 36-day period from 113 l/min to 119.8 l/min.

Four periods were used in the model to implement the WIPP-13 pumping test. From January 12 to January 27, a pumping rate of 113.4 l/min was used. The second period was from January 27 to February 4 and had a pumping rate of 116.4 l/min. The highest pumping rate of 119.4 l/min was implemented from February 4 to February 11. The fourth period lasted from February 11 until February 17 and had a pumping rate of 118.0 l/min. The pumping rates implemented in the model are illustrated in Figure 5.3.

G.4 Time-Step Considerations

The transient resolution of the simulation of each of the hydrologic disturbances is a direct function of the number and the length of the time steps. Taking into account the length of time to be simulated (more than 6 years) and the transient resolution of the observed head data (Appendix E), it was determined that a resolution of one day was appropriate. Consequently, the smallest time step used in this modeling study had a length of one day. In order to optimize the efficiency of the transient simulations, the minimum time step was only used at the beginning of a new activity, e.g., at the start of a test or after drilling a shaft. Similar to the common practice of reducing monitoring frequency during a hydraulic test, the length of subsequent time steps was increased (e.g., 2, 4, 8, 16 days). An arbitrary maximum of 32 days was chosen for the time-step size.

REFERENCES

Fenix and Scisson, Inc., 1982. SPDV Exploratory Shaft Hole History; Albuquerque, New Mexico. Consultants report prepared for the U.S. Department of Energy, 37 p.

Hydro Geo Chem, Inc., 1985. WIPP Hydrology Program, Waste Isolation Pilot Plant, SENM, Hydrologic Data Report #1. Sandia National Laboratories, Contractor Report SAND85-7206, 710 p.

INTERA Technologies, Inc., 1986. WIPP Hydrology Program, Waste Isolation Pilot Plant, SENM, Hydrologic Data Report #3. Sandia National Laboratories, Contractor Report SAND86-7109.

Kelley, V.A., and J.F. Pickens, 1986. Interpretation of the Convergent-Flow Tracer Tests Conducted in the Culebra Dolomite at the H-3 and H-4 Hydropads at the Waste Isolation Pilot Plant (WIPP) Site. Sandia National Laboratories, Contractor Report SAND86-7161.

Reeves, M., D.S. Ward, N.D. Johns, and R.M. Cranwell, 1986. Theory and Implementation for SWIFT II, the Sandia Waste-Isolation Flow and Transport Model, Release 4.84. Sandia National Laboratories, NUREG/CR-3328 and SAND83-1159, 189 p.

Stensrud, W.A., M.A. Bame, K.D. Lantz, A.M. LaVenue, J.B. Palmer, and G.J. Saulnier, Jr., 1987. WIPP Hydrology Program, Waste Isolation Pilot Plant, Southeastern New Mexico, Hydrologic Data Report #5. Sandia National Laboratories, Contractor Report SAND87-7125.

Stevens, K. and W. Beyeler, 1985. Determination of Diffusivities in the Rustler Formation from Exploratory Shaft Construction at the Waste Isolation Pilot Plant in Southeastern New Mexico. U.S. Geological Survey Water-Resources Investigations Report 85-4020, 32 p.

US Department of Energy (5)
Office of Civilian Radioactive Waste Management
Office of Geologic Repositories
Attn: Associate Director
W. J. Purcell, RW-20
Director, Repository Coordination Div.
T. H. Isaacs, RW-22
Director, Engineering & Licensing
R. Stein, RW-23
Director, Geosciences & Technology
R. Stein, Actg., RW-24
Director, Siting Division
E. Burton, RW-25
Forrestal Building
Washington, DC 20585

US Department of Energy (3)
Albuquerque Operations
Attn: R. G. Romatowski
D. L. Krenz
D. G. Jackson, Director, Public Affairs Division
PO Box 5400
Albuquerque, NM 87115

US Department of Energy (5)
Attn: J. Tillman,
WIPP Project Office (Carlsbad) (2)
T. Lukow, WPO (Carlsbad)
A. Hunt, WPO (Carlsbad)
B. Young, WPO (Carlsbad)
PO Box 3090
Carlsbad, NM 88221

US Department of Energy, SRPO (4)
Office of Nuclear Waste Isolation
Attn: J. O. Neff
R. Wunderlich
G. Appel
J. Sherwin
505 King Avenue
Columbus, OH 43201

US Department of Energy (2)
Idaho Operations Office
Nuclear Fuel Cycle Division
Attn: R. M. Nelson
J. Whitsett
550 Second Street
Idaho Falls, ID 83401

US Department of Energy (2)
Savannah River Operations Office
Waste Management Project Office
Attn: S. Cowan
W. J. Brumley
PO Box A
Aiken, SC 29801

US Department of Energy (3)
Office of Defense Waste and
Transportation Management
Attn: J. E. Dieckhoner, DP-122
L. H. Harmon, DP-121
A. Follett, DP-121
Washington, DC 20545

US Department of Energy
Research & Technical Support Division
Attn: D. E. Large
PO Box E
Oak Ridge, TN 37830

US Department of the Interior
Attn: E. Roedder
959 National Center
Geological Survey
Reston, VA 22092

US Nuclear Regulatory Commission (2)
Division of Waste Management
Attn: M. Bell
H. Miller
Mail Stop 623SS
Washington, DC 20555

US Geological Survey
Branch of Regional Geology
Attn: R. Snyder
MS913, Box 25046
Denver Federal Center
Denver, CO 80225

US Geological Survey (2)
Water Resources Division
Attn: C. Peters
P. Davies
Pine Tree Office Park
4501 Indian School Rd
Suite 200
Albuquerque, NM 87110

State of New Mexico (3)
Environmental Evaluation Group
Attn: R. H. Neill, Director
320 Marcy Street
PO Box 968
Santa Fe, NM 87503

New Mexico State Engineer's Office
District II
Attn: A. Mason
PO Box 1717
Roswell, NM 88201

NM Department of Energy & Minerals
Attn: K. Laplante, Librarian
PO Box 2770
Santa Fe, NM 87501

New Mexico Bureau of Mines and Mineral Resources (2)
Attn: F. E. Kottolowski, Director
J. Hawley
Socorro, NM 87801

Battelle Pacific Northwest Laboratories
Attn: D. J. Bradley
Battelle Boulevard
Richland, WA 99352

Battelle Memorial Institute (13)
Project Management Division
Attn: W. Carbiener, General Manager (3)
J. Treadwell
T. Naymik
J. Kirchner
V. Adams
O. Swanson
A. Razem
S. Gupta
W. Newcomb
A. LaSala
ONWI Library
505 King Avenue
Columbus, OH 43201

Bechtel Inc. (2)
Attn: E. Weber
M. Bethard
PO Box 3965
45-11-B34
San Francisco, CA 94119

IT Corporation (2)
Attn: W. E. Coons
S. Niou
2340 Alamo, SE
Suite 306
Albuquerque, NM 87106

IT Corporation (4)
Attn: W. Patrick
R. McKinney
D. Deal
M. Crawley
PO Box 2078
Carlsbad, NM 88221

INTERA Technologies, Inc. (13)
Attn: G. E. Grisak
J. F. Pickens
G. J. Saulnier
V. A. Kelly
A. M. LaVenue (5)
A. Haug
B. S. Ramarao
M. Reeves

INTERA Library
6850 Austin Center Blvd., #300
Austin, TX 78731

INTERA Technologies, Inc.
Attn: W. Stensrud
PO Box 2123
Carlsbad, NM 88221

Martin Marietta Energy Systems, Inc.
Oak Ridge National Laboratory
Attn: J. A. Carter
Box Y
Oak Ridge, TN 37830

Martin Marietta Energy Systems, Inc.
Oak Ridge National Laboratory
Environmental Science
Attn: E. Bondietti
X10 Area, Bldg. 1505, Rm. 322
Oak Ridge, TN 37831

RE/SPEC Inc.
Attn: P. Gnirk
PO 725
Rapid City, SD 57701

RE/SPEC Inc.
Attn: S. W. Key
PO Box 14984
Albuquerque, NM 87191

Rockwell International
Atomics International Division
Rockwell Hanford Operations
Attn: W. W. Schultz
PO Box 800
Richland, WA 99352

G. O. Bachman
Star Route Box 1028
Corrales, NM 87048

Stanford University
Department of Geology
Attn: K. B. Krauskopf
Stanford, CA 94305

Vanderbilt University
Department of Environmental and
Water Resources Engineering
Attn: F. L. Parker
Nashville, TN 37235

Oak Ridge National Laboratory
Attn: J. O. Blomeke
PO Box X
Oak Ridge, TN 37830

US Geological Survey
Water Resources Division
Attn: J. D. Bredehoeft
Western Region Hydrologist
345 Middlefield Road
Menlo Park, CA 94025

K. P. Cohen
928 N. California Avenue
Palo Alto, CA 94303

F. M. Ernsberger
1325 NW 10th Avenue
Gainesville, FL 32601

Johns Hopkins University
Department of Earth Sciences
Attn: H. P. Eugster
Baltimore, MD 21218

University of New Mexico
Department of Geology
Attn: R. C. Ewing
Albuquerque, NM 87131

University of Minnesota
Department of Geological Sciences
Attn: C. Fairhurst
Minneapolis, MN 55455

University of Texas at Austin
Department of Geological Sciences
Attn: W. R. Muehlberger
Austin, TX 78712

D. A. Shock
233 Virginia
Ponca City, OK 74601

National Academy of Sciences
Committee on Radioactive Waste Management
Attn: P. Meyers
2101 Constitution Avenue, NW
Washington, DC 20418

New Mexico Junior College
Panel Library
Attn: R. Hill
Lovington Highway
Hobbs, NM 88240

New Mexico Tech
Martin Speere Memorial Library
Campus Street
Socorro, NM 87810

New Mexico Tech (3)
Department of Geoscience
Attn: J. Wilson
D. Stephens
C. S. Chen
Socorro, NM 87801

New Mexico State Library
Attn: I. Vollenhofer
PO Box 1629
Santa Fe, NM 87503

US Geological Survey (2)
Water Resources Division
Attn: P. Hsieh
A. F. Moench
345 Middlefield Rd.
Menlo Park, CA 94025

University of New Mexico
Zimmerman Library
Attn: Z. Vivian
Albuquerque, NM 87131

Atomic Museum
WIPP Public Reading Room
Attn: G. Schreiner
Kirtland East AFB
Albuquerque, NM 87185

Carlsbad Municipal Library
WIPP Public Reading Room
Attn: L. Hubbard, Head Librarian
101 S. Hallagueno St.
Carlsbad, NM 88220

Thomas Brannigan Library
Attn: D. Dresp, Head Librarian
106 W. Hadley St.
Las Cruces, NM 88001

Roswell Public Library
Attn: N. Langston
301 N. Pennsylvania Avenue
Roswell, NM 88201

University of Minnesota
Dept. of Energy and Materials Science
Attn: R. Oriani
151 Amundson Hall
421 Washington Ave SE
Minneapolis, MN 55455

Texas A & M University
Center of Tectonophysics
Attn: J. Handin
College Station, TX 77840

Texas A & M University
Department of Geology
Attn: P. A. Domenico
College Station, TX 77843

University of British Columbia
Department of Geological Sciences
Attn: R. A. Freeze
Vancouver, British Columbia V6T 1W5
CANADA

University of Arizona (2)
Department of Nuclear Engineering
Attn: J. G. McCray
J. J. K. Daemen
Tucson, AZ 85721

University of Arizona
Department of Hydrology
Attn: S. P. Neuman
Tucson, AZ 85721

University of New Mexico (2)
Geology Department
Attn: D. G. Brookins
Library
Albuquerque, NM 87131

University of Texas at El Paso
Department of Geological Sciences
Attn: D. W. Powers
El Paso, TX 79968

Princeton University
Department of Civil Engineering
Attn: G. Pinder
Princeton, NJ 08504

Scientific Software-Intercomp
Attn: A. C. Gringarten
1801 California, 3rd Floor
Denver, CO 80202

University of California (2)
Lawrence W. Berkeley Laboratory
Attn: J. Long
S. M. Benson
Berkeley, CA 94720

Kansas Geological Survey
Attn: J. Butler
University of Kansas
1930 Constant Ave., Campus West
Lawrence, KS 66046

University of Wisconsin-Madison
Department of Geology and Geophysics
Attn: M. P. Anderson
1215 W. Dayton St.
Madison, WI 53706

Emcon Associates
Attn: F. W. Fenzel
1921 Ringwood Ave.
San Jose, CA 95131

Gartner-Lee Limited
Attn: K. G. Kennedy
140 Renfrew Dr.
Markham, Ontario L3R 6B3
CANADA

Atomic Energy of Canada, Ltd. (2)
Attn: C. C. Davison
D. R. Stevenson
Whiteshell Nuclear Research
Establishment
Pinawa, Manitoba ROE 1L0
CANADA

Netherlands Energy Research
Foundation ECN (2)
Attn: T. Deboer, Mgr.
L. H. Vons
3 Westerduinweg
PO Box 1
1755 ZG Petten
THE NETHERLANDS

Nationale Genossenschaft
für die Lagerung Radioaktiver
Abfälle (3)
Attn: P. Hufschmied
C. McCombie
M. Thury
Parkstrasse 23
CH5401 Baden
SWITZERLAND

National Ground Water
Information Center
Attn: J. Bix
6375 Riverside Dr.
Dublin, OH 43017

Ground Water Contamination Group
National Water Research Institute
Environment Canada
Attn: R. E. Jackson
PO Box 5050
Burlington, Ontario L2R 4A6
CANADA

Ecole des Mines
Attn: G. de Marsily
35 rue Sainte-Honore
77305 Fontainbleau
FRANCE

Exploration Consultants Ltd.
Attn: P. Hodgkinson
Highlands Farm Greys Road
Henley-on-Thames
Oxon RGO 4PS
ENGLAND

University of Virginia
Dept. of Environmental Sciences
Attn: G. Hornberger
Clark Hall
Charlottlesville, VA 22903

1540 W. C. Luth
6000 D. L. Hartley
6300 R. W. Lynch
6310 T. O. Hunter
6311 L. W. Scully
6312 F. W. Bingham
6314 J. R. Tillerson
6330 W. D. Weart
6330 Sandia WIPP Central Files
(700H INT) (2)
6331 A. R. Lappin
6331 R. L. Beauheim (2)
6331 D. J. Borns
6331 M. M. Gonzales
6331 A. L. Jensen
6331 S. J. Lambert
6331 K. L. Robinson
6331 M. D. Siegel
6332 L. D. Tyler
6333 T. M. Schultheis
6334 D. R. Anderson
6334 K. Brinster
6416 P. A. Davis
6416 C. D. Updegraff
7100 C. D. Broyles
7120 M. J. Navratil
7125 R. L. Rutter
7130 J. D. Kennedy
7133 J. W. Mercer
7135 P. D. Seward
8524 P. W. Dean
3141 S. A. Landenberger (5)
3151 W. L. Garner (3)
3154-1 C. H. Dalin (8)
For DOE/OSTI (Unlimited Release)